

Some pages of this thesis may have been removed for copyright restrictions.

If you have discovered material in AURA which is unlawful e.g. breaches copyright, (either yours or that of a third party) or any other law, including but not limited to those relating to patent, trademark, confidentiality, data protection, obscenity, defamation, libel, then please read our [Takedown Policy](#) and [contact the service](#) immediately

THE FRACTURE TOUGHNESS OF

A RANGE OF CAST STEELS

A Thesis Submitted at the University of Aston in Birmingham
for the Degree of Doctor of Philosophy

I. Al-Daimalani Robertson B.Sc., M.Sc.

April 1978

THE FRACTURE TOUGHNESS OF
A RANGE OF CAST STEELS

I. Al-Daimalani Robertson

A Thesis submitted at the University of Aston in Birmingham
for the degree of Doctor of Philosophy

April, 1978

SUMMARY

A range of plain carbon, carbon-manganese and low alloy cast steels were tested in order to determine their various fracture toughness values under elastic and elastic-plastic conditions. The main fracture toughness parameters which are considered are (1) Linear Elastic Fracture Mechanics (LEFM), (2) the J-Contour Integral, and (3) Crack Opening Displacement (COD). Results are obtained from fracture toughness specimens of various dimensions and the relevance of the validity criteria to cast steels is considered in some detail.

In addition, the effect of casting position on specimen toughness values was noted.

Valid K_{IC} results according to LEFM, were obtained for three of the eight cast steels tested. Although K_{IC} values from LEFM were not obtained from the remaining five steels, critical COD and J-integral values were determined. It is postulated that these values and particularly the critical J values can be used with confidence for material selection or in defect tolerance calculations using these steels.

Toughness values were found to vary with casting position in several of the steels tested and the possible reasons for such variations are discussed in the Thesis.

Cast Steels	Fracture Toughness	J-Integral	Crack Opening Displacement	Linear Elastic Fracture Mechanics
-------------	--------------------	------------	-------------------------------	--

CONTENTS

	<u>Page No.</u>
1. INTRODUCTION	1
2. LINEAR ELASTIC FRACTURE	
2.1 The Energy Approach to Fracture	4
2.2 The Stress Intensity Approach to Fracture	10
2.3 Equivalence of Stress Intensity Approach and Energy Approach	16
3. LIMITATIONS TO LINEAR ELASTIC FRACTURE MECHANICS	17
4. GENERAL YIELDING FRACTURE MECHANICS	
4.1 Introduction	25
4.2 The Crack Opening Displacement Approach	25
4.3 Elastic Plastic J-Integral Fracture Approach	30
4.3.1 J-Integral Estimation Techniques	
4.3.1.1 Experimental compliance calibration method	43
4.3.1.2 Analytical procedure for estimating J	48
4.3.1.3 Procedure based on specific fracture energy	48
5. MICRO-MECHANISMS OF FRACTURE	
5.1 Cracking Processes	50
5.2 Rupture Processes	60
6. EXPERIMENTAL TECHNIQUES AND MATERIALS	65
7. ANALYSIS OF RESULTS	86
8. RESULTS	96
9. DISCUSSION	166
10. CONCLUSIONS	181
11. ACKNOWLEDGEMENTS	188
12. APPENDICES	
12.A State of Plane Stress and Plane Strain	188
12.B Digital Computer Program for Determining J and K Values from Load-Load Point Displacement Curves	188
13. REFERENCES	188

1. INTRODUCTION

It is standard practice when designing structures, to apply a safety factor to the failure load in order to determine some safe working load. In many cases the failure load calculations are based on the supposed final collapse mechanism, e.g. buckling or yielding. There is an important mode of failure, classified under the general heading of fracture, and resulting from the propagation of pre-existing cracks or defects, which has received little attention from designers and material technologists. There are many examples of failure by fracture where the failure can be attributed to propagation of pre-existing starter cracks and where the failure load was a fraction of the limit or yield load, (1) and references contained therein. To counter this shortcoming in the methods of structural analysis the subject area known as fracture mechanics has been developed. Briefly, fracture mechanics exist as a branch of continuum mechanics to describe the response of a body containing one or more naturally occurring sharp cracks. With this more realistic approach to material behaviour, in structures prone to failure by fracture, the designer should ultimately be able to dispense with his empirical safety factors or at least be able to base such factors on a more realistic appreciation and quantification of actual material behaviour.

In general, fracture occurs by a two stage process - the first being crack nucleation or initiation and the second being crack propagation. As all engineering materials contain inherent defects it is perhaps more relevant to first quantify the 'conditions for propagation' of such pre-existing defects. This does not imply that crack nucleation studies are worthless, indeed this is an important area of research (2), particularly in studies of fatigue failure. In this thesis, however, attention is

focused on pre-existing cracks and the various methods for quantifying their behaviour under monotonic loading. For the methods of analysis, to be described in detail in this thesis the general aim is to identify a single parameter which is a function of the cracked body's geometry, applied load and crack length and which can be determined uniquely for any of these variables.

There are two basic analytical approaches to the problem of fracture, one based on an energy balance while the other is based on the magnitude of the stress field ahead of a crack tip. Both of these approaches are discussed in detail in this thesis. It is also shown that the two approaches are in fact equivalent for certain material behaviour.

In a later Chapter, the accuracy of the aforementioned techniques are discussed and it is noted that they have limited application to linear elastic/brittle materials. For materials which exhibit non-linear elastic behaviour, either a modified 'fracture parameter' is necessary or alternatively, a complete re-analysis of the problem is required. The requirement is generally determined by the amount of non-linearity or plastic flow that takes place prior to final fracture. As most common structural materials have the ability to deform plastically before fracture, this is obviously an important area for investigation. In sections (4.2) and (4.3) two methods are discussed, each of which make some allowance for non-linear material behaviour. The first of these is based on the hypothesis that a critical crack opening must be achieved before a given crack can propagate. In the second method, section 4.3, a fracture criterion is proposed which is based on a mathematical analysis of the stress and displacement field ahead of a crack tip in a material whose constitutive behaviour is not linear elastic.

The end product of any fracture analysis is the determination of critical crack lengths or applied loads for the particular cracked component under consideration. In order to achieve this, a value of the fracture parameter of interest is calculated theoretically for comparison with an experimentally measured critical fracture parameter. The experimentally determined value is a measure of the materials toughness, and if defined and measured correctly, is a unique property of the material under the given test conditions. The object of this thesis is to determine, experimentally, critical fracture data for a range of Cast Steels and to identify relevant metallurgical data for this important class of structural steels.

2. LINEAR ELASTIC FRACTURE MECHANICS

2.1 The Energy Approach to Fracture

The energy balance approach to the study of the fracture phenomenon in cracked bodies was originally proposed by Griffith (3) in 1920. Griffith postulated that a necessary condition for a crack to spread under the action of external loads is that the energy used in creating new fracture surfaces is supplied from the released energy in the elastic solid. Only if the total energy decreased would the crack extend spontaneously under the applied stress.

As an example, consider a centre cracked infinite plate of unit thickness loaded by a remote tensile stress σ as shown in Fig. 2.1. The changes in energy which occur as the crack extends an infinitesimal amount da , are two-fold:-

- a) As the new surfaces are created, the energy increase during crack extension is simply the 'work to fracture', $2\gamma da$. Here γ is the surface energy of the material and the factor 2 relates to the number of surface created.
- b) As the crack extends, energy in the elastic solid is released. Under 'fixed grip' conditions (fixed load point displacement) an increase in crack length results in a decrease in stored elastic strain energy while under constant loading conditions ($\sigma = \text{constant}$) the total potential energy is decreased. It can be shown, however (4), that for an infinitesimally small amount of crack extension, the decrease in stored elastic energy of a cracked body under fixed grip conditions is identical to the decrease in total potential energy under conditions of constant loading. Griffith (5) stated that 'the general conclusion may

be drawn that the weakness of an isotropic solids, as ordinarily met with, is due to the presence of discontinuities, or flaws, whose ruling dimensions are large compared with 'molecular distances'. The effective strength of technical materials might increase ten or twenty times at least if these flaws can be eliminated.

The Griffith Theory provides a means of estimating the theoretical strength of solids. It also gives, for brittle materials, a correct relationship between fracture strength (σ_F) and defect size ($2a$), in a large sheet by the equation:

$$\sigma_F = \sqrt{\frac{2E\gamma}{\pi a}} \quad (1)$$

γ = Surface energy per unit area.

E = Young's modulus of elasticity.

Where γ is the amount of energy required to form the new crack surface. For thick plates (plane strain conditions), the Griffith equation takes the form:

$$\sigma_F = \sqrt{\frac{2E\gamma}{(1-\nu) \pi a}} \quad (2)$$

Where ν = Poisson's ratio.

The stress analysis used to calculate the stored elastic energy was taken from Inglis's work (6). The Griffith analysis worked well for brittle materials such as glass where it can be assumed that γ was equal to the surface free energy. The energy rate analysis failed, however, to calculate fracture strength in metals (σ_F) where values were between two and three orders of

magnitudes too small. It was almost thirty years after Griffiths contribution that Irwin (7) and Orowan (8) suggested a modification to the original formulation so that limited plastic deformation prior to failure could be accommodated by the theory. They pointed out that the Griffith-type energy balance must be between the strain energy stored in the specimen and the surface energy plus the work done in plastic deformation. They also recognised that for relatively ductile materials, the work done against surface tension is generally not significant in comparison with the work done against plastic deformation. Both Irwin and Orowan argued that, provided plastic distortion takes place in a zone which is small in comparison with crack length and component thickness, the energy released by crack extension could still be calculated from elastic analysis with a sufficient degree of accuracy. Thus, in essence, the modified theory simply involves a redefinition of the energy absorption term.

Orowan (9) further demonstrated that the Griffith equation could be made more compatible with the actual fracture behaviour of metals by the inclusion of a term γ_p , expressing the plastic work required to create new surfaces. This proposition has been verified to some extent by experimental work which has revealed a thin layer of plastically deformed material in a metal which had fractured in a brittle manner was examined using X-ray diffraction techniques. The relationship between fracture stress and crack length then becomes from equation (2) (1):

$$\sigma_F = \sqrt{\frac{2E(\gamma + \gamma_p)}{\pi a}} \quad (3)$$

and since γ is two to three orders of magnitude less than γ_p , equation (3) can be approximated by:

$$\sigma_F = \sqrt{\frac{2E\gamma_p}{\pi a}} \quad (4)$$

Irwin's (10) modified theory consisted basically in evaluating the rate of strain energy release with respect to crack length at the point of fracture, i.e. the energy release rate was the controlling parameter. If the fracture process was to be similar for different loadings and geometries, the fracture event would occur when the strain energy release rate reached a critical value. It was proposed that this critical value could be regarded as a material property to be determined by a suitable fracture test. A means for determining the value of energy release rate for different loading conditions and geometries was proposed by Irwin and Kies (10). They noted that the strain energy stored in an elastic body could be represented by the relationship:

$$U = \frac{P^2 C}{2} \quad (5)$$

In this relationship P is a characterising applied load and C , the elastic compliance of the body, i.e. the displacement at the point of application of load due to unit applied load. From this expression it immediately follows that the strain energy release rate, with respect to crack extension, is given by:

$$\frac{dU}{da} = \frac{1}{2} P^2 \frac{dC}{da} \quad (6)$$

Irwin and Kies (10) suggested that by measuring the compliance of a test specimen, or a component model with different crack lengths,

the value of $\frac{dC}{da}$ as a function of crack length could be obtained. A fracture test could then be interpreted by evaluating $\frac{dU}{da}$ at fracture using the fracture load and the value of $\frac{dC}{da}$ for the appropriate crack length. On the basis of this result a considerable amount of work was carried out to determine the compliance of various specimen shapes; see for example Stawley et al (11). Irwin (12) proposed an alternative interpretation of critical strain energy release rate when he suggested that the surface energy term in the Griffith equation might be replaced by an experimentally determined 'crack extension force'. (This is also generally referred to as the 'strain energy release rate'). Since the crack extension process requires a fixed rate of release of energy, the crack extension force G (after Griffith) measured in units (in lb/in.^2) or MN/m is defined as the quantity of stored energy released from a cracking specimen as a result of the extension of an advancing crack by unit area. When G reaches a critical value, denoted as G_c , then release of strain energy just exceeds the rate of energy dissipation needed for the creation of the new crack surface. This critical value of G is known as the 'fracture toughness' and denoted as G_{Ic} or G_c according to whether the unstable propagation of crack occurs under plane strain or plane stress conditions. This ability to predict failure is sufficient justification for utilizing the concept as an engineering approach.

The concept of fracture toughness in terms of strain energy release rate has a number of drawbacks, principally because it is associated with the ambiguous 'surface energy'. The approach based on linear elastic fracture mechanics, now to be discussed, is therefore more attractive if only for its conceptual simplicity.

attention on the mechanical

of the crack

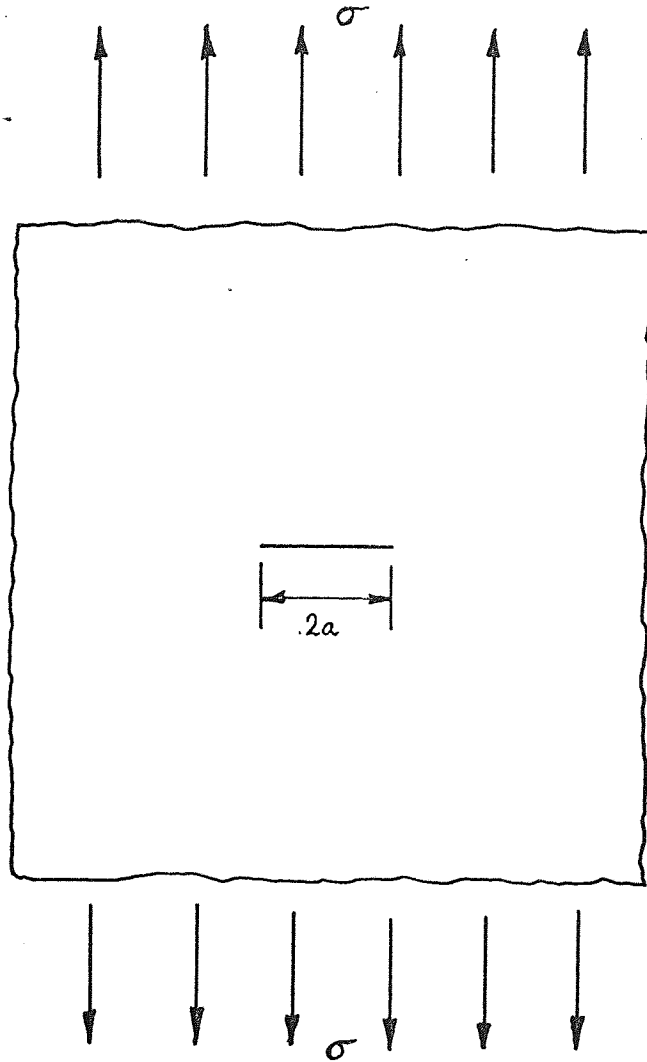


Fig. 2.1 Griffith's crack : geometrical configuration.

2.2 The Stress Intensity Approach

This approach to fracture focuses attention on the mechanical environment near the tip of a crack and is based on a linear elastic analysis of the crack tip region. The conditions at the root of a sharp crack were described in terms of the elastic stress field surrounding the crack tip and a stress intensity factor K was identified to express the magnitude of the local stress field. Westergaard's (13) stress field equations for a crack are used to express the local stress near the tip of the crack using a mathematical model of the crack as a flat, internal surface in a linear elastic solid. These equations can be written for the particular case where crack propagation takes place by the crack surfaces opening symmetrically as in Figure 2.2, as:

$$\begin{aligned}
 \sigma_x &= \frac{k_I}{\sqrt{2\pi r}} \left(\cos \frac{\theta}{2} \left(1 - \sin \frac{\theta}{2} \sin \frac{3\theta}{2} \right) \right) \\
 \sigma_y &= \frac{k_I}{\sqrt{2\pi r}} \left(\cos \frac{\theta}{2} \left(1 + \sin \frac{\theta}{2} \sin \frac{3\theta}{2} \right) \right) + \text{other terms} \\
 \tau_{xy} &= \frac{k_I}{\sqrt{2\pi r}} \left(\cos \frac{\theta}{2} \sin \frac{\theta}{2} \cos \frac{3\theta}{2} \right)
 \end{aligned}
 \tag{7}$$

bounded at $r = 0$

Symbols have their normal connotation with the local crack tip co-ordinate system as shown in Figure 2.2. The stress intensity factor, k_I (subscript I referring to the opening mode), is a function of applied stress and crack geometry and, for a central crack of length $2a$ placed symmetrically with respect to an applied stress σ , in an infinite plate is given by:

$$k_I = \sigma \sqrt{\pi a} \tag{8}$$

Analysis of other loading configurations reveal that equations of the form of (7) are obtained in each case but the value of k_I differs for each geometry and loading configuration considered. The stress intensity factor, therefore characterises the intensity of the stress field ahead of a crack. For any cracked body under load it is thus known that the local stresses will diminish as the inverse square root of the distance from the tip and that in general the stress intensity factor may be written in the form:

$$k_I = \sigma \sqrt{a} Y\left(\frac{a}{w}\right) \quad (9)$$

where σ is a characterizing stress, a is a characterizing crack length, w is a representative component dimension, and $Y\left(\frac{a}{w}\right)$ is a dimensionless calibration function which defines k_I for the specific body under consideration. Obviously, to interpret test results or to make design calculations, it is necessary to have explicit expressions for k_I for specific geometries and loading conditions. These expressions are usually derived theoretically and Figure 2.3 shows three configurations with the corresponding values of $Y\left(\frac{a}{w}\right)$. The important point to note is that it is always possible by theoretical or experimental means to determine k_I to a sufficient accuracy for any given geometry or set of loading conditions. An extensive review is given by Paris & Sih (14) including methods for estimating stress intensity factors for complicated geometries. The determination of stress intensity factors is a specialist task necessitating the use of a number of analytical and numerical techniques. The methods that have been used for evaluating the stress intensity factor Y are briefly described in (15).

The stress intensity factor criterion for failure states that, fracture will take place when the stress intensity factor reaches some critical value for the material, k_{IC} (16), this value being previously determined by experiments. This critical value is known as the fracture toughness and is taken as a material property. With the toughness value it is then possible to establish what flaws are tolerable in an engineering structure under given conditions or to compare materials as to their utility in situations where fracture is of relevance. The difference between k_I and k_{IC} can be considered analogous to the difference between stress and yield strength as in conventional stress analysis.

As noted previously, the subscript I refers to the opening mode of crack behaviour. There are, however, two other possible modes by which a crack may extend, these are the Shear Mode II and the Antiplane Shear Mode III. These modes are illustrated diagrammatically in Figure 2.4.

The shear mode II and the antiplane shear mode III fracture mechanisms may be analysed in a similar manner (4) to the opening mode I case where the stress intensity factors are denoted k_{II} and k_{III} respectively. It is found from such analyses that each mode has the characteristic inverse square root singularity similar to that for k_I found from equation (7). k_{II} and k_{III} are, therefore, analogous to k_I in that they characterise the magnitude of the near crack tip stress field for these modes of crack extension. The three modes are sufficient to describe all possible modes of crack behaviour. Any particular problem may be treated as one or a combination of these modes. The emphasis here shall be placed initially on the opening mode, which corresponds to the usual case of tensile loading.

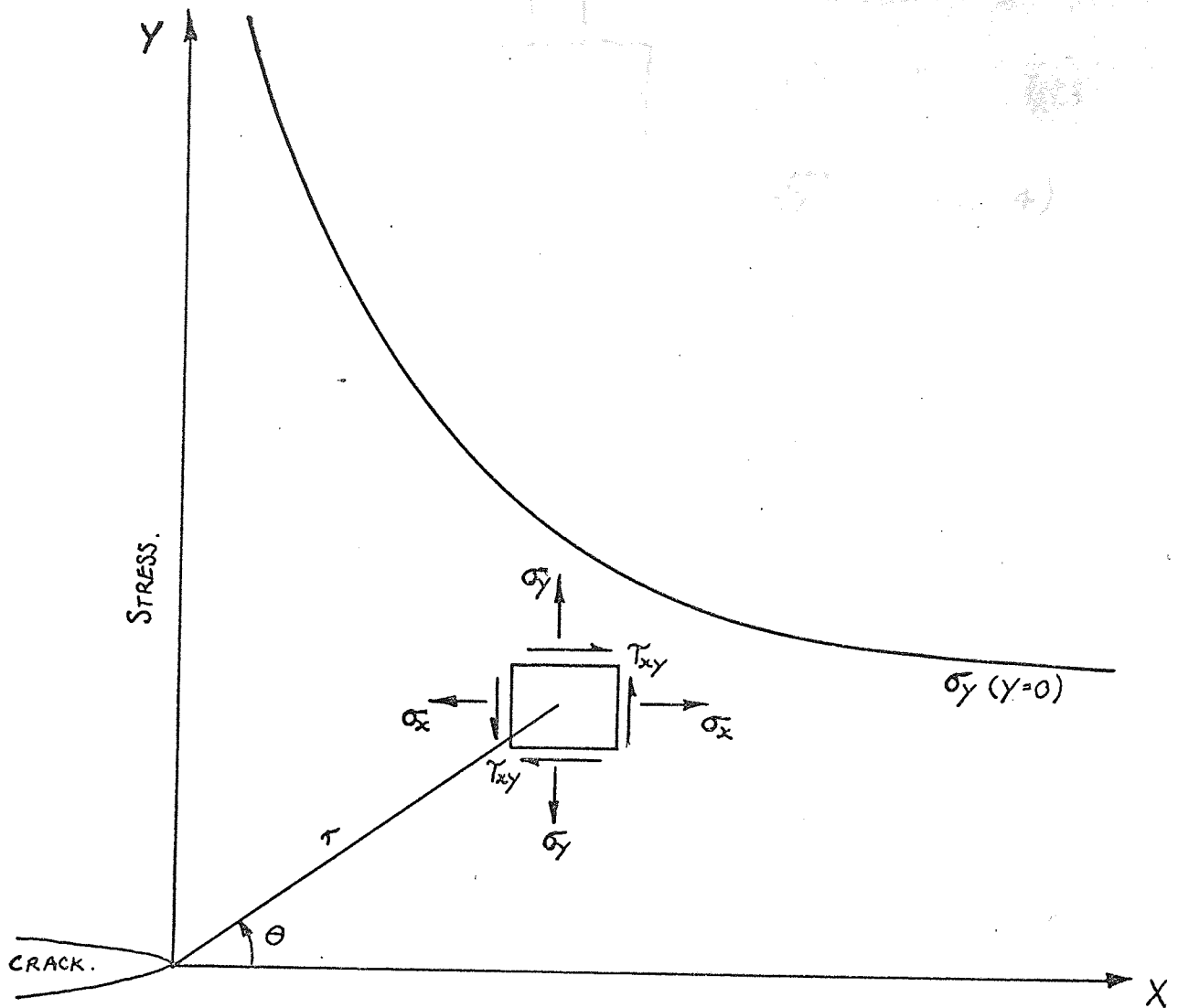
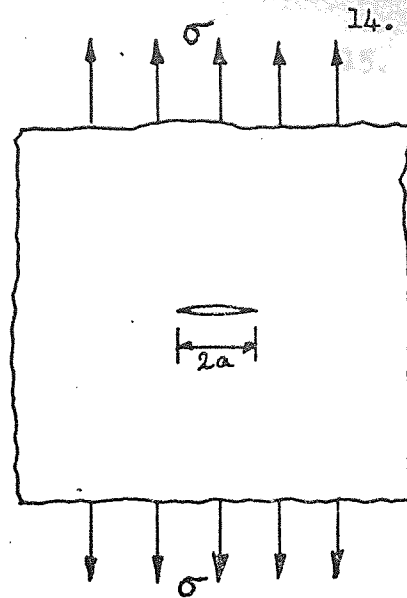
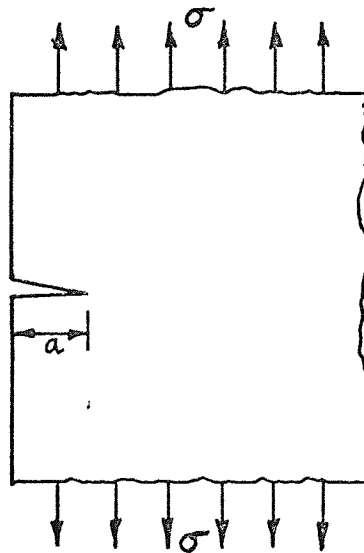


Fig. 2.2 Schematic illustration of the elastic stress distribution near the tip of a crack.



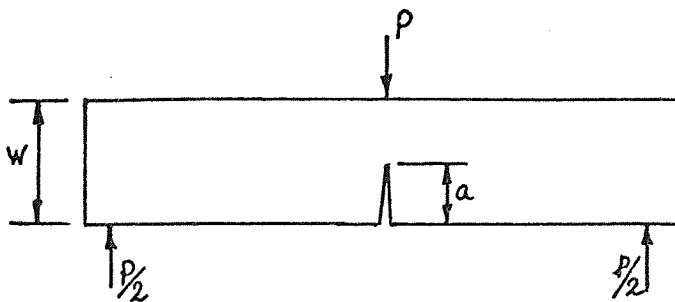
$$Y = \sqrt{\pi} \quad (\text{REF. 14})$$

a) Isolated crack in an infinite plate.



$$Y = 1.12\sqrt{\pi} \quad (\text{REF. 17})$$

b) Surface crack in a semi-infinite plate.



$$Y\left(\frac{a}{w}\right) = 1.93 - 3.07\left(\frac{a}{w}\right) + 14.53\left(\frac{a}{w}\right)^2 - 25.11\left(\frac{a}{w}\right)^3 + 25.8\left(\frac{a}{w}\right)^4 \quad (\text{REF. 18})$$

c) Surface crack in a three-point bend specimen.

Fig. 2.3 Three crack configurations with corresponding $Y(a/w)$ values.

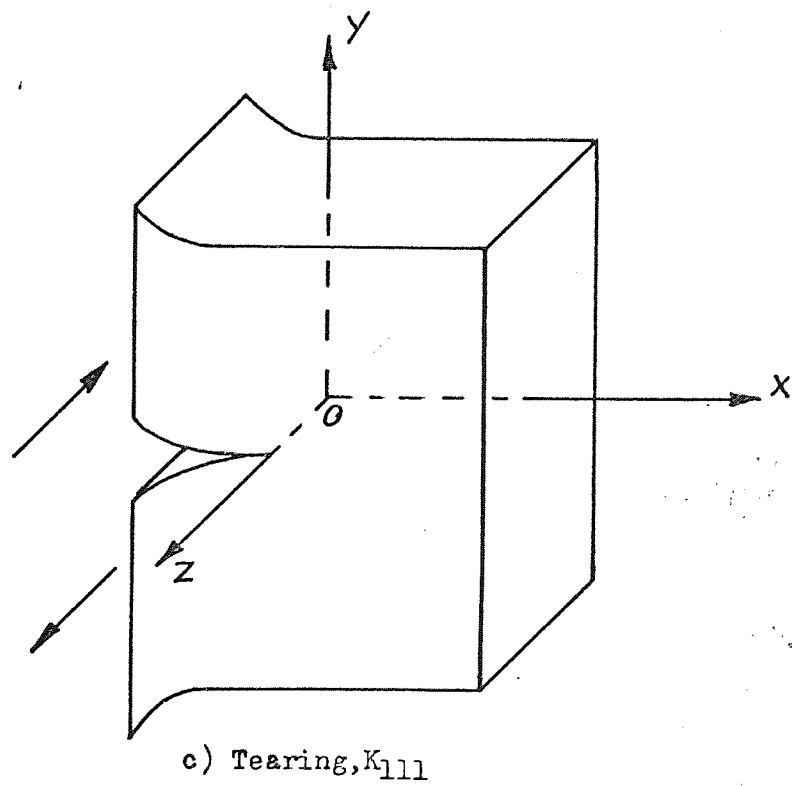
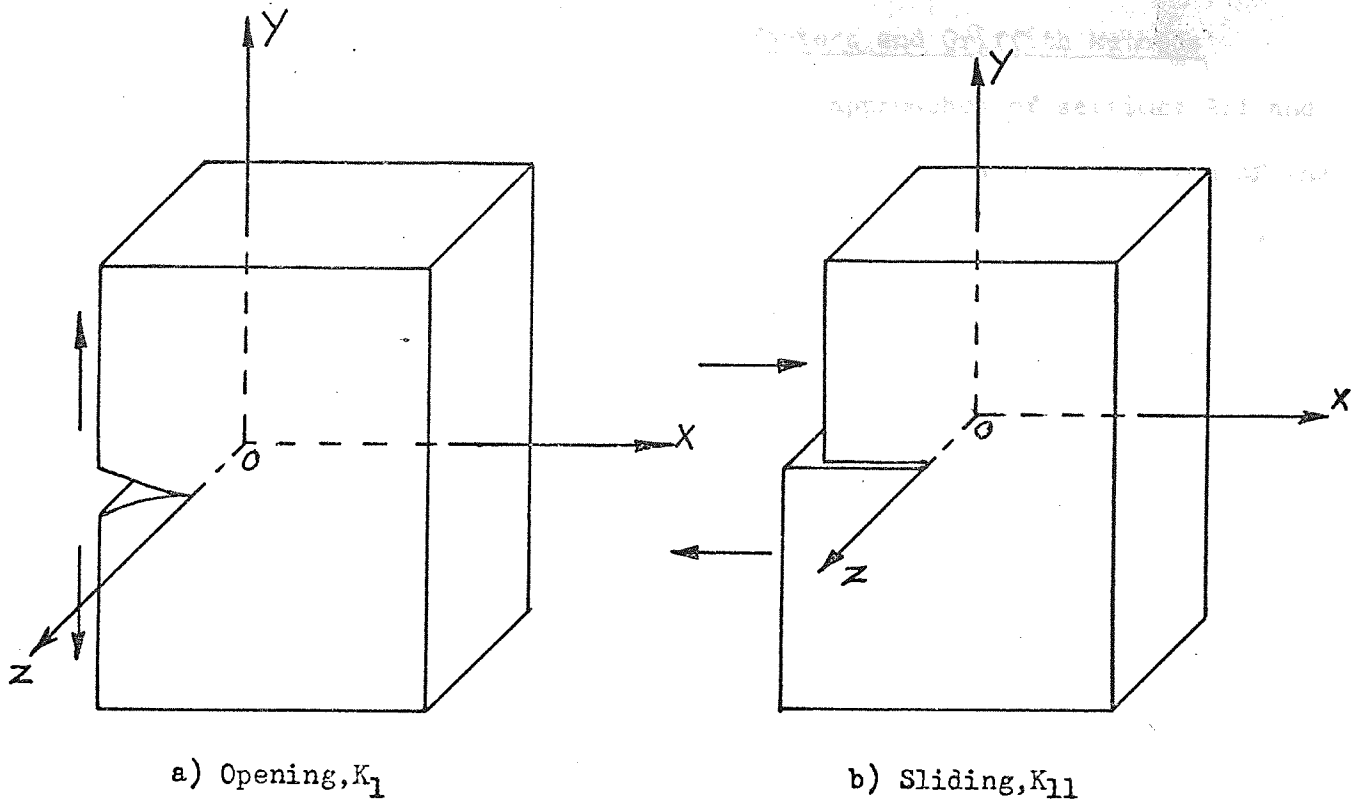


Fig. 2.4 Basic modes of crack extension.

2.3 Equivalence of Stress Intensity Factors and Griffith Methods

For the linear elastic case, the two approaches of sections 2.1 and 2.2 may be shown to be equivalent (12). From a consideration of the work done in extending the crack by a small increment, it can be shown that, for plane strain:

$$G_I = \frac{k_I^2}{E} (1 - \nu^2) \quad (10)$$

and for plane stress:

$$G_I = \frac{k_I^2}{E} \quad (11)$$

where ν = Poisson's ratio

E = Young's modulus.

3. LIMITATIONS OF LINEAR ELASTIC FRACTURE MECHANICS

The plane strain fracture toughness, k_{IC} , represents the minimum value of the critical stress intensity for any material, and is the more important quantity from the standpoint of brittle fracture in low alloy cast steels. However, as a result of experimental investigation it became apparent that, except in cases where fracture occurred at very low stress levels (in comparison with material yield stress), plastic flow was significant and some account of plastic behaviour was necessary. Irwin (19) found that the value of k_I at the point of fracture was strongly dependent on plate thickness, and only after a certain thickness had been exceeded could the critical value be regarded as a material property, k_{IC} , dependent only on the testing environment. The variation in the apparent value of k_I has been attributed to through-the thickness change in constraint across the crack front. The plastic regions that are near a free surface are practically in a condition of plane stress whilst those remote from such a surface approach conditions of plane strain. The conditions of plane stress and plane strain are discussed in Appendix 12.A. With reference to fracture, these conditions are shown schematically in Figure 3.1. When plate thickness is sufficiently large the fracture behaviour will be dominated by the region of constrained plastic deformation, in which the fracture surface is flat and normal to the applied stress and conditions are described as plane strain. Plane stress conditions are associated with an oblique shear mode of fracture, occurring predominantly in thin sheets. Figure 3.2 indicates schematically the fracture mode transition from plane stress to plane strain which results from increasing thickness, expressed in terms of a change from k_C to k_{IC} (For simplicity of notation, k_C is used to signify toughness under plane stress while k_{IC} refers to predominantly plane strain behaviour. This is sufficient in this work as opening mode fracture only is being considered).

However, there exists no method to predict whether the fracture mode will be plane stress or plane strain prior to a given test. ASTM Committee E24(21) has set minimum specimen size limits and recommendations for determining test validity. One recommendation for plane strain is that no specimen dimension should be less than $2.5 \left(\frac{k_{IC}}{\sigma_Y} \right)^2$. These limits are based on experimental results from tests on what might now be considered as materials of medium toughness. The Committee has not yet attempted to solve the problems for materials in which the toughness k_{IC} exceeds the tensile yield strength σ_Y . In such cases, specimen sizes become prohibitive under the proposed recommended practice.

A continuing effort is being made to adjust or correct values obtained from undersized specimens to reflect true plane strain values. k_Q determined from a LEFM analysis using the load at instability will be less than k_{IC} for geometrically invalid specimens. This can be seen by adding Irwin's plasticity term (22), $\beta \left(\frac{k_{IC}}{\sigma_Y} \right)^2$ to the measured crack length to give a first order plastically corrected estimate of the toughness k'_Q where

$$k'_Q(a_1) = \frac{P_Q}{B\sqrt{w}} f \left(\frac{a_1}{w} \right) \quad (12)$$

and

$$a_1 = a + \beta \left(\frac{k_{IC}}{\sigma_{YS}} \right)^2$$

β is about $\frac{1}{6\pi}$ for plane strain. Clearly k'_Q is a better approximation to k_{IC} than k_Q . A graphical correction method, based on the Irwin plasticity correction, has been proposed by Stonesifer and Smith (23). These authors have also proposed another method (24), known as the scaling method, which is based on equivalent elastic fracture strain and this technique appears

to work better over a larger range of specimen sizes than earlier suggestions (23). This more recent correction technique is based on the assumption that if the specimen had been of sufficient size, general yielding would not have occurred before crack propagation or instability and the total strain at failure would have been completely elastic. Failure would then have occurred at the load represented by the intersection of a line extending through the elastic portion of the load/deflection curve and a constant strain, or deflection line through the point of crack instability. The load corresponding to this intersection is used in k_{IC} calculation. Figure 3.3 illustrates the method used to determine this load. This method appeared to work well on the 12% Ni Martensitic steel examined by Stonesifer and Smith. Using this approach it should be possible to calculate the k_{IC} value corresponding to the point of crack instability and hence to compare the k_{IC} value obtained by this method with that determined using the various techniques to be described subsequently.

An alternative method of determining a toughness value from an invalid test has been proposed by Witt (25). Using Witt's method, a normalised load-displacement curve, such as that shown in Figure 3.4, can be constructed for geometrically similar specimens. The load-displacement record of any geometrically similar specimen should lie on this curve up to the point of failure. In order to apply this method, for the determination of the toughness values, an appropriate displacement record must be made for some point in the specimen while carrying out a fracture toughness test. The actual points chosen for recording displacements should be close to the crack tip region and are usually taken as the crack opening displacements, δ . From the record of displacement a critical value can be found which is associated with crack instability, this value can then be employed in the curve of Figure 3.4. Large specimens generally fail on the

linear part of the normalised load displacement curve, say at A, in Figure 3.4, where linear elastic fracture mechanics is applicable. Smaller specimens, however, generally fail well into the non-linear part of the curve, at say, B. Consider a fracture test on a specimen that fails at the point B. According to the equivalent-energy method the toughness k_{1C}^W is obtained from:

$$k_{1C}^W = \frac{P_A}{B\sqrt{w}} f\left(\frac{a}{w}\right) \sqrt{\frac{U_B}{U_A}} \quad (13)$$

where P_A is any load which lies on the linear part of the load-displacement curve and U_B and U_A are the areas under the load-displacement curve up to the points B and A respectively. Witt (25) has demonstrated, that for A533B steel

$$k_Q < k_{1C}^W < k_{1C}$$

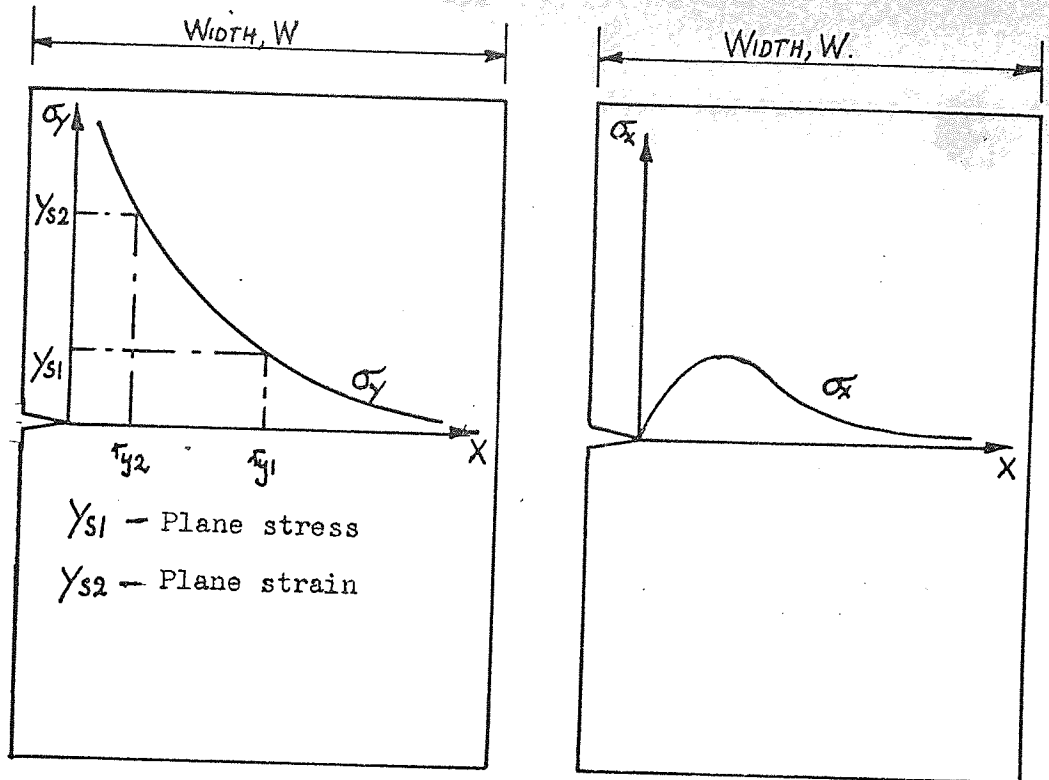
where

$$k_Q = \frac{P_B}{B\sqrt{w}} Y\left(\frac{a}{w}\right)$$

is the apparent toughness, k_{1C} the true fracture toughness of the material and P_B is the maximum load recorded up to failure. This method was used by Chell et al (26) for the determination of valid plane strain fracture toughness data from ASTM invalid tests obtained for two low-pressure turbine-disc steels.

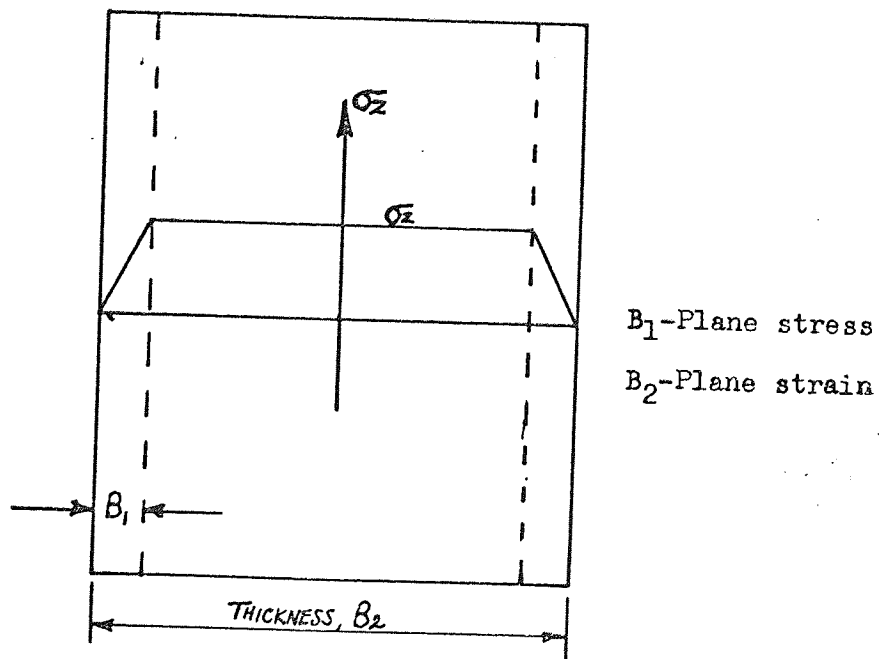
It is easy to appreciate the attraction and potential usefulness of being able to use 'invalid' data to determine 'valid' k_{1C} results. The results of virtually any fracture test could be employed to yield valid

data that otherwise would have required fracture specimens of considerable size. Although the methods described above have each been shown, by their respective supporters, to give acceptable results in many cases, it is inconceivable that such methods could be expected to be of sufficient generality to handle all types of material behaviour. The material to material variability in the fracture process necessitates a more fundamental mathematically rigorous and realistic approach to the quantification of material fracture parameters. In view of this, the preceding methods are presented for completeness and as possible techniques for the evaluation of approximate material toughness values.



a) Variation of σ_y across width

b) Variation of σ_x across width



B_1 -Plane stress
 B_2 -Plane strain

Fig. 3.1 Development of constraint through width and thickness of a notched plate. (Ref. 20)

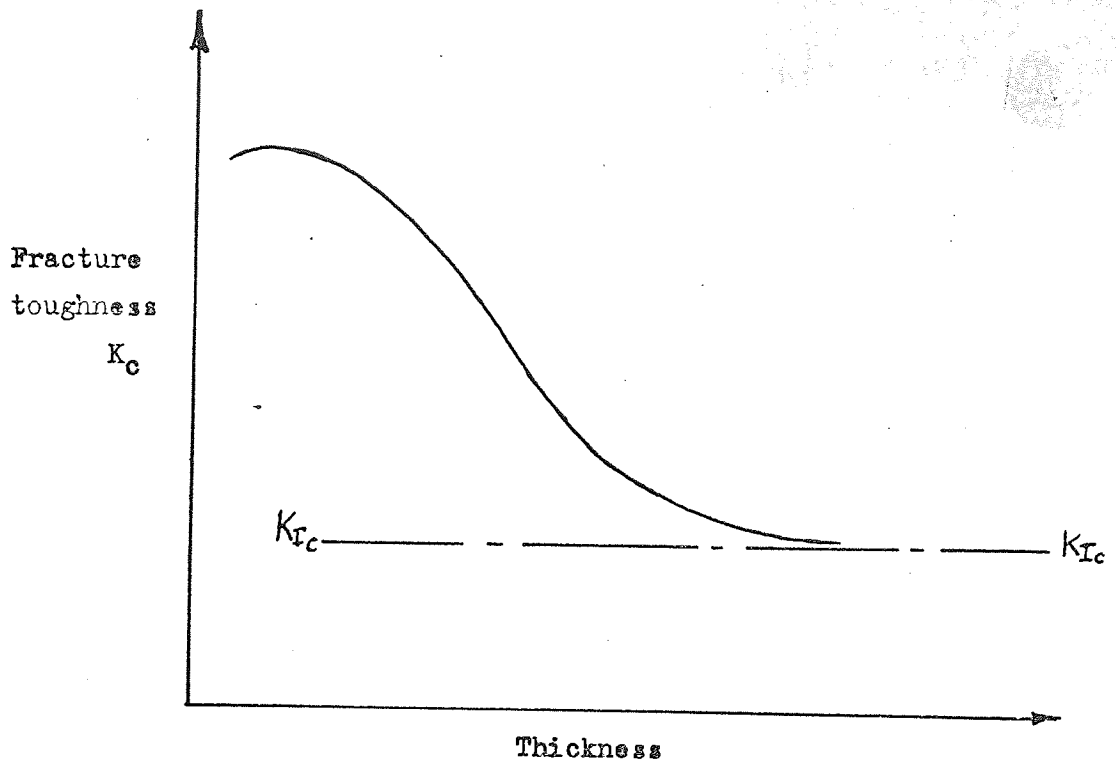


Fig. 3.2 General form of the variation of toughness with thickness.

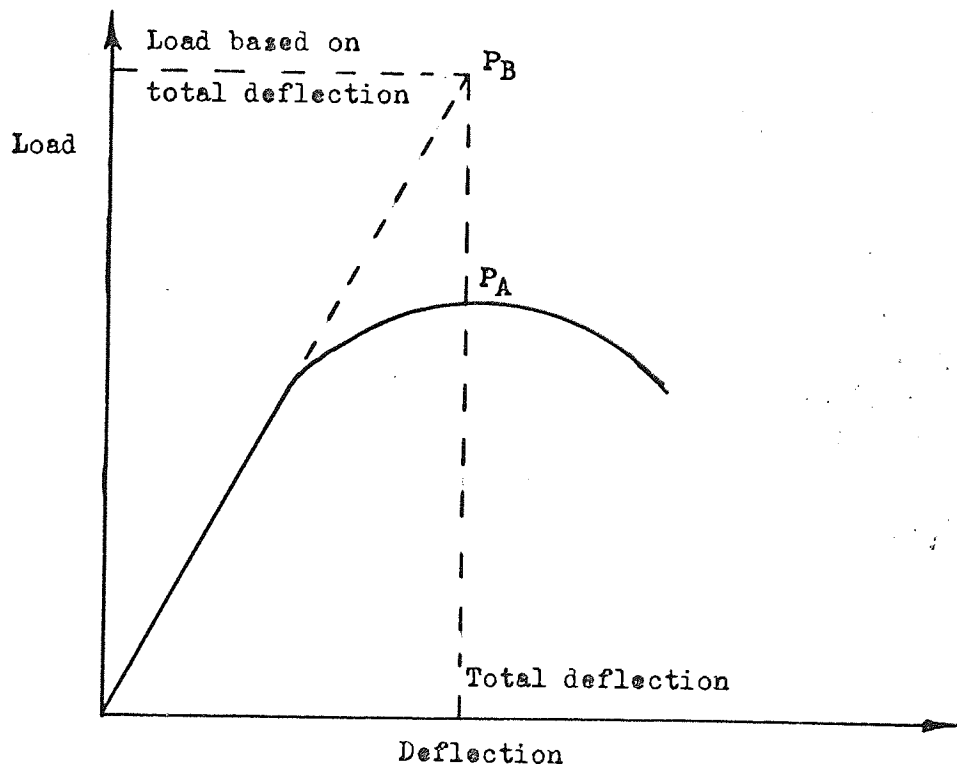


Fig. 3.3 Method used to determine load used in scaling method. (Ref. 24)

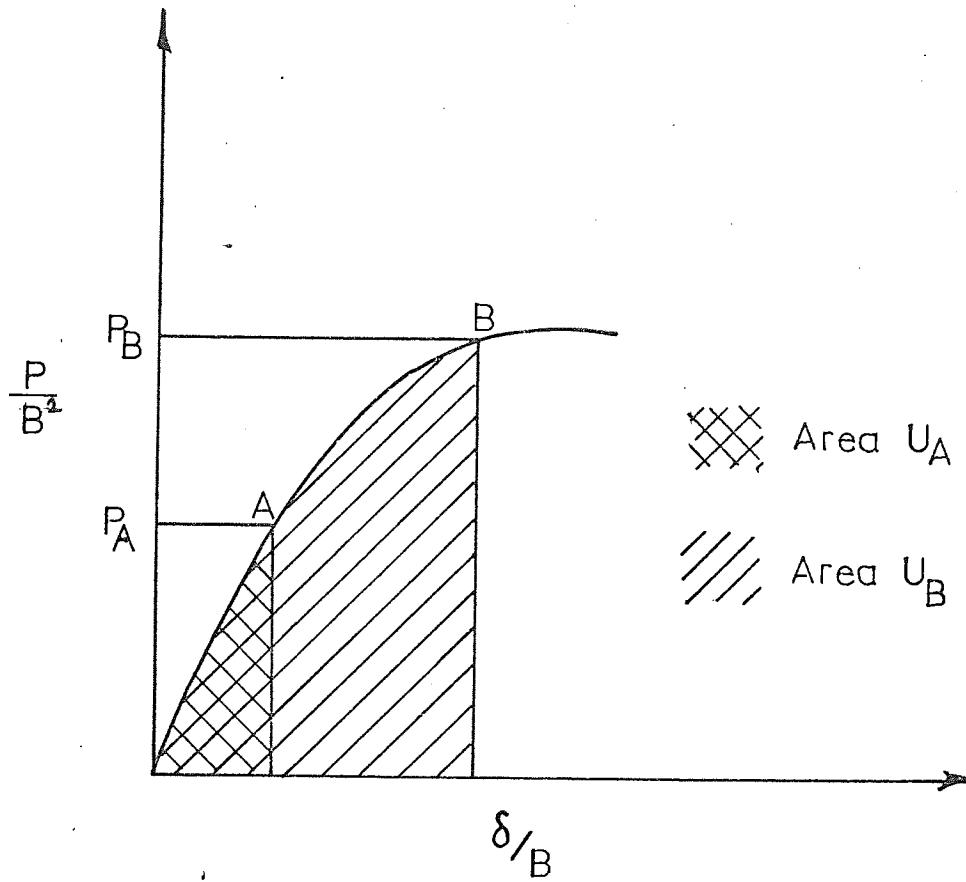


Fig. 3.4 Normalised load-displacement curve. (Ref. 25)

4. GENERAL YIELDING FRACTURE MECHANICS

4.1 Introduction

Linear elastic fracture mechanics (LEFM) where the near crack tip stress and strain fields at fracture are adequately described by a purely elastic analysis, has been shown to provide an acceptably accurate prediction of critical fracture conditions. However, since very few structural materials have a sufficiently high yield strength to behave elastically at the crack tip, the (LEFM) approach is inappropriate in many cases of practical interest. Consequently considerable research effort has been devoted to the development of an elastic plastic fracture theory. At the present time no fully proven approach has emerged, but two concepts which seem promising are those based on crack opening displacement (COD), and the J contour integral. The theoretical and experimental evidence in support of these methods will now be reviewed.

4.2 The Crack Opening Displacement Concept

The concept of crack opening displacement (COD), which forms the basis of general yielding fracture mechanics is used to extend the basic linear elastic fracture mechanics theory to situations where the fracture process is accompanied by significant plastic deformation. The recognition of the consequences of yielding at a crack tip, giving rise to a physical displacement of the crack surfaces at the tip, was first applied as a possible fracture criterion by Wells (27) and independently by Cottrell (28). With this fracture concept it is implicitly assumed that any opening takes place without any crack extension.

Burdekin and Stone (29) found from theoretical analysis that the crack opening displacement δ , at the tip of the real crack is, using the model employed by Dugdale (30), Figure 4.1, given by the displacement at the point $x = \pm a$ within the elastically stressed crack $2a_1$. This displacement was shown by Burdekin and Stone to be:

$$\delta = \frac{8ey}{\pi} a \log_e \sec \frac{\pi\sigma}{2\sigma_Y} \quad (14)$$

where $ey = \frac{\sigma_Y}{E}$, is the yield strain

a = crack length.

σ, σ_Y = applied and yield stresses respectively.

Equation 14 may be expanded as a series in $\frac{\pi\sigma}{2\sigma_Y}$,

$$\delta = \frac{8\sigma_{YS}a}{\pi E} \left\{ \frac{1}{2} \left(\frac{\pi\sigma}{2\sigma_Y} \right)^2 + \frac{1}{12} \left(\frac{\pi\sigma}{2\sigma_Y} \right)^4 + \frac{1}{45} \left(\frac{\pi\sigma}{2\sigma_Y} \right)^6 + \dots \right\} \quad (15)$$

Taking the first term from equation 15,

$$\delta = \frac{\pi\sigma^2 a}{E\sigma_{YS}} \quad (16)$$

It will be recalled from the analysis of a centre cracked plate that the strain energy release rate G was found as:

$$G = \frac{\pi\sigma^2 a}{E}$$

Re-arranging this equation:

$$\frac{G}{\sigma_{YS}} = \frac{\pi\sigma^2 a}{E\sigma_{YS}} \quad (17)$$

and hence from equation 16:

$$G = \delta\sigma_{YS} \quad (18)$$

Further, with the first and second terms from equation 14:

$$\delta = \frac{\pi\sigma^2 a}{E\sigma_{YS}} \left\{ 1 + \frac{\pi^2}{24} \left(\frac{\sigma}{\sigma_y} \right)^2 \right\} \quad (19)$$

and comparing this with the A.S.T.M. treatment for small plastic zones (16):

$$\text{i.e. } \frac{G}{\sigma_{YS}} = \frac{\pi\sigma^2 a}{E\sigma_y} \left\{ 1 + \frac{1}{2} \left(\frac{\sigma}{\sigma_{YS}} \right)^2 \right\} \quad (20)$$

Thus it can be seen that for $\frac{\sigma}{\sigma_Y} \ll 1$, which corresponds to a requirement for a crack tip plastic zone which is small compared to the crack length, the expression derived for δ is related to the crack extension force parameter G by the simple expression given by equation 18. Equation 18, has also been derived from a consideration of the energy released by incremental increase in crack length by Wells (31) and by Bilby et al (32). Burdekin and Stone have confirmed experimentally the validity of the basic concept of a critical crack opening displacement prior to fracture using notched tensile and notched bend specimens of mild steel over a wide temperature range (29).

Note that in an analogous manner to G and G_c , it is postulated that fracture will occur in a given thickness of material when δ reaches a critical value δ_c . Equation 18 indicates the physical nature of the relationship between crack extension force and crack opening displacement. That is, as loading progresses, the plastic zone develops at the crack tip which permits the faces of the crack to move apart. If the COD is large enough for a specified value of yield stress such that the product $\sigma_{YS}\delta$ exceeds the critical crack extension force for the material, then fracture follows. This

expression does not, however, take account of effect of stress triaxiality in the near tip region, except in the choice of the value of yield stress across the plane of incipient cracking. As noted by Irwin et al (33), this equation was originally believed to be invariant with stress state. Work by Wells (34) and Turner (35), however has shown that for plane strain conditions a constraint factor of the order of 2 or 3 is required to balance the above equation. Equation 18 therefore has the modified form:

$$G = n \sigma_y \delta \quad (21)$$

where n - constraint factor = 1, 2, 3.

Recent work by Robinson and Tatelman (36), calculated k_{IC} values from measurements of critical COD values under plane strain conditions using measurements obtained at the specimen midsection of small specimens deformed beyond general yield, by making use of the theoretical relationship between COD, G_{IC} equation 18. The value of n has been theoretically estimated as 1.0 by Bilby et al (32). Robinson and Tatelman gives an experimental value of n equal to 0.93, thereby confirming theoretical estimates. This confirms the work by Smith and Knott (37) who found that notched bend specimens of mild steel, 0.2", 0.4" and 0.67" thick, all showed the same value of critical COD at room temperature. Finally, work by Wilshaw (38), demonstrates that the average degree of transverse constraint at the root of the notch, in a Charpy V bend specimen, is high well after general yield.

It can be seen that the basic equation, $G = n \sigma_{YS} \delta$, linking the crack extension force concept of linear elastic fracture mechanics and crack opening displacement is accurate provided the constraint factor n is known.

The accuracy with which COD can be measured is very important to the usefulness of the technique. Measurement of COD requires the use of equipment capable of recording the opening at a crack tip during loading. In early results a paddle type COD meter (29) was used, normally with notches of perhaps .006" in width. As the crack opens, the paddle rotates and provides a continuous, direct measurement of the COD. Following the standard recommendation that the test piece notch should be extended by fatigue cracking, however, the location of a measuring device at the crack tip becomes a practical impossibility.

A method was devised by Fearnehough and Watkins (39) who used a photographic technique to record the crack opening displacement. The displacement measurements were taken from a series of photographs using microhardness indentations made on either side of the slits, the indentations being made close to the crack surfaces. An image of these impressions is projected via the objective lens from a microscope into a ground glass screen. The magnified image is photographed at various load increments during the test and the COD can subsequently be determined from the displacement of the indentations.

Fearnehough and Watkins employed small notched bend specimens to construct a calibration curve of load point displacement against COD, determined using the photographic technique. Using such a calibration curve, the critical COD at the onset of fracture can be determined from a knowledge of the specimen's load point deflection at the point of instability. During fracture toughness testing it is therefore necessary only to record the specimen load point deflection. There are two main objections to the photographic method:

- a) it requires considerable experimental skills in setting up the equipment and co-ordinating photographs with applied load values
- and b) photographs record surface displacements only and for certain materials or thin specimens where there are appreciable shear lips/plane stress effects, then such photographs may not be representatives of say mid-section crack opening displacements.

In more recent work, crack opening displacement measurements have been made using a clip gauge attached to specimen with fatigue sharpened cracks. A sketch of a typical clip gauge in position is shown in Figure 4.2. The notch or clip gauge displacement (not COD at this stage) is determined from the strains in the clip gauge arms which bend as the crack opens. This method is proposed as standard in the draft British Standard on COD testing, DD19 (40), further details on the technique can be obtained from this reference. In contrast to the photographic technique described above, it is a simple matter to obtain continuous simultaneous records of applied loads and clip gauge displacements using conventional pen-recording equipment.

The clip gauge displacement values (V_c) are subsequently converted into the crack tip COD (δ_c) using the methods discussed below.

In DD19 (40) two methods are proposed for the calculation of crack tip COD values from V_c values. The first method is based on the theoretical work of Wells (34) and treats the relationship between V_c and δ_c in two parts. The first, up to general yield, is parabolic and the second, beyond general yield, is linear. The equations for each part are as follows:-

Up to general yield:

$$\delta_c = \frac{0.45 (W-a)}{0.45 W + 0.55 a + Z} \left[\frac{V_c^2 E}{4\gamma \sigma_y W (1-v^2)} \right]$$

for $V_c < \frac{2\gamma \sigma_y W (1-v^2)}{E}$ (22)

Above general yield:

$$\delta_c = \frac{0.45 (W-a)}{0.45 W + 0.55 a + Z} \left[V_c - \frac{\gamma \sigma_y W (1-v^2)}{E} \right]$$

for $V_c \geq \frac{2\gamma \sigma_y W (1-v^2)}{E}$ (23)

Here Z is the distance of clip gauge from test piece surface and γ is a non-dimensional limiting value of elastic clip gauge displacement,

$$\gamma = \frac{V^1 E}{\sigma_y W (1-v^2)}$$

where:

V^1 = limiting elastic clip gauge displacement

σ_y = material yield strength

E = Young's modulus of elasticity

v = Poisson's ratio.

Values of γ corresponding to a range of $\frac{a}{W}$, for notched three point bend test pieces are tabulated in DD19 (40). The derivation of this formula is based on the assumption that the crack opening displacement is composed of an elastic component based on linear elastic fracture mechanics (LEFM) and a plastic component based on rotation (hinging)

about a fixed centre. The position of the centre of rotation is taken to be a constant value equal to $0.45 (W-a)$ from the crack tip. In reality however, on taking account of both components the centre of rotation varies in position with increasing load point displacement moving from the crack tip towards a maximum value of $0.45 (W-a)$. Sumpter's analysis (41) indicates that under plane stress conditions, the centre of rotation approaches this position at very large displacements, while for predominantly plane strain conditions for such large displacements the centre is at a depth $0.4 (W-a)$.

The second method of calculating δ_c from V_c is based upon experimental calibrations (40). Tests on specimens up to 50 mm thick have shown that, for the COD range 0.0625 mm to 0.625 mm good approximations to the crack opening displacement can be obtained by using the equation:

$$\delta_c = \frac{V_c}{3 \frac{(a+Z)}{W-a} + 1}$$

$$\text{i.e. } \delta_c = \frac{(W-a) V_c}{W + 2a + 3Z} \quad (24)$$

This is the simplest relationship and is based on the observed behaviour of COD specimens up to about 50 mm in thickness. The predicted relationship between δ_c and V_c is linear being based on the assumption that deformation occurs by a hinge mechanism about a centre of rotation at a depth of $1/3 (W-a)$ below the crack tip. The centre of rotation was first considered to be at a point $0.5 (W-a)$ below the crack tip but it was found that $\frac{W-a}{3}$ gave results more compatible with experimental observations.

A third method for calculating δ_c from V_c is given by Venzi (42) who suggests that:

$$\delta_c = \alpha \left(V_c + \frac{e}{\beta} e^{-\beta V_c} \right) + C_0 \quad (25)$$

where

$$\alpha = \frac{0.4 (W-a)}{a + Z + 0.4 (W-a)}$$

$$\beta = \frac{\alpha/50}{W-a}$$

$$C_0 = -\frac{\alpha}{\beta}$$

This relationship was obtained by expressing an equation similar to (24) in differential terms and integrating it. The values of the constants were obtained by analysing some experimental results. Recent work suggests that the experimentally determined equation is optimistic at low COD's (43). From Robinson and Tetelman's work (36), it was found that the position of centre of rotation varies with COD values see Figure 4.3 and therefore in order to find accurate COD values the correct position of centre of rotation must be found.

After deciding on which method is to be used for calculating COD, a question arises as to which point on a load/COD curve characterises the critical COD. In the past, the critical point has been taken as the maximum load point on a load/COD trace and the COD for this has been measured (44). However, this approach has no real justification from a physical viewpoint as the maximum load COD probably coincides with the critical event when the plastic zone size is small but does not correspond to a unique event when the plastic zone size is large. A number of authors have also shown that maximum load condition does not necessarily define the onset of slow tearing.

Harrison and Fearnough (45) showed that the COD at initiation of ductile tearing was relatively independent of specimen dimensions, but the extent of slow crack growth was affected by specimen dimensions, as was the maximum load/COD relationship. In bend tests, Smith & Knott (46) reported that the maximum load is attained in thick test pieces after slow crack growth has occurred in the "thumbnail", but just before the growth spreads to the specimen surfaces. Terry and Barnby (47) showed that the critical COD taken for the point of initiation of slow tearing δ_I in two structural steels is constant, independent of the range of specimen geometries tested, unlike maximum COD which varies with geometry. A critical COD defined on a δ_I basis provides a material constant on which it may be possible to base safe engineering designs. Throughout this thesis δ_I is taken as the critical COD value. The actual instant when δ_I is reached is obtained from a record of 'potential drop' across the specimen as a function of time. The potential drop technique (48) is normally used as a measure of crack length and is described in detail later in this thesis.

COD values at the notch root were determined using the clip gauge technique as described in DD19 (40) for all of the cast steels. Since, at the present time, this is the only document which gives details of a recommended procedure for COD testing.

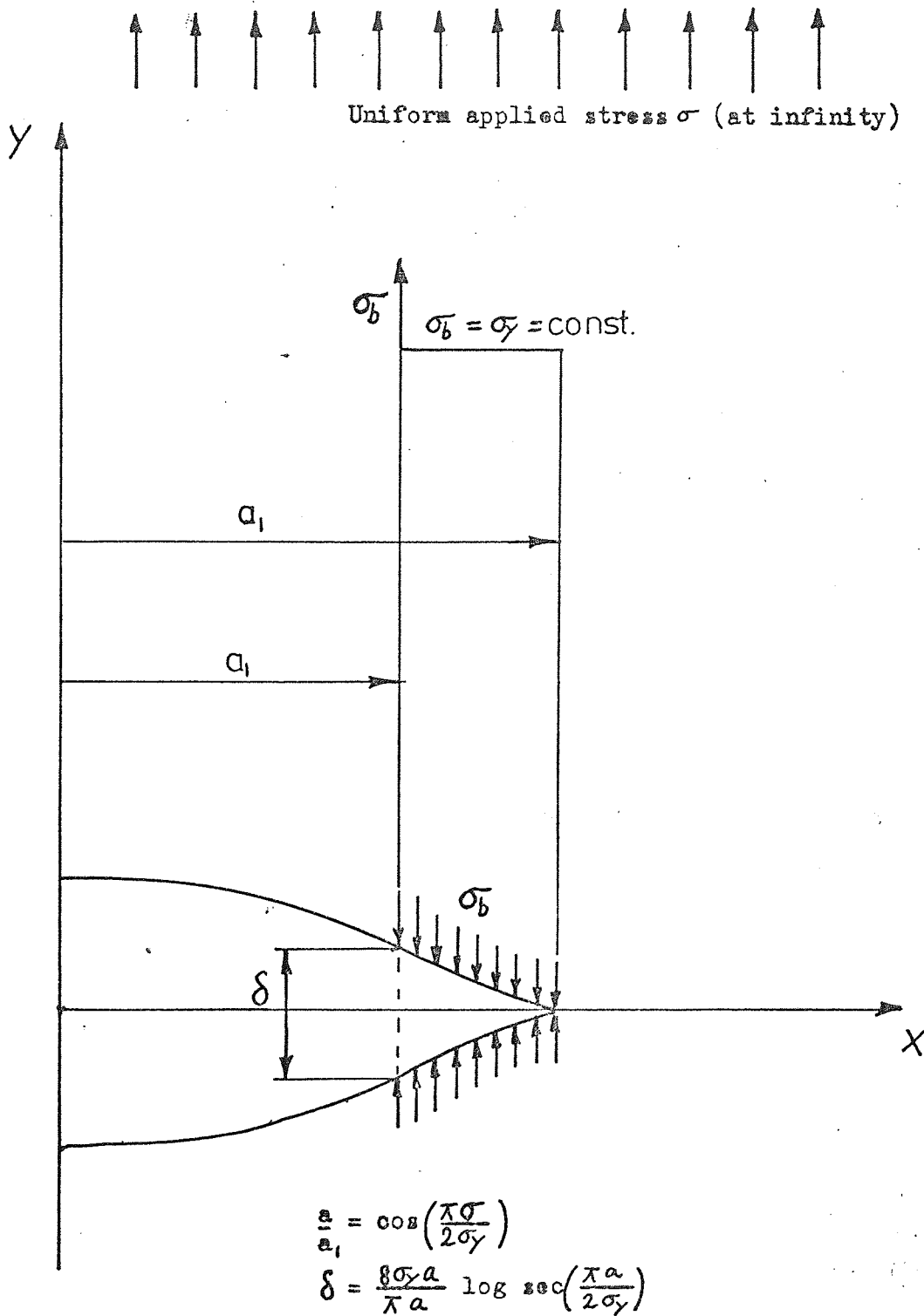


Fig. 4.1 Schematic crack tip and plastic zone. (Ref. 29)

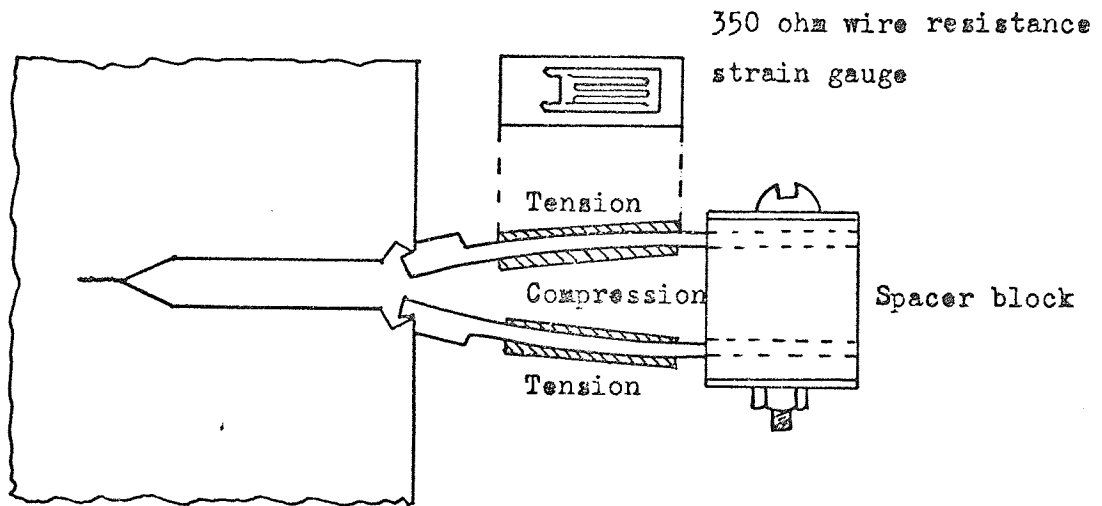


Fig. 4.2 Design and assembly of clip gauge.(Ref. 40)

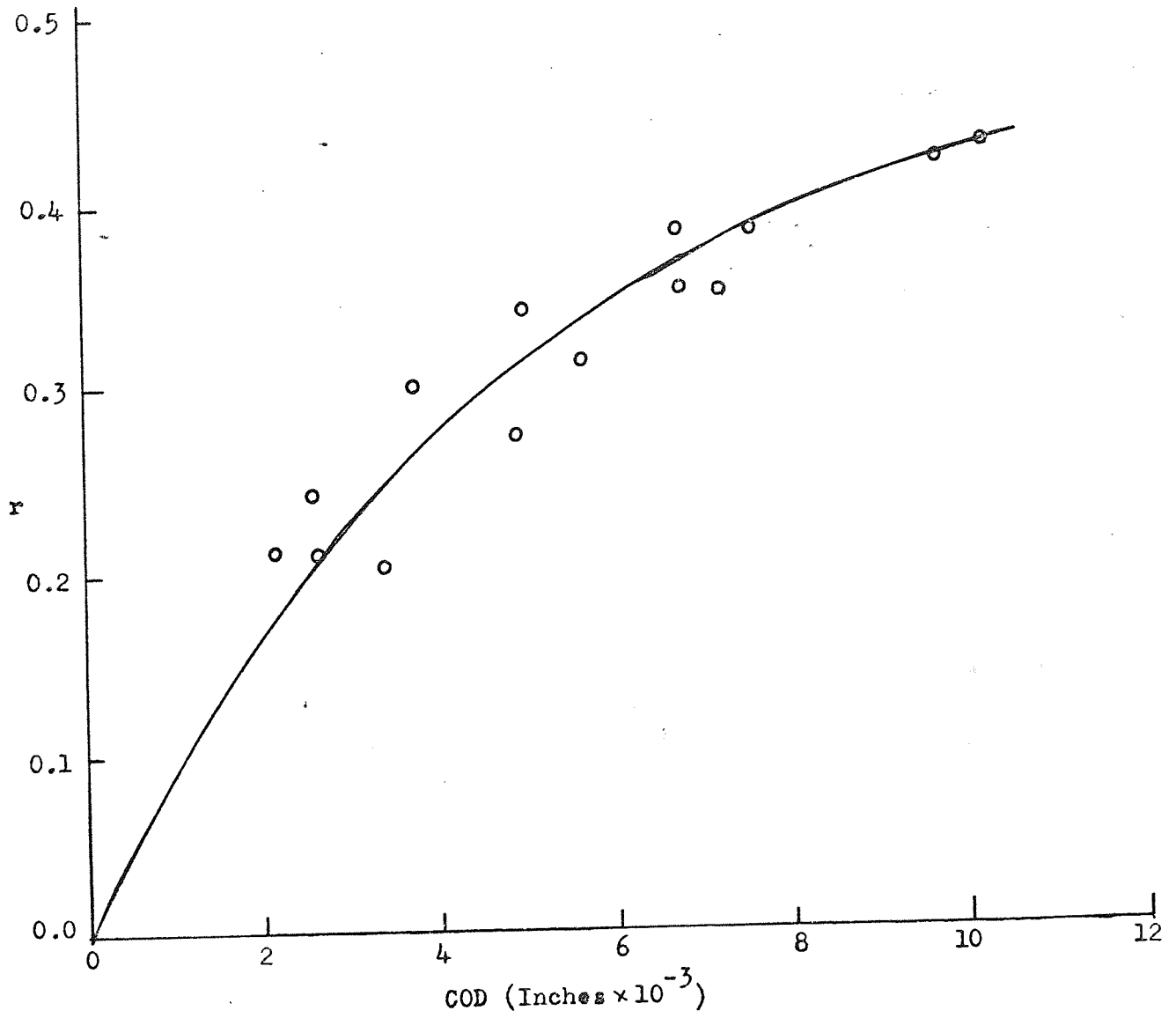


Fig. 4.3 Position of centre of rotation versus COD for A533B(Ref. 36)

4.3 Elastic Plastic J Integral Fracture Approach

The elastic plastic fracture criterion based on the J integral evolved from the need to extend the concepts of linear elastic fracture mechanics to include cases of large scale plastic yielding. The basis of the elastic plastic J integral fracture criterion is the path independent integral J proposed by Rice (49).

J integral as defined for two dimensional crack problems is given by the equation:

$$J = \int_{\Gamma} \left(W dy - T \frac{du}{dx} ds \right) \quad (26)$$

Where Γ is any contour surrounding the crack tip (Note Figure 4.4), T is the traction vector defined according to the outward normal on Γ , u is the displacement vector, δ_s is the arc along Γ , $W(x,y)$ is the strain energy density.

J may be interpreted (50), for elastic bodies, as the potential energy difference between two identically loaded specimens of unit thickness having neighbouring crack sizes, that is:

$$J = - \frac{1}{B} \frac{dU}{da} \quad (27)$$

where U , the potential energy of the body, is given by:

$$U = B \left\{ \int_{\text{Area}} W dx dy - \int_{S_T} T u dS \right\} \quad (28)$$

The first term in this expression is the integrated elastic strain energy density, and in the second term, T , is the traction vector,

which specifies the stresses on the boundary over which surface tractions are prescribed as boundary conditions. From the experimental viewpoint, the potential energy may be evaluated in terms of testpiece deflection by integration of the area under the load versus load point displacement record, being equivalent to strain energy for imposed displacement.

When deformation is not reversible, as in the general elastic-plastic problem, J loses its physical significance as a crack driving force, because the in-elastic energy is not available for crack extension. The in-elastic energy is dissipated in regions away from the crack. However, the value of J is still equal to $\frac{dU}{da}$ and this permits J to be determined experimentally. As discussed by Begley & Landes (51), the physical significance of J for elastic-plastic materials is that it is a measure of the characteristic crack tip elastic-plastic strain fields within extensive plastic zones. This is related to the work of Hutchinson (52) and Rice & Rosengen (53) which showed that a singularity does exist which is uniquely dependent upon the material flow properties. They indicate that the product of stress and strain approaches a $\frac{1}{r}$ singularity as r tends to zero,

i.e.

$$\sigma_{ij} \epsilon_{ij} \rightarrow \frac{\text{a function of } \theta}{r} \text{ as } r \rightarrow 0$$

McClintock (54) has shown that by combining the work of Hutchinson (52) and Rice (49) the crack tip elastic stress and strain singularities can be expressed as a function of J . Therefore, fracture will be governed by a characteristic crack tip singularity in the plastic range. This aspect is analogous to the role of stress intensity factor, k , in linear elastic fracture mechanics, which shows a

unique stress-strain field with a singularity at the crack tip. The strength of the crack tip singularity is the stress intensity factor, k . The crack tip region can then be characterised by the single parameter k with fracture occurring at a critical value of k .

Rigid plastic slip line field analysis shows that fully plastic flow fields and hydrostatic stress elevation are greatly influenced by geometry, which might have an effect on J_{1C} . However, Landes and Begley (55) found that the J_{1C} values obtained for the two geometries, centre cracked panels and bend bars, are not affected by the radically different slip line fields. This gives support to the reasoning of Begley & Landes (51), that the local plastic crack tip singularity and subsequent crack tip blunting overrides the effect of slipline in determining J . Hence the J integral is a valid fracture criterion for elastic-plastic behaviour. Begley & Landes (51) calculated J experimentally and found that it can be used to predict fracture in low to intermediate strength steels for plane strain conditions ranging from linear elastic to fully plastic fracture behaviour. The value of J at the onset of initial crack growth, J_{1C} , was constant over the entire range and was equal to G_{1C} , the energy release rate per unit crack extension in the linear elastic range. Therefore, a J fracture criterion for the linear elastic case is identical to the K_{1C} fracture criterion. In addition, if J_{1C} is a valid fracture criterion, it must be constant from essentially elastic to fully plastic conditions. Thus, J_{1C} must equal G_{1C} , where J_{1C} is defined as the J level causing the first significant crack growth.

4.3.1 J Integral Estimation Techniques

4.3.1.1 Experimental compliance calibration method

Begley and Landes (51, 55), measured J experimentally by a specimen compliance method which is applicable from linear elastic to fully plastic material behaviour.

Load versus load point displacement curves are generated for specimens with different crack lengths. These curves are integrated graphically to determine the work done in loading to a specified displacement. For each specimen the work done was determined at four different specified displacements. In each case work done was calculated to the same four displacement values for each specimen so that a plot of work versus crack length could be made for each of the specified displacements.

As discussed by Rice (50), the J integral can be interpreted as the potential energy difference between two identically loaded specimens of unit thickness having neighbouring sizes that is:

$$J = - \frac{1}{B} \frac{dU}{da}$$

J at constant load point displacement for a specimen of thickness B, is measured by taking the negative of the slopes of the curves and dividing by B, J is then a function of crack length and load point displacement. A plot of J versus load point displacement can then be constructed. To determine the critical value of J for crack initiation, J_{1C} , a critical value of load point displacement must be determined from experiment. Hence, J_{1C} can then be determined by taking the critical displacement and determining its corresponding value of J.

Begley & Landes (51, 55), found that crack initiation corresponds to the point where the maximum load first begins to drop off. This was found to be true for the particular material tested (Ni Cr Mo V and A533B steels) and only with the relatively small fully plastic test specimens employed. This method requires both procurement and analysis of a large number of experimental load displacement record a process which is both time consuming and costly.

4.3.1.2 Analytical procedure for estimating J

R.J. Bucci, et al (56) derived load versus load point displacement curves analytically for specimens of the particular geometry of interest. In reality actual load versus load point displacement characteristics border the two extremes exhibited by purely elastic and rigid plastic behaviour, Figure 4.5a. For low loads and associated small scale plasticity the load-load point displacement behaviour can always be approximated by linear elastic giving a slope (or compliance) which is a function of crack size, specimen geometry, and elastic material constants

$$\delta_{LPD} = P \times F \left(\frac{a}{W}, S, B, W, E, \nu \right)$$

As loading progresses, increased plasticity introduces nonlinearity. Nonlinearity is affected by amending the linear elastic portion of the load-load point displacement relationship by use of a plasticity adjustment factor (56) and references contained therein which considers the leading edge of the crack to be given a central location within the plastic zone (57). The plasticity adjustment results in an equivalent elastic or effective crack size, a_{eff} , given by:

$$a_{\text{eff}} = a + ry$$

$$\text{where } ry = \frac{1}{2\pi} \left(\frac{K}{\sigma_{\text{YS}}} \right)^2 \text{ for plane stress and}$$

$$ry = \frac{1}{6\pi} \left(\frac{K}{\sigma_{\text{YS}}} \right)^2 \text{ for plane strain.}$$

where a is the actual crack size, K the stress intensity factor (based on actual crack size) and σ_{YS} is the yield stress.

Employing the plasticity adjustment, a family of load-displacement records can be generated by using the plastically adjusted elastic analysis up to limit load and limit load analysis thereafter. For small load point displacement (δ_{LPD}) and consequently small scale plasticity, J can be represented by the linear elastic solution, $J=G$, which is parabolic in (δ_{LPD}) for constant crack length. For large (δ_{LPD}) where the limit load is attained prior to fracture, J as a function of (δ_{LPD}) becomes a linear relationship, Figure 4.5b. The offset between parallel segments of the rigid plastic and actual J versus δ_{LPD} curves of Figure 4.5 is governed in part by the non-linearities in the load versus load point deflection records which occur in the transition region. Hence, estimation of the actual J versus δ_{LPD} relationship rests on the ability to effectively approximate the elastic to plastic transition, or more specifically, the variation with crack length of the curved portion of the load - load point displacement relationship up to limit load, as well as the limit load itself.

The analytical load-displacement records were curve fitted by computer using an orthogonal polynomial relationship. The computational process was carried out as described (51, 55).

Employing these procedures, analytical prediction of critical plane strain J (J_{1C}) were found to agree with J_{1C} results (51, 55). Moreover, the estimated critical J was found to agree quite well with G_{1C} as determined from valid plane strain (K_{1C}) fracture toughness tests.

Adams & Munro (58) followed the procedure outlined above for calculating the value of J from a single load - load point displacement test record for centre cracked sheets, compact tension specimens and single edge notch beams in bending. In their analysis the non-linear effects are accounted for in a more detailed manner. They adapted a general form of yield zone correction, having the form:

$$r_y = \frac{k_{\text{mod}}}{2\pi} \left(\frac{K}{\sigma_Y} \right)^2$$

where k_{mod} is a constant for each fracture test. This constant is appropriate to the specimen configuration, the material properties and the load-displacement record. This was taken from (59) where it was shown that the size of the yield zone, changes considerably for different specimen configurations. It has also been shown (60) that due to the nature of the crack growth resistance, the plane stress fracture toughness is highly dependent on specimen width. This would imply that yield zone is also influenced by specimen width. In addition, if the variation in post-yield characteristics of different materials is also considered, then it becomes apparent that the yield zone correction as originally proposed, cannot be applied generally. However, the results obtained in (59) indicate that it may be unreasonable to expect to establish a critical J value for the plane stress failure mode, in the manner that J_{1C} appears to quantify plane strain failure (55).

4.3.1.3 Procedure based on specific fracture energy

Rice (61) developed a formula to evaluate J integral from a single load-load point displacement record for certain geometrical configurations. These configurations have the feature that there is only one geometrical dimension of interest, namely, the uncracked ligament length. For specimens subjected to bending, Rice's formula is given by:

$$J = \frac{2}{Bb} \int_0^{\delta_{\text{crack}}} Pd \delta_{\text{crack}} \quad (29)$$

where b , is the uncracked ligament length, B thickness of the specimen and $\int_0^{\delta_{\text{crack}}} Pd \delta_{\text{crack}}$ is simply the work done in loading or area under the $P-\delta_{\text{LPD}}$ curve to the displacement of interest. This result, equation 29, is applicable to the deeply notched 3-point bend specimens. Rice (61) specified that notch depths must at least be sufficient so that plasticity encountered is confined to the uncracked ligament region ahead of the crack tip.

In the case of the 3-point bend specimen, elastic displacements with no crack ($\delta_{\text{no crack}}$) may be appreciable (compared to displacements, elastic and plastic due to the crack) and would have to be eliminated in evaluating J . However, the displacement of the load point in a deeply notched compact tension specimen with no crack present would be negligible compared to displacements due to the crack, therefore, the raw load versus load point displacement record could be analysed using equation 29 with good results. Moreover for cases where the plastic displacement becomes very large compared to elastic contribution equation 29, can be used on the raw load-displacement record with little error.

On the very important point of plane strain validity in J testing Paris (discussion 51) suggests that a min. dimension $B > 50 \frac{J_{1C}}{\sigma_Y}$ might be adequate. In the second paper, Landes & Begley (55) suggest about $B > 25 \frac{J_{1C}}{\sigma_Y}$. These figures 50 or 25 are based predominantly on the data presented in these papers which cannot therefore have sufficient generality to cover all possible materials. More work will be done before specifying a limit to the thickness.

The method described above is used for calculating J throughout this thesis with the limitation on specimen sizes quoted above and the elastic contribution on J values also being investigated. This method is chosen for it is far more direct than the other two procedures described previously, requiring one test record and no analytical work to establish a value of J at any stage of loading.

To calculate the critical value of J (J_{IC}) a way must be found for pinpointing the point of crack initiation on the test record. A possible method in solving the problem of identifying a measurement point may come from presenting the J data in the form of a resistance (R) curve (63). However, a number of specimens are required to construct a resistance curve for calculating a single J_{1C} value, and since the scope of this work is to determine valid fracture toughness and also the effect of casting position from a fixed number of Keel blocks, this method was impossible to use. The point of initiation was found directly using the potential drop technique, during which, the potential drop was plotted as a function of time while the fracture test was in progress.

More work was done on evaluating J_{IC} in order to evaluate its usefulness as an alternate fracture criteria for the elastic plastic

and fully plastic fracture regimes. The major reasons for favouring the use of J over δ are its unambiguous continuity with K for near elastic behaviour, also its greater flexibility and ease of definition. Also the δ_c criteria often focuses attention on the region immediately surrounding the crack tip where the accuracy of analysis becomes uncertain, and because of the contradictions over the COD's, the J integral can be calculated analytically by utilizing a stress-strain analysis of regions somewhat removed from the crack tip.

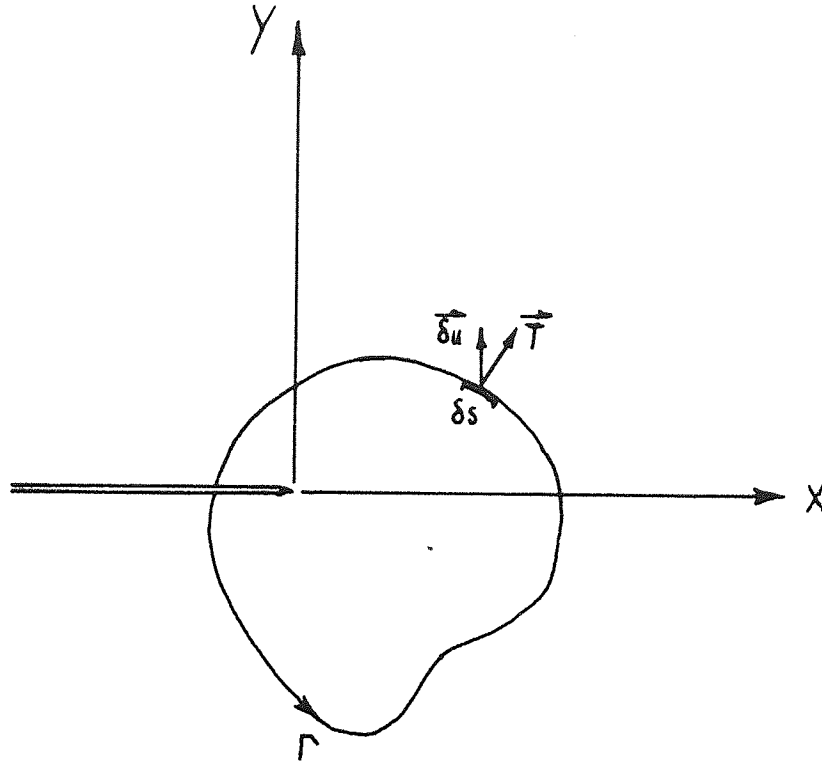


Fig. 4.4 Crack tip coordinate system and arbitrary line integral contour. (Ref. 49)

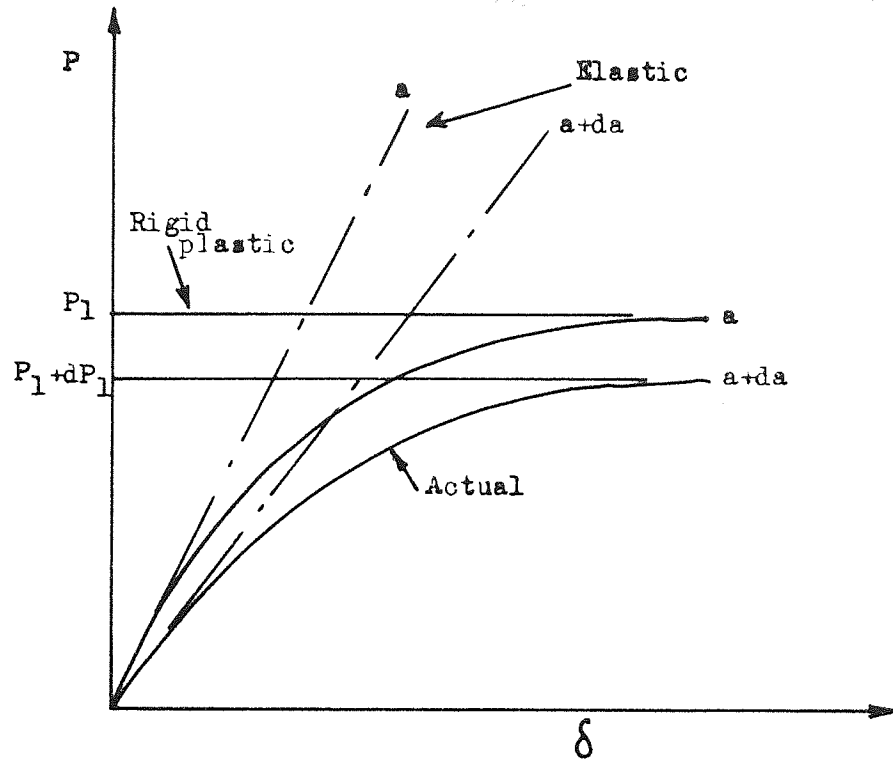
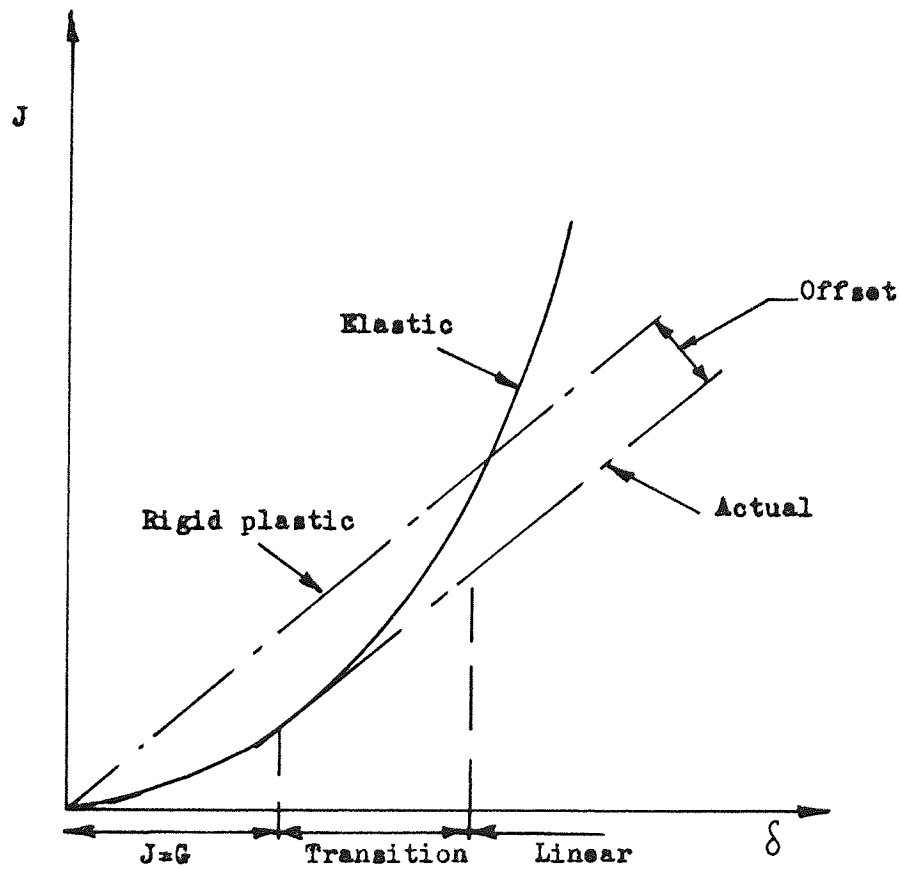
(a) Typical load-displacement (P v's δ) records.(b) Typical (J v's δ) Curves (a =constant)

Fig. 4.5 Idealised versus actual behaviour for load-displacement and J -displacement. (Ref.56)

5. MICRO-MECHANISMS OF FRACTURE

Micro-mechanisms of fracture may be divided into cracking processes typified by cleavage or low temperature intergranular fracture, and rupture processes; typified by void coalescence by internal necking or shear linkage.

5.1 Cracking Processes

Cleavage can be defined as the separation of a crystal along certain crystallographic planes. Metals with body-centred cubic and closed packed hexagonal structures are prone to cleavage fracture along atomic planes of high density. Cleavage fracture is produced, usually at low temperature, under a condition of high triaxial stress, that is, at the root of a notch, or at a high deformation rate, as for example, by impact loading.

Griffith (5) states that cracks of finite length must be present for crack propagation. Whilst it is known that cracks, as such, of this magnitude are not present before yielding. This leads to the conclusion that, even in very brittle notched bars, cleavage fracture is preceded by a small amount of local yielding around the notch root, because yield is necessary to produce a cleavage crack nucleus. The yield may take the form of slip or twinning.

Petch (64) noted that yielding occurs at a lower stress in coarse grained than in fine grained steel, due to the large stress concentration arising from the longer slip lines in the coarse grained material, promoting unlocking of dislocations and yielding in the next grain. Petch has developed a relationship connecting yield characteristics with the frictional stress resisting deformation, σ_1 , and the grain size dependence:

$$\sigma_Y = \sigma_i + kyd^{-\frac{1}{2}} \quad (30)$$

where σ_Y , lower yield strength, σ_i and ky are material constant, the σ_i is in fact the friction stress on the slip plane, the material constant ky is a function of the stress needed to unlock the source and of the distance of the source from the boundary, d , grain size. The Petch relationship is illustrated in Figure 5.1.

Stroh (65) made the first attempt to associate slip bands with the initiation of fracture. He supposed that the dislocations at the head of the slip-band were squeezed together to produce a crack nucleus and calculated the magnitude of the local tensile stress $\sigma_{\theta\theta}$, needed to spread this nucleus as a Griffith crack. Stroh's expression for the conditions under which the nucleus will spread may be written as:

$$Y_{\text{eff}} = Y_y - Y_i \geq \left[\frac{\pi A \gamma}{2(1-\nu)d} \right]^{\frac{1}{2}} \quad (31)$$

where Y_{eff} , effective shear stress, γ surface energy, A , shear modulus, ν poisson ratio, and d , average grain size. Stroh's model for cleavage fracture is illustrated in Figure 5.2.

Stroh (65) suggests that once the nucleation barrier has been overcome and a micro-crack initiated this crack would be of critical size and result in immediate failure. Stroh's nucleation mechanism failed to explain the role of the tensile stress parameter for fracture which indicates that fracture must be growth-controlled rather than nucleation controlled.

In view of the inadequacy of the Stroh model, Smith and Barnby (66) suggested a mode of fracture initiation in two phase material.

Consideration of dislocations piled up against a barrier such as a carbide, as in Figure 5.3, leads to the following equation for the stress to cause failure of the carbide:

$$\sigma_{\text{eff}} = \left(\frac{2c}{d} \right)^{\frac{1}{2}} \left[\frac{2\gamma G}{\pi(1-\nu)d} \right]^{\frac{1}{2}} \quad (32)$$

where $2c$ average carbide size, d average grain size, γ surface energy. Thus if $2c$ is small and d long (i.e. long slip band and thin precipitate), the precipitate will fracture at a lower stress than postulated by Stroh. Once the crack is formed, equal lengths of slip lines cancel out leaving an unpropagated void. Unbalancing will cause the crack to propagate into the matrix on the weaker side.

Cottrell (67) proposed a dislocation mechanism for cleavage fracture, which allowed growth to be the controlling factor, by providing an easy nucleation process, as indicated in Figure 5.4. The combination of dislocation on (101) and $(10\bar{1})$ planes with Burger's vector $\frac{a}{2} [\bar{1}1\bar{1}]$ and $\frac{a}{2} [111]$ respectively produces a dislocation of (001) with a nett lowering of the elastic strain energy:

$$\frac{a}{2} [\bar{1}1\bar{1}]_{(101)} + \frac{a}{2} [111]_{(10\bar{1})} \rightarrow a [001]_{(001)}$$

The value of the tensile stress needed to propagate a nucleus has been derived as:

$$P \geq \frac{2\mu\gamma}{K_Y^S} d^{-\frac{1}{2}} \quad (33)$$

Cottrell's model therefore emphasises the role of tensile stress and explains effect of grain size ($d^{-\frac{1}{2}}$) and yielding parameters (K_Y^S) on fracture.

Hull (68) found that a cleavage crack was initiated on the (001) cleavage plane, not by the intersection of slip bands, but by the intersection of twins. Similar events have been observed in polycrystalline mild steel (69). McMahon & Cohen (70) have examined the initiation of cleavage cracking in polycrystalline iron, containing up to 0.035% carbon. Their results showed that coarse carbides promoted cleavage, whilst fine carbides allowed the material to behave in a ductile manner.

Smith (71) has suggested an alternate mode for growth-controlled cleavage fracture in two phase material, such as ferrite matrix containing grain boundary carbides. It is found that the conditions for propagating a crack formed by slip-band impingement have been derived as:

$$\left(\frac{Co}{d}\right) \sigma_F^2 + Y_{eff}^2 \left[1 + \frac{4}{\pi} \frac{Co}{d} \frac{Y_i}{Y_{eff}} \right]^2 \geq \frac{4E\gamma_p}{\pi(1-\nu^2)d} \quad (34)$$

where σ_F is the tensile stress across the nucleus, d is the grain diameter, Co is the carbide thickness, γ_p is the effective surface energy of the ferrite matrix, Y_i is the (shear) lattice friction stress and Y_{eff} is the effective shear stress acting on the slip band as shown in Figure 5.5. The first term in this expression represents the effect of the tensile stress alone; the second shows the effect of the dislocation pile-up in the slip band. If the dislocation contribution is absent equation 33 reduces to:

$$\sigma_F > \left[\frac{4E\gamma_p}{\pi(1-\nu^2)Co} \right]^{\frac{1}{2}} \quad (35)$$

This model emphasises the importance, not only of yield parameters and grain size, but also of carbide thickness and indicates clearly that coarse carbides give rise to low fracture stresses. By appropriate substitution in equation 34, it may be shown that σ_F is predicted to be independent of grain size, other factors being equal. Yet a large number of results, drawn from several workers, show a clear dependence of σ_F on $d^{-\frac{1}{2}}$. In practice, however, fine grains are associated with thin carbides, and other cracking mechanism may be operative rather than the Smith's model for propagation. A further model for crack nucleation in a ferrite/carbide microstructure is that crack nuclei are formed in the carbide as a result of fibre-loading of the carbide by a generally plastically-deformed ferrite matrix (72).

The various micro-mechanisms proposed for the formation of cleavage cracks involve the nucleation of cracks by the high stresses developed locally at the ends of slip bands and the propagation of the nuclei under the applied tensile stress to produce the final fracture. At present, no single growth controlled mechanism has been shown to cover all possible cases.

It is now well established that the propensity of body-centred cubic metals to fail by cleavage is influenced by a host of compositional and structural factors. For example, the deleterious effects of sulphur and other trace impurities have been quantitatively determined (73, 74). Increasing the aluminium content in cast steels has been shown (75) to favour the formation of type II manganese sulphides which have a marked influence on fracture toughness. Also, the relative merits of steels with bainitic, martensitic, or tempered martensite microstructures, have been well documented with respect

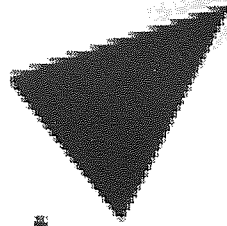
to their strength and fracture toughness (76, 77). Auto-tempered martensite (with no interlath carbide) forming during the quenching operation is tough. Lower bainite, and tempered martensite free from lath boundary films of carbides, are also tough. The presence of retained austenite films around auto-tempered laths of martensite adds substantially to the inherent toughness of the auto-tempered martensitic structure (78, 79, 80). The sub-structure of martensite itself is also important, e.g. transformation twinning in carbon steels lower toughness (81). The assumption is generally made that the high hardenability of commercial quenched and tempered steels leads to uniform microstructures throughout the thickness of fracture toughness specimens, because the hardness is nearly constant throughout the thickness. Recent studies showed (82) that fracture toughness is highly dependent on relatively small amounts of embrittling microconstituents such as the presence of upper bainite in a martensitic matrix which results in poor toughness, whereas such microconstituents have little effect on the hardness. However, small amount of austenite in a martensitic matrix enhance the fracture toughness (83). Free ferrite grains and ferrite plates in upper bainite are regions that are mechanically weak. They can fail readily by either plastic flow or by cleavage, and thus they tend to initiate microcracks at relatively low levels of plastic strain. This results in low values of fracture toughness. Austenite is not sensitive to high local stress concentrations and does not fail by cleavage, as does ferrite.

Wood (84) studies the effect of austenitizing temperature, the quenching media on the fracture toughness of five quenched and tempered low alloy commercial steels. The fracture toughness of these alloys was significantly increased with higher austenitizing

temperature and for some alloys increasing the severity of the quench from oil to ice brine, when used after austenitizing at 1200°C , led to still further increases in the fracture toughness. Each step in the heat treatment used has its effects on the resulting microstructure and mechanical properties. The increase in fracture toughness is attributed to many factors, e.g. in Wood's studies the fracture toughness specimens were quenched into iced brine directly from 1200°C . The cooling rate in this case was fast enough to suppress the formation of upper bainite. In other cases (83, 81), increases in fracture toughness of more than 50% were obtained in, as quenched specimens by the use of high austenitizing temperatures on a secondary hardening 5M.0.3C steel. In this case, the improvement was attributed to the reduction of undissolved alloy carbides.

In general, for low alloy quenched and tempered steels, resistance to cleavage fracture is improved by ensuring that any high temperature transformations products, such as upper bainite, are eliminated from the microstructure, but it is also important to control the amounts of minor impurity elements such as (Sn, Sb, As) in the steel, because these can segregate to prior austenite grain boundaries and give rise to intergranular brittle fractures. Similarly, carbide particles undissolved during austenitizing lower toughness. For carbon steels and C.Mn steels cleavage fracture are promoted by coarse carbides and large grain size. High work-hardening rate is detrimental, because high stresses are obtained in association with low strains together with all the factors concluded for low alloy steels.

Low

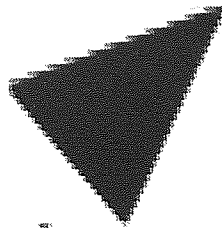


ins

Aston University

Illustration removed for copyright restrictions

Fig. 5.2 Stroh's model for cleavage fracture.(Ref.65)



Aston University

Illustration removed for copyright restrictions



Fig. 5.4 Cottrell's model for cleavage fracture. (Ref. 67)

5.2 Rupture Processes

The fracture mechanism important in most ductile and tougher materials is by microvoid initiation, growth and coalescence. Beachem et al (85) showed that microvoids usually initiate during plastic flow at inclusions, undissolved second-phase particles (such as carbides), grain boundaries, cleavage planes, or at any site where a discontinuity concentrates the plastic flow. Separation at the site of microvoid initiation can occur across a second-phase particle or at a particle-matrix interface. As the plastic strain increases, the existing microvoids grow, new microvoids are initiated, and eventually the enlarged microvoids grow into close enough proximity so that the thin ridges, or membranes, separating them rupture and fracture occurs. The resultant fracture surfaces have numerous cuplike depressions or "dimples" first identified by Crussard (86).

Beachem (87) has been able to show from the shape of a dimple, the relative stress directions operating to make the microvoid grow. When the fracture is caused by simple tension, dimples usually have an equiaxed appearance. When a shearing motion takes place, as in a shear lip or torsion fracture, the dimples have an elongated, parabolic shape, and the dimples on opposing fracture surfaces point in the same direction (toward the fracture origin). Recently (88), however, precision matching of surface replicas has shown that there are at least eight varieties and that there may be as many as fourteen ways of forming dimples, depending on the crack-tip stress states. This is an important advance in theory because detailed analysis of dimple shapes permits the reconstruction of local crack-tip strain conditions, thereby shedding some light on local crack tip stress states. In ductile fractures, the sizes and shapes of dimples are seldom uniform. In engineering materials with an appreciable variation

in size and distribution of precipitate particles, dimples may exhibit a wide range of dimensions. Dimple size (diameter and depth) appears to depend on the number of microvoid-initiation sites available and the amount of plastic growth permitted before the void coalesces with another free surface. The most important single structural effect on ductile fracture, is that due to second phase particles, such as inclusions, precipitates, and dispersions. As early as 1949, Tipper (89) showed that voids forming around non-metallic inclusions in mild steel were the first stage of the ductile fracture process. Some later workers (90, 91) have confirmed this observation whilst others have suggested carbide cracking may be the first stage in certain steels (92). The fibrous mode is common to ductile low-strength ferritic steels, to high strength steels, to austenitic steels and to aluminium alloys. Since work must be done in the nucleation of the cavities, and in the subsequent coalescence process, the toughness of the alloy will depend on the distribution, size and characteristics of the dispersed particles. That is, particle spacing (93), the spacing of void-nucleating particles can vary by an order of magnitude in the various systems, and the details of void coalescence may be different.

Several theories have been proposed to explain the growth of voids to final coalescence most notably McClintock (94), Gurland (95) and Thomson (96). McClintock (94) considered the case of the expansion of cylindrical holes. With longitudinal axis parallel to the X_3 direction and subject to generalised plane strain. As a result of this work he arrived at the conclusion that, large volume fractions of voids, high transverse stresses and low work-hardening rates all promote low-strain fracture.

Gurland and Plateau (95) have examined cavity nucleation in Al/Si alloy and pearlitic steel and have related the elongation to rupture to the volume fraction of inclusions, with the micro-cracks growing into cavities by concentration of plastic strain. From this work Gurland and Plateau expressed the elongation to rupture as a function of the volume fraction only, for the conditions of hard precipitates and inclusions able to deform within the matrix. The model is shown to hold well for the experimental results of Edelson and Baldwin (97) on copper, strengthened with precipitates of Cr, alumina, Fe and Mo. A similar effect has been found by Turkalo and Low (98) on the effect of volume fraction of carbide particles on the ductility of steels. The data reveals that the steels were almost an order of magnitude more ductile for a given volume fraction. This is the case because all the types of inclusion were minimally bonded to the matrix. Gladman (91) shows the effect of particle shape in addition to those of interface bonding and found that disc-shaped sulphide are more detrimental to ductility than sulphides elongated parallel to the tensile axis. Pearlitic carbides, although plate-like, are less detrimental because void initiation occurs by particle cracking and this is stress dependent, so that a significant strain is required before voids initiate. Spheroidal carbides increase the ductility still further, because very large true strain (>0.7) are required to initiate the voids.

Thomason (96) employs a different model to describe void coalescence. As shown in Figure 5.6 he takes an initially square array of square holes in a matrix whose flow behaviour is rigid/plastic. The deformation is assumed to be plane strain and is usually composed of two parts. If the voids are widely spaced, it is easier to deform the body as a whole, by gross-section yielding, than it is to produce

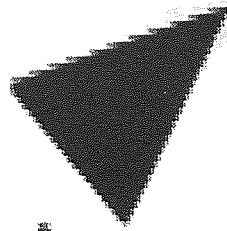
internal necking between the voids. The effect of applying a tension is to draw the voids out in the X_1 direction and to bring their centres closer together in the X_2 direction. Eventually, the voids are spaced sufficiently closely for localised internal necking between them to become possible. Final void coalescence then occurs rapidly. If the mean tensile stress in the X_1 direction, necessary to cause flow in the internal neck is σ_n , the general condition for the onset of coalescence is given by:

$$\sigma_n (1 - \sqrt{v_f}) + P < \sigma_{22} + 2 Y_Y \quad (36)$$

where σ_{22} is any tensile stress applied in the X_2 direction, P is the superimposed hydrostatic pressure, v_f is the volume fraction of voids and Y_Y is *the shear yield stress*.

Coalescence cannot occur if $P > 2 Y_Y + \sigma_{22}$. For a uniaxial tension specimen, Thomason shows that the majority of the elongation comprises the uniform elongation, with only a small amount being attributable to the non-uniform internal necking.

The model is able to treat effects of volume fraction on ductility both in uniaxial tension and in the triaxial stress field ahead of a sharp crack. The importance of high volume fractions in reducing crack-tip ductility is again apparent. Therefore, in fibrous fracture, high work-hardening rate is beneficial, because it prevents strain concentrations. In general, *clean* steels, that is reducing the inclusion content (vacuum melting), fine grain size, fine carbide distribution and increased inclusion spacing all improve resistance to ductile fracture.



Aston University

Illustration removed for copyright restrictions

(b)

The diagram consists of a grid of small dots arranged in approximately 10 rows and 10 columns. A horizontal band of grey shading is drawn across the middle of the grid, roughly between the 5th and 7th rows. On the left side of the grid, a curved line starts from the middle row and curves downwards towards the bottom row.

Fig. 5.6 Thomason's model for void coalescence. (Ref. 96)
(b), (c), (d) progressive stages of deformation.

6. EXPERIMENTAL TECHNIQUES AND MATERIALS

6.1 The Materials

The materials for testing were supplied as keel blocks through the Steel Castings Research and Trade Association who obtained them from different foundaries.

The specifications, compositions and heat treatments of the steels are shown against their code letters in Tables 6.1, 6.2 and 6.3 respectively. The heat treatments carried out on the keel blocks, to simulate commercial practice, and the resultant mechanical properties are as shown in Table 6.4.

Briefly, the various cast steels were prepared as follows, materials A and B were melted in an arc furnace using the double slag procedure and cast in self-setting silicate moulds. Material C was melted in a basic electric furnace (5 ton) and cast in green sand moulds, while materials F and G were melted in an acid electric furnace. Finally, materials L and M were melted in a high induction (2 ton) furnace.

Code Letter	General Specification
A	B.S. 1456 Grade A
B	$\frac{1}{2}\%$ Cr.- $\frac{1}{2}\%$ Mo.- $\frac{1}{4}\%$ V.
C	B.S. 1458(A) Mn-Ni-Cr-Mo
D	B.S. 592(B)
F	B.S. 1458(A) $1\frac{1}{2}\%$ Mn-Mo
G	B.S. 1458(B) Ni-Cr-Mo
L	B.S. 1760 Grade B
M	B.S. 1956 Grade A

Table 6.1 General Material Specifications.

Material	C	Si	Mn	S	P	Ni	Cr	Mo	Al	Cu	V	Sn
A	0.24	0.41	1.26	0.008	0.022	—	—	—	—	—	—	—
A 1276	0.18	0.48	1.22	0.019	0.016	0.30	0.12	0.04	0.107	—	—	—
A 1277	0.28	0.51	1.23	0.021	0.017	0.04	0.12	0.05	0.110	—	—	—
B	0.11	0.42	0.61	0.015	0.019	0.08	0.37	0.48	0.034	0.10	0.30	0.006
C	0.22	0.63	1.58	0.026	0.028	0.72	0.62	0.35	0.074	0.13	—	—
D	0.34	0.40	0.85	0.018	0.030	0.17	0.10	0.04	0.019	0.32	0.01	—
F	0.26	0.42	1.45	0.021	0.024	0.07	0.08	0.27	0.044	0.15	—	—
G	0.32	0.38	0.02	0.018	0.013	1.60	0.71	0.28	0.060	0.04	—	—
L	0.54	0.85	0.02	0.033	0.013	0.02	0.01	0.02	0.023	—	—	—
M	0.50	0.76	0.82	0.021	0.013	0.08	1.06	0.03	0.03	—	—	—

Table 6.2 Material Chemical Compositions

Material	Heat Treatment
A	3 hours 960°C Furnace Cool 3 hours 960°C Air Cool
Al276	3 hours 955°C Furnace Cool
Al277	3 hours 955°C Furnace Cool
B	8 hours 950°C Furnace Cool 8 hours 980°C Air Cool 8 hours 680°C Furnace Cool RE-HEAT TREATED 4 hours 980°C Air Cool 4 hours 680°C Furnace Cool+ 8 hours 700°C Furnace Cool
C	680 C Air Cool 3 hours 930°C Water Quench 4 hours 600°C Water Quench
D	4 hours 950°C Furnace Cool
F	4 hours 900°C Furnace Cool 4 hours 900°C Water Quench 3 hours 600°C Water Quench 1 hour 610°C Water Quench
G	4 hours 900°C Furnace Cool 4 hours 880°C Oil Quench 1 hour 640°C Air Cool
L	5 hours 900°C Furnace Cool
M	4 hours 920°C Furnace Cool 5 hours 870°C Air Cool 5½ hours 635°C Furnace Cool

Table 6.3 Heat Treatments.

Material	A	B	C	D	F	G	L	M
Tensile Strength, MN/m ²	639	651	869	577	764	940	734	920
Yield Stress, MN/m ²	427			330			360	460
0.5% Proof Stress, MN/m ²		504	759		661	853		
%Elongation	17.0	19.6	16.8	27.0	17.1	16.8	20.0	17.5
%Reduction in area	32.5	66.0	51.5	44.5	45.0	49.5	35.1	38.0
Charpy, +20° C J		6.8, 6.8		33.9, 31.2	78.0, 75.9	67.8, 73.2	19.0, 20.3	8.5 6.5
		6.8, 6.8		31.2, 33.2	78.6	71.8	16.3, 23.0	6.5 7.5

Table 6.4 Material Mechanical Properties

6.2 Material Preparation and Experimental Programme

The first keel blocks of materials A, B, C, F and G were sectioned according to the numbering system shown in Figure 6.1. In a similar manner the first keel blocks of materials D, L and M which were of different dimensions to those of the materials above, were sectioned with the numbering system shown in Figure 6.2.

In each case, six specimens were cut from each keel block. The overall size of these specimens was felt to be the minimum representative of the cast metal. By taking specimens from the positions shown it is possible to examine the effect of casting position on fracture toughness.

In all the fracture toughness tests carried out in this work, the three-point bend specimen geometry as shown in Figure 6.3 was employed. This particular geometry was chosen for its simplicity of manufacture, its general popularity and the fact that relatively low loads are required for substantial specimens. The basic specimen dimensions were, width $W = 45$ mm, thickness $B = 25$ mm and span $S = 265$ mm. Note that S/W ratio lies between 4 and 8, the two values generally recommended, $W = 45$ mm being due to physical limitations on keel block size. It is felt however that this will not affect results to any great extent.

The British Institute for toughness testing requires that for plane strain behaviour the specimen thickness B , and crack length a , must be such that:

$$a \text{ and } B \geq 2.5 \left(\frac{kQ}{\sigma_Y} \right)^2$$

where kQ = apparent toughness and σ_Y = yield stress. From the

preliminary tests on the first batch of specimens, it was found that the above condition was fulfilled for steel B; M and material C at the centre of the block, but for the other cast steels, the calculated thickness required to give plane strain behaviour was larger than the actual specimen thicknesses tested. However for these materials most specimens showed small shear lips which is generally taken to indicate that fracture conditions are predominantly plane strain. In any case there is considerable contradictory evidence as to whether the factor 2.5 in the above validity criterion is universally applicable for all materials (99, 100). In order to examine the thickness validity test with relevance to cast steels, specimens with varying thicknesses but constant width were sectioned from the second keel block, (the specimen dimensions are tabulated together with the k_Q values in Chapter 8). The heat treatments previously described in Table 6.3 being carried out on the block before sectioning.

Towards the later stages of the work two keel blocks A (1277) and A (1276) were cast and sectioned, this was done for up to this stage no valid fracture toughness values were available for material A. (The specimen dimensions are tabulated together with the k_Q and K_{1C} values in Chapter 8).

Finally, smaller specimens of a similar design were cut from the halves of the previously tested specimens, these specimens were prepared for the determination of values of Rice's J integral.

Unfortunately, specimen dimensions to yield valid fracture toughness data cannot be calculated prior to experimental testing. It is therefore virtually impossible to predict the likely cost of a programme of work to determine valid K_{1C} data by the linear elastic fracture mechanics technique for a range of materials, in this case

cast steels. Also, for the determination of valid K_{1C} data it may be found necessary to use large test pieces which may not be representative of the behaviour of sections actually used in service. In view of these points, therefore, it is worthwhile summarising the objectives of the work before proceeding to a description of specimen preparation. Firstly, no specific attempt is made to determine valid fracture toughness data by the LEFM technique for all the cast steels examined. Several of the steels did in fact yield valid data for modest specimen dimensions and these results are noted where appropriate. Secondly the 'validity criteria' for LEFM testing are often called into question regarding their universality of application for all material types. These criteria are examined critically as to their relevance for cast steels. Finally, several different fracture criteria are examined as to their relevance in quantifying fracture behaviour in cast steels. These include the J integral method and the crack opening displacement method.

6.3 Specimen Preparation

The specimens were first rough machined from the cast and heat treated keel blocks. Final machining to the required dimensions was by wet grinding giving tolerances of ± 0.01 mm on linear dimensions. All faces, except the ends, were parallel and perpendicular to within 0.02 mm per 10 mm run. The side faces were ground in the length direction to facilitate the observation of growing fatigue cracks, i.e. grinding scratches normal to the direction of crack growth.

A notch was cut centrally on the top face of each specimen having a notch root radius of 0.1 mm. This was achieved with a radiused

slitting wheel having a nominally zero flank angle and a 60° lead-in angle to the radiused tip.

The notch machining was carried out using liberal quantities of lubricant, a maximum cut of 0.25 mm and a feed rate of less than 10 mm/minute.

Fatigue pre-cracking of the bend test specimens was carried out in a 50 kN capacity electro-hydraulic test machine (Servotest 177-F8). The waveform in all cases was sinusoidal with a frequency of 80 Hz.

The fatigue machine was switched on at least thirty minutes before the start of any experimental work to ensure complete thermal and electrical stabilisation. In some cases, it was difficult to get a fatigue crack with a straight crack front. This problem was overcome by spark machining with a 0.1 mm thick copper electrode prior to fatiguing. For some cast steels, the initiation of a fatigue crack was conducted at a fatigue intensity larger than the recommended figure of $0.005E$ suggested by B.I.S.R.A. (101), since the fatigue crack would not propagate at this level. As soon as the crack had initiated, the maximum load used was calculated using the relation:

$$\Delta K = K_{\max} - K_{\min} = \frac{Y P_{\max}}{B W_2^{1/2}} - \frac{Y P_{\min}}{B W_2^{1/2}}$$

The final stage of crack propagation was carried out at a reduced load to satisfy the condition:

$$\frac{da}{dN} \leq \frac{1.27 \text{ mm}}{50,000 \text{ cycles}}$$

6.4 Fracture Toughness Measurements

Fracture toughness testing was performed on both 5000 kg and 50000 kg capacity Instron machines with variable crosshead speed. All test specimens were loaded in three point bending, the span/width ratio used was 4:1 in accordance with the recommendations contained in DD3 (102). The specimen was then loaded at a constant crosshead speed of 0.2 mm/min. A clip gauge was constructed to a design suggested in BSI Draft for Development DD3 and illustrated in Figure 4.2. Four 350 ohm strain gauges were connected in a Wheatstone Bridge balanced circuit, excited by a Boulton Paul C52 transducer amplifier unit. The amplified response from the clip gauge together with the load signal from the Instron load cell, was fed into a Bryan's X-Y plotter.

An autographic record of clip gauge displacement against applied load was plotted on the X-Y plotter. Location of the clip gauge across the notch was by means of knife edges glued to the specimen by Araldite with a fixed spacing on either side of the notch. The clip gauge was calibrated and checked for linearity with a micrometer.

Bend specimens were located for testing on a rig with friction free hard steel rollers, supported on adjustable bosses to accommodate a span up to 300 mm. Plane strain fracture toughness testing was carried out in accordance with the recommendation of BSI Draft for Development DD3 (102). The procedure is explained in Chapter 7.

In addition to K_Q results, values of Rice's J-integral were also determined for each cast steel. The theory, for the experimental determination of J, is developed and applied to three-point specimens in Chapter 7. The load cell output from an Instron machine was

supplied to the Y axis of a Bryan's X-Y plotter. Load point deflection was measured using a direct current-linear displacement transducer (DC-LVDT). Transducer output was used to drive the X-axis of the plotter.

Prior to each test, a calibration of the load cell and the transducer was performed. Plates 1, 2, 3 show the experimental set up. The transducer being mounted as close as possible to the load application point, to exclude rig displacements, as shown in plate 3.

The experimental set up was such that all information necessary for the calculation of K_Q , J and COD values could be obtained from one test on each specimen.

The photographic method as described in section 4.2 was tried for several specimens in the early stages of the work. This was found to be a difficult experimental technique, particularly with the number of recordings being made during a test and consequently it was abandoned in later work. In any case, there are doubts as to the usefulness of the photographic method for detecting the onset of crack instability, this is also discussed in detail in section 4.2. It was decided to use the clip gauge technique recommended in DD19 (40). This was easily done since a fully instrumented toughness test includes the clip gauge and it was a simple matter to calculate COD's using equations in section 4.2.

The initiation of cracking for COD and J measurements was detected by the electrical potential method (48). The principle of this technique is measurement of the electrical potential between two points on a uniform specimen through which a steady current distribution is flowing. The current supply consisted of a constant

source (Farnell F24M 7/50 ST) with an output, variable between zero and thirty five amperes. A current of 1 amp/1 mm thickness ± 0.02 amps was passed through the specimens. Since it was found from various trials that the sensitivity of the method increases with increasing current up to a maximum then decreases as the current is further increased.

The current was introduced to the specimen through multiple lengths of the flattened screen from multi-core cable. This type of input load was extremely flexible and had sufficient cross-sectional area to reduce resistive heating in the leads to a negligible degree. The lead terminations were prepared such that good electrical contact was obtained between the power supply and the specimen. Actual contact was made at each end of the specimen using Toolmakers Clamps, the clamping faces of which were lined with strips of electrical purity copper. Having connected the clamps to each end of the specimen, the current supply was switched on, and left for a period of one hour in order to ensure electrical stability across the specimen. The potential drop was measured across the notch using 0.15 mm Nichrome wire probes, spot welded in the same positions for each specimen. Spot welding was carried out using a converted battery charger. To ensure consistency between different specimens, the location chosen for the probes was the specimen top surface at each side of the notch as illustrated in Figure 6.4. The voltage between the potential probes, normally of the order of 0.15 mV, was measured using a D.C. chart recorder (Tekman TE200). This potential was opposed by a variable millivolt source (Time Electronics Type 2003 0.006%) enabling a 50 μ V full scale deflection to be used on the chart recorder. As the crack grows, the total current density across the uncracked section is kept constant by external means, and the measured potential

difference across the increasingly resistive cracked section becomes greater.

A view of the specimen complete with potential leads, mounted in the machine is shown in plate 2. A schematic diagram for the electrical potential circuit is shown in Figure 6.5. To gain confidence and familiarity in using the potential drop technique a calibration of the potential from $\frac{a}{w} = 0.4$ to $\frac{a}{w} = 0.6$ was established using sawn notches and also using fatigue cracked notches where the change in crack length was by further fatigue cracking. The sawn notches gave an accurate calibration while fatigue cracks shows scatter on the calibration curve probably arising from crack closure in the off load condition. It is worth noting here that the potential drop technique is not used to measure actual values of crack lengths and so the calibration described previously is unnecessary. Rather, a trace of potential drop against time is employed to detect the point of initiation of fracture or crack instability. The onset of crack growth can be identified from a sharp change in slope of the potential drop versus time curve, however this is discussed in greater detail in Chapter 7. The point of instability obtained as above can be relayed to the Load/COD and Load/Load point displacement curves by using a trace of load against time, each trace being plotted simultaneously as the experiment proceeds.

A diagrammatic sketch of a fully instrumented fracture toughness test is shown in Figure 6.6. In carrying out the test, four plotters are employed to produce, simultaneously, the following records:

- a) Applied Load versus Load point displacement. Load point displacement is recorded using the signal from the linear displacement transducer.

- b) Applied load versus clip gauge opening. Output from the clip gauge is fed to the X axis of Bryan's X-Y plotter. The load cell output from an Instron machine was supplied to the Y axis of the plotter.
 - c) Potential drop versus elapsed time. The chart recorder paper is fed under the recorder head at a constant rate while a recording of potential drop across the specimen is being made.
- and
- d) Applied Load versus elapsed time. Elapsed time is recorded in a similar manner to that described in c) above with the applied load trace taken from the load cell output from the Instron machine.

Briefly, to summarise the setting up procedure; the steps were as follows:-

- a) The specimen was positioned centrally on the test rig.
 - b) A small load was applied to hold the specimen in position and to overcome the effects of crack closure on potential drop measurements.
 - c) Current input clamps were fixed to the specimen ends.
 - d) Output from the Load cell, displacement transducer, etc. were connected to chart recorders as shown diagrammatically in Figure 6.6.
 - e) Backing off voltage from the millivolt source was increased until the excess potential was approximately $10 \mu\text{V}$
- and
- f) The crosshead speed was set at 0.2 mm/min. and the test was started.

6.5 Metallography and Fracture Surface Examination

Microstructures were prepared for examination using an electro-polishing technique developed by Holder (2) from a method described by Jacquet (103). With this method, a stainless steel cathode, as shown in Figure 6.7, is used as both an electrode and the electrolyte cell, a small length of polythene tubing extends beyond the end of the steel tube and the cavity so formed is filled with a wad of cotton-rayon wool (Boots Surgery wool). The electrode is then dipped in the electrolyte which has the following composition:

90% glacial Acetic Acid
10% Perchloric Acid (Specific Gravity 1.75)
0.01% Wetting agent (Kodak 'Photoflo')

The specimen to be polished is made the anode in the circuit with a potential of between 24 and 30 volts applied between it and the cathode. The cathode is then placed on the area of the specimen to be polished and the voltage dropped to between 20 and 25 volts and the initially high current density rapidly decreased. Finally the electrode was removed after approximately thirty seconds and the brown ferrous perchlorate flushed off with water.

This technique was found suitable for both optical and Scanning Electron microscope (SEM) examination. Preparation was conventional wet grinding down to 400 grade paper. Specimens were etched using the same electrode and solution as described previously but with a smaller potential of between 2 and 8 volts. The optimum etching conditions were determined for each material experimentally.

Normal metallographic techniques were also used. The etchant used on the specimens of each material were 5% aqueous solution of ammonium

perchlorate or 10% nitric acid in alcohol. The first technique was used extensively because of its rapid preparation, in some cases for Scanning Electron microscope investigation, the electro-polishing and etching took less than one minute.

The volume fraction of the ferritic - pearlitic steels (A, L, M, D) was estimated on a Quantimet microscope, ten areas were selected at random at known magnification, for each determination. The results were recorded.

A comprehensive fractographic survey was made on a Cambridge Scanning Electron Microscope. The fracture surfaces of a random area of the specimens tested to failure were sectioned and examined. Fractographs of representative features of the fracture surfaces at the interface between the fatigue area and fast fracture and the area next to the fatigue region were then taken for each sample for comparison purposes.

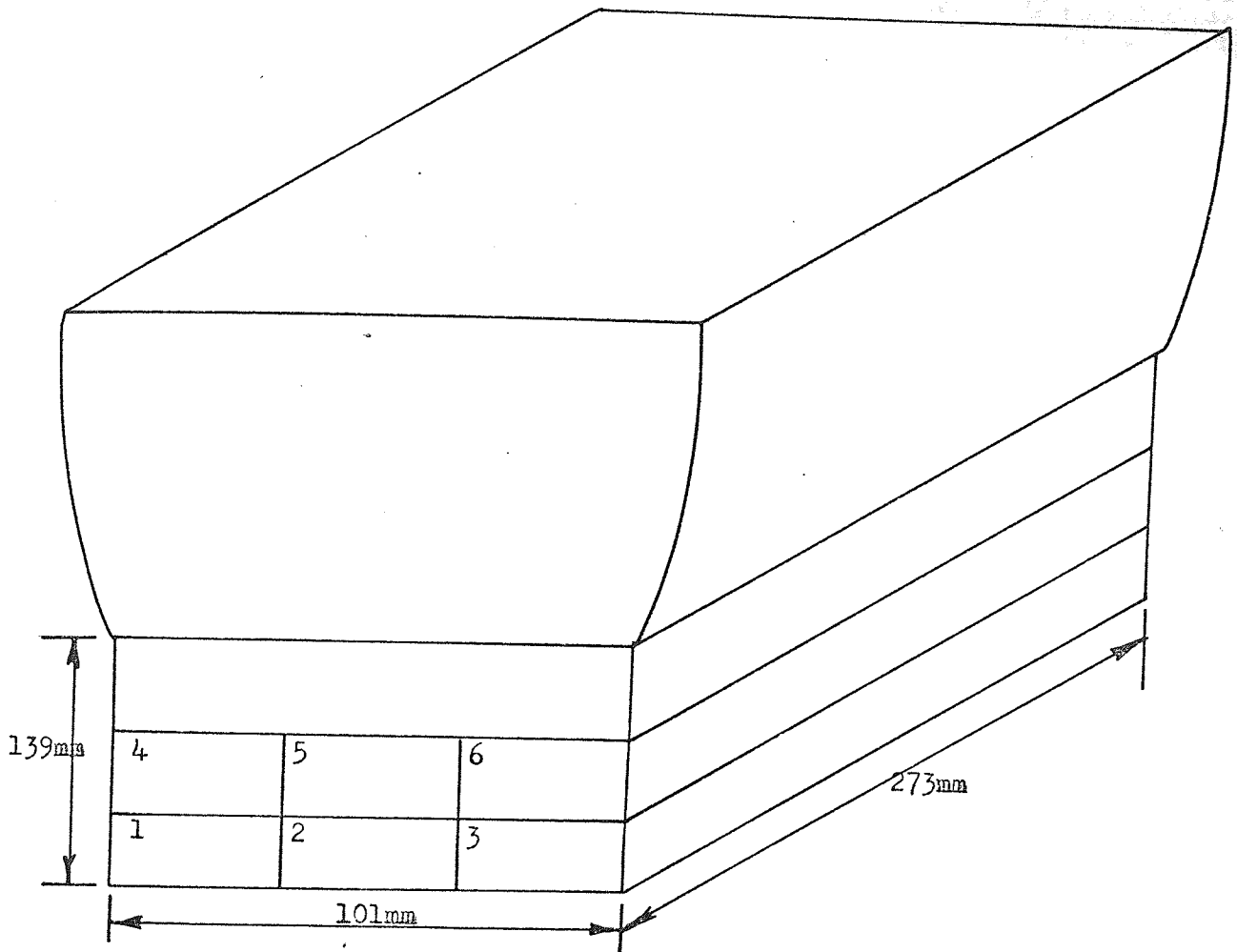


Fig. 6.1 Keel Block Casting of Materials A,B,C,F and G.

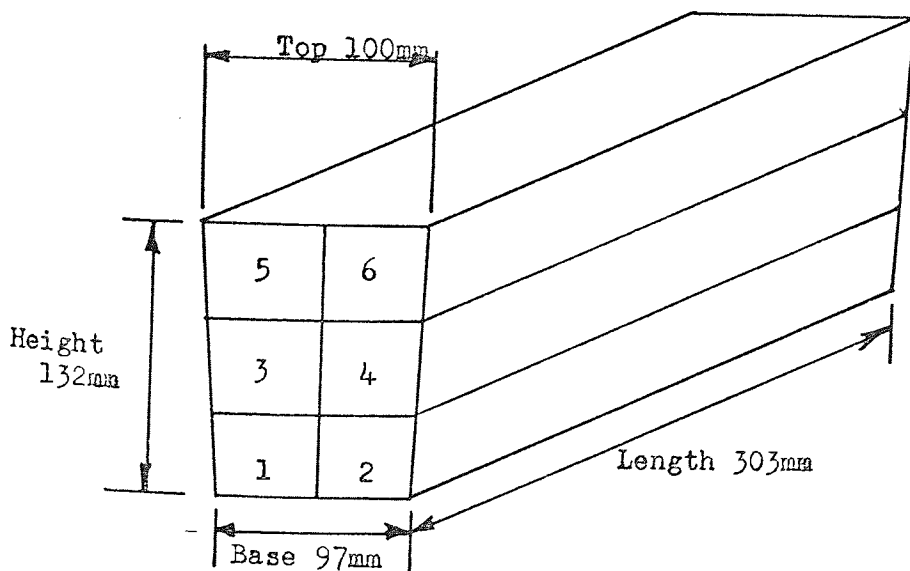


Fig. 6.2 Keel Block Casting of Materials D,L and M.

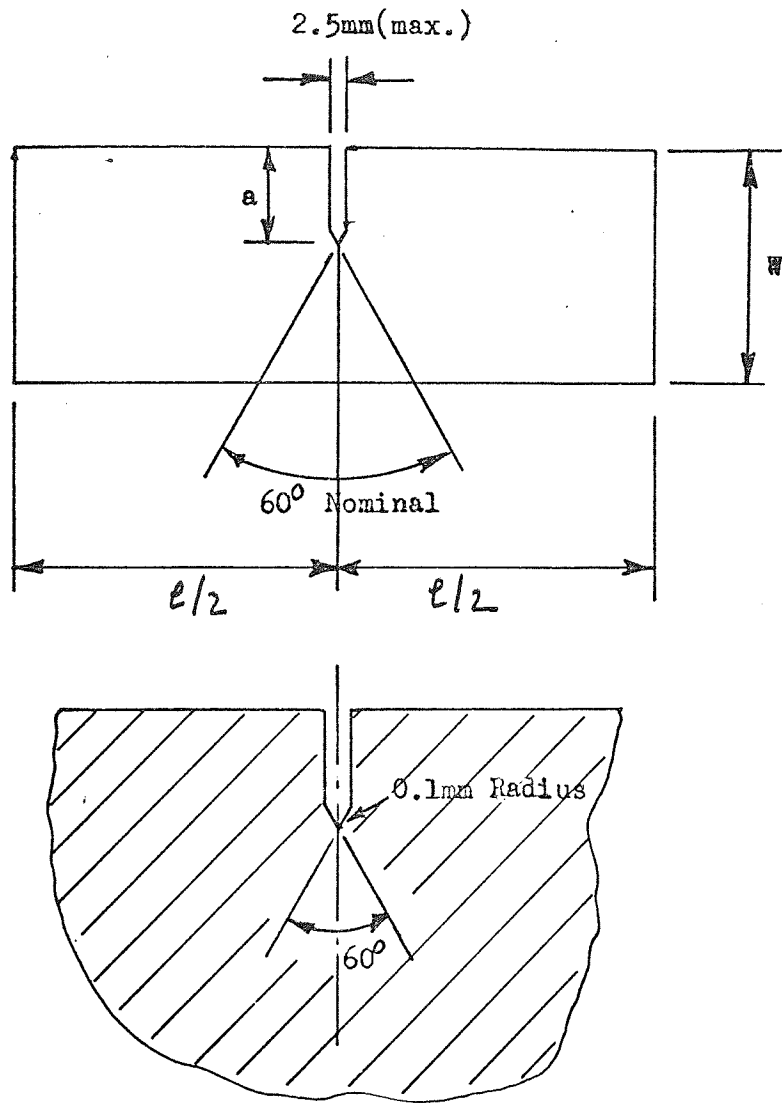


Fig. 6.3 Three Point Bend Specimen.

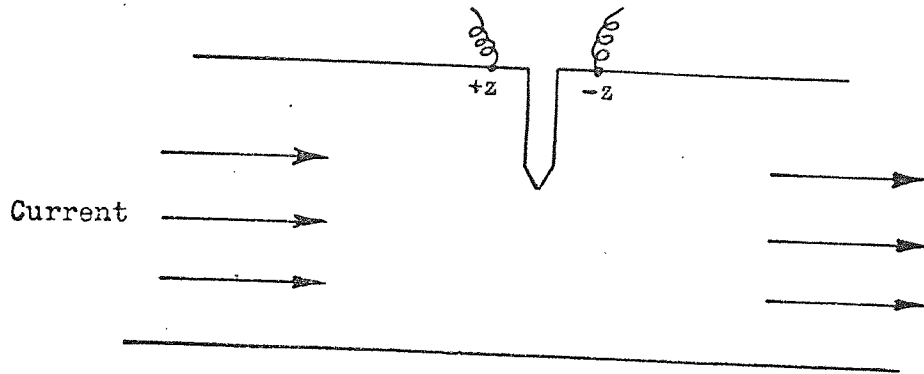


Fig. 6.4 Potential Probes Positions for the Three-Point Bend Specimen

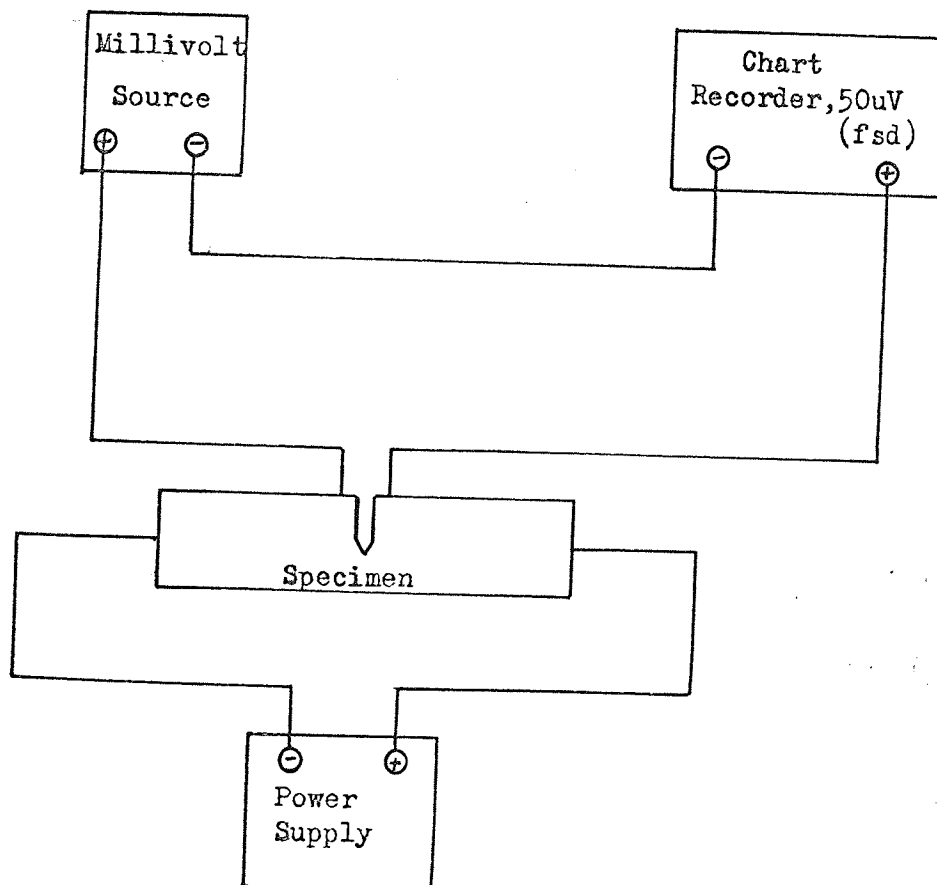


Fig. 6.5 Schematic Diagram of the Electrical Potential Drop Apparatus.

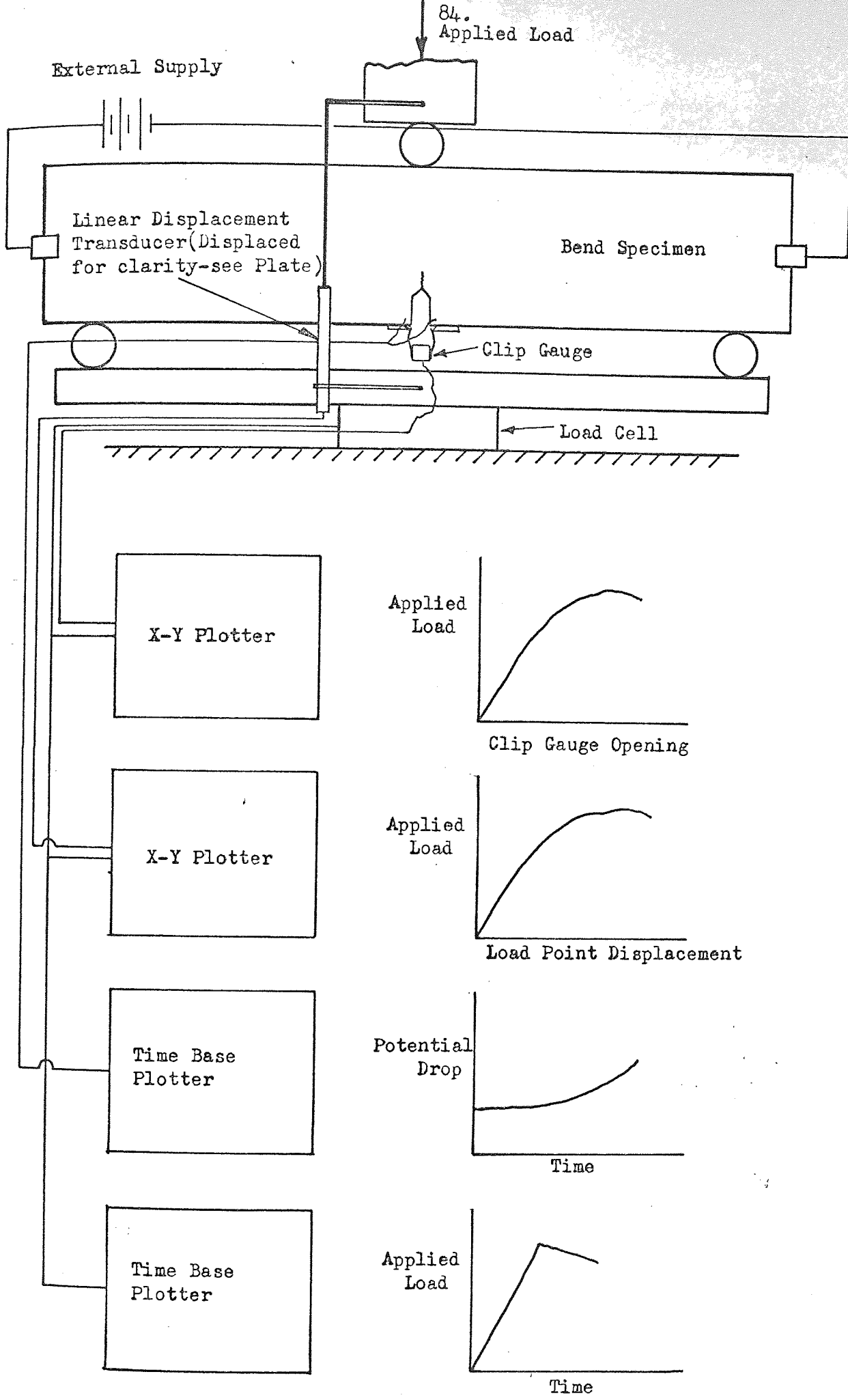


Fig. 6.6 Schematic Arrangement of Recording Equipment on Fully Instrumented Fracture Toughness Test.

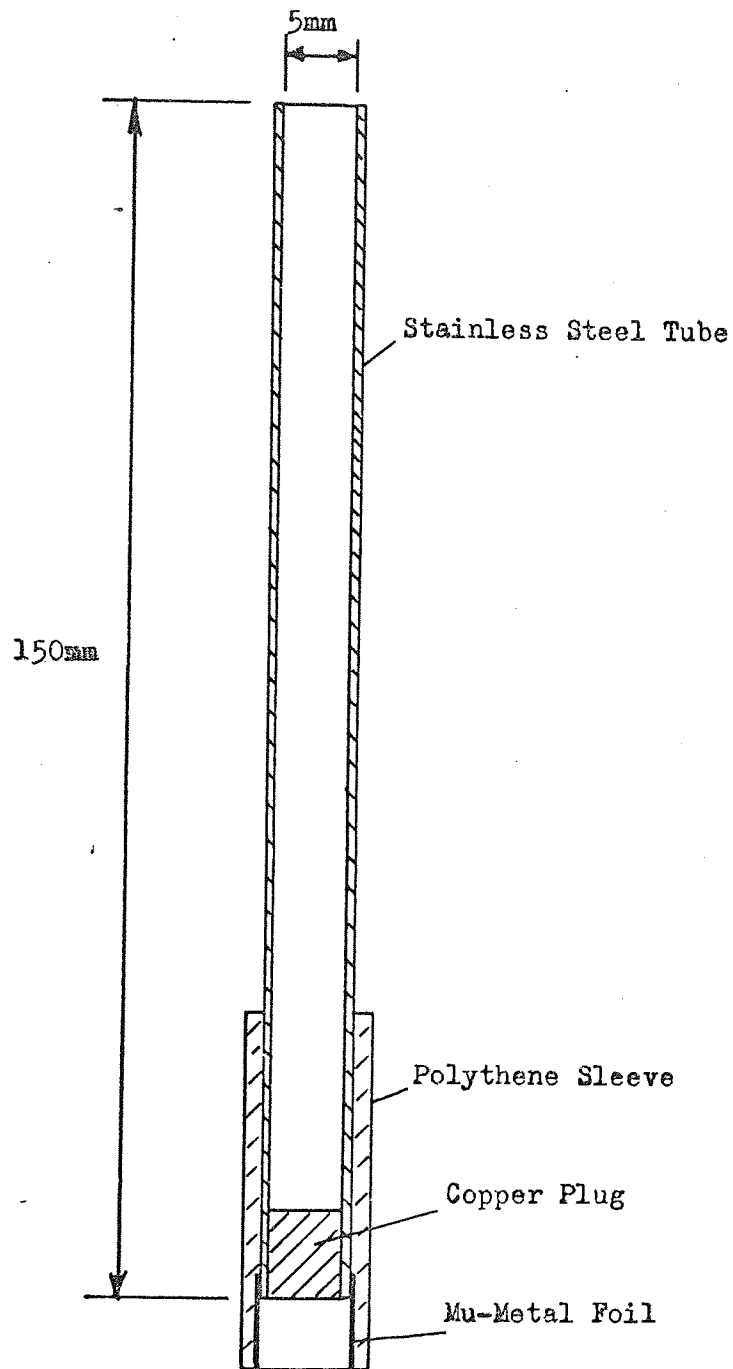


Fig. 6.7 The Cathode used in the Electropolishing Method.

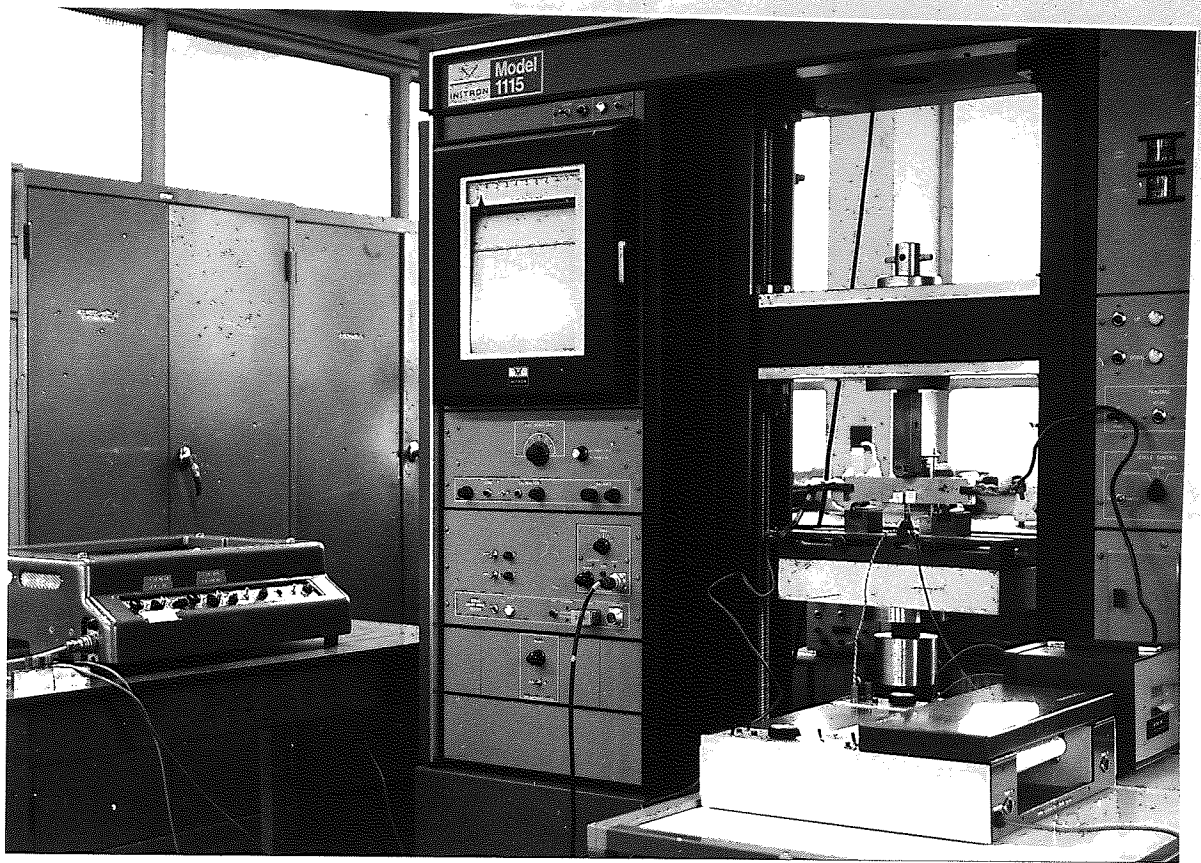


Plate 1 General View of Equipment used.

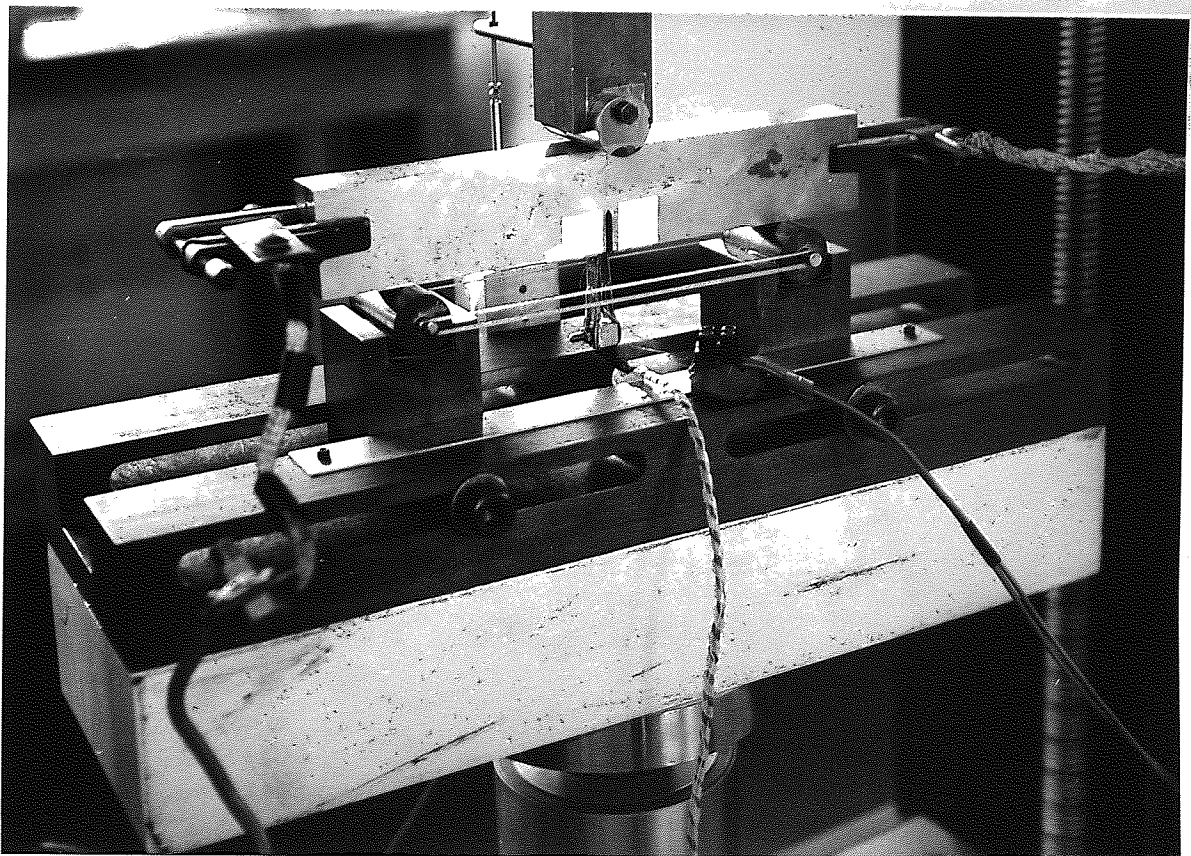


Plate 2 Three-Point Bend Rig showing Potential Drop Apparatus.

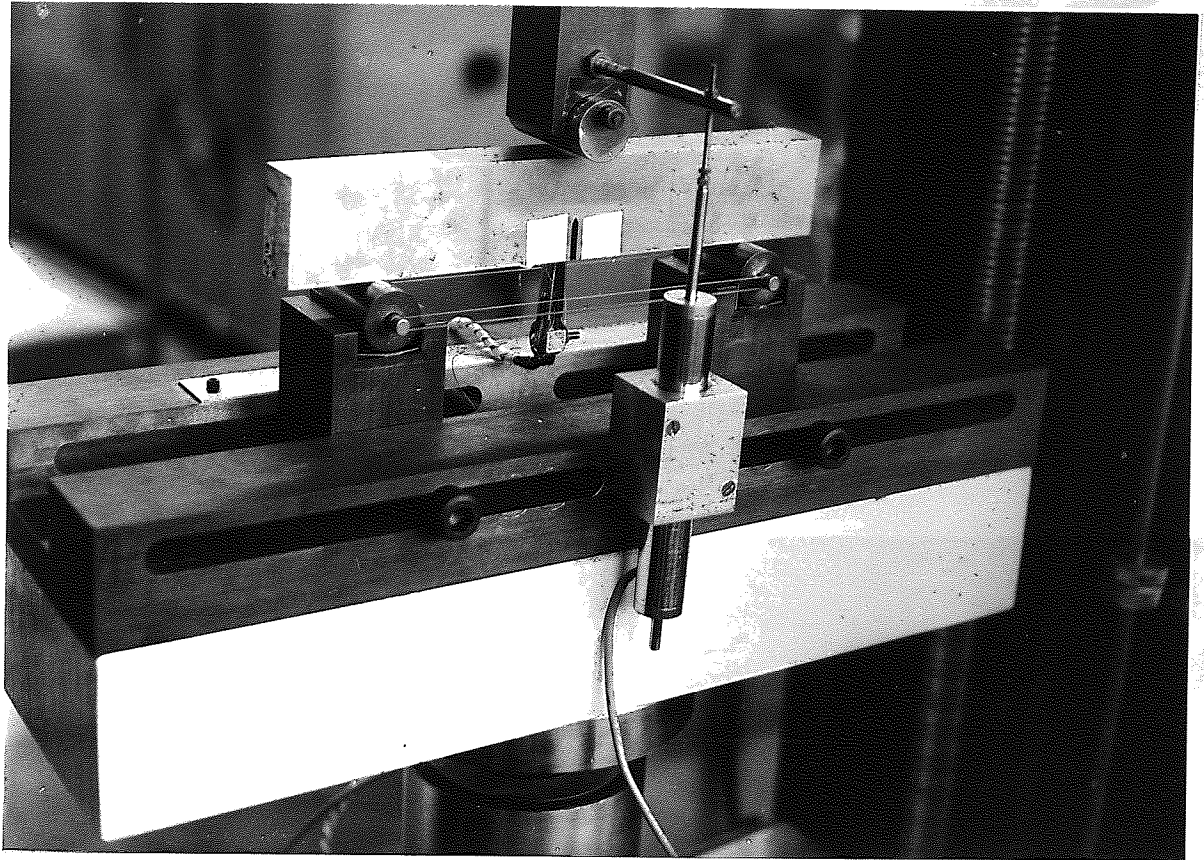


Plate 3 Test Rig for Three-Point Bend Tests showing the
Load Point Displacement Transducer.

7. ANALYSIS OF RESULTS

The experimental records of load, clip gauge and load point displacement values are used to calculate K_Q (K_{1C}), J_I and δ_c values as described in the following sections.

7.1 Analysis for K_Q

For each test, K_Q is calculated using the following relationship:

$$K_Q = \frac{P_Q Y}{BW^{\frac{3}{2}}} \quad (37)$$

Where the value of Y is obtained from the polynomial equation (18)

$$Y = 1.93 - 3.07 \left(\frac{a}{w}\right) + 14.53 \left(\frac{a}{w}\right)^2 - 25.11 \left(\frac{a}{w}\right)^3 + 25.8 \left(\frac{a}{w}\right)^4$$

The value of P_Q is the load at fracture. This load was determined from the load/displacement record using the 5% offset procedure. After each test has been completed, measurements of the effective crack length are made and the value of Y determined from the appropriate compliance calibration.

All of the criteria in DD3 (102) were used in judging the validity of the results, together with the more recent criterion added to the 1972 version of the ASTM E399-72 (104). This most recent criterion states that if P_{max}/P_Q exceeds 1.10, there is too much plastic deformation, and K_Q is not judged a valid measure of K_{1C} . This was explained by the fact that a rising load - COD curve through the region in which P_Q is measured indicates that a relatively great amount of plastic deformation is likely to be masking crack growth.

If K_Q satisfies all these criteria, then K_Q is considered a valid measure of K_{1C} .

7.2 Analysis for J

J integral values were estimated from single load/load point displacement curves, following Rice, Paris and Markle technique (61), using the expression:

$$J = \frac{2}{Bb} \int_0^{\delta_{\text{crack}}} Pd(\delta_{\text{crack}}) \quad (38)$$

Where

b = (w-a) uncracked ligament length, m,

B = Specimen thickness, m,

$$\int_0^{\delta_{\text{crack}}} Pd(\delta_{\text{crack}}) = \text{work done in cracking the specimen (Mn. m)}$$

and δ_{crack} is the load point displacement arising from the presence of the crack.

The total load point displacement is given, using the principle of superposition, by:

$$\delta_{\text{total}} = \delta_{\text{crack}} + \delta_{\text{no crack}}$$

To obtain δ_{crack} from the measured δ_{total} the $\delta_{\text{no crack}}$ is calculated from simple beam theory for the test piece containing no crack as:

$$\delta_{\text{no crack}} = \frac{PS^3}{48EI} \quad (39)$$

where

P = Load, MN;

S = Span of 4W, m;

E = Young's Modulus, MN/m²;

I = Moment of Inertia, m⁴

E = Young's Modulus, MN/m²

V = Poisson's Ratio.

The point of crack initiation was detected by the electrical potential method, and this measurement fixed δ_{total} and how far to integrate the Load/Load point displacement curve.

The procedure described above, for the determination of J from a Load-Load point displacement record, has been programmed for a digital computer. This computer programme enables J values to be determined accurately for a range of specified load point displacement values and the program is described in detail in Appendix 12.B.

7.3 Analysis for Crack Opening Displacement COD

Relative displacements at the open end of the notch are measured using a clip gauge such as that described in 4.2. These clip gauge displacements were converted to crack opening displacement for the three point bend specimen geometry using equations 22, 23 and 24.

Using the potential drop technique to identify the point of crack initiation, a value of critical crack opening displacement at this point can then be calculated, δ_{IC} . This value should, therefore be the COD corresponding to initiation. Having determined δ_{IC} , the stress intensification factor, n can be calculated using equation:

$$\text{i.e. } n = \frac{K_{1C}^2 (1-V^2)}{\delta \sigma_Y E} \quad (42)$$

The value of K_{1C} used in this equation was determined from the LEFM experimental results and also through the J integral values found experimentally.

$$I = \frac{BW^3}{12}$$

and

B = Thickness of the specimen, m;

W = Width of the specimen, m.

The area under the Load-Load point deflection curve Figure 7.1, was calculated from:

$$\int_0^{\delta_{\text{crack}}} Pd(\delta_{\text{crack}}) = \int_0^{\delta_{\text{total}}} Pd(\delta_{\text{total}}) - \int_0^{\delta_{\text{no crack}}} Pd(\delta_{\text{no crack}}) \quad (40)$$

The area under the Load-Load point displacement curve $\int_0^{\delta_{\text{total}}} P(\delta_{\text{total}})$

can be determined numerically by fitting a curve to the experimental results and integrating the resulting polynomial. The integral

$\int_0^{\delta_{\text{crack}}} Pd(\delta_{\text{crack}})$ can now be calculated by subtracting the elastic

component of the work done. The elastic component can be evaluated explicitly from equation 39. Using the calculated value of

$\int_0^{\delta_{\text{crack}}} Pd(\delta_{\text{crack}})$, J can be evaluated from equation 38. The calculated J

will be equivalent to J_{1C} since the load and Load point displacement

were taken at the point of crack initiation, finally K_{1C} was estimated

from J using

$$K_{1C}^2 = \frac{J_{1C} E}{1-\nu^2} \quad (41)$$

where

K_{1C} = Critical plane strain fracture toughness parameter,
MN. m^{-3/2}

J = G, the crack driving force, MN/m, for the linear elastic case. For any non linear elastic body, J may be interpreted as the energy available for crack extension per unit increase in crack length.

Wells (34) estimated n , the stress intensification factor, defined as the local elevation of the yield stress arising from constraints, as about 2.1 for plane strain, and 1.0 for plane stress conditions ahead of a crack tip. Intermediate values, between 1 and 2.1 occurring in mixed fractures. In this thesis, n was determined for each of the steels tested and found to be between 1.0 and 2.0 for the lower toughness steels and approximately equal to 1 for the higher toughness steels.

From an experimental viewpoint, clip gauge displacements and hence crack opening displacements can be determined more accurately with higher toughness steels than those with a lower toughness. This arises from the smaller absolute magnitude of the notch displacements in the lower toughness steels.

Since the COD values are determined at the point of initiation as identified from the potential drop record, they are therefore equivalent to δ_{1C} values for each cast steel. All such δ values are tabulated together with the stress intensification factor, n for each material tested.

7.4 Analysis of Potential Drop Technique

The potential drop technique was used to find the point of crack initiation. In the early stages of this work, a 2% crack extension was used for calculating J and δ as in the usual LEFM testing procedure. This technique was later abandoned however for it was found that the measurement point was affected by specimen size and this artificial size effect was reflected in calculating values of J and δ . It was concluded from this early result that an absolute measure of crack initiation is more desirable. To establish the

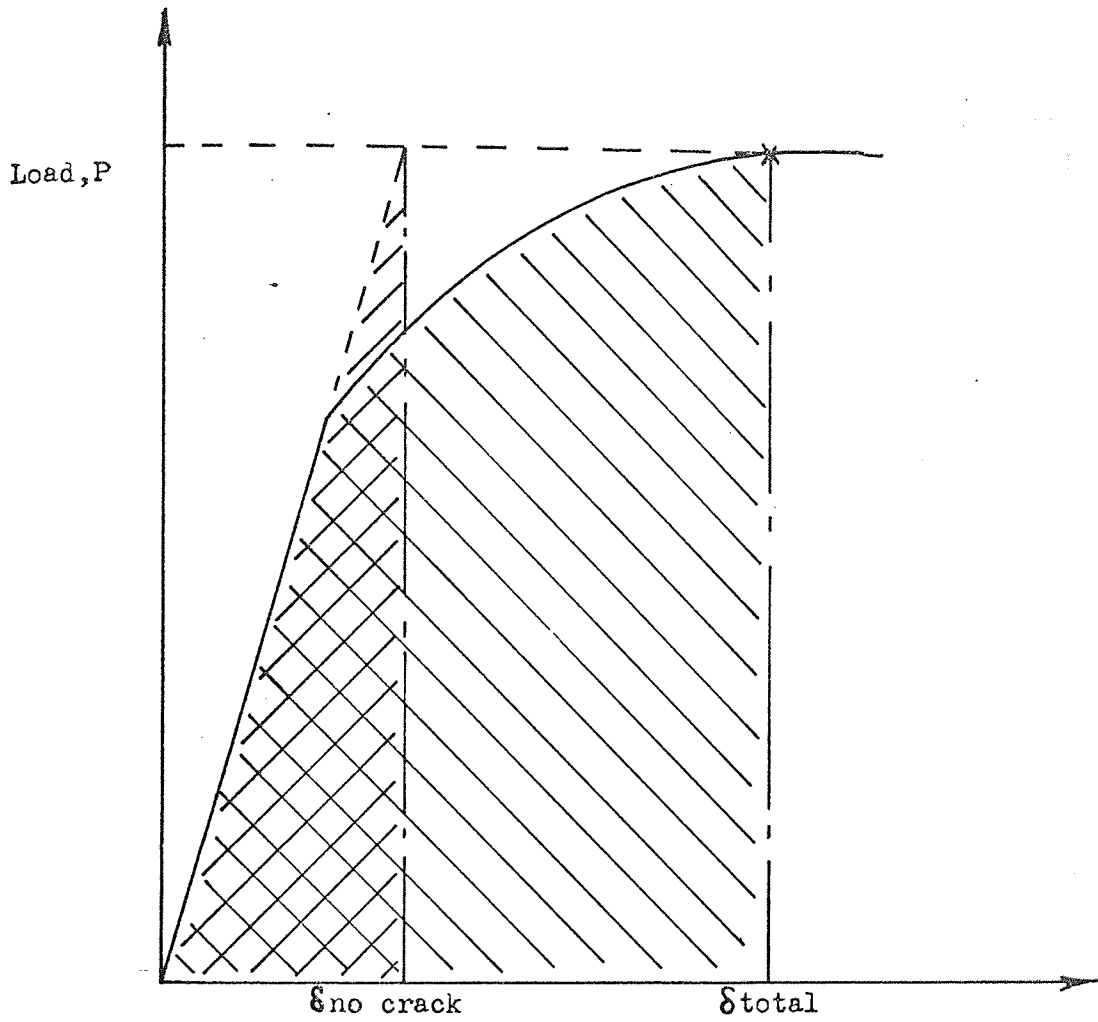
point of initiation, it is necessary to locate a point on the potential drop trace of p.d versus elapsed time where crack extension has taken place by actual surface separation rather than by crack front geometry changes. Of course, the accuracy and consistency of the final results (J_C and δ_C) depends on the operator's ability to locate the point of initiation.

There are two basic forms which the potential drop trace has, as shown in Figures 7.2 and 7.3. The first, exhibited by materials M, B and C at the centre of the keel block, corresponds to the case where the material behaves in an elastic/brittle manner. In this case the point of initiation can be easily located, shown as A in Figure 7.2. For these materials, the J-integral calculated using this point of initiation gave valid toughness data which compared well with K_{1C} values determined using normal linear elastic methods. This is of course to be expected, considering the equivalence of J and G, but it nevertheless provides confirmation of the potential drop technique as used for identifying the exact point of crack initiation.

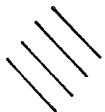
For the second form of the potential drop trace as shown in Figure 7.3, where the material behaves in an elastic/plastic manner, the point of crack initiation is not so easily pinpointed. From physical considerations, macroscopic crack extension probably takes place as a result of the following three interacting microscopic effects/processes:-

- a) Blunting of the crack tip.
- b) Crack tunnelling at the specimen centre where conditions of full stress triaxiality exists.
- c) Macroscopic growth by normal ductile mechanisms, e.g. void coalescence.

In view of this, it is difficult to identify an actual point of initiation, and in order to overcome the problem, the potential drop trace is visualised as composed of two distinct stages as shown in Figure 7.3. Stage I, where there is a small deviation from linearity at constant slope, this is considered to be due to the opening of the crack (blunting) and the effect of the stretch zone formation. The point of initiation for material separation is taken when slope of the trace changes sharply (stage II) and continues to do so, this is taken to indicate crack growth. The actual fixing of the point of crack initiation however still is to some extent a matter of choice, particularly in cases where the change of slope is not easily located. In such cases upper and lower limits are set. Values of J can be calculated for these upper and lower limits and from the results of this thesis these were found to differ from each other by only a few percent.



'Elastic' Area for bend specimen with no crack.



'Total' Area under P- δ curve to the point of initiation.

Fig. 7.1 Representative curve of load against load point displacement.

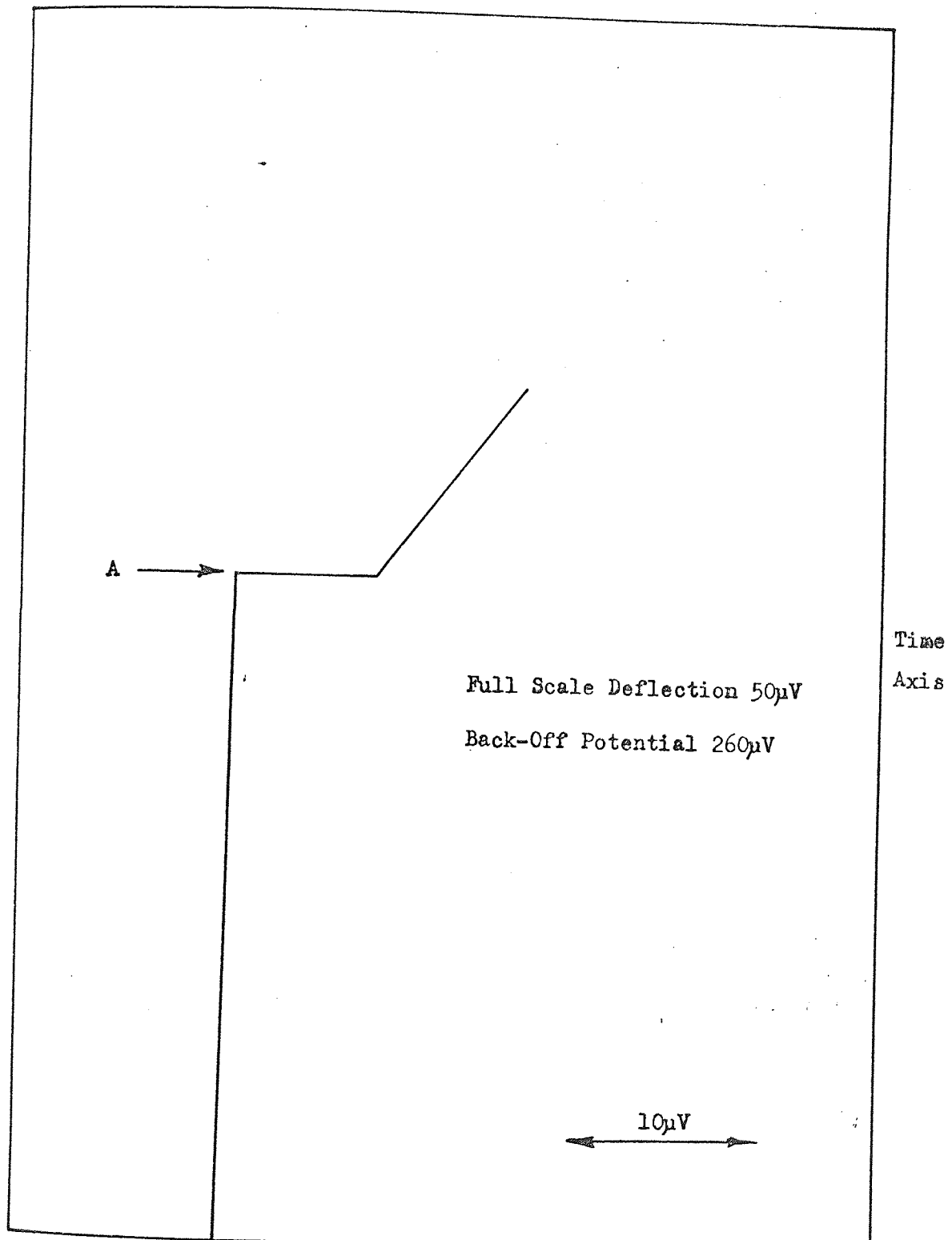


Fig. 7.2 Typical Electrical Potential Trace showing Crack Initiation for Elastic Material.

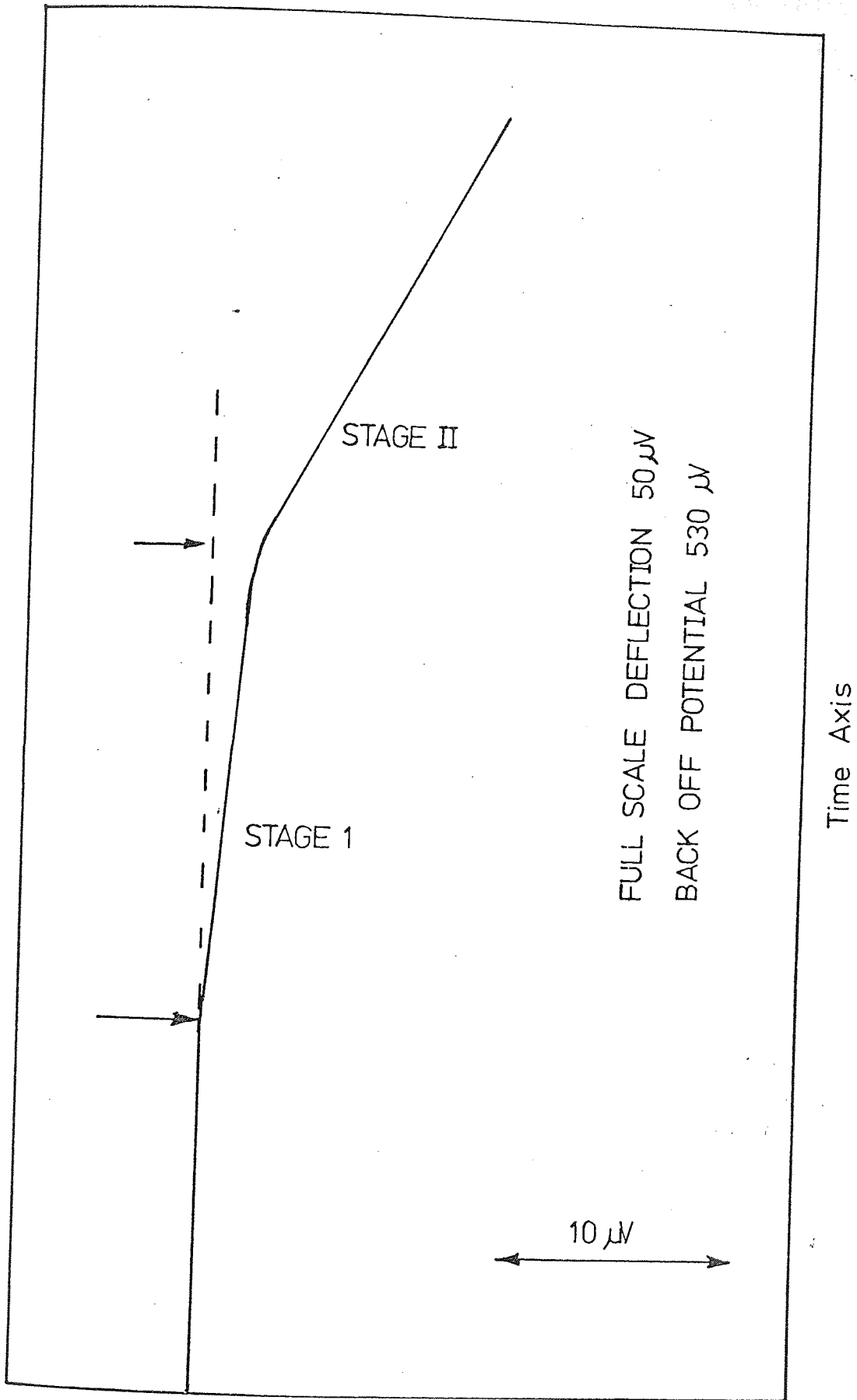


Fig. 7.3 Typical Electrical Potential Trace Showing Crack Initiation for Elastic/Plastic Material.

8. RESULTS

8.1 Introduction

This Chapter contains the results of all the experiments carried out to determine toughness values for each cast steel. Each material is treated separately in the following sections which also contain brief explanations on the results obtained. The actual discussion of the results is contained in Chapter 9, however, where appropriate certain features of the results are discussed in this Chapter.

In each of the sections, results are presented as follows:

- a) K_Q values, determined using the methods of Linear Elastic Fracture Mechanics, are listed in tables and also shown graphically, plotted as a function of specimen thickness. The K_Q values are checked against the various 'validity' criteria for valid plane strain results, K_{1C} , and in those cases where all criteria are fulfilled, K_{1C} results are noted. Where appropriate explanations are given on which criteria were satisfied and which were not.
- b) A representative trace of applied load versus clip gauge opening is reproduced for each material. Such curves give an indication of type of fracture behaviour exhibited by the material, i.e. brittle, ductile.
- c) K values determined from values of the J-Integral are listed in tables and shown graphically as in (a) above. In these tests, the potential drop technique is employed to detect the onset of crack growth rather than the 5% offset procedure used in LEFM testing. The intention is to demonstrate that this procedure leads to more consistent toughness values which can be obtained

using specimens of virtually any reasonable proportions. Where various specimen dimensions were tested, these results are also presented.

- d) Crack opening displacements, δ , calculated from the clip gauge openings are tabulated for each material. In each case the stress intensification factor, n , was determined using the material's toughness value. The n values are tabulated with the COD values.
- e) Representative micrographs showing the microstructure of each material are given with an explanation of the microstructure.
- and f) Fractographs showing the topography of the fracture surface are presented for each material. These fractographs give an indication as to the fracture mechanism(s) operating during specimen failure.

8.2 Steel M, Ni - Cr - Mo

The results obtained from Linear Elastic Fracture Mechanisms (LEFM) tests are presented in Table 8.1 where thickness, width, average crack length, K_Q , K_{1C} and K_{max} values are tabulated for each specimen tested. For this steel all the validity tests were satisfied and the K_Q values calculated are therefore K_{1C} values. It can be seen from these results that K_{1C} is virtually independent of casting position, the maximum variation in toughness values throughout the keel block being approximately 9%. $K_{1C} = 48 \pm 3 \text{ MN m}^{-3/2}$ for this steel, tested at room temperature using specimens of 25 mm thick. Plate 4 shows fracture surfaces for two of the specimens. Fatigue crack fronts are straight, fracture is predominantly by cleavage and shear lips are negligible - classic plane strain fracture.

Table 8.2 and Figure 8.1 show the results using specimens of varying thicknesses with all other specimen dimensions being kept approximately constant. Using a material yield stress of 480 MN m^{-2} (Table 6.4) the K_{1C} of $48 \text{ MN m}^{-3/2}$ all thicknesses of 25 mm or more generate valid K_{1C} values. At specimen thicknesses of 10 mm the fracture mode still corresponds to plane strain fracture as shown in Figure 8.1. Using the K_{1C} value determined above, a plastic zone size of approximately 1.6 mm was determined using:

$$r_y = \frac{1}{2\pi} \left(\frac{k_{1C}}{\sigma_Y} \right)^2 \quad (43)$$

Such a plastic zone constitutes almost 10% of the ligament. This being the case it is surprising that valid K_{1C} data was obtained with such a small specimen. In fact the original size (25, 45, 180) appears to be just sufficiently large to meet the linearity condition.

These results were analysed using the 5% secant method. However both visual inspection and the electrical potential result showed that no crack extension has taken place at the apparent P_Q , for thickness (10 mm and 15 mm). These apparent K_{IC} values arose from a sudden onset of plastic behaviour, rather than from fracture by crack propagation. Plate 5 shows fracture surfaces of specimens with different thicknesses. Fracture is predominantly by cleavage.

As part of the work on Rice's J-integral, tests were performed on smaller specimens with $\frac{a}{w}$ and $\frac{B}{w}$ ratios outside the range permitted by the ASTM test method. Table 8.3 and Figure 8.2 show the results of these tests. Results were again analysed using the 5% secant method for the determination of K_Q . Whereas those in Table 8.4 and Figure 8.3 are derived using the J-integral method. Analysis of these small specimen tests by the J-integral technique gave the results as shown in Figure 8.3. The average K_{IC} value obtained using LEFM theory for the larger specimens tested is also shown for comparison in Figure 8.3. In this case therefore the J-integral and LEFM methods gave similar results. The K_{IC} values for the smaller specimens was determined using the potential drop technique rather than the more usual offset procedure. These results clearly demonstrate the soundness of using potential drop to determine the point of instability linked with the calculation of K through J.

Typical crack opening displacement versus applied load traces for the larger and smaller specimens are shown in Figures 8.4 and 8.5 respectively. Note that the larger specimens produced valid fracture toughness values while the smaller specimens did not.

Crack opening displacement results together with the calculated values of the stress intensification factor, n , are shown in Table 8.5. The crack opening displacement, δ , was estimated using equations 22 and 23, with n being calculated using equation 42. From these results it can be seen that there is no significant variation of δ with thickness for specimens whose thicknesses ranged from 15 mm to 35 mm. The average δ was 0.018 ± 0.003 mm with a variation in n from 1.0 to 1.5 with an average of 1.25. In calculating n , the average K_{1C} of $48 \text{ MN m}^{-3/2}$ from LEFM test at $B = 25$ mm was employed.

Material M consists of a ferrite - pearlite aggregate with approximately 98% volume fraction pearlite. Representative photomicrographs are presented in plates 6 and 7 at low and high magnification respectively.

Plates 8 and 9 show a typical fractograph for the large specimen. The area examined was adjacent to the fatigue crack and at the fatigue crack tip which indicates that fracture occurred by a cleavage mechanism.

Specimen Number	Dimensions			K_Q MN/m ^{3/2}	K_{Ic} MN/m ^{5/2}	K_{max} MN/m ^{3/2}
	B mm	W mm	a mm			
M1x1	24.98	46.98	23.43	48.88	48.88	48.88
M1x2	24.98	47.00	22.96	49.08	49.08	49.08
M1x3	25.00	44.98	24.65	50.16	50.16	50.16
M1x4	25.01	44.98	24.19	47.19	47.19	47.19
M1x5	25.00	44.98	23.97	45.98	45.98	45.98
M1x6	25.00	44.98	25.03	46.20	46.20	46.20

Table 8.1 Fracture Toughness Results : Cast Steel M (Block 1)

Specimen Number	Dimensions			K_Q MN/m ^{3/2}	K_{Ic} MN/m ^{5/2}	K_{max} MN/m ^{3/2}
	B mm	W mm	a mm			
M1(10,45)	10.03	44.96	22.53	46.08		65.53
M2(10,45)	10.03	45.03	21.98	46.97		67.17
M1(15,45)	15.06	45.02	22.42	51.05		63.20
M1(20,45)	20.01	45.00	23.36	50.74		54.72
M2(20,45)	20.02	45.00	23.32	47.91		53.20
M1(30,45)	30.00	45.00	22.22	46.48		46.48
M2(40,45)	40.01	44.97	22.03	50.84		50.84

Table 8.2 Fracture Toughness Results : Cast Steel M at various Thicknesses (Block 2).

Specimen Number	Dimensions			K _Q MN/m ^{3/2}	K _{Ic} MN/m ^{3/2}	K _{max} MN/m ^{3/2}
	B mm	W mm	a mm			
M1(15,30,120)	14.99	30.00	15.47	37.96		64.78
M2(15,30,120)	14.98	30.00	15.05	40.95		64.59
M1(10,20,80)	10.02	19.98	11.61	39.85		47.63
M2(10,20,80)	10.03	20.00	10.11	41.76		52.91
M1(35,25,100)	34.99	24.99	13.75	40.85		40.85
M2(35,25,100)	34.99	25.00	13.92	38.94		43.27
M3(35,25,100)	34.99	24.97	11.94	38.64		41.45
M4(35,25,100)	34.99	24.99	14.03	45.09		45.09
M1(30,25,100)	30.00	24.98	14.20	45.41		45.41
M2(30,25,100)	30.01	24.99	13.18	46.33		46.33
M3(30,25,100)	30.00	24.98	12.28	40.66		40.66

Table 8.3 Fracture Toughness Results using LEFM Techniques.

Cast Steel M (small specimens)

Specimen Number	Dimensions			J with elastic corr'n MN/m	K _{1c} from J + el. corr'n MN/m ^{3/2}	J without elastic corr'n MN/m	K _{1c} from J no el corr'n MN/m ^{3/2}
	B mm	W mm	a mm				
M1(15,30,120)	14.99	30.00	15.47	9.79x10 ⁻³	47.08	1.23x10 ⁻²	52.80
M1(10,20,80)	10.02	19.98	11.61	1.17x10 ⁻²	51.50	1.33x10 ⁻²	55.00
M2(10,20,80)	10.03	20.00	10.11	1.10x10 ⁻²	49.96	1.34x10 ⁻²	55.04
M2(15,15,60)	14.99	14.98	8.00	1.08x10 ⁻²	49.45	1.30x10 ⁻²	54.28
M4(15,15,60)	14.97	15.02	6.86	8.62x10 ⁻³	44.17	1.02x10 ⁻²	48.17
M1(10,15,60)	10.01	14.31	6.92	1.03x10 ⁻²	48.35	1.25x10 ⁻²	53.12
M1(35,25,100)	34.99	24.99	13.75	1.04x10 ⁻²	48.44	1.23x10 ⁻²	52.72
M2(35,25,100)	34.99	25.00	13.92	9.22x10 ⁻³	45.69	1.08x10 ⁻²	49.52
M3(35,25,100)	34.99	24.97	11.94	9.05x10 ⁻³	45.27	1.13x10 ⁻²	50.64
M4(35,25,100)	34.99	24.99	14.99	1.21x10 ⁻²	52.37	1.42x10 ⁻²	56.77
M1(30,25,100)	30.00	24.98	14.20	1.04x10 ⁻²	48.62	1.23x10 ⁻²	52.76
M2(30,25,100)	30.01	24.99	13.18	9.27x10 ⁻³	45.81	1.12x10 ⁻²	50.45
M3(30,25,100)	30.00	24.98	12.28	8.73x10 ⁻³	44.45	1.11x10 ⁻²	50.23
M1(20,45,180)	20.01	45.00	23.36	1.01x10 ⁻²	47.92	1.28x10 ⁻²	53.79
M2(20,45,180)	20.02	45.00	23.32	1.19x10 ⁻²	51.85	1.47x10 ⁻²	57.78

Table 8.4 K_{1c} values derived from J_{1c} at fracture in small scale

specimens : Cast Steel M

Specimen Number	Dimensions			δ mm	n
	B mm	W mm	a mm		
M1(15,30,120)	14.99	30.00	15.47	0.017	1.1
M1(20,45,180)	20.01	45.00	23.36	0.014	1.5
M2(20,45,180)	20.02	45.00	23.32	0.017	1.45
M2(30,25,100)	30.01	24.99	13.18	0.017	1.2
M1(35,25,100)	34.99	24.99	13.75	0.019	1.1
M2(35,25,100)	34.99	25.00	13.92	0.016	1.2
M3(35,25,100)	34.99	24.97	11.94	0.017	1.1
M4(35,25,100)	34.99	24.99	14.99	0.020	1.2

Table 8.5 Crack Opening Displacement (δ) and the Stress Intensification Factor : Results for Steel M.

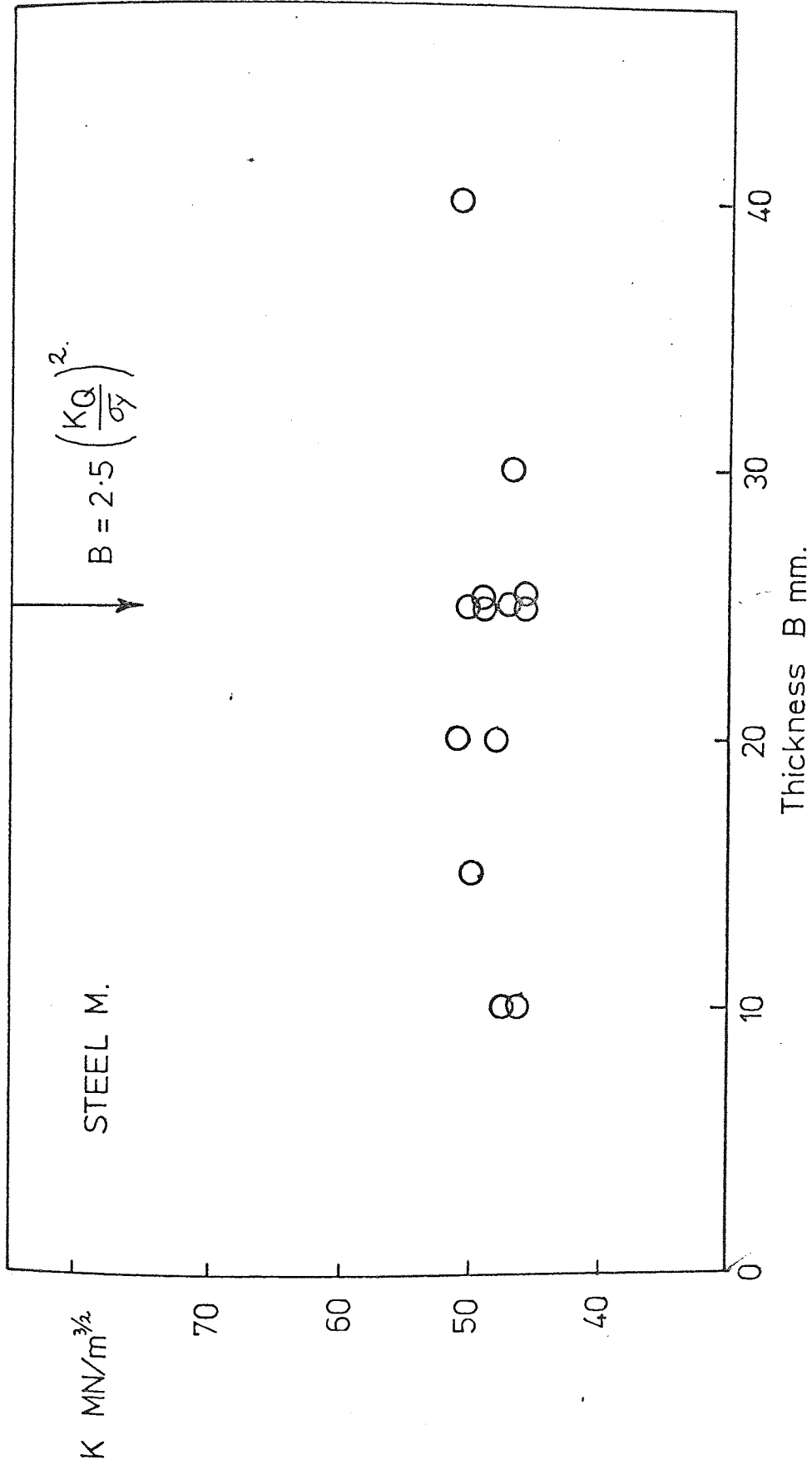


Fig. 8.1 K_{Ic} and K_C values from LEFM tests for steel M at various thicknesses.

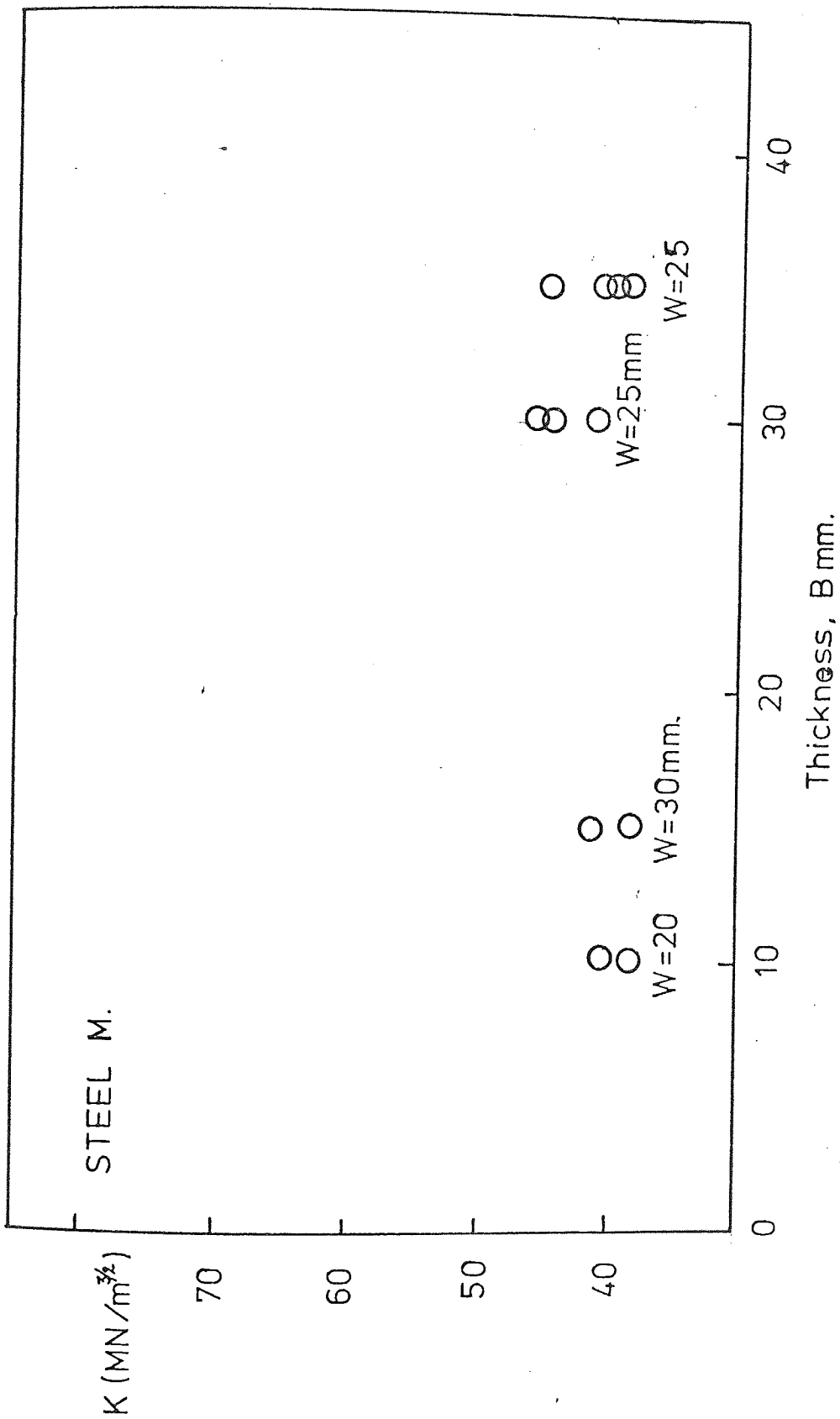


Fig 8.2 K_{Ic} values corresponding to the onset of yielding in small scale specimens of steel M.

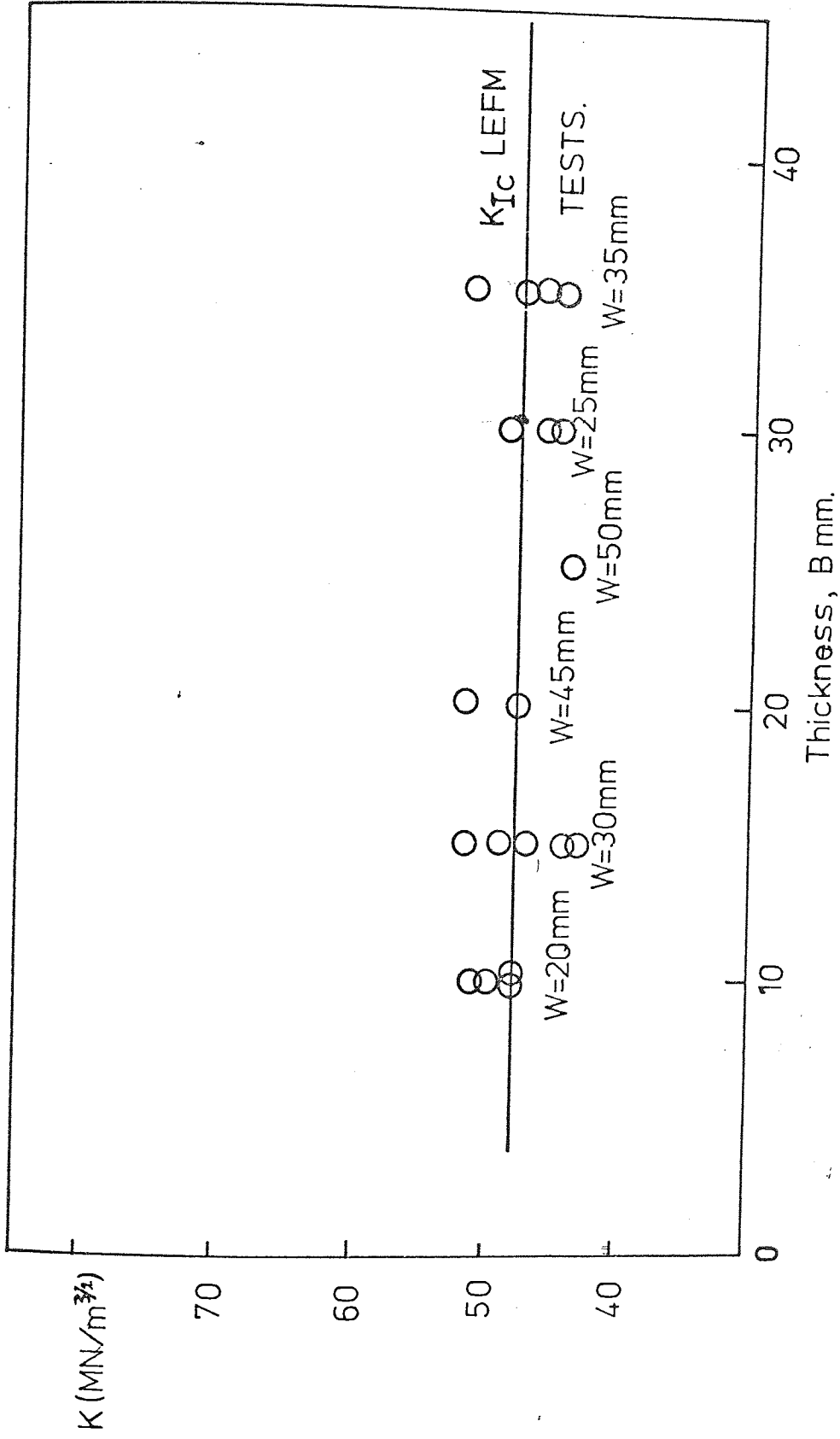


Fig. 8.3 K_{Ic} values for steel M derived from J_{Ic} at fracture.
Line indicates average K_{Ic} from LEFM tests.

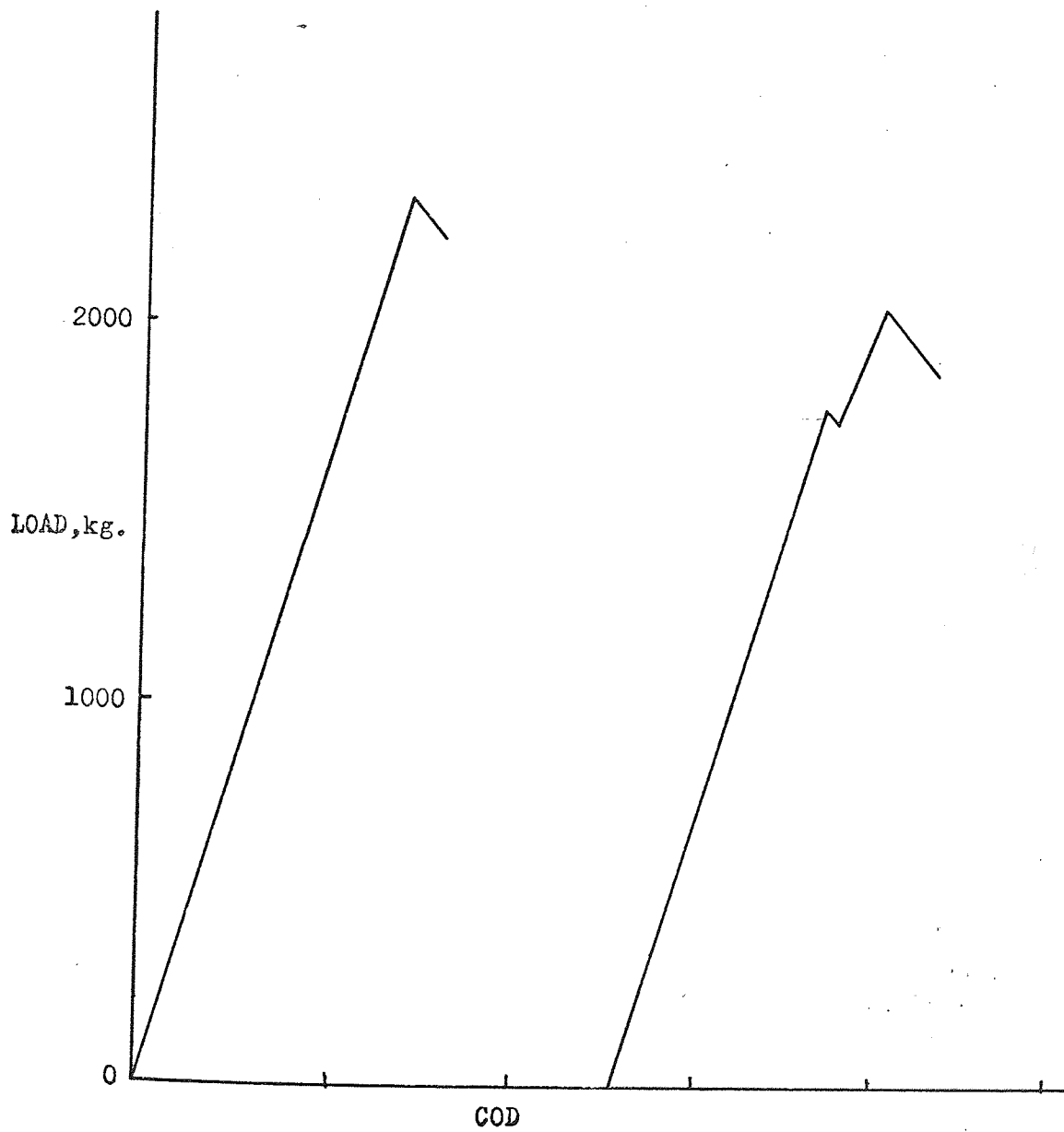


Fig. 8.4 Crack Opening Displacement versus Applied Load
for Steels Mlx1 and Mlx5.

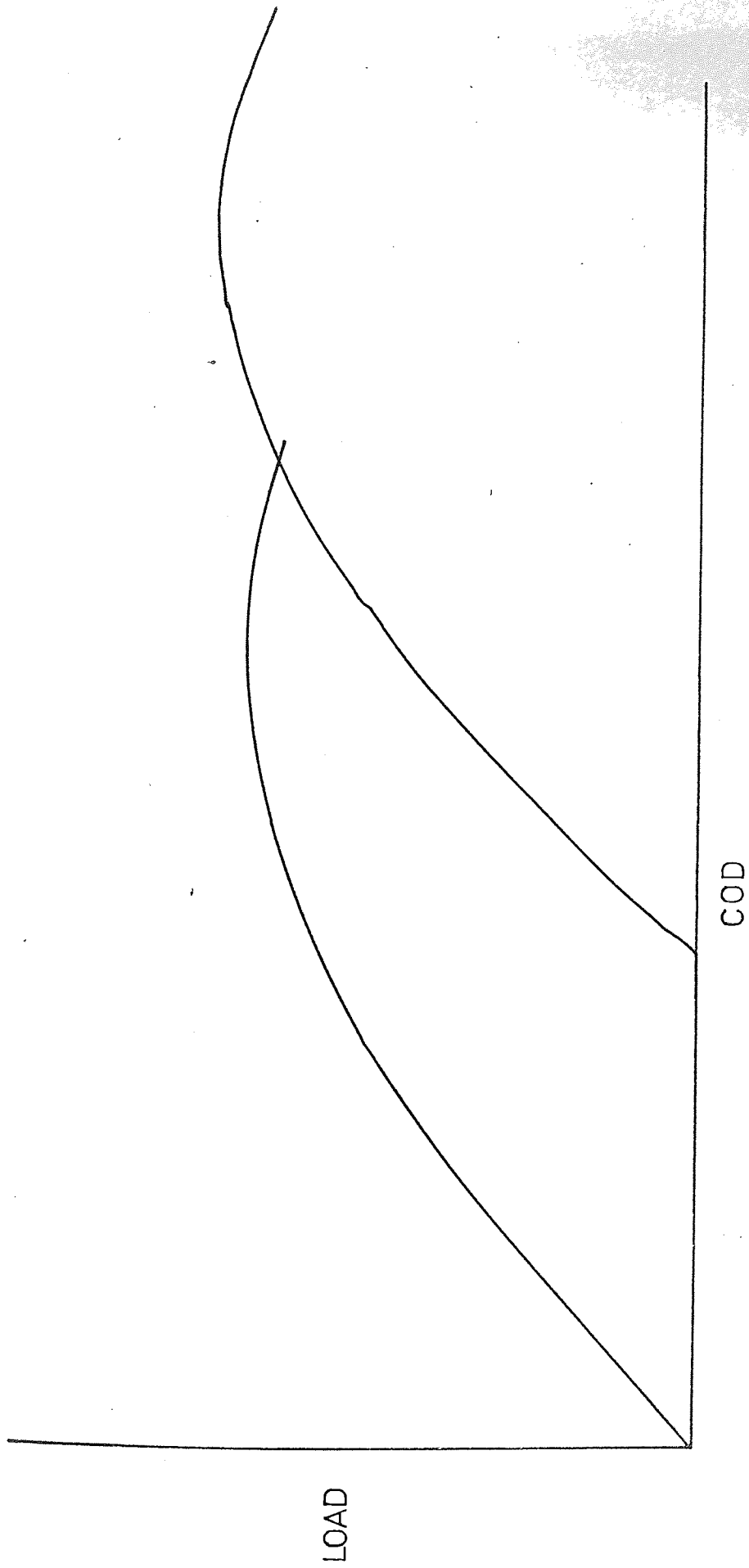


Fig. 8.5 Crack Opening Displacement versus Applied Load for Steel M1 (15, 30, 120) and M2(15, 30, 120).



Plate 4 Fracture surfaces from 25mm thick specimens of Steel M.

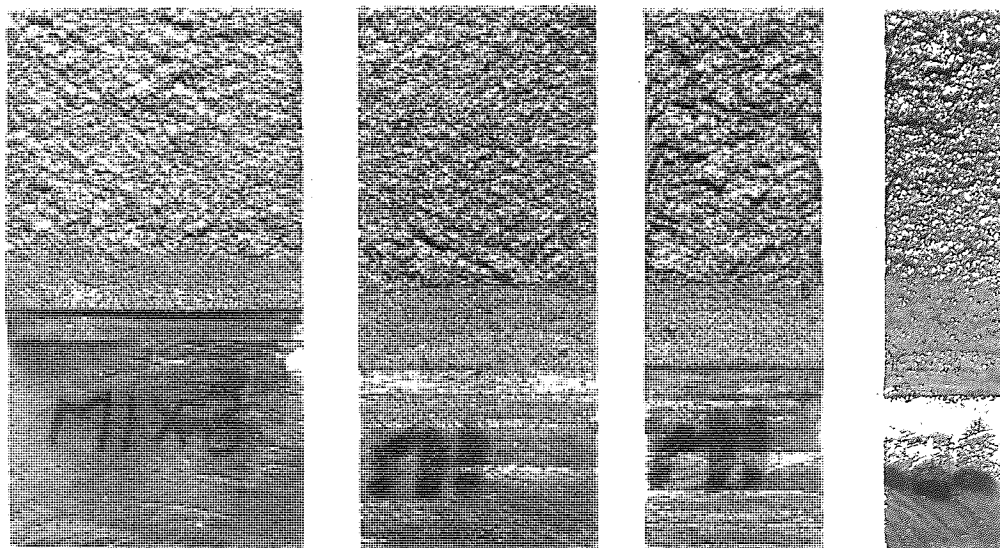


Plate 5 Fracture surfaces from 10mm, 15mm, 20mm and 25mm thick specimens of Steel M.

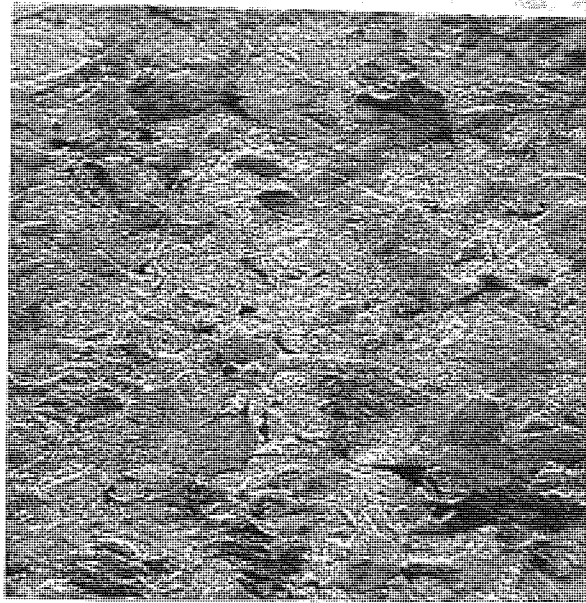


Plate 6 Steel M ,Microstructure - ~~Electro~~ Electro Etching(x650).

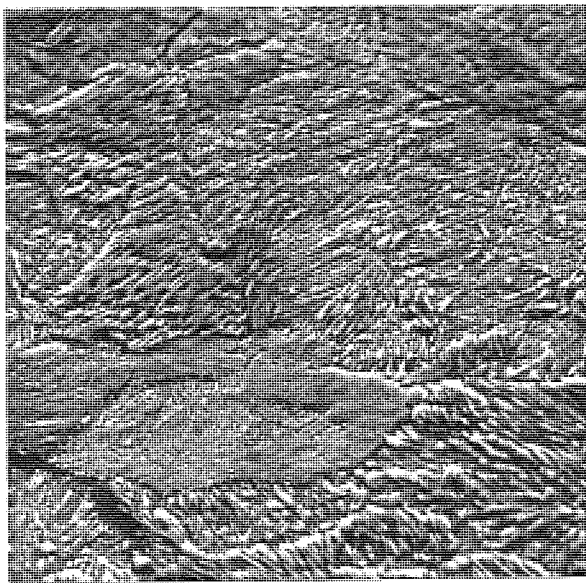
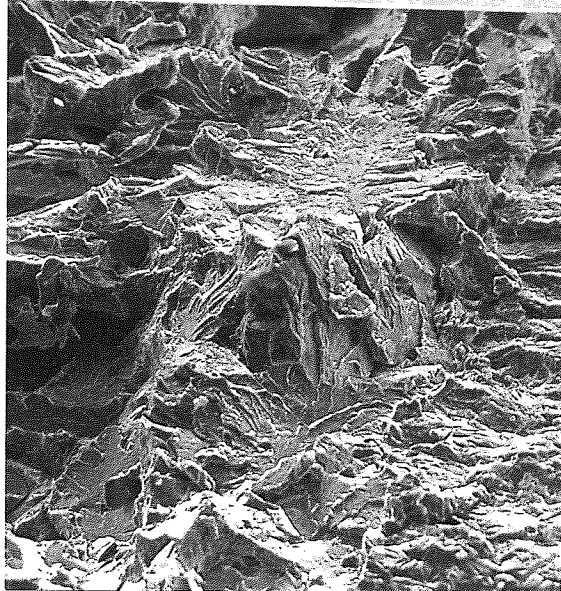


Plate 7 Steel M ,Microstructure - ~~Electro~~ Electro Etching (x2.4K).



Direction of crack propagation ←

Plate 8 Material M - Fracture surface at the fatigue crack tip showing cleavage fracture. Scanning Electron Fractograph (x280)

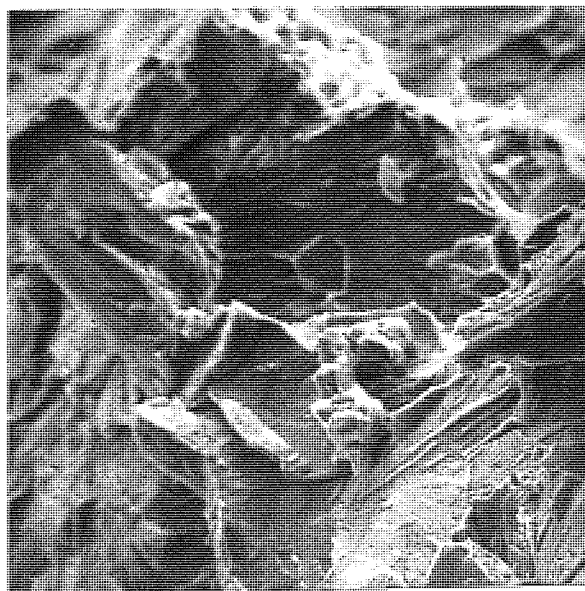


Plate 9 Material M - Fracture surface next to the fatigue crack tip showing details of cleavage fracture. Scanning Electron Fractograph (750).

8.3 Steel B, Cr - Mo - V

The results of fracture toughness tests carried out on samples of cast steel B are shown in Table 8.6. The K_Q values satisfy all the validity criteria of DD3 (102), and hence these results represent valid fracture toughness values K_{1C} for this cast steel. Plate 10 shows fracture surfaces which exhibit mostly cleavage fracture and small shear lips. A representative load versus COD trace is shown in Figure 8.6.

A further series of tests was conducted where specimen thickness B was varied with a constant specimen width $W = 42$ mm. These specimens were instrumented for the determination of K, J and δ values.

Results from the LEFM experiments are tabulated in Table 8.7, and shown graphically in Figure 8.7. The acceptable limit on specimen thickness for valid K_{1C} values is also shown in Figure 8.7. At thicknesses of 10 mm, 15 mm and 20 mm these tests did not meet the thickness requirement for K_{1C} , but met the deviation from linearity test for LEFM conditions and are therefore K_C values at the particular specimen thicknesses tested. According to potential drop records the P_Q values for these thicknesses did correspond to crack initiation so in fact they are most likely the plane strain fracture toughness and the fact that they are lower than the K_{1C} at 25 mm thickness probably arises from a variation in the actual toughness of the material.

J-integral results for these specimens are shown in Table 8.8 and in Figure 8.8 and show comparable toughness values to the LEFM results, confirming that in this case the 5% secant method was indeed detecting crack initiation. J-integral tests on further specimens with $B = 25$ mm and $W = 50$ mm fell on the average value of the LEFM tests at $B = 25$ mm.

Finally, results of crack opening displacement (δ) measurements are shown in Table 8.9 together with calculated values of the stress intensification factor, n . Values of n were calculated assuming a K_{1C} of $44 \text{ MN m}^{-3/2}$ from the previous tests. These results appear to show a variation of δ , and consequently n , with specimen thickness. As the n values increase with thickness this seems a reasonable experimental confirmation of the estimate by Wells (34) that n varies from about 2.1 for plane strain conditions to about 1.0 for plane stress conditions.

Micrographs showing the typical microstructure^{variation} of material B are shown in plates 11 and 12. It can be seen from these photographs that the microstructure consists mainly of bainite in a ferritic matrix.

A fractographic survey of the fracture surfaces was made using Cambridge scanning electron microscope. The areas studied were adjacent to the fatigue crack where rapid crack propagation is initiated and also at the interface between the fatigue crack and fast fracture. Plates 13 and 14 show that fracture occurred by cleavage. This cleavage fracture was observed in all the specimens tested. Finally a study of crack path was made on this material and crack branching was observed. Plates 15 and 16 show that branching of the crack appeared to take place at the boundary between bainite colonies and ferrite.

Specimen Number	Dimensions			K_Q MN/m ^{3/2}	K_{Ic} MN/m ^{3/2}	K_{max} MN/m ^{3/2}
	B mm	W mm	a mm			
Blx1	25.01	42.12	21.17	44.18	44.18	50.26
Blx2	24.99	44.91	23.96	48.25	48.25	57.00
Blx3	25.01	46.16	25.08	42.35	42.35	46.54
Blx4	25.00	44.81	24.24	46.36	46.36	52.64
Blx6	25.02	44.68	23.23	43.51	43.51	47.18
B3x1	24.90	49.99	25.61	41.78	41.78	53.47
B3x2	24.97	49.99	25.84	39.91	39.91	54.22

Table 8.6 K_{Ic} values from LEFM tests : Cast Steel B (Block No's 1 & 3)

Specimen Number	Dimensions			K_Q MN/m ^{3/2}	K_{Ic} MN/m ^{3/2}	K_{max} MN/m ^{3/2}
	B mm	W mm	a mm			
B1(10,42)	10.00	42.00	21.02	45.40		63.45
B2(10,42)	9.99	41.98	21.57	41.00		53.24
B1(15,42)	14.97	42.00	25.19	39.19		52.42
B2(15,42)	14.97	41.99	25.71	42.55		52.87
B1(20,42)	19.98	41.93	21.80	37.95		49.58
B2(20,42)	19.98	41.93	22.92	38.72		50.34

Table 8.7 Fracture Toughness values at various Thicknesses from LEFM tests : Cast Steel B (Block 2).

Specimen Number	Dimensions			J with elastic corr'n MN/m	K _{1c} from J + el. corr'n MN/m ^{3/2}	J without elastic corr'n MN/m	K _{1c} from J no el corr'n MN/m ^{3/2}
	B mm	W mm	a mm				
B1(10,42)	10.00	42.00	21.02	9.75x10 ⁻³	46.99	1.25x10 ⁻²	53.22
B2(10,42)	9.99	41.98	21.51	8.35x10 ⁻³	43.49	1.02x10 ⁻²	48.19
B1(15,42)	Inadequate potential drop record.						
B2(15,42)	14.97	41.99	25.71	8.14x10 ⁻³	42.94	9.61x10 ⁻³	46.64
B1(20,42)	19.98	41.93	21.80	7.39x10 ⁻³	40.90	9.09x10 ⁻³	45.36
B2(20,42)	19.98	41.93	22.92	6.72x10 ⁻³	39.01	8.33x10 ⁻³	43.43
B1(25,50)	24.90	49.99	25.61	8.48x10 ⁻³	43.82	1.08x10 ⁻²	49.38
B2(25,50)	24.97	49.99	25.84	8.58x10 ⁻³	44.07	1.01x10 ⁻²	47.73

Table 8.8 K_{1c} values from J_{1c} for tests on Steel B.

Specimen Number	Dimensions			δ mm	n
	B mm	W mm	a mm		
B1(10,42)	10.00	42.00	21.02	0.016	1.0
B2(15,42)	14.97	41.99	25.71	0.014	1.3
B2(20,42)	19.98	41.93	22.92	0.010	1.7
B1(25,50)	24.90	49.99	25.61	0.010	1.7

Table 8.9 Crack Opening Displacement (δ) and Stress Intensification Factor values for Steel B.

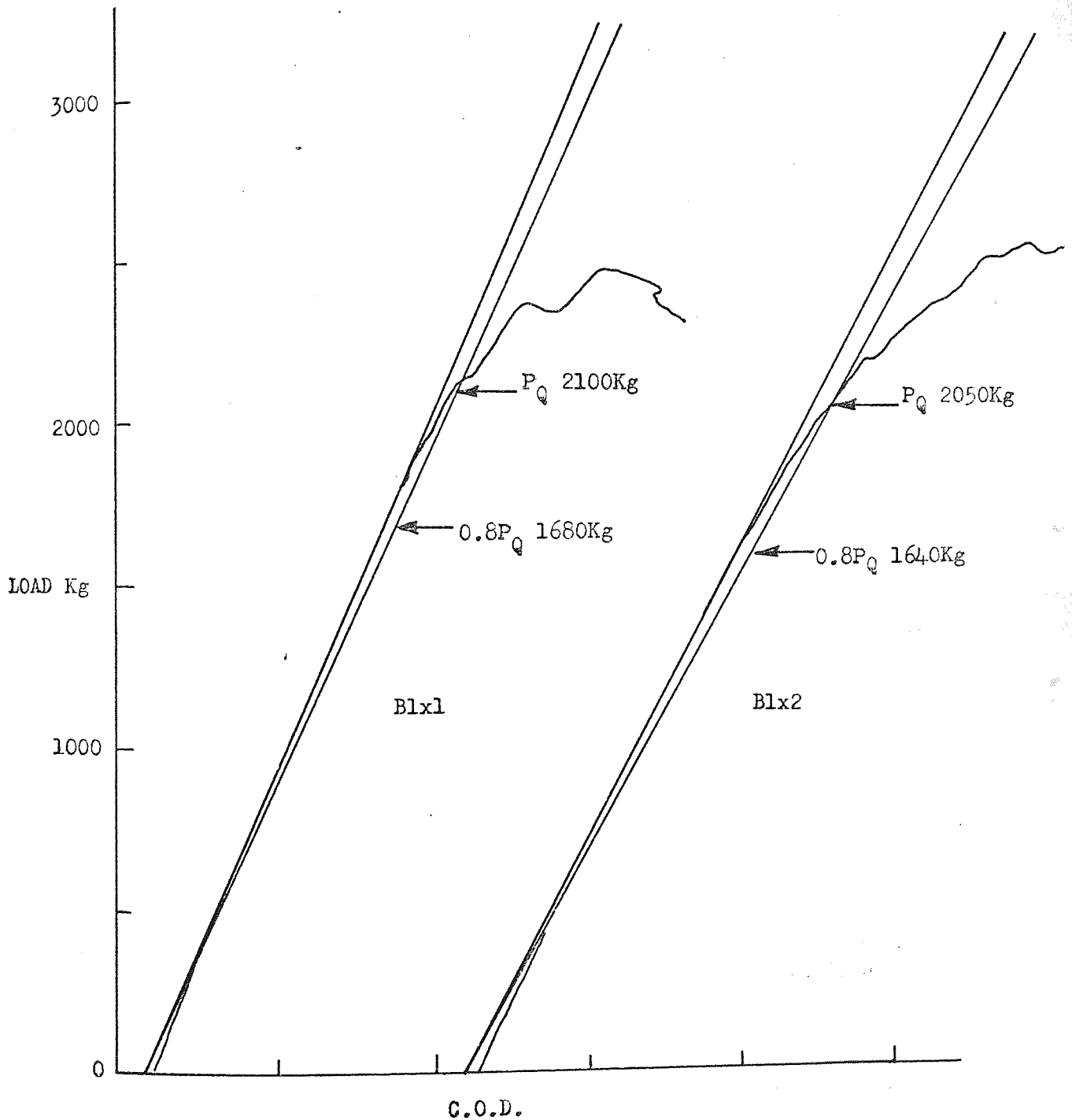


Fig. 8.6 Load-displacement curves for 3-point notch bend fracture toughness tests of Blx1 and Blx2.

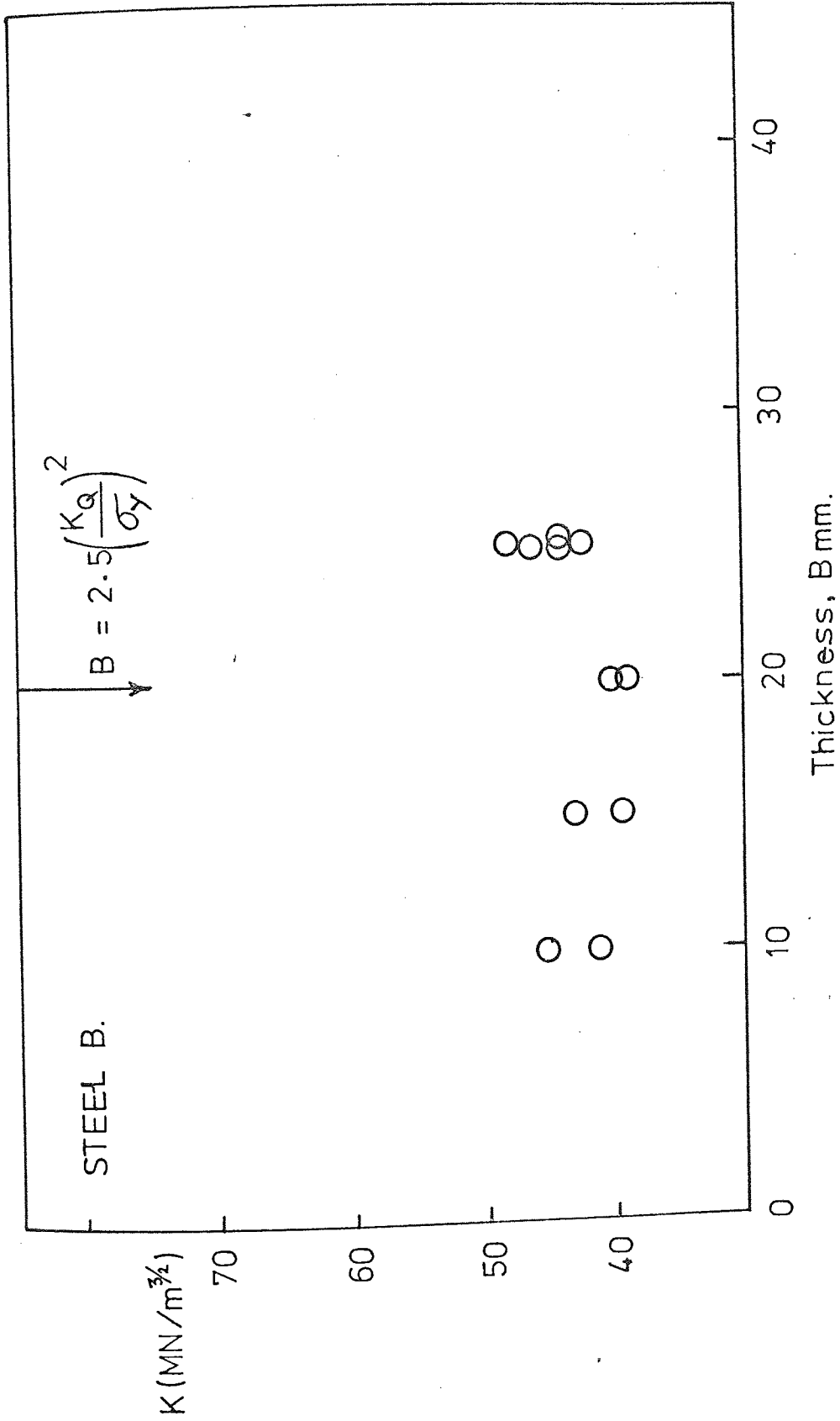


Fig. 8.7 K_C and K_{Ic} values from LEFM tests on steel B.

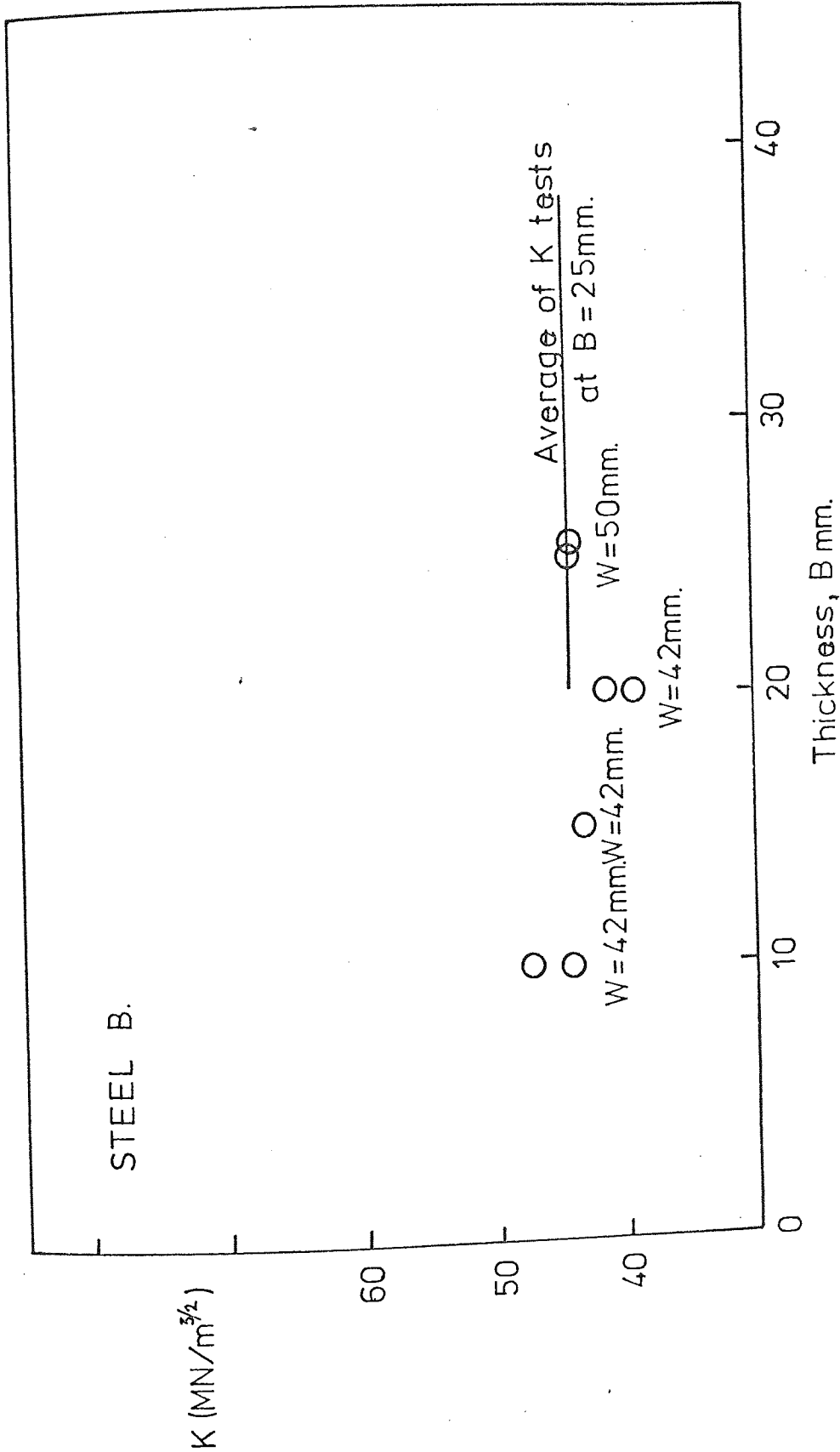


Fig. 8.8 K_{1c} from J_{1c} for tests on steel B. Line indicates average K_{1c} from LEFM tests analysed by the secant method

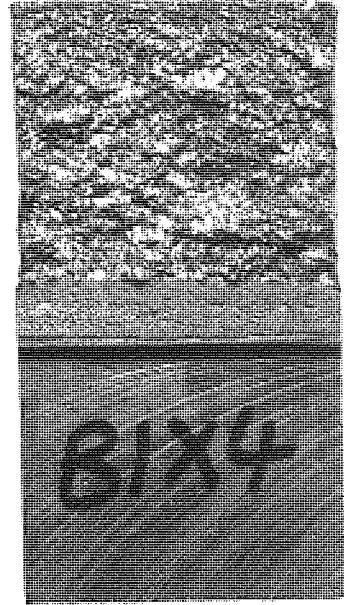
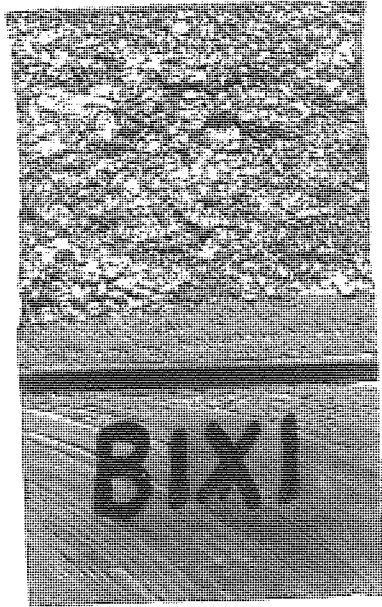


Plate 10 Fracture surfaces from 25mm thick specimens of Steel B.

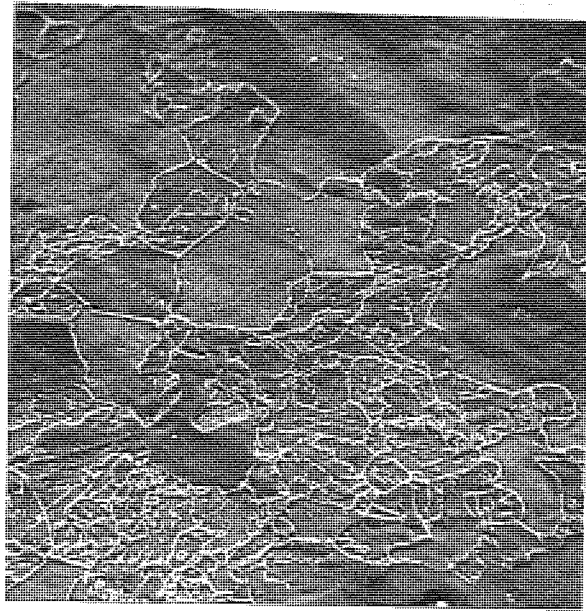


Plate 11 Material B - Microstructure Electro-etching
Scanning Electron Micrograph (x670)

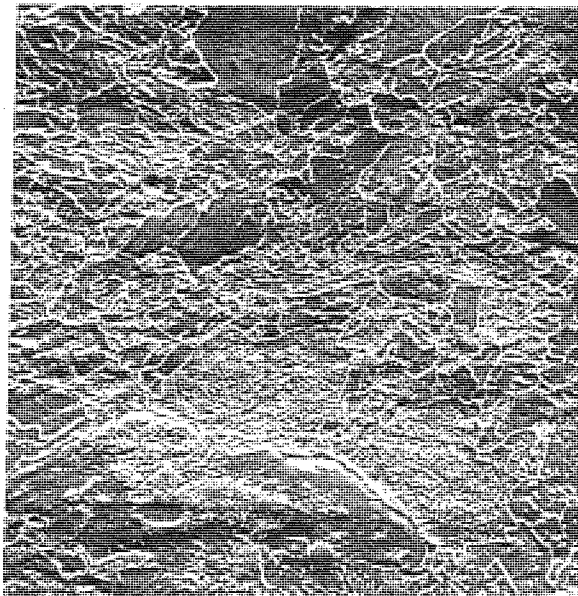
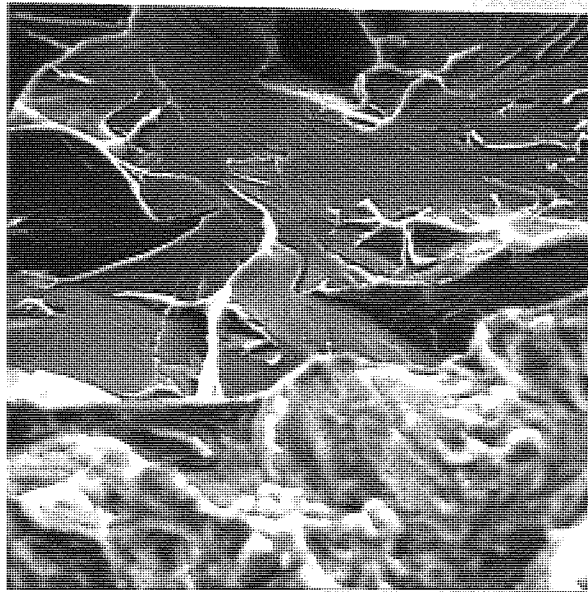


Plate 12 Material B - Microstructure Electro-etching
Scanning Electron Micrograph (x665)



Direction of
crack prop-
agation.

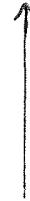


Plate 13 Material B - Fracture surface at the fatigue crack tip showing cleavage fracture. Scanning Electron Fractograph (x13K)

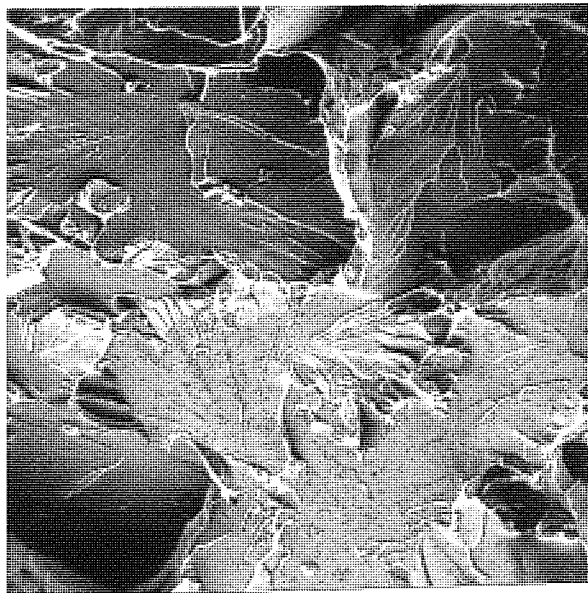


Plate 14 Material B - Fracture surface next to the fatigue crack tip showing details of the cleavage fracture. Scanning Electron Fractograph (x3.7K)

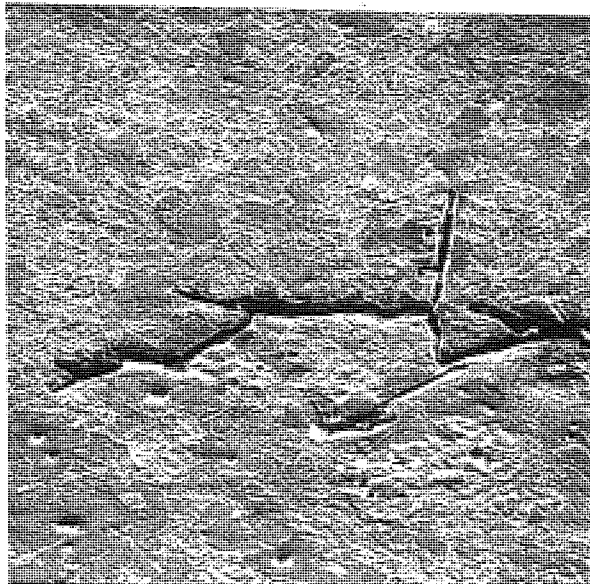


Plate 15 Steel B - crack path. SEM (x225)

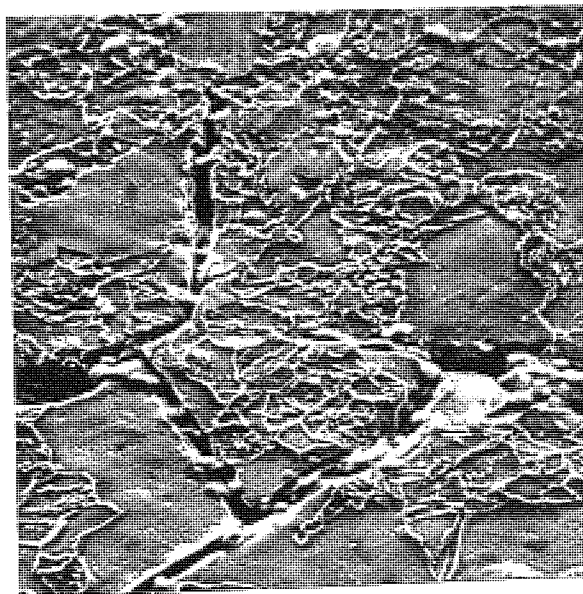


Plate 16 Steel B - crack path. SEM (x600)

8.4 Cast Steel C, Mn - Ni - Cr - Mo

Table 8.10 shows results of fracture toughness tests carried out on cast steel C (block No. 1). The fracture toughness values of the specimens at the centre of the block gave valid K_{1C} results and these results are shown in Figure 8.9. A representative trace of applied load against COD is shown in Figure 8.10. The variation in K_Q values across the keel block shows that there is some effect of casting position on fracture toughness values. K_Q values are higher at the corner of the block by about 16% than those at the centre of the block. Also shown in Figure 8.9 and Table 8.11 are results for tests with varying B but with W constant at 45 mm. The two low toughnesses arrowed in Figure 8.9 met the LEFM linearity condition, but not the thickness condition. In fact, for these two points alone, the P_Q did not correspond to crack initiation but to the sudden onset of plastic behaviour. Crack initiation occurred at a higher load as detected by the electrical potential method. These results would also be ruled out by (104) since the ratio P_{max}/P_Q was about 1.7 above the limit of 1.1 set to exclude this type of plastic behaviour. Plate 17 shows the fracture surfaces with small but recognizable shear lips.

The results obtained from J-integral tests are presented in Table 8.12 and Figure 8.11, Figure 8.11 shows the same results arrowed as in Figure 8.9. The K values at crack initiation derived from the J-integral method show higher toughnesses than those derived anomalously from the 5% secant method in Figure 8.9. Tests at B = 25 mm give fracture toughnesses in agreement with the K_{1C} values of Figure 8.9. The circled results indicate the overestimate of toughness which arises if the δ_{total} is used to determine J without subtracting $\delta_{no\ crack}$. Scatter on other values in this figure is thought to be a reflection of the variation in the materials toughness.

Smaller specimens were prepared to induce 'non valid' specimen behaviour. These specimens were cut from the halves of the centre specimens in an offer to eliminate the effect of casting position and to compare the results of K_{1C} obtained from J-integral methods with those obtained by normal linear elastic method. Table 8.13 shows the K_Q values for the smaller specimens and it can be seen that all the K_Q values were below the valid K_{1C} . The point of initiation according to the potential drop technique was always higher than P_Q indicating that all of the displacement at the load corresponding to K_Q was due to plasticity at the crack tip. A representative trace of applied load versus COD is shown in Figure 8.12. Table 8.14 and Figure 8.13 show the results of K_{1C} derived using the J-integral method. The results of these tests are in agreement with those derived by LEFM on J-integral methods from the larger test specimens. Table 8.15 contains the results of crack opening displacements for steel C which show a small variation of δ with thickness, $\delta = 0.026$ mm at $B = 15$ mm and $\delta = 0.018$ at $B = 35$ mm. Assuming a K_{1C} of $72 \text{ MN m}^{-3/2}$ from the LEFM results this indicates a variation of n from 1.0 to 1.8.

Micrographs of material C are shown in Plates 18 to 22 at various magnifications and positions in the keel block. It can be seen from these photographs that the microstructure consists of tempered martensite. Note that in Plate 18 alternate light and dark areas can be seen which is an indication of compositional differences which leads to different microstructure, tempered martensite and maybe bainite, which may account for the fall in toughness. In order to confirm this assumption a detailed study using an electron microscope would be required. As such a study was beyond the scope of this present work, all that can be said are general comments concerning

the likely variation in fracture properties across a cast section. For the particular case of material C, there is a decrease in fracture toughness from the edges to the centre of the keel block, probably due to the different cooling rates and the corresponding variation in grain size and microstructures.

A fractographic study of the various fracture surfaces showed that a variety of cracking or fracture mechanisms were operating during failure. For example, Plate 23 for specimen (20, 45) (1) shows that fracture took place by cleavage while in Plate 24 for specimen (20, 45) (2) the fracture mechanism is clearly by void coalescence. In fact, in most cases a mixed mechanism was apparent with areas of cleavage separated by areas of microvoid coalescence as in Plate 25.

Specimen Number	Dimensions			K_Q MN/m ^{3/4}	K_{Ic} MN/m ^{3/4}	K_{max} MN/m ^{3/2}
	B mm	W mm	a mm			
C1x2	25.00	44.95	22.39	72.19	72.19	85.32
C1x3	24.97	37.81	16.48	85.66		114.58
C1x4	24.98	41.98	21.98	84.99		115.50
C1x5	24.99	44.00	25.89	71.95	71.95	76.93
C1x6	24.97	44.95	23.43	84.20		138.80
C4x5	26.18	46.18	24.02	74.69	74.69	84.68

Table 8.10 Fracture Toughness values from LEFM tests : Cast Steel C
(Blocks 1 and 4)

Specimen Number	Dimensions			K_Q MN/m ^{3/4}	K_{Ic} MN/m ^{3/4}	K_{max} MN/m ^{3/2}
	B mm	W mm	a mm			
C1(10,45)	10.02	44.98	22.22	85.26		117.68
C2(10,45)	10.03	44.98	21.52	91.36		125.62
C1(15,45)	14.96	44.95	21.85	83.23		117.47
C2(15,45)	15.00	45.01	27.29	61.54		106.53
C1(20,45)	19.90	45.01	20.18	61.19		96.54
C2(20,45)	19.89	45.03	21.71	79.26		93.26
C1(30,45)	29.90	45.01	22.42	79.91	79.91	79.91
C2(30,45)	29.99	45.02	21.98	67.74	67.74	73.20

Table 8.11 Fracture Toughness values at various Thicknesses from
LEFM tests : Cast Steel C (Block 2)

Specimen Number	Dimensions			J with elastic corr'n MN/m	K _{1c} from J + el. corr'n MN/m ^{3/2}	J without elastic corr'n MN/m	K _{1c} from J no el. corr'n MN/m ^{3/2}
	B mm	W mm	a mm				
C1x2	25.00	44.95	22.39	2.16x10 ⁻²	70.02	2.74x10 ⁻²	78.71
C1x5	24.99	44.00	25.89	2.40x10 ⁻²	73.77	2.81x10 ⁻²	79.77
C4x5	26.18	46.18	24.02	2.01x10 ⁻²	67.54	2.64x10 ⁻²	77.39
G1(15,45)	14.96	44.95	21.85	2.34x10 ⁻²	72.76	2.96x10 ⁻²	81.89
G2(15,45)	15.00	45.01	27.29	2.64x10 ⁻²	77.29	3.00x10 ⁻²	82.47
G1(20,45)	19.90	45.01	20.18	2.05x10 ⁻²	68.16	2.76x10 ⁻²	79.06
G2(20,45)	19.89	45.03	21.71	2.59x10 ⁻²	76.56	3.29x10 ⁻²	86.26
G1(30,45)	29.90	45.01	22.42	3.66x10 ⁻²	91.05	4.55x10 ⁻²	101.51
G2(30,45)	29.99	45.02	21.98	2.89x10 ⁻²	80.95	3.56x10 ⁻²	89.78

Table 8.12 K_{1c} values from J_{1c} for tests on Steel C.

Specimen Number	Dimensions			K_Q MN/m ^{3/2}	K_{Ic} MN/m ^{3/2}	K_{max} MN/m ^{3/2}
	B mm	W mm	a mm			
C3(30,25) (FromC1x2)	30.00	24.99	14.08	57.11		100.88
C4(30,25) (FromC1x2)	30.00	24.97	12.28	64.20		106.78
C2(30,25) (FromC1x5)	29.99	24.97	11.86	67.07		108.64
C3(35,25) (FromC1x5)	35.00	25.00	14.05	55.63		99.67
C4(35,25) (FromC4x5)	34.98	24.99	12.15	63.02		101.74

Table 8.13 Fracture Toughness Results using LEFM Techniques :
Cast Steel C (Small Specimens)

Specimen Number	Dimensions			J integ- ral with el. corr MN/m	K_{Ic} calc from J_{Ic} MN/m ^{3/2}	J integ ral wit hout el corr'n MN/m	K_{Ic} from J no el corr'n MN/m ^{3/2}
	B mm	W mm	a mm				
C3(30,25) (FromC1x2)	30.00	24.99	14.08	2.05×10^{-2}	68.22	2.46×10^{-2}	74.61
C4(30,25) (FromC1x2)	30.00	24.97	12.28	2.22×10^{-2}	70.96	2.81×10^{-2}	79.83
C2(30,25) (FromC1x2)	29.99	24.97	11.86	2.21×10^{-2}	70.75	2.90×10^{-2}	81.08
C3(35,25) (FromC1x5)	35.00	25.00	14.05	2.06×10^{-2}	68.25	2.51×10^{-2}	75.39
C4(35,25) (FromC4x5)	34.98	24.99	12.15	2.00×10^{-2}	67.30	2.49×10^{-2}	75.06

Table 8.14 K_{Ic} Results using the J-Integral Technique :
Cast Steel C (Small Specimens)

Specimen Number	Dimensions			δ mm	n
	B mm	W mm	a mm		
C2(15,45)	14.50	45.01	27.29	0.028	1.1
C2(20,45)	19.89	45.03	21.71	0.026	1.1
C1(20,45)	19.90	45.01	20.18	0.031	1.0
C2(30,45)	29.99	45.02	21.98		1.3
C3(30,25) from C1x2	30.00	24.99	14.08	0.0195	1.6
C4(35,25) from C4x5	34.98	24.99	12.15	0.018	1.8
C4(30,25) from C1x2	30.00	24.97	12.28	0.019	1.6

Table 8.15 Crack Opening Displacement (δ) and the Stress
Intensification Factor : Results for Steel C.

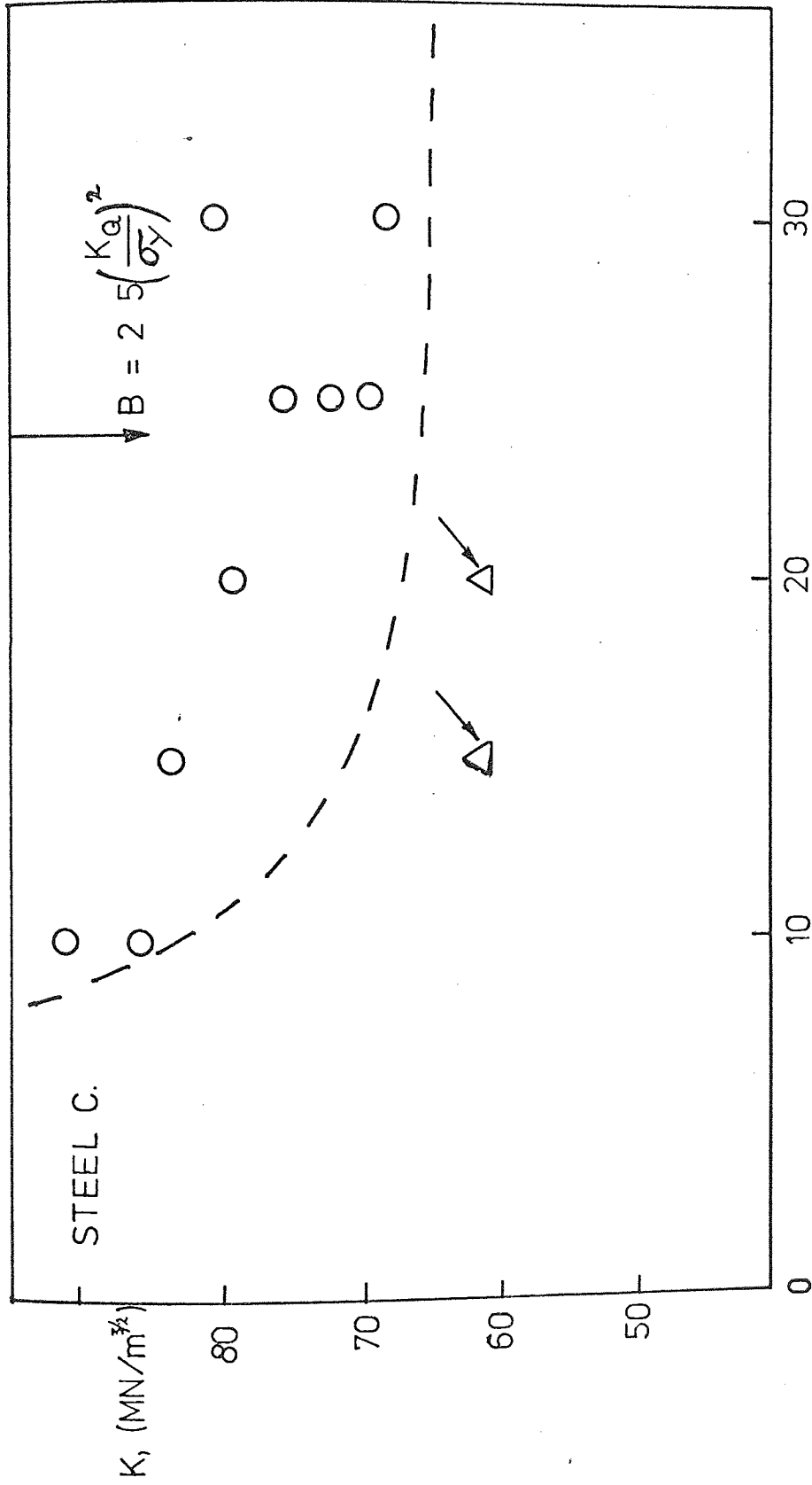


Fig. 8.9 K_C and K_{1C} for tests on steel C derived from LEFM tests and the secant method.

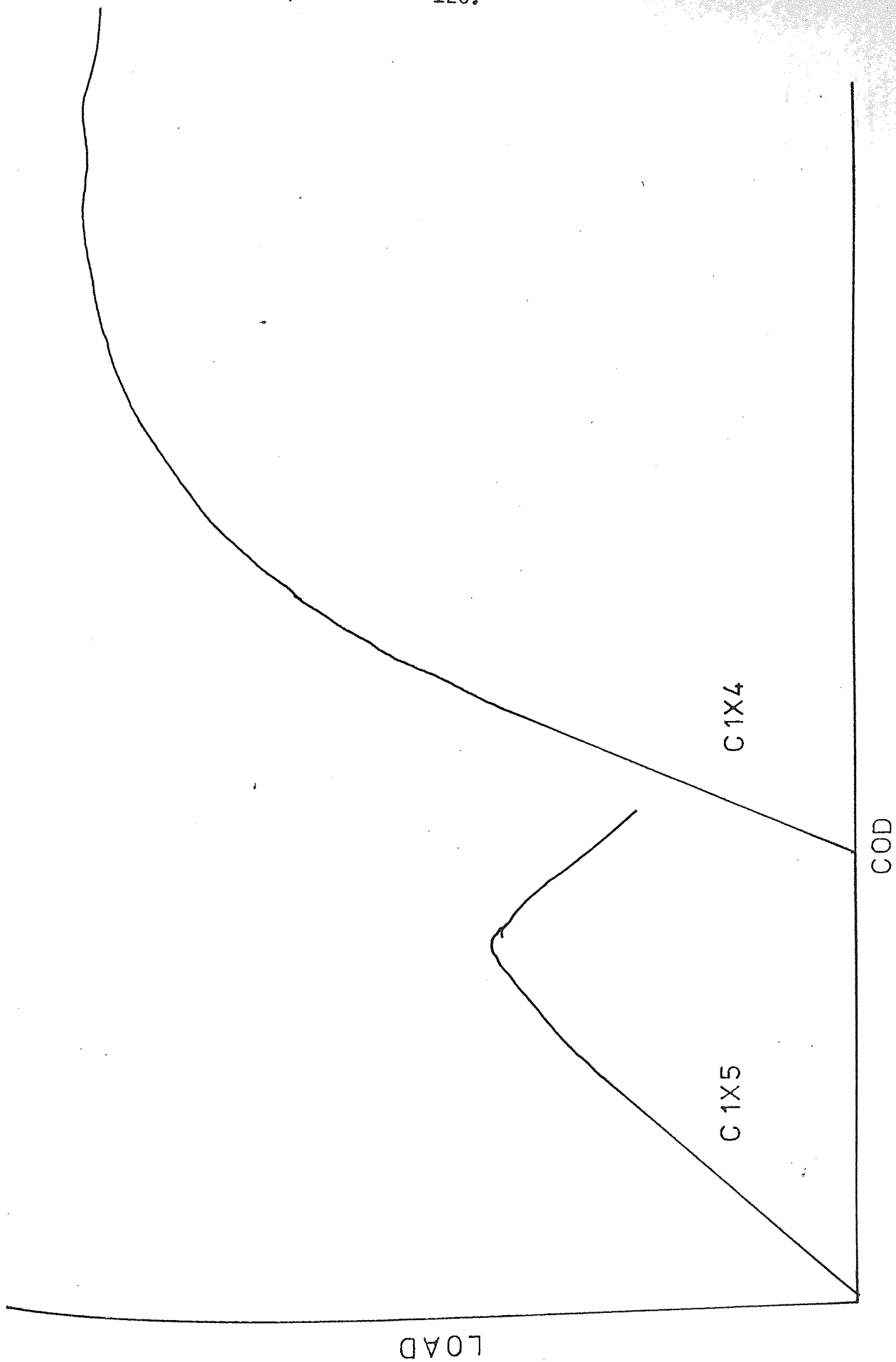


Fig. 8.10 Crack opening displacement versus applied load for C1x5 and C1x4.

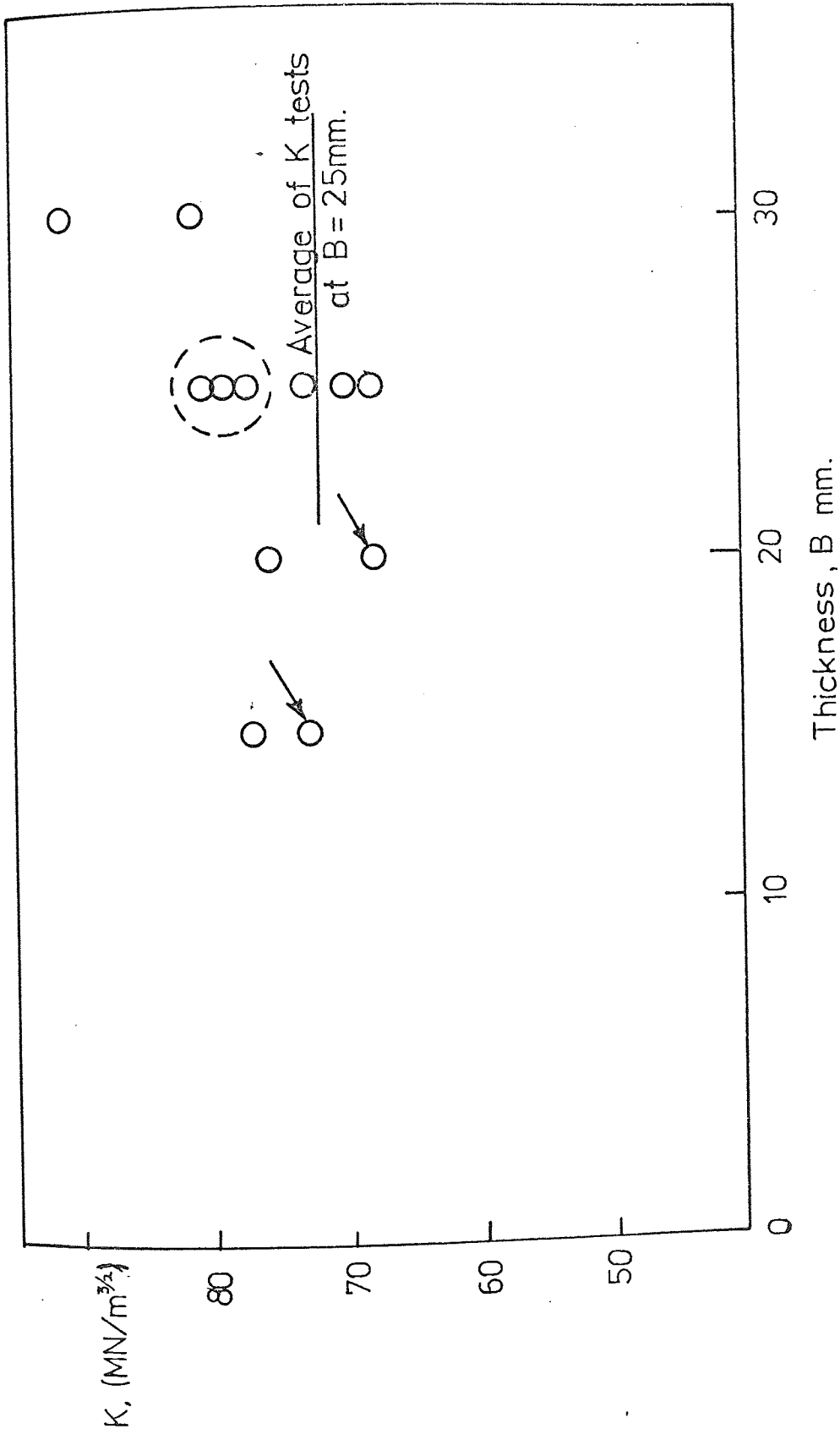


Fig. 8.11 K_{Ic} and K_{IIc} from J values for steel C.

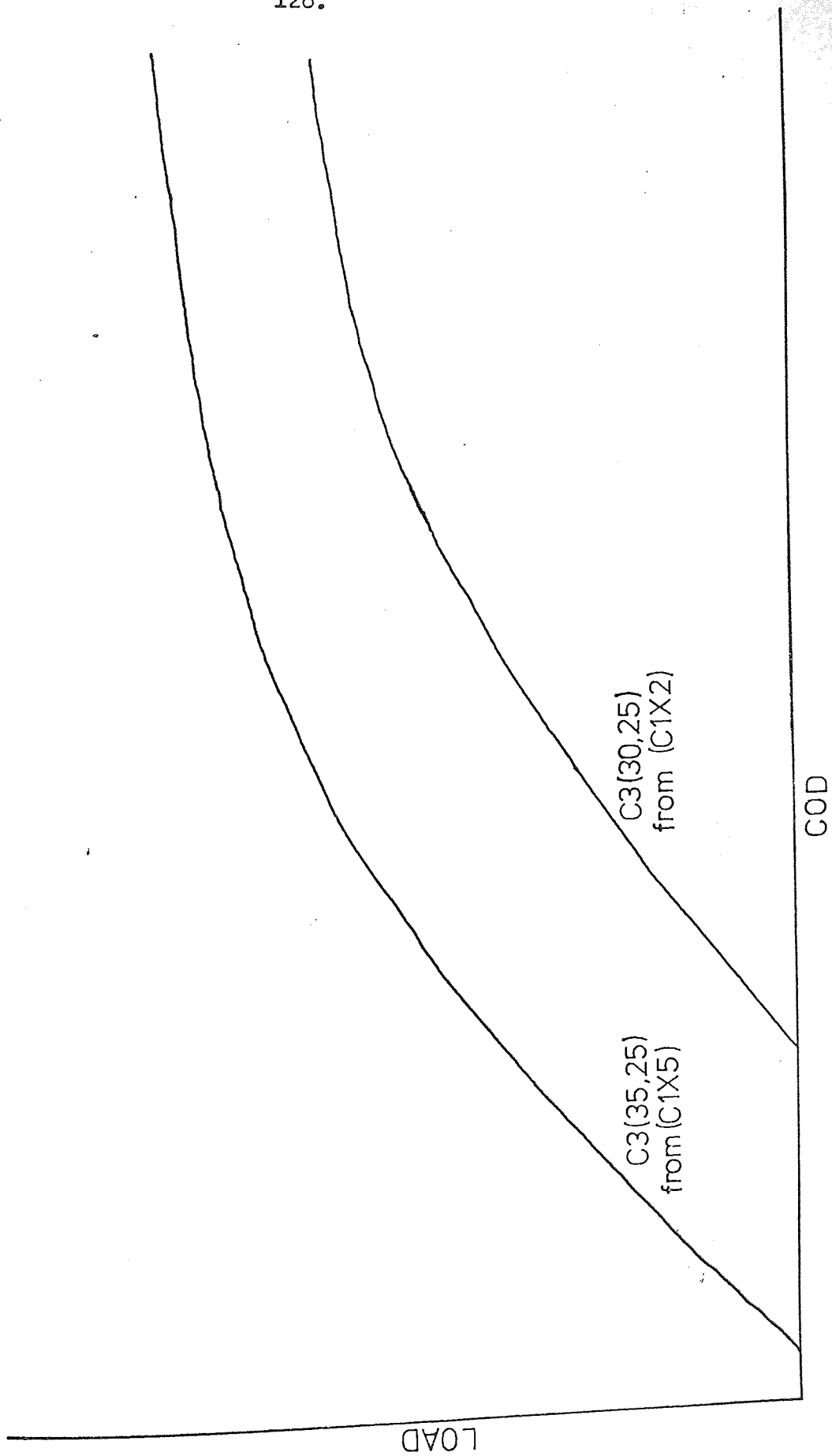


Fig. 8.12 Crack opening displacement versus applied load traces for C3(35,25) and C3(30,25).

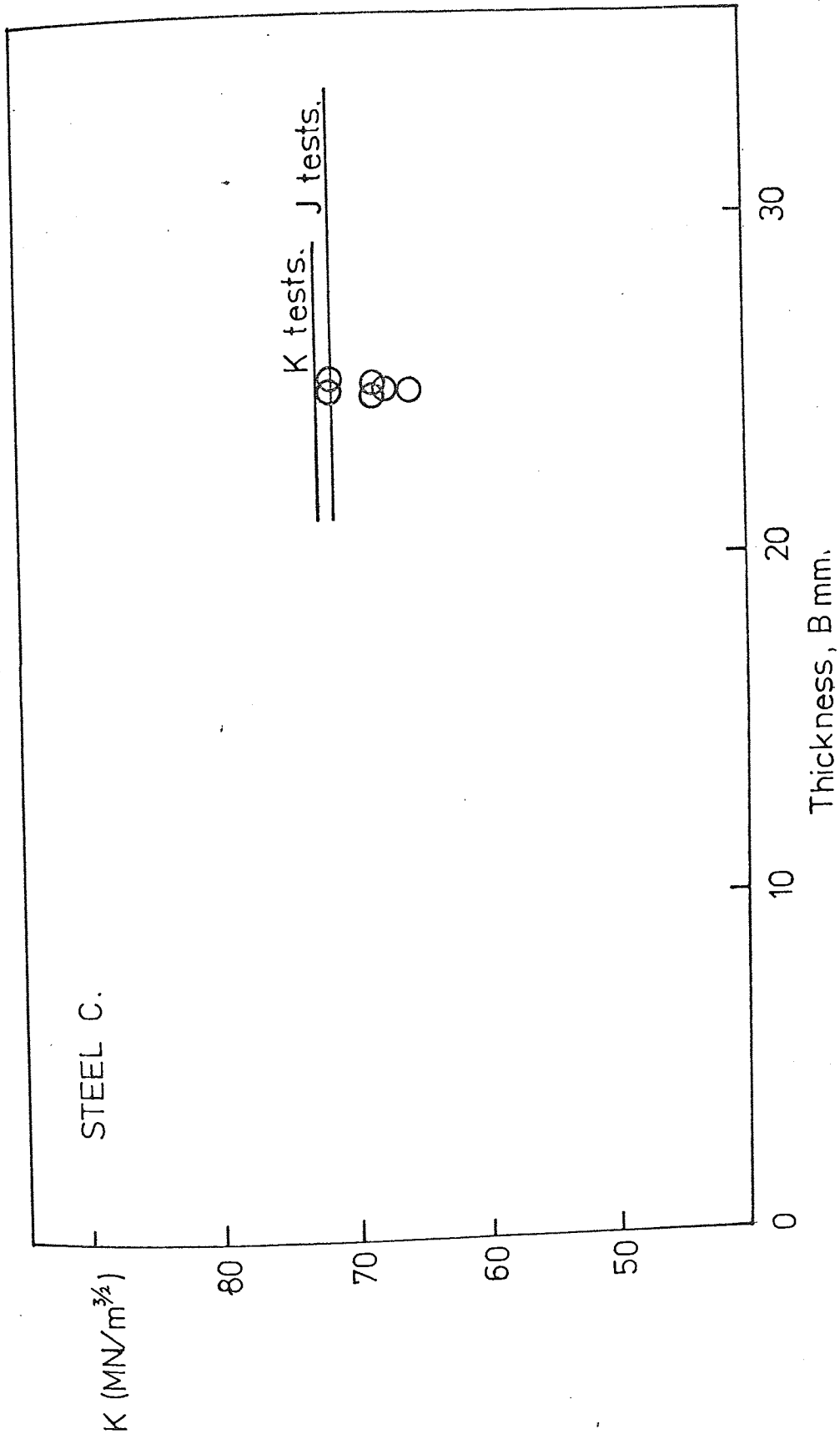


Fig. 8.13 K_{1C} from J_{1C} for tests on small scale specimens of steel C.



Plate 17 Fracture surfaces from 25mm thick specimens of Steel C.

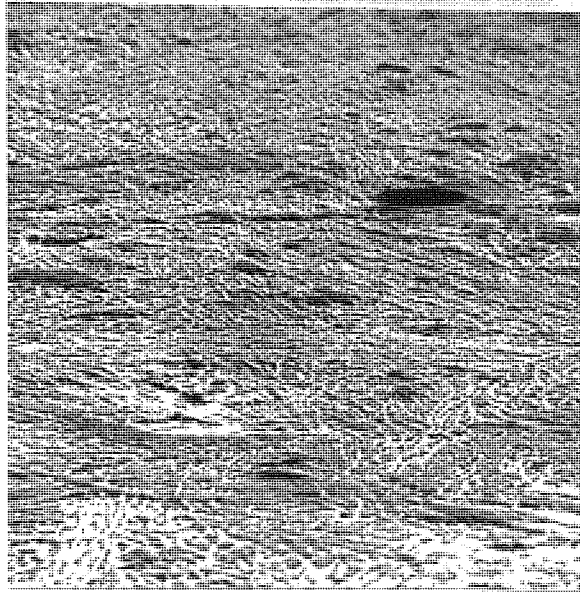


Plate 18 Microstructure of Material C at the centre of the block.
Electro-etching. Scanning Electron Micrograph (x1.2K)

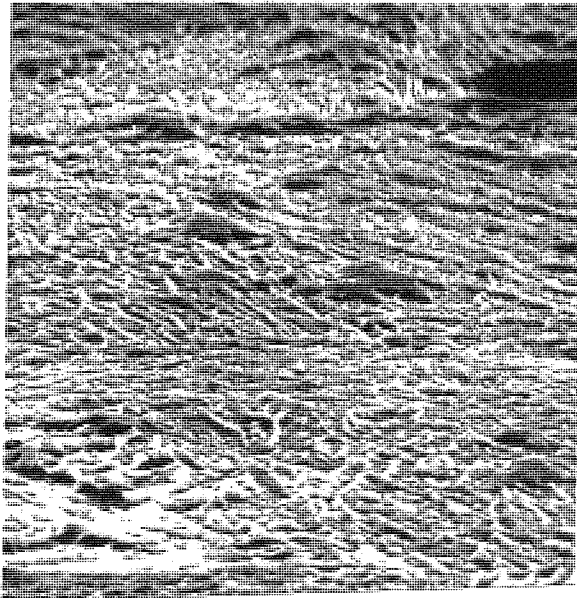


Plate 19 Microstructure of Material C at the centre of the block.
Electro-etching. Scanning Electron Micrograph (x2.4K)

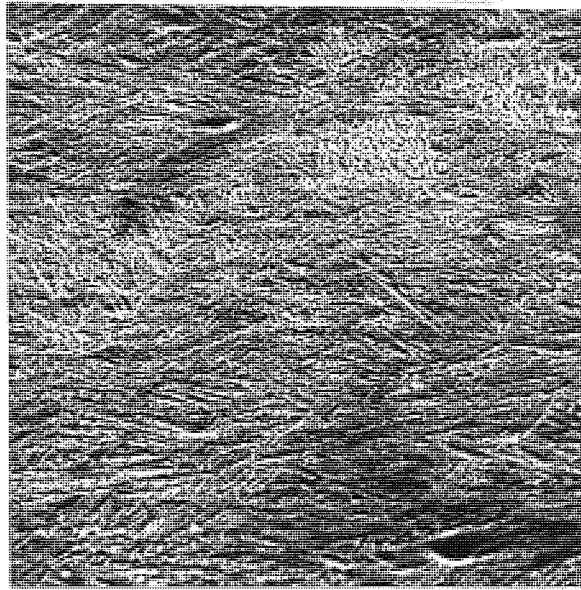


Plate 20 Microstructure of Material C at the corner of the block.
Electro-etching. Scanning Electron Micrograph (x1.2K)

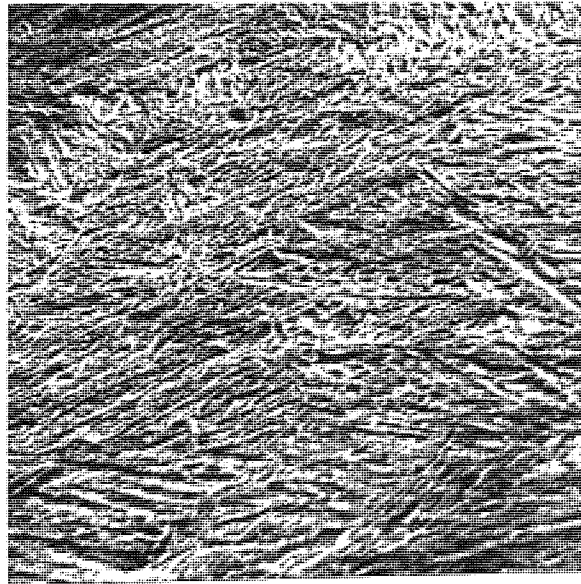


Plate 21 Microstructure of Material C at the corner of the block.
Electro-etching. Scanning Electron Micrograph (x2.4K)

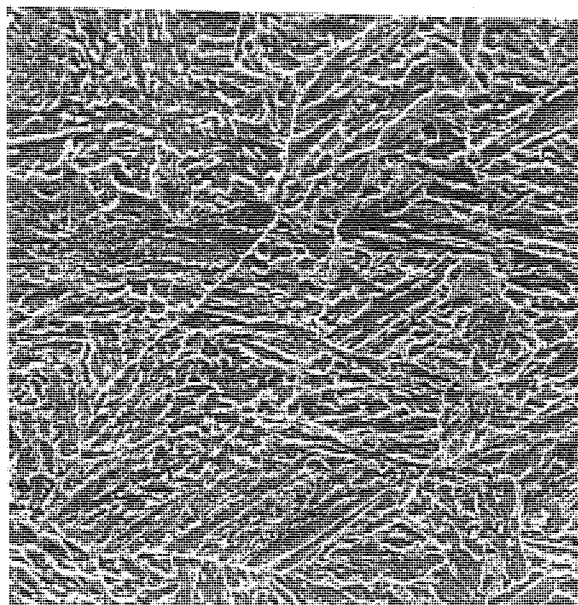
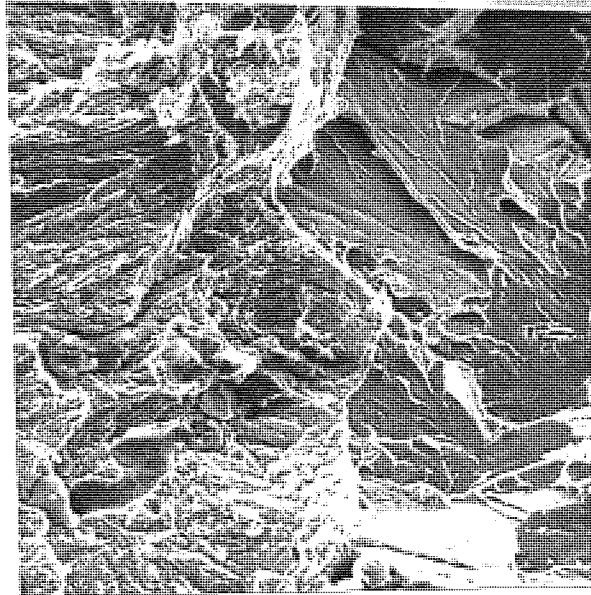


Plate 22 Microstructure of Cl(20,45).Conventional etching.

Scanning Electron Micrograph (x630)



→ Direction of crack propagation

Plate 23 Material C - Fracture surface at the fatigue crack tip showing cleavage fracture. Scanning Electron Fractograph (x650).

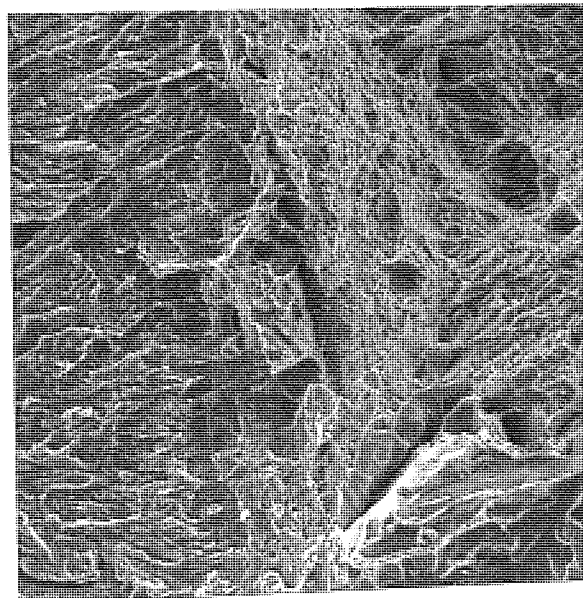


Plate 24 Material C - Fracture surface at the fatigue crack tip showing fracture by micro-void coalescence. Scanning Electron Fractograph (x600)

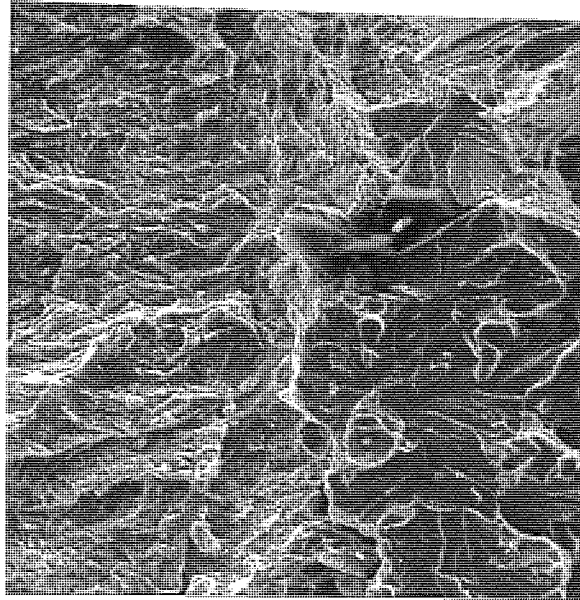


Plate 25 Material C. Fracture surface at the fatigue crack tip showing mixed fracture mechanisms of cleavage and microvoid coalescence. Scanning Electron Fractograph(x600)

8.5 Steel G, Ni - Cr - Mo

Steel G had the highest strength of the eight steels tested and it might have been expected at the onset of the work that its toughness would be obtained for moderately sized specimens. In fact it was one of the toughest steels as is apparent from the shear lips on the basic test specimen shown in Plate 26. Table 8.16 and Figure 8.14 shows results of K_Q values using the LEFM testing method for specimens taken from two different keel blocks. It can be seen from these results that there is a large scatter in the K_Q values and that the specimen size was not generally large enough to give LEFM conditions. K_Q values appear to be larger at the corners than those at the centre of the block. A representative trace of applied load versus COD is shown in Figure 8.15.

The results in Table 8.16 and Figure 8.14 fulfilled the deviation from linearity condition, however the tests for adequate thickness and crack length, according to DD3 (102), were borderline for most of the specimens. Consequently specimens having various thicknesses were tested and results are shown in Table 8.17 and Figure 8.14.

The K_Q values for all the specimens with different thicknesses were within the values previously found for blocks 1 and 2. Results from the J-integral tests are shown in Table 8.18 and Figure 8.14 which show a similar scatter to that found for the K_Q values.

Examination of the fracture surfaces using the scanning electron microscope showed the presence of a great deal of sulphur in the form of Manganese Sulphide. A typical fractograph, showing the sulphur is given in plate 27 for specimen G(30, 25) (3). The segregation of the sulphur varied considerably over the blocks examined. The scatter in all experimental results was almost

certainly due to this segregation coupled with the secondary effect of variation in casting position. In view of this, therefore, the only reasonable estimate of toughness must be the lowest value found in all the experiments. This will of course be the most conservative value for the purpose of design.

Table 8.19 and 8.20, show the results obtained using the J-integral for the smaller specimens and those obtained by LEFM method respectively. It is worth noting that with these specimens the point of initiation according to potential drop technique were above P_Q point. Once again, results exhibited some scatter to those found previously using the LEFM method.

Table 8.21 shows the results of crack opening displacements. In view of the scatter in test results, a check on the value of n is not feasible. Also the δ appeared to increase rather than decrease with increasing thickness from $\delta = 0.026$ mm at $B = 15$ mm to $\delta = 0.050$ mm at $B = 30$ mm. Such results probably arise from variation of the material toughness from place to place in the cast block.

Plates 28 and 29 show the microstructure of material G at low and high magnifications. The structure consists of dark and light areas which may be due to compositional differences deriving from the peritectic reaction on solidification. This leads to martensite forming at different temperatures and having differing tempering behaviour.

A comprehensive fractographic survey was made on this material, the areas studied in all cases being adjacent to the fatigue crack where rapid crack propagation is initiated and at the fatigue crack tip.

The fracture surfaces of all specimens investigated were very similar with predominantly ductile fibrous fracture as shown in Plates 30 and 31.

The fracture was in the form of dimple rupture. Experimental observations show large voids due to sulphide inclusions, as in Plate 27. This is fairly typical of the fracture surfaces obtained in high S-content steels. Note the shallow voids associated with the large MnS inclusions and the small ligaments between them, fracture in this steel proceeds by the coalescence of these voids. All of the specimens examined contained large manganese sulphide particles and it was found that the specimens with a lower toughness contained a higher percentage of the particles as shown in Plate 32 which are characteristic of interdendritic segregation of the particles.

Specimen Number	Dimensions			K_Q $MN/m^{3/2}$	K_{Ic} $MN/m^{3/2}$	K_{max} $MN/m^{3/2}$
	B mm	W mm	a mm			
G1x1	24.97	44.99	23.25	109.80		144.40
G1x2	25.00	44.98	23.67	90.93		140.03
G1x3	24.97	44.99	24.34	103.73		148.44
G1x4	24.97	44.99	23.17	90.90		140.45
G1x5	25.00	44.99	23.02	87.08		138.27
G1x6	24.98	44.88	23.27	89.71		139.48
G2x1	25.00	44.96	23.70	96.62		140.62
G2x2	25.01	42.97	23.37	85.86		127.61
G2x3	24.99	44.98	23.76	107.29		148.43
G2x4	24.99	44.97	24.53	95.85		128.88
G2x5	24.99	44.98	23.74	92.68		121.67
G2x6	25.00	44.98	24.32	93.40		141.79

Table 8.16 Fracture Toughness Results : Cast Steel G (Blocks 1 and 2)

Specimen Number	Dimensions			K_Q MN/m ^{3/2}	K_{Ic} MN/m ^{3/2}	K_{max} MN/m ^{3/2}
	B mm	W mm	a mm			
G(10,45)(1)	10.03	44.90	24.68	89.56		119.37
G(10,45)(2)	10.03	44.98	22.14	88.10		130.96
G(15,45)(1)	15.02	45.03	22.31	88.57		131.98
G(15,45)(2)	15.02	44.85	22.92	92.36		131.65
G(20,45)(1)	19.99	44.61	22.76	89.08		127.39
G(30,45)(1)	29.98	45.01	21.65	93.37		138.13
G(30,45)(2)	29.98	44.87	22.65	91.50		133.06

Table 8.17 Fracture Toughness Results : Cast Steel at various thicknesses
(Block 3)

Specimen Number	Dimensions			J with elastic corr'n MN/m	K_{Ic} from J el. corr'n MN/m ^{3/2}	J without elastic corr'n MN/m	K_{Ic} from J no el. corr'n MN/m ^{3/2}
	B mm	W mm	a mm				
G(15,45)(1)	15.02	45.03	22.31	2.96×10^{-2}	81.80	3.79×10^{-2}	92.67
G(15,45)(2)	15.02	44.85	22.92	2.96×10^{-2}	81.92	3.74×10^{-2}	91.97
G(20,45)(1)	19.99	44.61	22.76	3.98×10^{-2}	94.98	5.02×10^{-2}	107.04
G(30,45)(1)	29.98	45.01	21.65	4.63×10^{-2}	102.40	5.93×10^{-2}	115.90
G(30,45)(2)	29.98	44.87	22.65	3.96×10^{-2}	94.78	4.99×10^{-2}	106.27

Table 8.18 K_{Ic} results derived from J_{Ic} at Fracture for Cast Steel G at various Thicknesses (Block 3).

Specimen Number	Dimensions			J with elastic corr'n MN/m	K _{1c} from J + el. corr'n MN/m ^{3/2}	J without elastic corr'n MN/m	K _{1c} from J no el. corr'n MN/m ^{3/2}
	B mm	W mm	a mm				
G1(30,25) from G(1x5)	30.00	25.00	12.32	4.42x10 ⁻²	100.01	5.27x10 ⁻²	109.20
G3(30,25) from G(1x5)	30.00	24.99	12.87	2.81x10 ⁻²	79.84	3.43x10 ⁻²	88.16
G3(35,25) from G(1x6)	35.00	25.00	12.23	5.97x10 ⁻²	116.29	7.03x10 ⁻²	126.14
G5(35,25) from G(1x4)	35.01	25.00	15.27	5.30x10 ⁻²	109.51	5.94x10 ⁻²	110.61

Table 8.19 K_{1c} values derived from J_{1c} at fracture in small scale specimens : Cast Steel G.

Specimen Number	Dimensions			K _Q MN/m ^{3/2}	K _{1c} MN/m ^{3/2}	K _{max} MN/m ^{3/2}
	B mm	W mm	a mm			
G1(30,25) from G(1x5)	30.00	25.00	12.32	76.98		106.96
G3(30,25) from G(1x5)	30.00	24.99	12.87	76.07		110.67
G3(35,25) from G(1x6)	35.00	25.00	12.23	72.60		109.80
G5(35,25) from G(1x4)	35.01	25.00	15.27	82.28		108.65

Table 8.20 Fracture toughness results using LEFM techniques.
Cast Steel G (small specimens)

Specimen Number	Dimensions			δ from eq'n derived expt. mm	n	δ from eq'n derived theoret. mm	n
	B mm	W mm	a mm				
G1(15,45)	15.02	45.03	22.31	0.073		0.027	
G2(15,45)	15.02	44.85	22.92	0.070		0.026	
G1(20,45)	19.99	44.61	22.76	0.085		0.038	
G1(30,45)	29.98	45.01	21.65	0.091		0.042	
G2(30,45)	29.98	44.87	22.65	0.099		0.050	
G3(35,25) fromG(1x6)	35.00	25.00	12.23	0.069		0.047	
G5(35,25) fromG(1x4)	35.00	25.00	15.27	0.059		0.046	
G1(30,25) fromG(1x5)	30.00	25.00	12.32	0.061		0.035	
G3(30,25) fromG(1x5)	30.00	24.99	12.87	0.047		0.028	

Table 8.21 Crack opening displacement and stress intensification factors for Steel G.

Fig. 8.16 K from 1.5 to 5 ft ft
secant mod

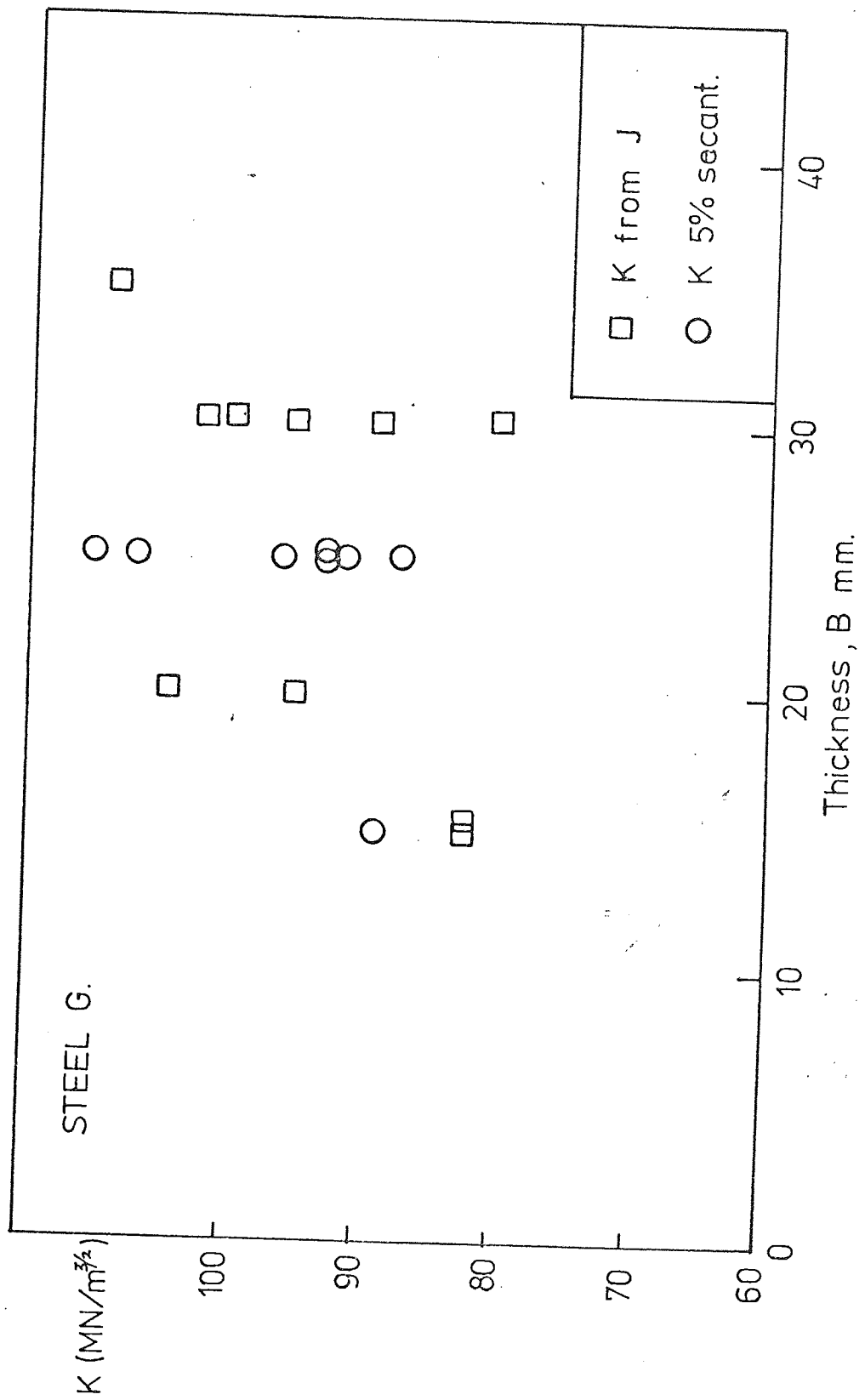


Fig. 8.14 K from J values at fracture and K_Q values using the secant method for steel G.

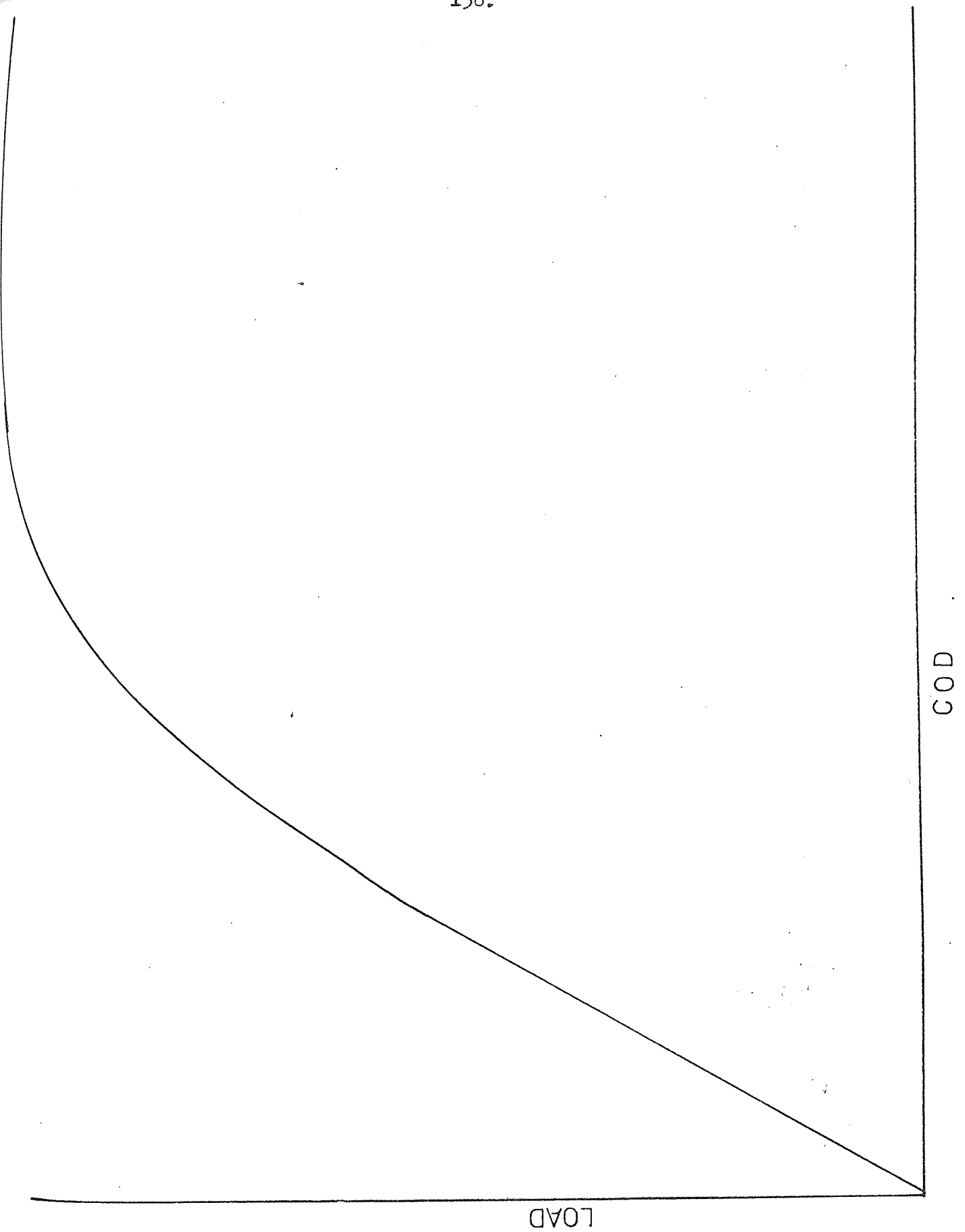


Fig. 8.15 Crack opening displacement versus applied load trace for G1x1.

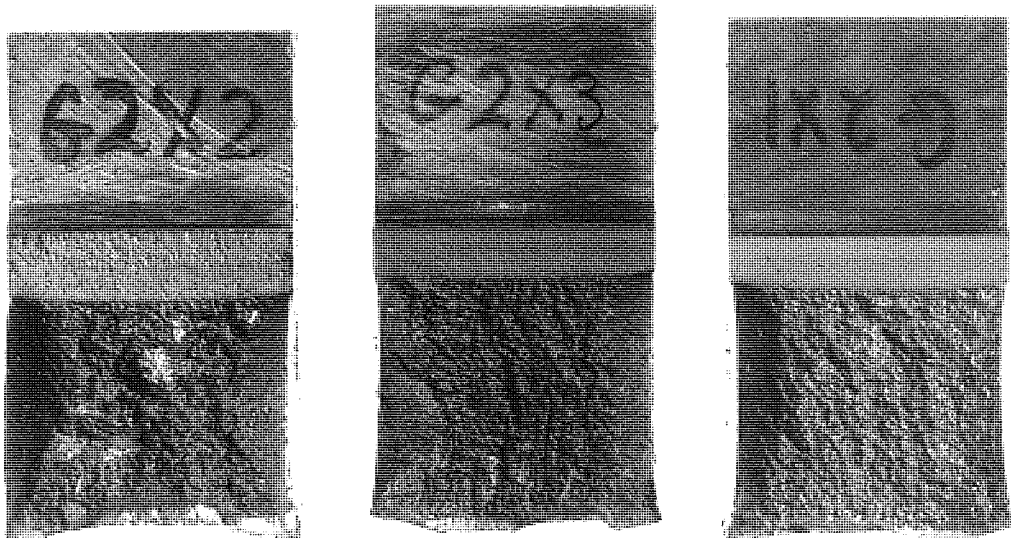


Plate 26 Fracture surfaces from 25mm thick specimens of Steel G.

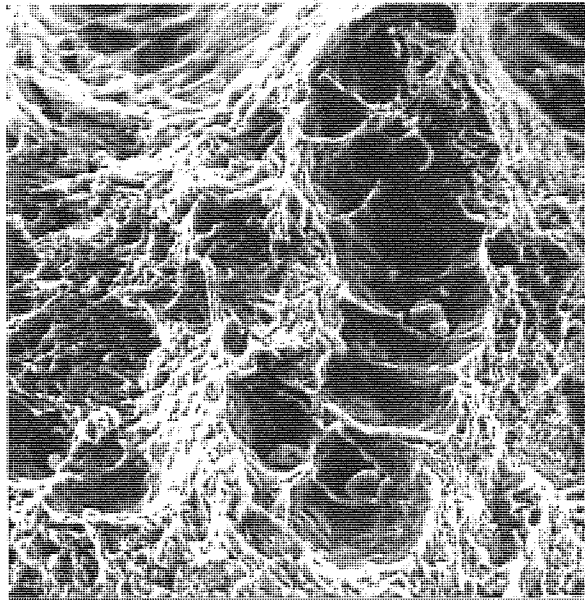


Plate 27 Material G. Fracture surface next to the fatigue crack tip showing details of the fracture. SEM (x1.1K)

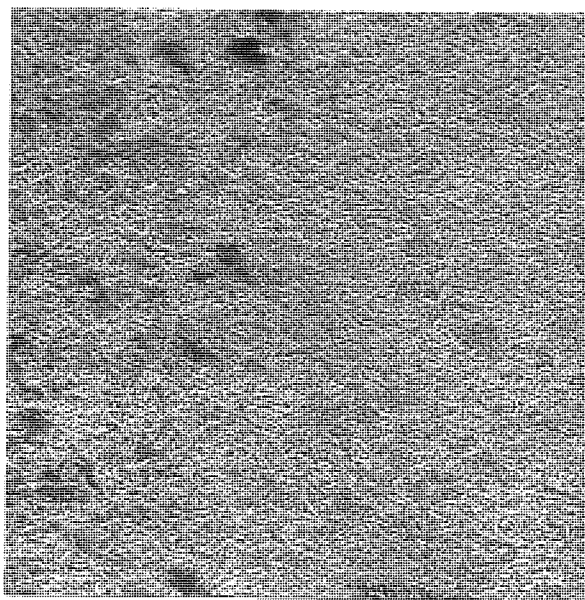


Plate 28 Steel G. Microstructure - Electroetching SEM (x260)

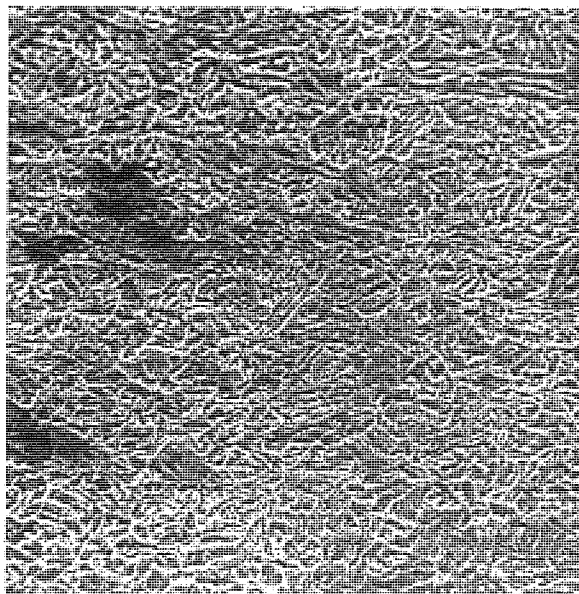
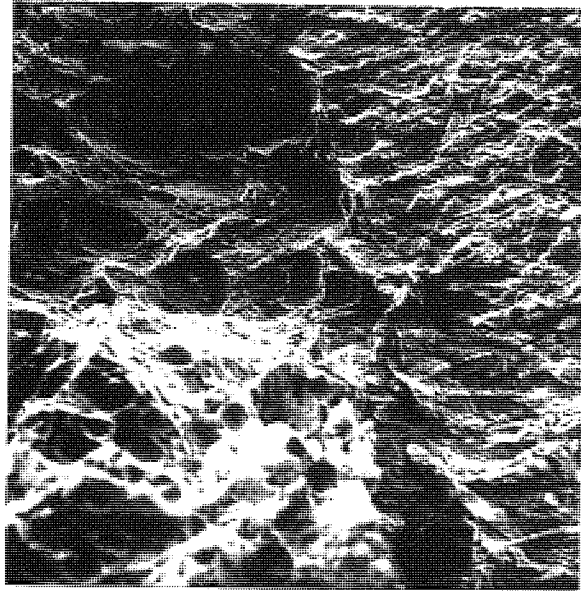


Plate 29 Steel G. Microstructure - Electroetching SEM (x640)



Direction of crack propagation

Plate 30 Steel G. Fracture surface at the fatigue crack tip.

SEM (x310)

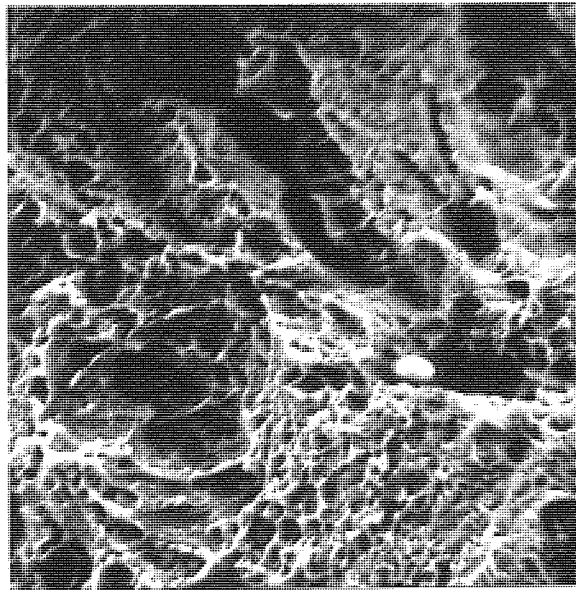


Plate 31 Steel G. Fracture surface next to the fatigue crack tip.

SEM (x330)

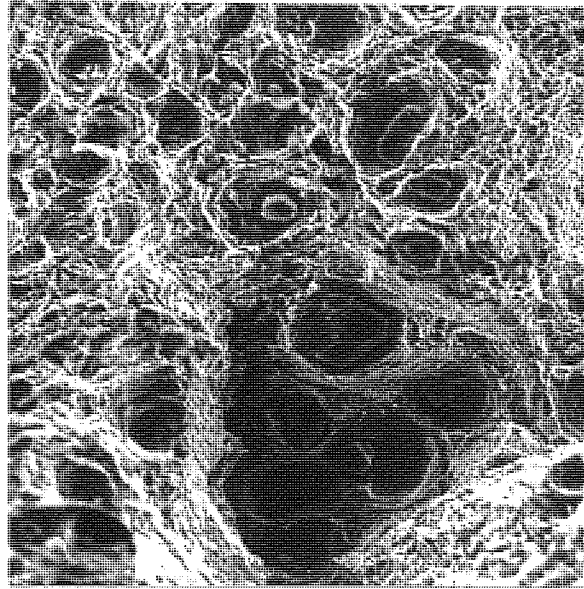


Plate 32 Steel G. Fracture surface next to the fatigue crack tip.

SEM (x560)

8.6 Steel D, Plain Carbon

Table 8.22 contains the results obtained from LEFM tests. Also tabulated are the thicknesses, widths, average crack lengths, K_Q and K_{max} values. Results are also shown graphically in Figure 8.16.

These results fulfilled the elastic linearity test in that the deviation from linearity on the load/COD curve was negligible at $0.8 P_Q$ as compared with that at P_Q as determined by the secant method. In spite of this the ratio P_{max}/P_Q was about 1.7 in all cases, showing that the deviation was plastic in origin, the rise in load occurring due to work hardening as a plastic zone began to cross the ligament. The electrical potential detection showed crack initiation well beyond P_Q . This sudden onset of plastic behaviour is akin to the sudden yielding which gives the upper and lower yield point and a Luders extension in wrought mild steels. A representative trace of load versus COD shown in Figure 8.17. The fracture surfaces shown in Plate 33 indicate conditions close to plane strain judging from the relatively small shear lips. The progression of cracking appears to oscillate between cleavage and fibrous fracture, probably because of repeated crack initiation and arrest.

Table 8.23 and Figure 8.16 show the K_{1C} values derived from J-integral tests. These tests were conducted on a range of thicknesses but with width constant at 45 mm. Also the K_{1C} values derived from J-integral tests were obtained for two small specimens cut from the halves of the large specimens.

The K_{1C} values obtained from these small specimens compared well with the results obtained from the bigger specimens.

A simpler method than the J-integral was introduced by Stonesifer et al (24) to derive K_C by a scaling method for tests just beyond the limits of LEFM. Figure 3.3 indicates their method. The fracture load is not taken as P_Q , but as the extrapolated linear elastic load at the fracture COD. Thus P_Q is estimated at P_B rather than P_A in Figure 3.3.

The above method was experimented with on the results generated here, but in this case the COD at fracture was detected by the electrical potential method and not the COD at maximum load as introduced by Stonesifer et al (24). These results are shown in Table 8.24 and in Figure 8.18 upon which is superimposed the K_{1C} from the J-integral method and the K_Q from the P_Q average for test pieces 25 mm thick. The method does not appear to have any special advantages and is based on less rigorous concepts than the J-integral.

Crack tip COD values, δ , using the linear relation between clip gauge COD values and δ (22, 23) and the experimental relation between clip

gauge displacement and crack opening displacement (24) are presented in Table 8.25. δ values were between 0.04 mm and 0.05 mm over a thickness range of 15 mm to 30 mm, obtained using the linear relation, while δ values were between 0.057 mm and 0.061 mm over the same thickness range, obtained using the experimental relation. In both cases the results showed no significant variation of δ with thickness. Using a K_{1C} value of $67 \text{ MN m}^{-3/2}$ from the J-integral results gives an average estimated value of the stress intensification value (the factor by which the yield stress is elevated by constraints) of 1.

A photomicrograph showing the typical microstructure of steel D is shown in Plate 34. The microstructure consists of fine grained ferrite-pearlite aggregate, with approximately 30% pearlite.

Fractography showed that the fracture mechanism was primarily by microvoid coalescence, as shown in Plate 35. The area examined was at the fatigue crack tip. Note that the dimples are small which accounts for the high toughness of this steel.

Specimen Number	Dimensions			K_Q MN/m ^{3/2}	K_{Ic} MN/m ^{3/2}	K_{max} MN/m ^{3/2}
	B mm	W mm	a mm			
Dlx1	24.99	44.98	23.83	41.83		80.10
Dlx2	25.01	44.97	23.55	53.07		74.29
Dlx3	25.02	44.51	24.51	47.92		68.40
Dlx4	24.97	44.99	23.74	51.61		77.53
Dlx6	25.00	44.98	23.76	49.55		68.30

Table 8.22 Fracture Toughness Results : Cast Steel D (Block 1)

Specimen Number	Dimensions			J with elastic corr'n MN/m	K _{1c} from J + el. corr'n MN/m ^{3/2}	J without elastic corr'n MN/m	K _{1c} from J no el corr'n MN/m ^{3/2}
	B mm	W mm	a mm				
D1(15,45)	15.10	44.83	22.03	1.62x10 ⁻²	60.71	2.03x10 ⁻²	67.78
D1(20,45)	19.95	45.02	23.15	1.99x10 ⁻²	67.23	2.24x10 ⁻²	71.31
D1(30,45)	29.70	44.71	22.58	2.17x10 ⁻²	70.05	2.55x10 ⁻²	76.06
D3(30,45)	29.98	44.83	22.71	2.04x10 ⁻²	67.97	2.40x10 ⁻²	73.74
D1(25,30,100)	24.97	29.94	17.29	1.92x10 ⁻²	65.95	2.10x10 ⁻²	68.98
D2(25,30,100)	25.02	29.95	14.92	2.12x10 ⁻²	69.25	2.42x10 ⁻²	74.00

Table 8.23 K_{1c} results derived from J_{1c} at fracture for Cast Steel D at various thicknesses (Block 2)

0.048	1.25
0.043	1.25
0.04	1.25
0.04	1.25

Specimen Number	Dimensions			K_Q $MN/m^{3/2}$	Corrected K_Q using the scaling method, $MN/m^{3/2}$	K_{max} $MN/m^{3/2}$
	B mm	W mm	a mm			
D1(15,45)	15.00	44.83	22.03	46.04	68.37	72.30
D1(20,45)	19.77	44.63	23.23	38.58	58.69	49.99
D2(20,45)	19.95	45.02	23.15	46.55	57.14	74.73
D1(30,45)	29.70	44.71	22.58	47.99	75.70	70.72
D3(30,45)	29.98	44.83	22.71	49.54	65.98	77.95

Table 8.24 Corrected K values according to the scaling method for steel D at various thicknesses.

Specimen Number	Dimensions			δ from eq'n derived expt. mm	n	δ from eq'n derived theoret. mm	n
	B mm	W mm	a mm				
D1(15,45)	15.00	44.83	22.03	0.063	0.95	0.048	1.25
D2(20,45)	19.95	45.02	23.15	0.057	1.05	0.043	1.39
D1(30,45)	29.70	44.71	22.58	0.059	1.02	0.044	1.36
D3(30,45)	29.98	44.83	22.71	0.060	1.00	0.048	1.25

Table 8.25 Crack opening displacement δ and stress intensification results for Steel D.

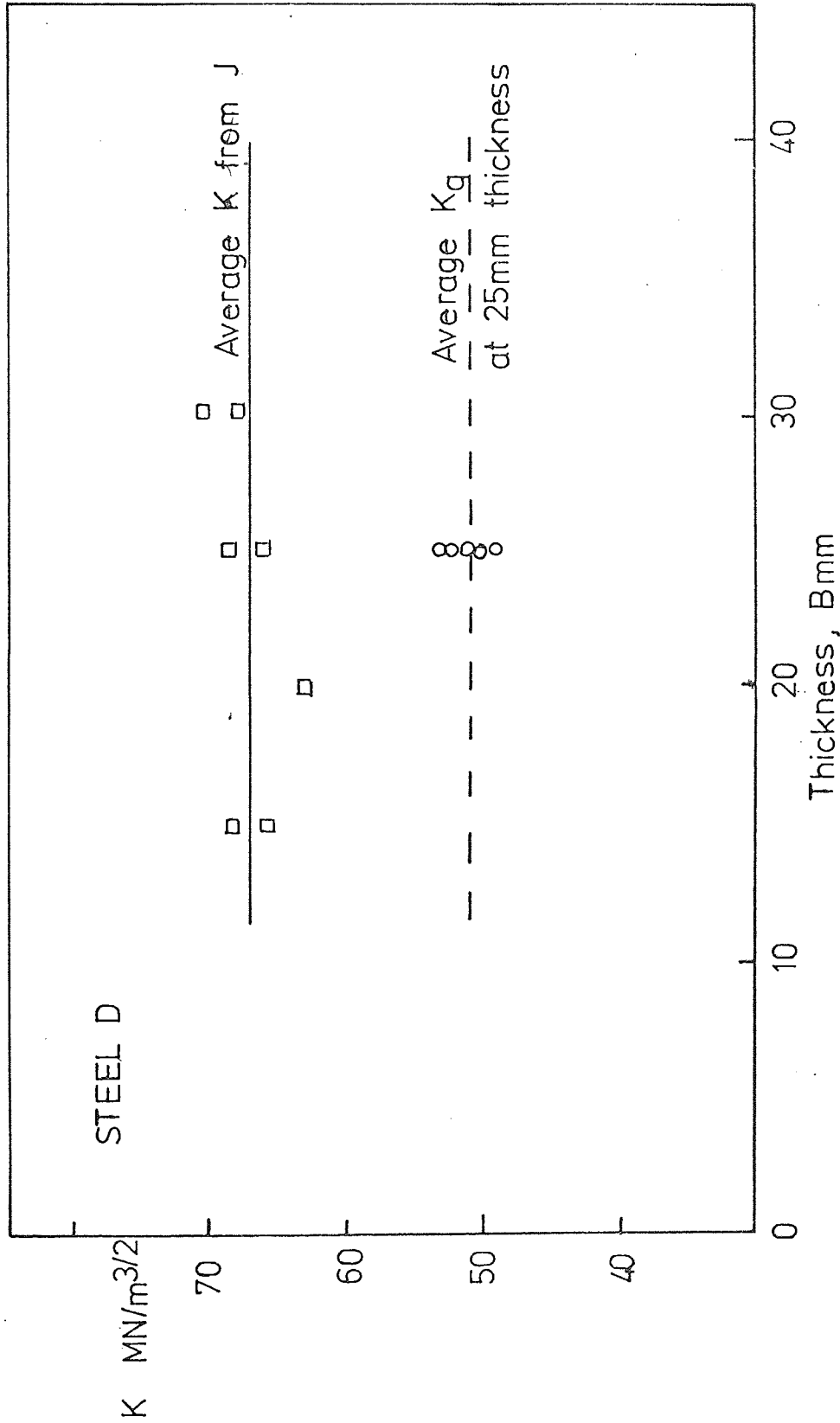


Fig. 8.16 K_{Ic} values derived from J at fracture initiation for steel D, compared with K_q values corresponding to sudden yield.

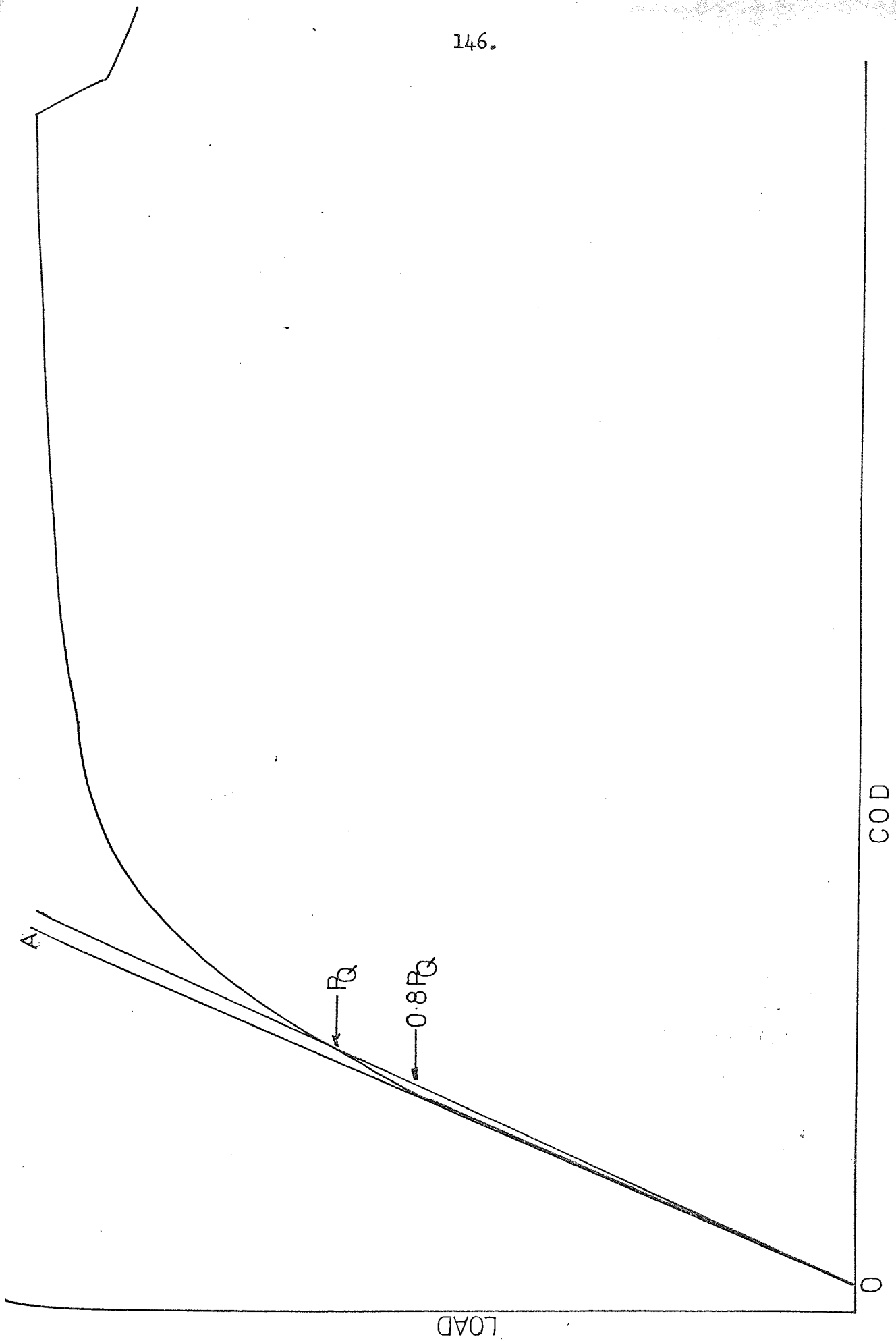


Fig. 8.17 Crack opening displacement versus applied load trace for

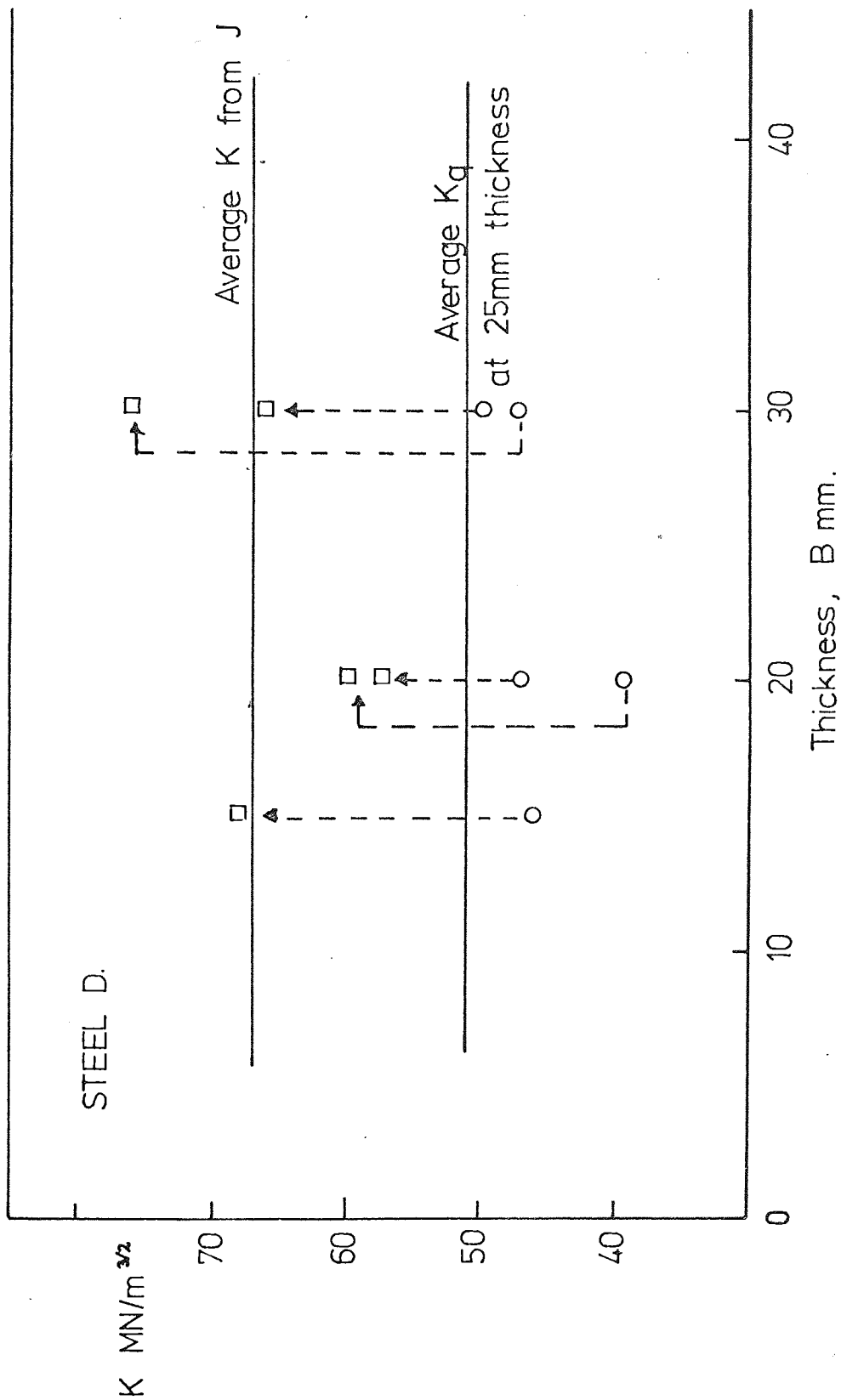


Fig 8.18 Squares indicate estimates of K_c using the scaling method, circles indicate K estimates from the load at fracture COD, P_A

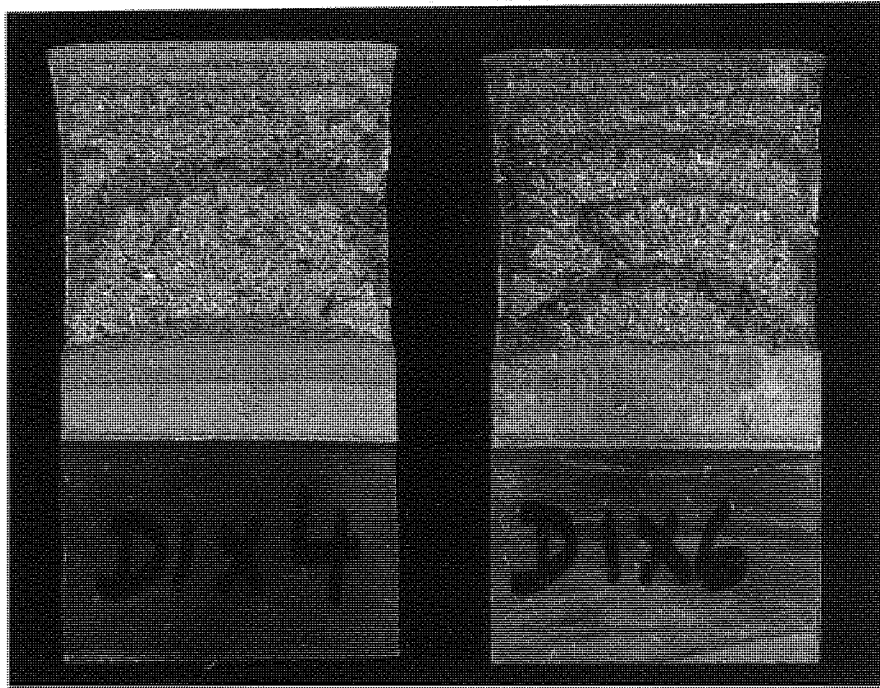


Plate 33 Fracture surfaces from 25mm thick specimens of Steel D.

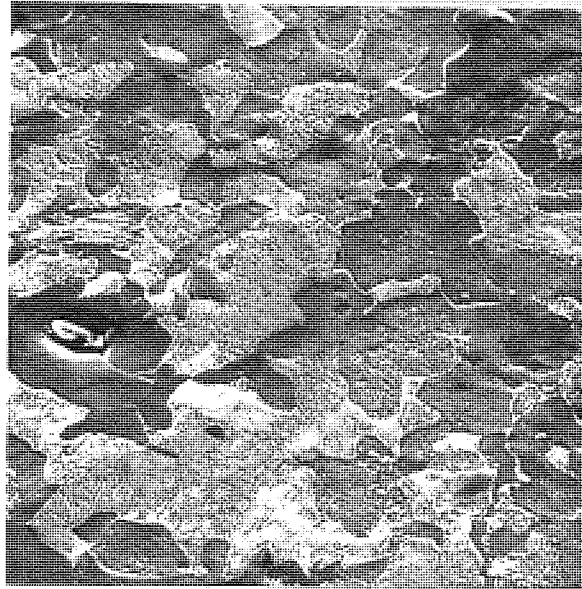
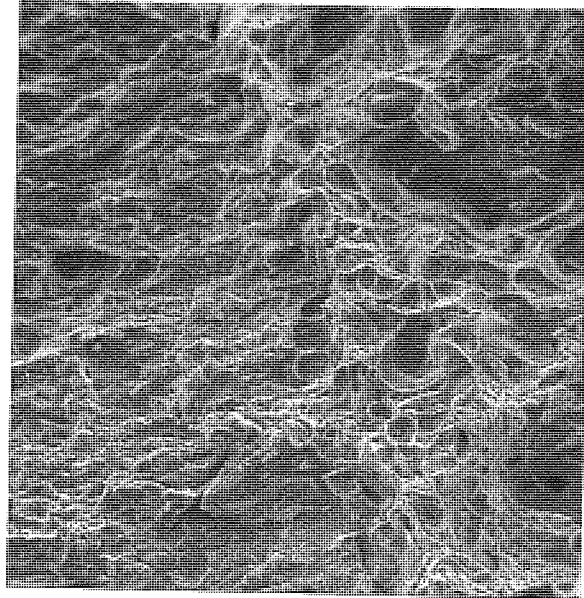


Plate 34 Steel D. Microstructure Electroetching. SEM (x680)



→ Direction of crack propagation

Plate 35 Steel D. Fracture surface at the fatigue crack tip.

SEM (x260)

8.7 Steel L, Plain Carbon

Steel L is a slightly higher strength plain carbon steel than steel D. Tests on the 25 mm thick specimen showed the same characteristics as those for steel D, the anomalous P_Q values again corresponding to no crack initiation and P_{\max}/P_Q about 1.7 in all cases. The K_Q values derived from P_Q values are shown in Table 8.26 and Figure 8.19. All the surface fractures were predominantly cleavage, as shown in Plate 36, and the lack of shear lips is consistent with plane strain fracture. A representative load versus COD trace is shown in Figure 8.20.

The results of K_{1C} derived from the J-integral test are presented in Table 8.27 and are shown in Figure 8.19. Toughness values derived from the J-integral tests remained at about $86 \text{ MN m}^{-3/2}$ down to a specimen thickness of 10 mm. The K_{1C} derived from the J-integral test using two small specimens cut from the halves of the large specimens also obtained and compared well with those results obtained from the large specimens.

Crack tip COD values, δ , were estimated using the linear relation between clip gauge COD values and δ (22, 23) and the experimental relation between clip gauge displacement and crack opening displacement (24) and are presented in Table 8.28. Crack opening displacements were in the range 0.05 to 0.10. Assuming a K_{1C} of $86 \text{ MN m}^{-3/2}$ the stress intensification value, n , varied from about 1.0 at a thickness of 10 mm, 45 mm width to 1.9 at 25 mm thick, 30 mm wide.

A photomicrograph showing the typical microstructure of steel L is shown in Plate 37. It can be seen from this plate that the microstructure consists of fine grained ferrite-pearlite aggregates, with approximately 85% pearlite.

The inclusion content of all the samples examined was very low. The level of porosity in all the specimens examined was also very low and consisted of evenly distributed micropores rather than large scale macroporosity.

The fractographic examination revealed that a mixed fracture mechanism had taken place with areas of microvoid coalescence separated by areas of tearing as shown in Plate 38. Also, it can be seen that the dimples are fine. This explains the high toughness of this material for generally it is more difficult (i.e. requiring greater energy input) to nucleate microvoids at small particles rather than large ones.

Specimen Number	Dimensions			K_Q MN/m ^{3/2}	K_{Ic} MN/m ^{3/2}	K_{max} MN/m ^{3/2}
	B mm	W mm	a mm			
L(1x2)	24.98	46.98	23.17	49.09		69.48
L(1x3)	25.01	44.97	24.21	49.02		62.95
L(1x4)	25.02	44.97	23.26	51.26		71.10
L(1x5)	24.98	44.97	23.64	47.20		62.69
L(1x6)	25.00	44.98	24.48	54.54		67.07

Table 8.26 Fracture Toughness Results : Material L (Block 1)

Specimen Number	Dimensions			J with elastic corr'n MN/m	K_{Ic} from J + el. corr'n MN/m ^{3/2}	J without elastic corr'n MN/m	K_{Ic} from J no el. corr'n MN/m ^{3/2}
	B mm	W mm	a mm				
L1(10,45)	10.00	45.01	22.75	3.28×10^{-2}	86.19	3.76×10^{-2}	92.32
L2(10,45)	10.01	45.01	22.85	2.56×10^{-2}	76.13	3.02×10^{-2}	82.75
L1(15,45)	15.01	45.01	22.88	3.63×10^{-2}	90.64	4.17×10^{-2}	97.13
L2(15,45)	14.68	45.02	22.77	3.02×10^{-2}	82.73	3.50×10^{-2}	89.01
L1(20,45)	19.76	45.01	22.37	3.42×10^{-2}	88.03	3.85×10^{-2}	93.37
L2(20,45)	19.96	45.00	25.13	2.90×10^{-2}	81.09	3.24×10^{-2}	85.60
L1(30,45)	29.99	45.01	23.03	3.02×10^{-2}	82.68	3.56×10^{-2}	89.84
L(1x5)	24.98	44.97	23.64	2.92×10^{-2}	81.25	3.31×10^{-2}	86.58
L1(25,35,120)	25.00	29.95	14.20	3.05×10^{-2}	83.15	3.50×10^{-2}	89.41
L2(25,30,120)	24.99	30.02	14.26	3.20×10^{-2}	85.15	3.68×10^{-2}	91.35

Table 8.27 K_c derived from J at crack initiation for Steel L with various thicknesses and for small specimens.

Specimen Number	Dimensions			δ from eq'n derived expt. mm	n	δ from eq'n derived theoret. mm	n
	B mm	W mm	a mm				
L1(10,45)	10.00	45.01	22.75	0.10	0.93	0.093	1.00
L2(15,45)	14.68	45.02	22.77	0.095	0.98	0.088	1.06
L1(20,45)	19.76	45.01	22.37	0.073	1.28	0.059	1.58
L2(20,45)	19.96	45.00	25.13	0.073	1.28	0.066	1.41
L1(25,30, 120)	25.00	29.95	14.20	0.055	1.70	0.049	1.90
L2(25,30, 120)	24.99	30.02	14.26	0.060	1.56	0.050	1.86

Table 8.28 Crack opening displacement and stress intensification factor
results for Steel L.

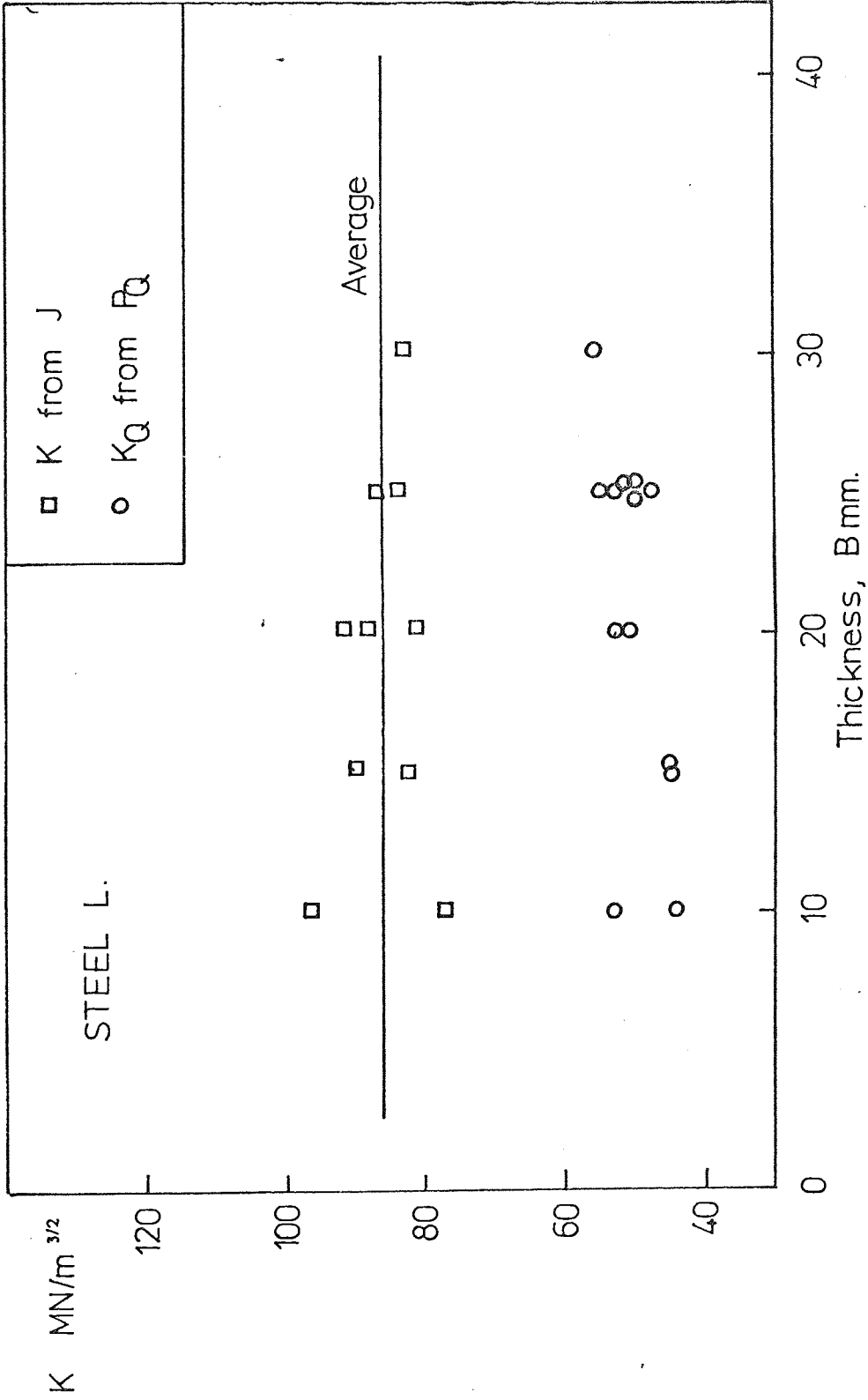


Fig. 8-19 K_{1c} estimates from J at fracture initiation in steel L, and K_Q values corresponding to sudden yielding.

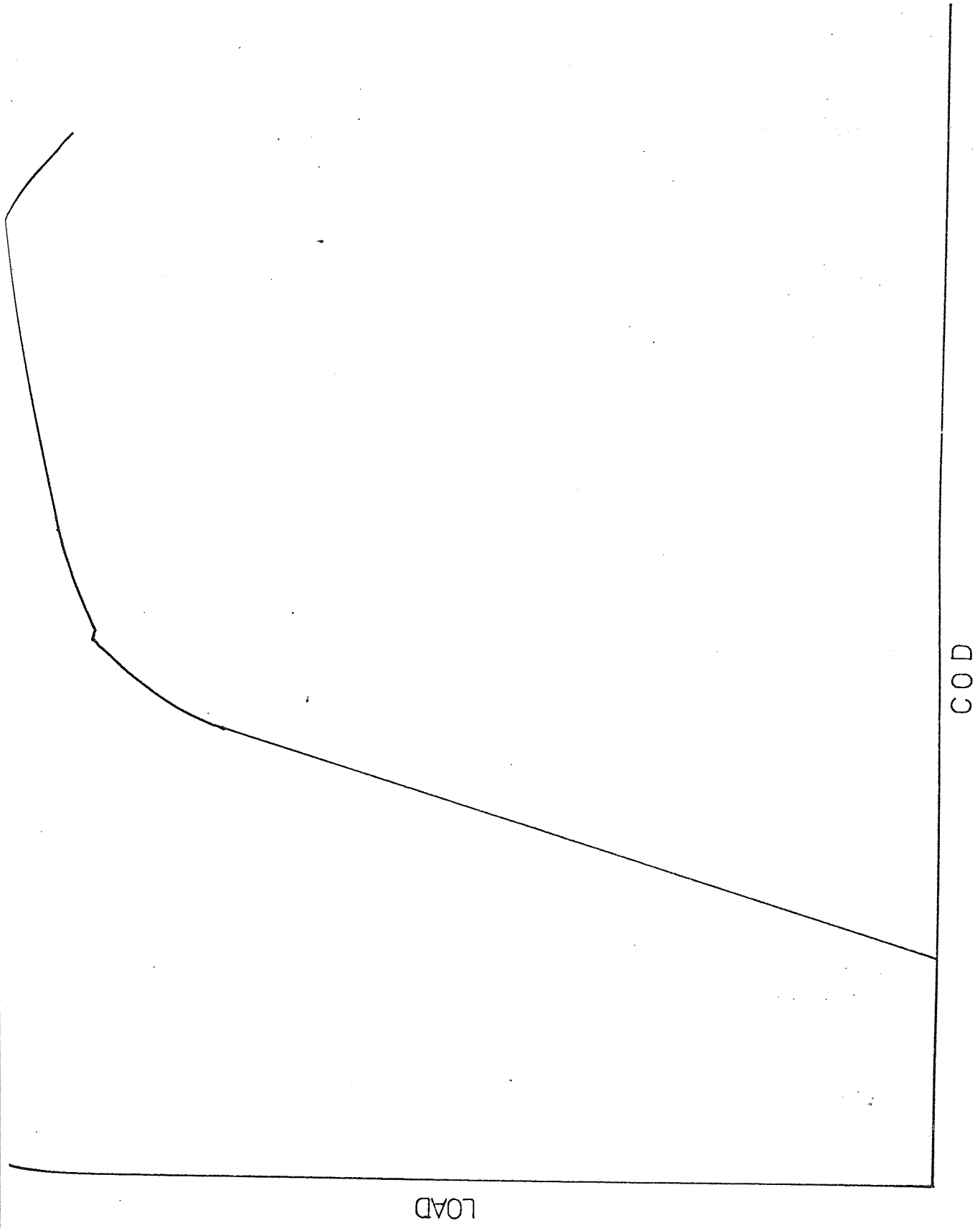


Fig. 8.20 Crack opening displacement versus applied load trace for Llx4.



Plate 36 Fracture surfaces of 25mm thick specimens from Steel L.

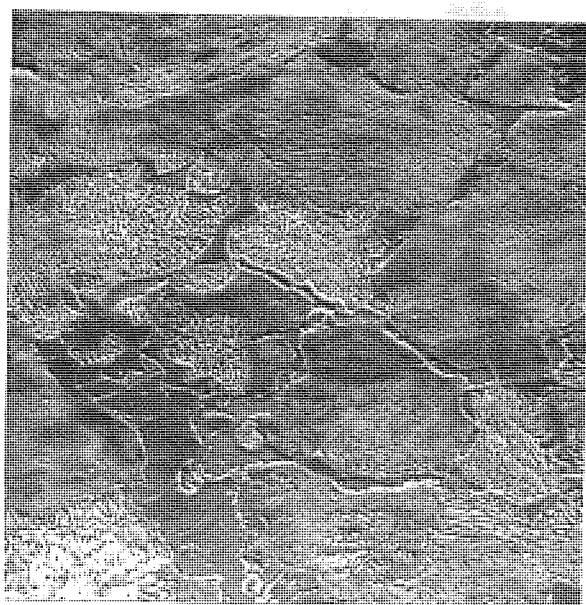
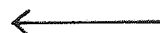
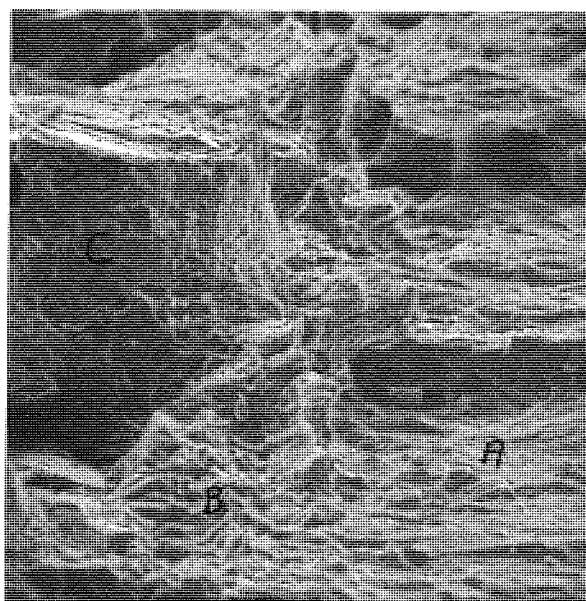


Plate 37 Steel L. Microstructure-Electroetching SEM (x1.15K)



Direction of crack propagation

Plate 38 Steel L. Fracture surface at the fatigue crack tip.

A-fatigue area, B-small dimples and C-tearing. SEM(x650)

8.8 Steel A, Carbon Manganese Steel

Steel A has a very high toughness but again showed the linear elastic behaviour followed by sudden development of a plastic zone. The K_Q values are listed in Table 8.29 and shown graphically in Figure 8.21. These values do not correspond to crack initiation but to plastic failure, once again the ratio P_{max}/P_Q was close to 1.7 in all cases. A representative load/COD trace is shown in Figure 8.22. These toughnesses correspond to predominantly cleavage surface fractures as shown in Plate 39.

Detection of crack initiation by the electrical potential allowed K_{1C} values to be estimated from J. These are around $140 \text{ MN m}^{-3/2}$ as shown in Figure 8.21 and Table 8.30. Crack tip displacement values, δ , using the linear relation between clip gauge displacement values and crack opening displacement (22, 23) and the experimental relation between clip gauge displacement and COD (24) are presented in Table 8.31. The crack tip δ varied from 0.18 to 0.29 mm and gave a stress intensification factor, n , of 0.9 ± 0.2 , assuming a K_{1C} of $138 \text{ MN m}^{-3/2}$.

Micrographs showing the typical microstructure of material A, A (1277), A (1276) are presented in Plates 40, 41 and 42 respectively. (Note that these different keel blocks were cast at different foundaries). It can be seen from these micrographs that the microstructure consists of a fine ferrite-pearlite aggregate, with approximately 50% pearlite, but it is worth noting that only material A contained colonies of bainite surrounded by large colonies of pearlite which suggests segregation of Manganese as shown in Plate 43. No valid fracture toughness value was obtained for this block and so it is difficult to relate these effects to material toughness.

A fractographic study of the fracture surfaces of three blocks tested, i.e. A, A(1277) and A(1276) showed that a variety of fracture mechanisms were operating during failure. For example, Plates 44 and 45 for specimen A indicate that fracture took place by cleavage with a small stretch zone. The actual areas examined in Plates 44 and 45 were at the fatigue crack tip which is the transition between the fatigue region and the main fracture area, in this case the fracture took place by cleavage.

Material A(1277) showed that crack extension process took place by the formation of a large stretch zone at the crack tip, resulting from shear deformation and slip associated with the development of the plastic zone. A typical stretch zone is shown in Plate 46. Distinct wavy marking can be seen running essentially normal to the crack propagation direction, these are characteristic of slip deformation. The subsequent fracture is by a cleavage mechanism as shown in Plate 47.

Material A(1276), however failed by void coalescence as can be seen in Plates 48 and 49. Plate 48 shows the fracture surface at the fatigue crack tip from which it can be seen that the width of the stretch zone was small in comparison to material A(1277). Plate 49 shows the fracture surface adjacent to the fatigue crack from which it is clear that fracture took place by the nucleation growth and coalescence of voids originating from second phases.

Specimen Number	Dimensions			K_Q MN/m ^{3/2}	K_{Ic} MN/m ^{3/2}	K_{max} MN/m ^{3/2}
	B mm	W mm	a mm			
Alx1	25.01	44.53	23.01	49.60		65.43
Alx2	25.01	44.88	25.39	49.16		71.23
Alx3	25.03	44.66	21.85	45.63		71.17
Alx5	25.03	44.85	23.28	48.06		70.68
A1 block3 A(1276)	29.99	59.95	29.88	53.13		84.98
A1 block4 A(1277)	30.00	60.01	30.42	56.39		86.89
A2 block4 A(1277)	30.00	60.01	31.25	56.39		91.05
A2 block3 A(1276)	24.98	50.01	25.39	51.64		77.39
A3 block4 A(1276)	24.63	49.95	25.98	51.09		80.83

Table 8.29 Fracture Toughness Results : Cast Steel A,A(1276),A(1277)
Blocks 1,3 and 4

Specimen Number	Dimensions			J with elastic corr'n MN/m	K_{Ic} from J + el. corr'n MN/m ^{3/2}	J without elastic corr'n MN/m	K_{Ic} from J no el. corr'n MN/m ^{3/2}
	B mm	W mm	a mm				
A1 block3 A(1276)	29.99	59.95	29.88	8.32×10^{-2}	137.23	9.04×10^{-2}	143.05
A2 block3 A(1276)	24.98	50.01	25.39	1.11×10^{-1}	158.54	1.17×10^{-1}	162.72
A1 block4 A(1277)	30.00	60.01	30.42	8.63×10^{-1}	139.80	9.44×10^{-2}	146.16
A2 block4 A(1277)	30.00	60.01	31.25	1.00×10^{-1}	150.55	1.08×10^{-1}	156.13
A3 block4 A(1277)	24.63	49.95	25.98	1.04×10^{-1}	153.23	1.10×10^{-1}	158.22

Table 8.30 K_{Ic} values derived from J at initiation for Steels A(1276) and A(1277)

Specimen Number	Dimensions			δ from eq'n derived expt. mm	n	δ from eq'n derived theoret. mm	n
	B mm	W mm	a mm				
A1 block 3 A(1276)	29.99	59.95	29.88	0.21	0.94	0.21	0.94
A2 block 3 A(1276)	24.98	50.01	25.39	0.22	0.95	0.23	0.91
A1 block 4 A(1277)	30.00	60.01	30.42	0.19	1.1	0.24	0.87
A2 block 4 A(1277)	30.00	60.01	31.25	0.19	1.1	0.19	1.1
A3 block 4 A(1277)	24.63	49.95	25.98	0.23	0.91	0.26	0.81

Table 8.31 Crack opening displacement and stress intensification factor values for A(1277) and A(1276).

The axes
Fig. 8.21 (a) values estimated from
values corresponding to (a)

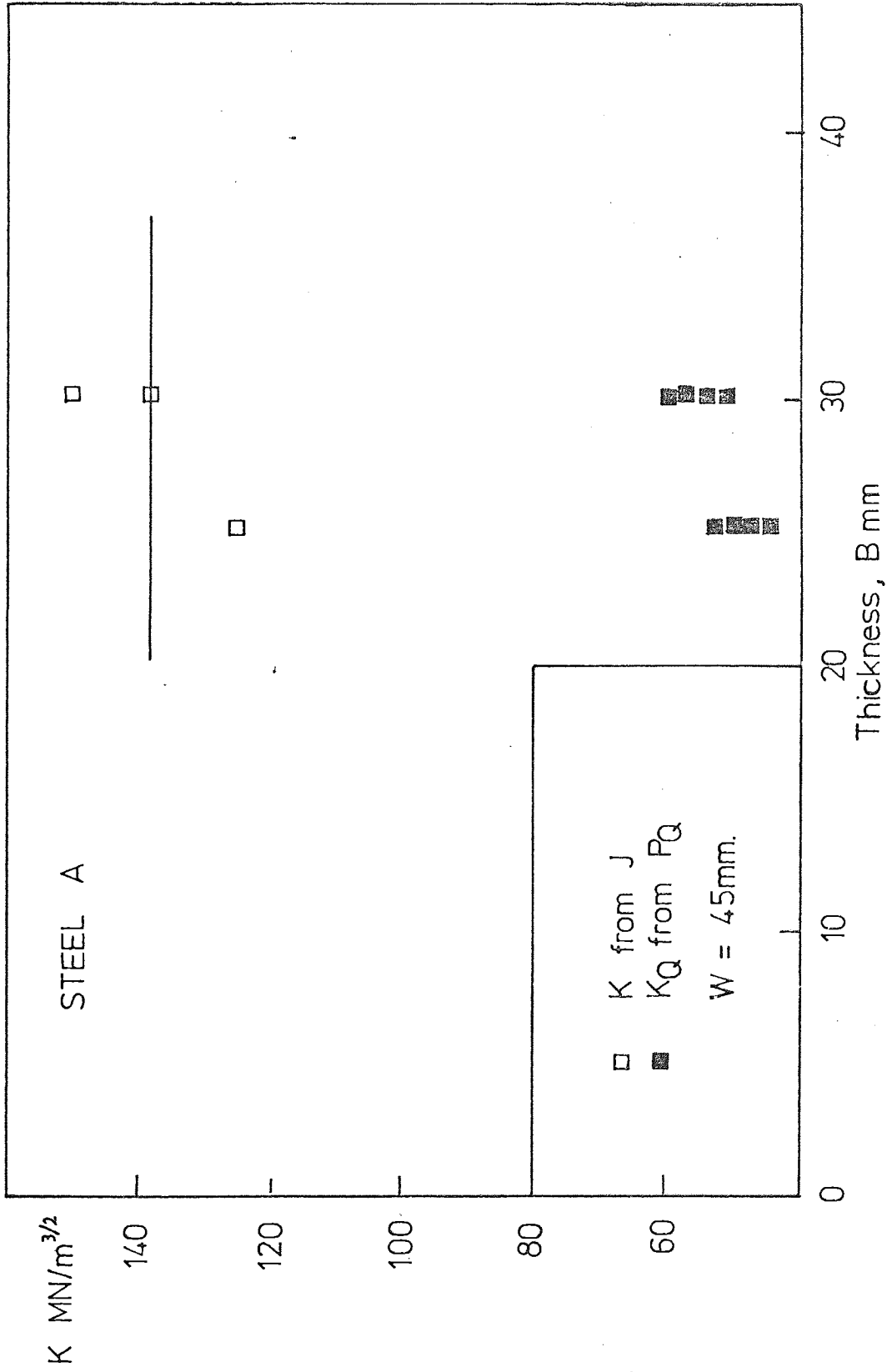


Fig. 8.21 K_{Ic} values estimated from J at fracture initiation and K_{Ic} values corresponding to sudden yield in steel A.

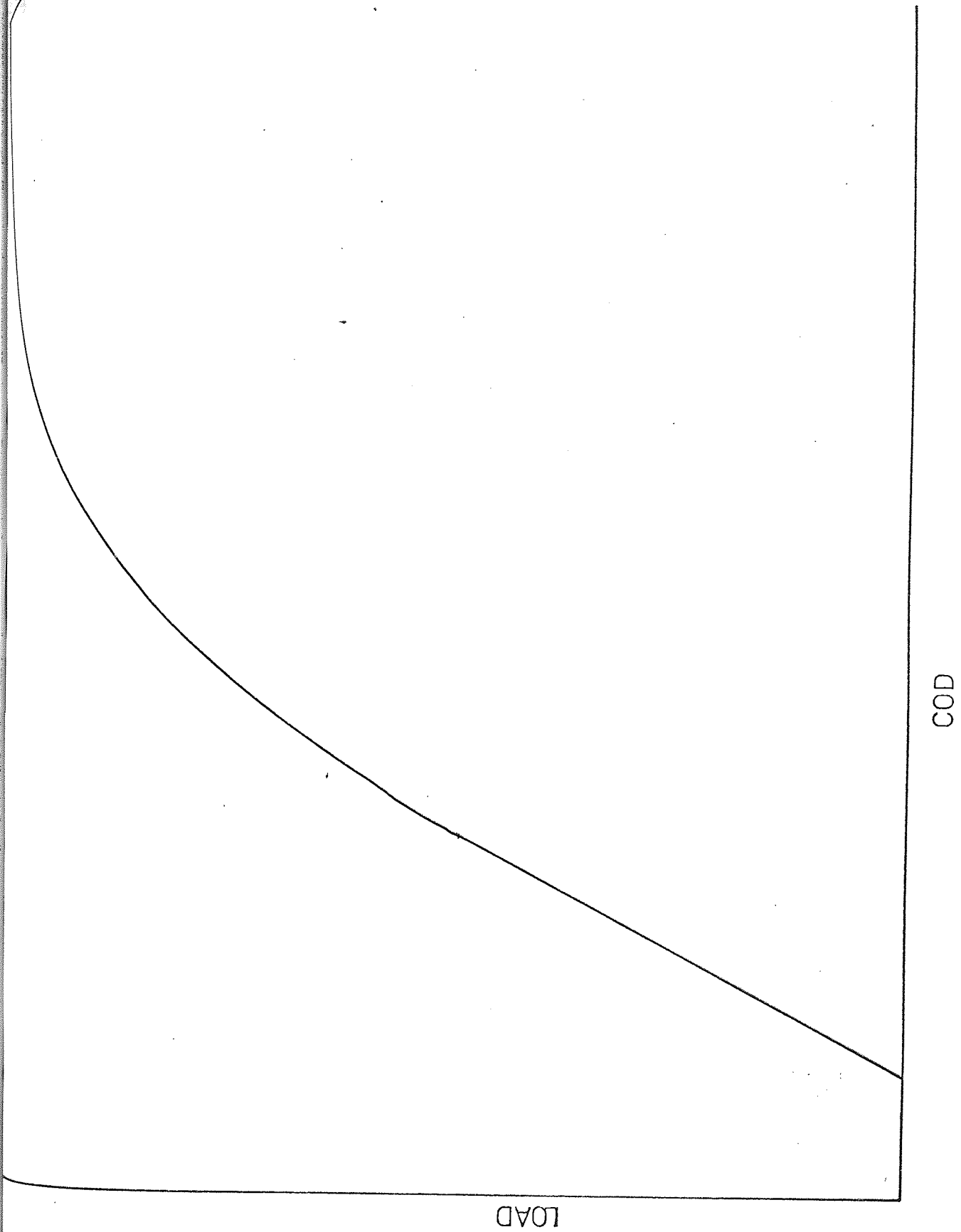


Fig. 8.22 Crack opening displacement versus applied load for A(1x5)



Plate 39 Fracture surfaces of 25mm thick specimens of Steel A.

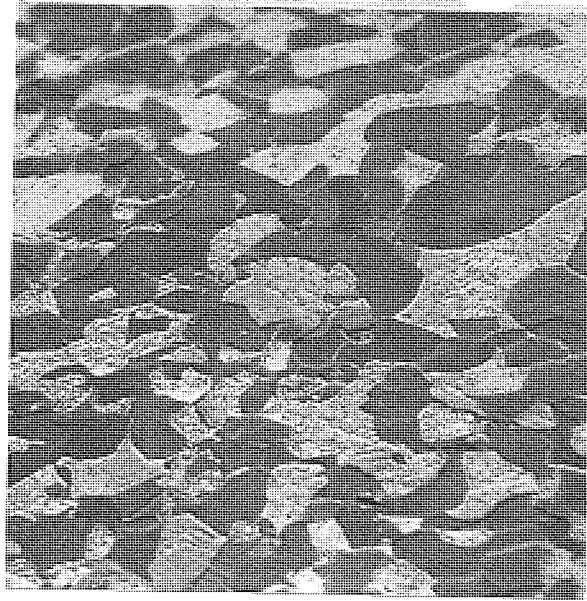


Plate 40 Steel A. Microstructure, conventional etching (x650)

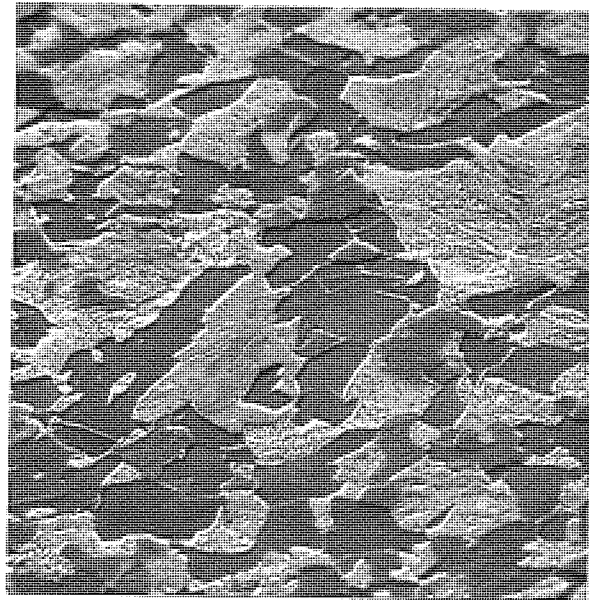


Plate 41 Steel A(1277). Microstructure, conventional etching (x750)

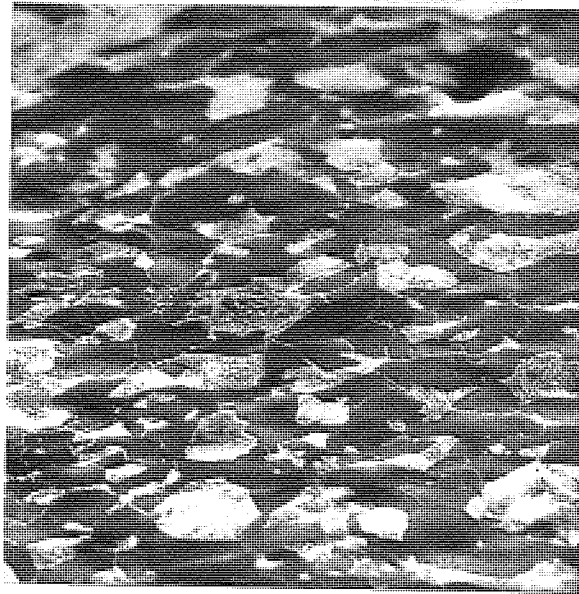


Plate 42 Steel A(1276). Microstructure, conventional etching (x650)

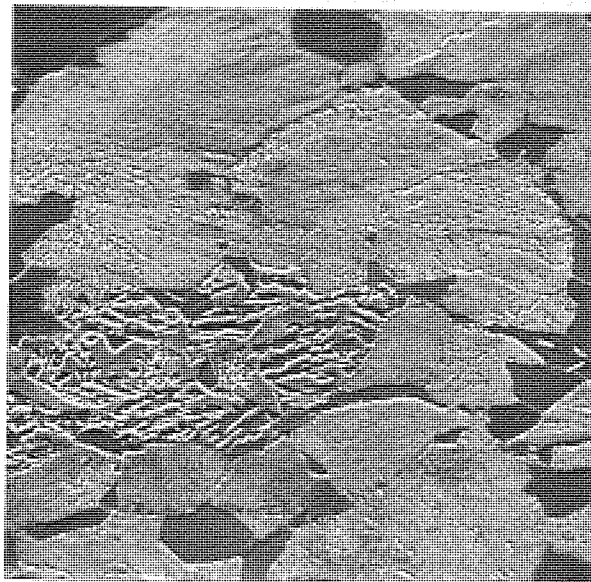
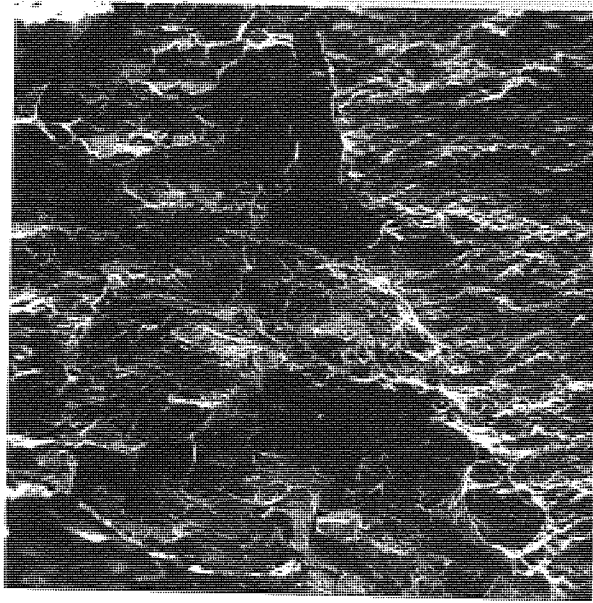


Plate 43 Steel A. Microstructure, conventional etching (x650)



Direction of crack propagation

Plate 44 Steel A. Fracture surface at the fatigue crack tip.
SEM (x150)

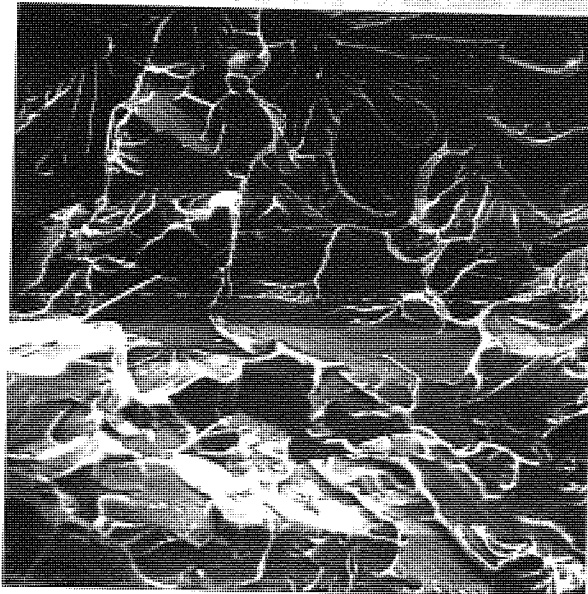
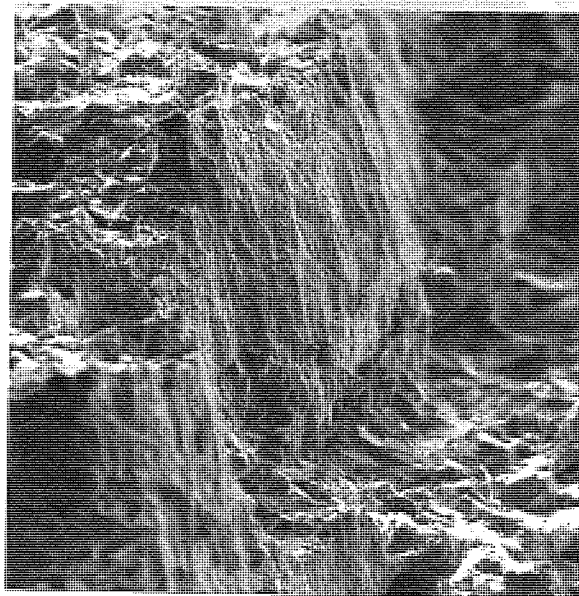


Plate 45 Steel A. Fracture surface next to the fatigue crack tip.
SEM (x750)



Direction of crack propagation

Plate 46 Steel A(1277). Fracture surface at the fatigue crack tip showing stretch zone. SEM (xl40)

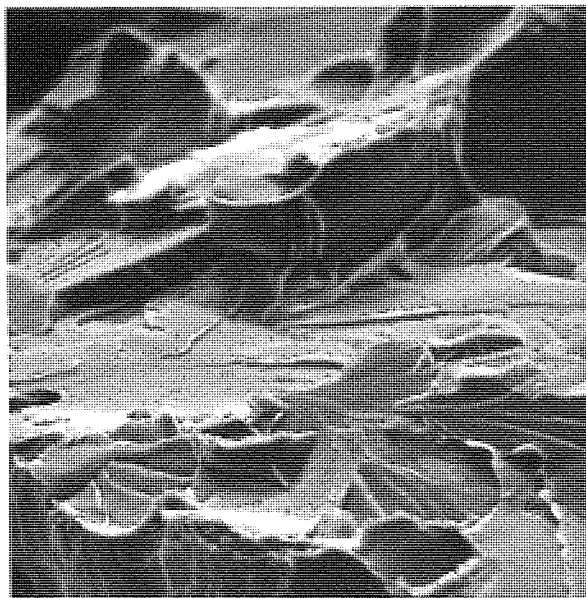
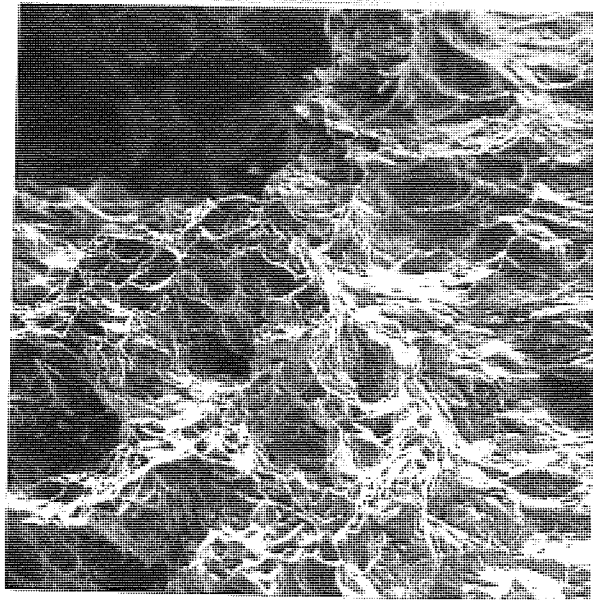


Plate 47 Steel A(1277). Fracture surface next to the fatigue crack tip. SEM (xl.45K)



Direction of crack prppagation

Plate 48 Steel A(1276). Fracture surface at the fatigue crack tip.

SEM (x260)

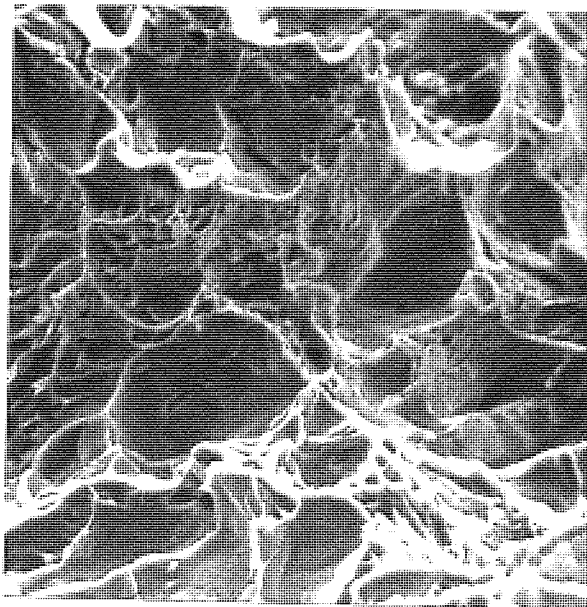


Plate 49 Steel A(1276). Fracture surface next to the fatigue crack tip.

SEM (x1.3K)

8.9 Steel F, $\frac{1}{2}$ Mn - Mo

Table 8.32 and Figure 8.23 contain the K_Q values obtained from LEFM tests. These results indicate an apparent toughness of around 61-75 $\text{MN m}^{-3/2}$. Two of the test results in Table 8.32 met the deviation from linearity condition for valid toughness values while the other tests did not. The P_Q values again correspond to no crack initiation with $P_Q/P_{Q_{\max}}$ about 1.7 in all cases. A representative trace of applied load versus COD is presented in Figure 8.24.

This steel was one of the toughest of the steels tested, as apparent from the size of the shear lips on the basic test specimens as shown in Plate 50. Unfortunately the test results showed the same scatter as those of steels G and steel C. K_Q values at the centre of the block were found to be lower than those at the outer edges.

Table 8.33 and Figure 8.23 contain the K_{1C} values estimated from J-integral. These tests were conducted on a range of specimen thicknesses but with W constant at 45 mm. Scatter on these results is felt to reflect variation in the material toughness.

Table 8.34 contains the COD results, obtained using the linear relation between clip gauge displacement and crack opening displacement (22, 23). δ varied from 0.19 mm at 10 mm to about 0.14 mm at 30 mm thickness. However because of the scatter in test results arising from variation of the material toughness in the cast block, it is not feasible to conclude anything from these results. The stress intensification factor, n, was found to be equal to 0.8 ± 0.2 when the individual K_{1C} results estimated for each specimen were used in the calculation.

Plates 51 and 52 show the microstructure of material F. For Plate 51 the first specimen was polished and etched using the conventional method while for Plate 52, the second specimen was prepared by electropolishing as described in Chapter 6. Note that, like materials G and C, light and dark areas can be seen in the microstructure which is an indication that the constituents have formed at different temperatures and have different mechanical behaviour. However in order to adequately correlate material microstructure with the toughest results a considerable amount of work would have to be done involving the electron microscope. This was beyond the scope of this thesis, the object of which was to obtain valid fracture data for a range of cast steels.

Fractography of the fracture surfaces revealed that the fracture mechanism was by microvoid coalescence. An example showing the fracture surfaces is shown in Plate 53, with the important area being immediately beyond the fatigue crack tip. Examination of the crack path shows that the fracture mode is fully ductile taking place by nucleation, growth and coalescence of voids as shown in Plate 54. In contrast to steel G, very few MnS particles were present in this steel.

Specimen Number	Dimensions			K_Q MN/m ^{3/2}	K_{Ic} MN/m ^{3/2}	K_{max} MN/m ^{3/2}
	B mm	W mm	a mm			
F2x1	21.01	42.00	22.06	72.17		101.52
F2x2	18.00	41.99	21.51	61.41		96.20
F2x4	21.00	41.99	21.06	75.29		109.33
F2x5	20.98	41.98	20.68	60.82		94.16

Table 8.32 Fracture Toughness Results : Material F (Block 2)

Specimen Number	Dimensions			J with elastic corr'n MN/m	K_{Ic} from J + el. corr'n MN/m ^{3/2}	J without elastic corr'n MN/m	K_{Ic} from J no el. corr'n MN/m ^{3/2}
	B mm	W mm	a mm				
F2x1	21.01	42.00	22.26	1.05×10^{-1}	154.3	1.16×10^{-2}	162.2
F2x2	18.00	41.99	21.51	7.65×10^{-2}	131.60	8.66×10^{-2}	140.05
F2x5	20.98	41.98	21.20	8.38×10^{-2}	137.73	9.29×10^{-2}	145.02
F1(10,45)	9.89	44.90	22.15	1.01×10^{-1}	151.50	1.21×10^{-1}	165.4
F2(10,45)	9.98	44.53	21.84	1.00×10^{-1}	150.59	1.21×10^{-1}	165.4
F2(15,45)	15.02	44.65	27.37	7.93×10^{-1}	133.96	8.87×10^{-2}	141.69
F1(20,45)	19.95	45.01	22.77	7.75×10^{-1}	132.49	9.37×10^{-2}	145.63
F2(20,45)	19.86	44.61	22.55	7.56×10^{-2}	130.83	9.10×10^{-2}	143.52
F1(30,45)	29.98	44.73	22.58	1.03×10^{-1}	152.63	1.23×10^{-1}	166.74
F2(30,45)	29.98	44.73	22.58	9.99×10^{-2}	150.40	1.17×10^{-1}	163.16

Table 8.33 K_{Ic} values derived from J at initiation for material F

(Block No's 2 and 3).

Specimen Number	Dimensions			δ mm	n
	B mm	W mm	a mm		
F1(10,45)	9.89	44.90	22.15	0.18	
F2(10,45)	9.98	44.53	21.84	0.19	
F2(15,45)	15.02	44.73	27.37	0.15	
F1(20,45)	19.95	45.01	22.77	0.10	
F2(20,45)	19.86	44.61	22.55	0.11	
F1(30,45)	29.98	45.01	22.62	0.13	
F2(30,45)	29.98	44.73	22.58	0.13	

Table 8.34 Crack Opening Displacement Results for material F
at various thicknesses.

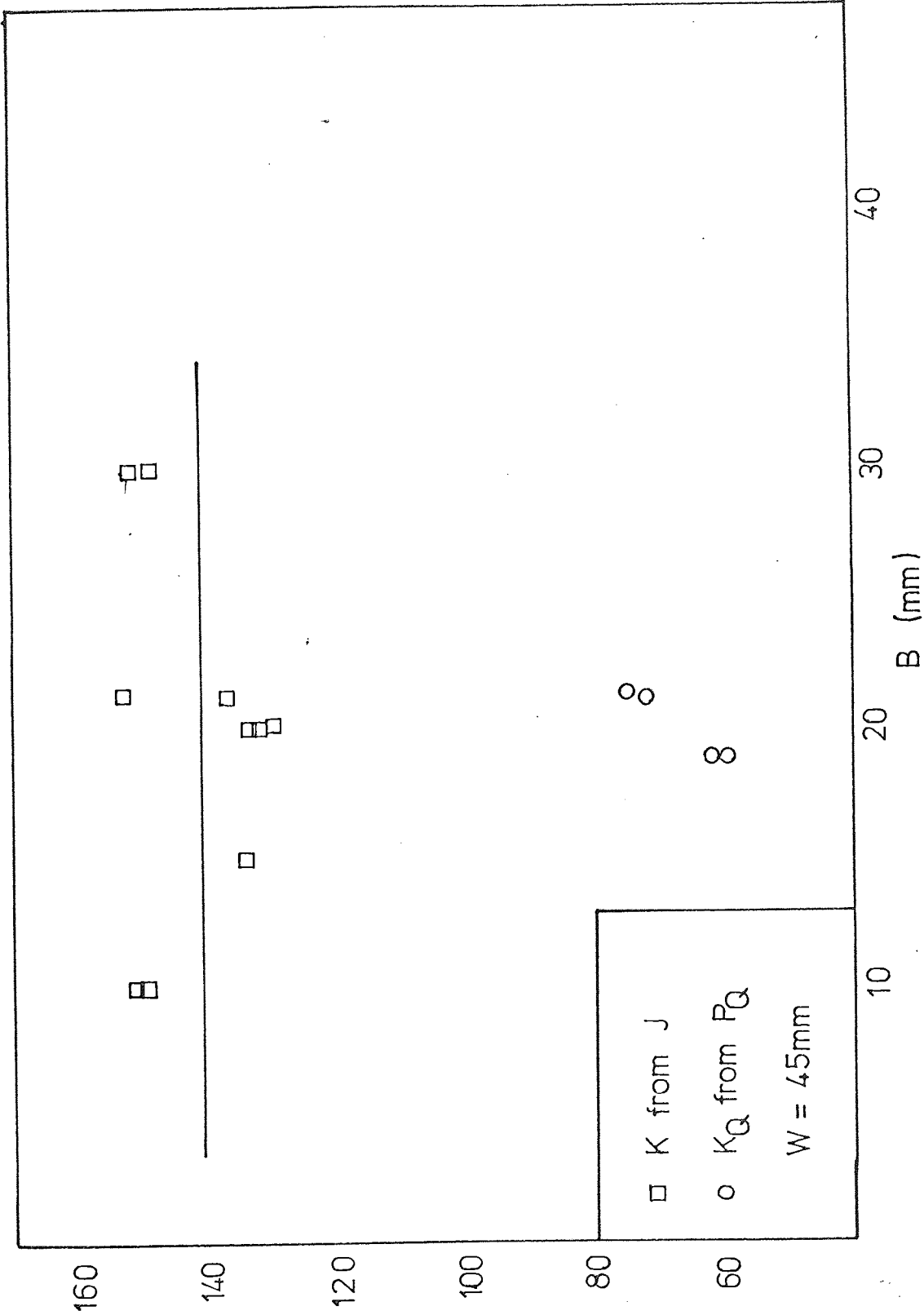


Fig. 8.23 K_{1c} values estimated from J at fracture initiation and K_Q values from P_Q in Steel F

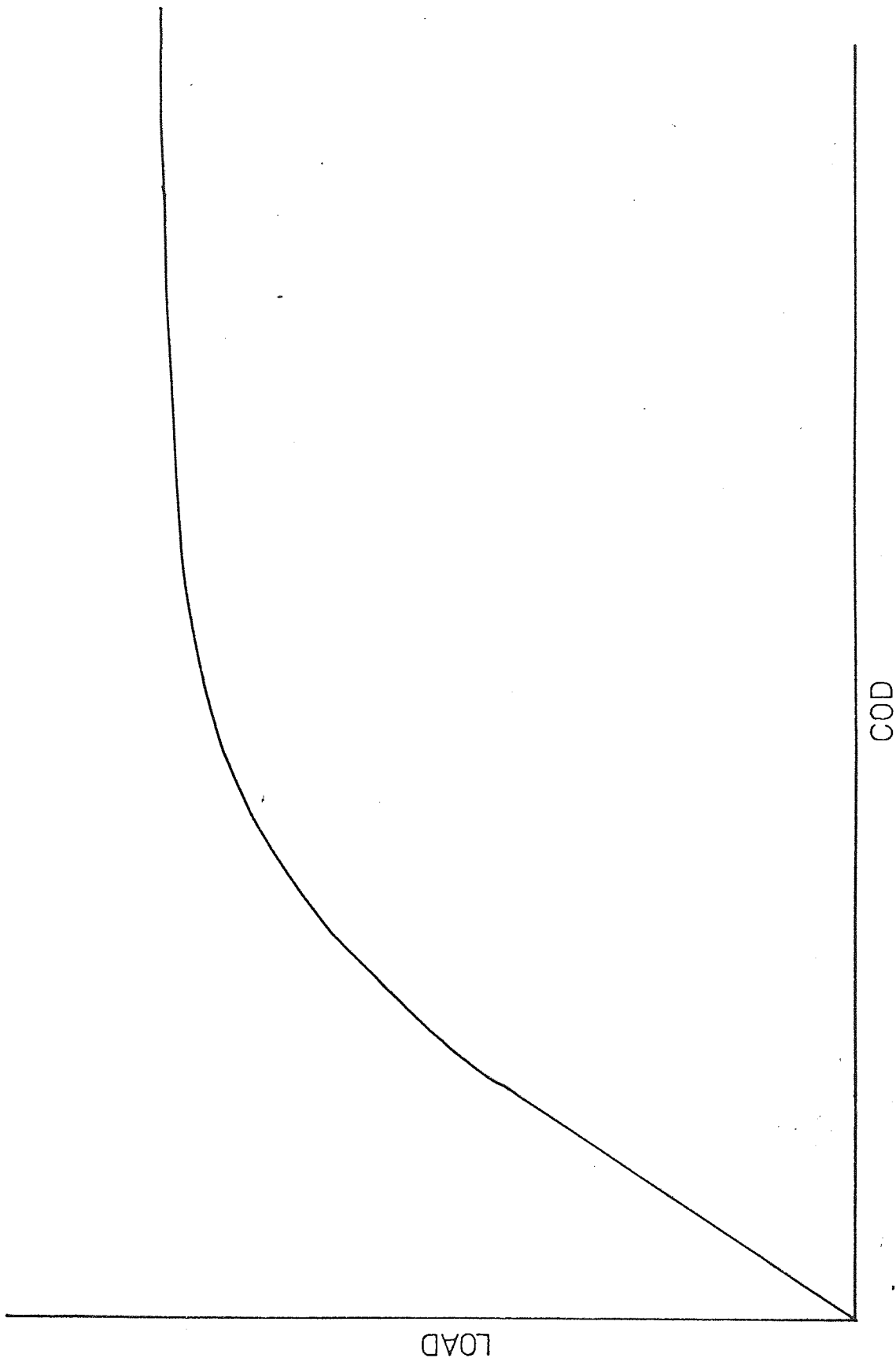


Fig. 8.24 Crack opening displacement versus applied load for F(2x4).

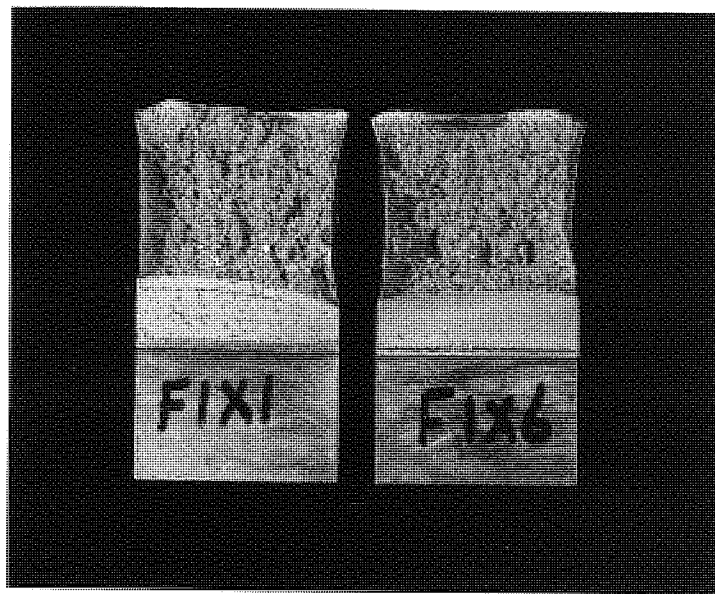


Plate 50 Fracture surfaces of 20mm thick specimen from Steel F.

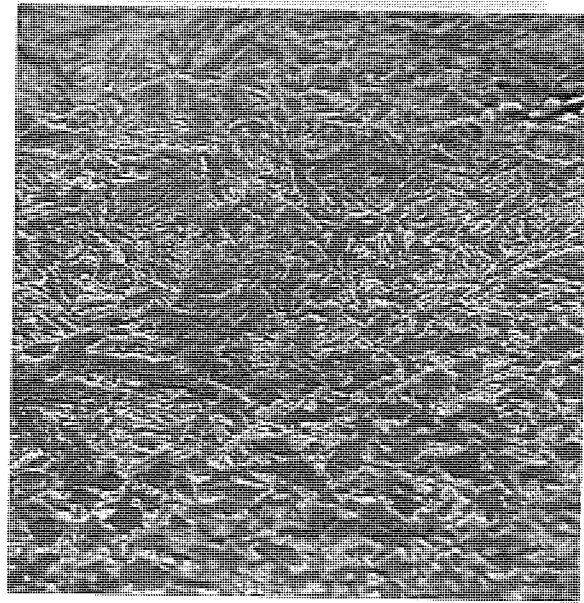


Plate 51 Steel F. Microstructure, conventional etching. SEM (x650)

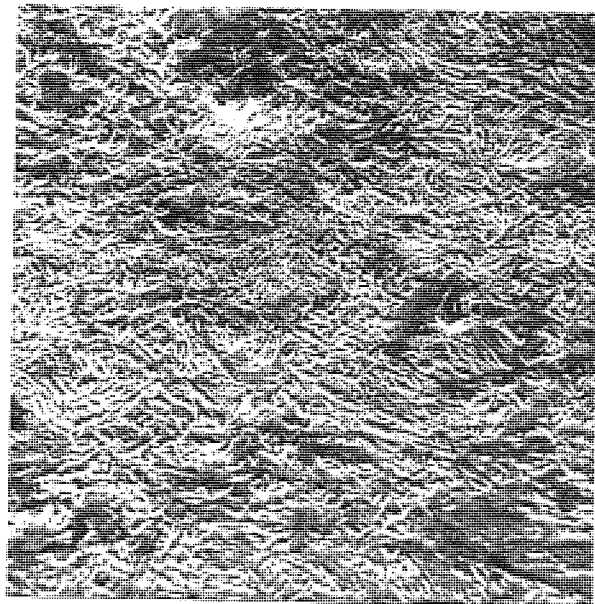
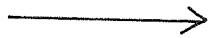
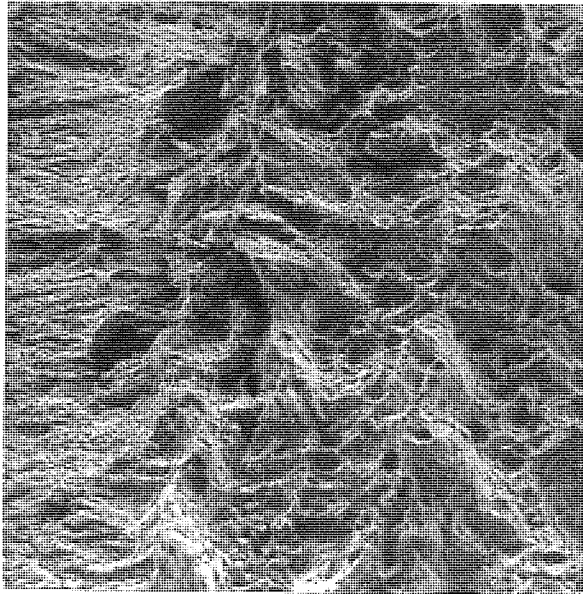


Plate 52 Steel F. Microstructure, electroetching. SEM (x650)



Direction of crack propagation

Plate 53 Steel F. Fracture surface at the fatigue crack tip.

SEM (x240)

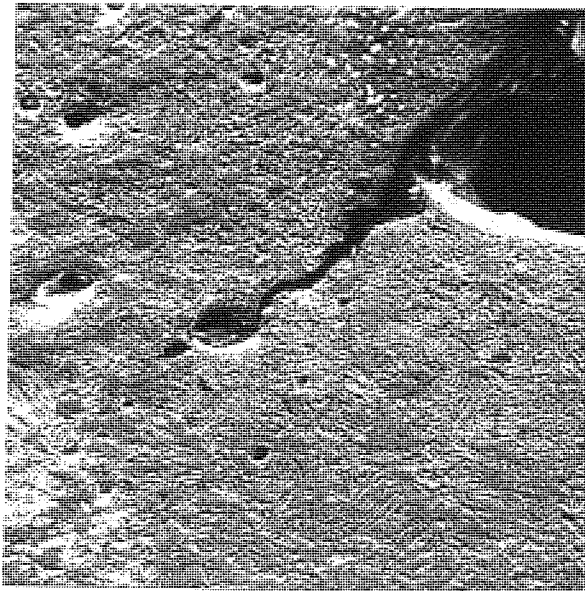


Plate 54 Steel F. Crack path. SEM (x260)

9. DISCUSSION

Cast steels are used extensively as engineering materials, often in situations where high dynamic stresses and unfavourable environments place large demands on the structural integrity of the materials. The obvious example of such a situation is in the case of pressure vessel components although there are other applications where cast steel has been employed or at least proposed as the material. Indeed, such is the use and potential of steel castings that they are now treated as a special class of engineering materials controlled by their own standards, (105) governing their composition. In view of these comments, it is perhaps surprising to discover that defect control in cast steels bears little or no relation to the defect tolerance of the particular steel based on fracture toughness considerations. According to current practice, defects are classed as deleterious more or less on the basis of whether they are detectable by radiographic methods. Although these methods are probably adequate, when combined with practical experience, for the higher strength steels, they bear little reference to the real defect tolerance of the more commonly used steels. In the case of plain carbon or carbon manganese steels, which are used extensively as casting materials, although they have a high toughness they are controlled by concepts of defect tolerance generally applicable to higher strength steels which are often more brittle.

It is worth noting in passing that the practice of removing defects castings (generally by grinding) then re-filling with weld material can have an adverse affect on the structural integrity of the casting, (106). Or, stated more bluntly, in certain cases it is better to leave the original defect rather than attempt a repair weld. Clearly, a greater understanding of the fracture characteristics of cast steels is required if steels are ever to realise their potential as cast components.

In view of these comments, and since little information on K_C or K_{IC} values for cast steel is available (107,109) a programme to examine the fracture properties of some of the common types of steel castings was set-up. For convenience, all experimental testing was to be carried out on a single edge-notched specimen geometry loaded in three-point bending. Each specimen was to be assessed using the three main currently available methods of fracture toughness testing, namely:-

- a) Linear Elastic Fracture Mechanics (LEFM).
- b) The J-Integral Method.
- and c) Crack Opening Displacement Measurement (COD).

An experimental set-up was proposed such that all measurements necessary for the above methods could be recorded simultaneously during testing of a single specimen. This was desirable since it was envisaged at the outset that the lower strength steels would not behave in a linear elastic manner, and that by using all methods conjointly on the higher strength steels which were expected to behave in a linear elastic manner this would give useful comparisons and confidence in the toughness assessments on the lower strength steels using general yielding fracture mechanics. This was in fact borne out by the experimental results obtained.

For clarity of presentation, the following general discussion has been divided into five sections. The first three of these deal with the results obtained from and the usefulness of three methods of fracture toughness assessment mentioned above while the fourth contains a comparison of the J-integral method and the COD method and their relative merits. The last section contains general comments on the metallography and fractography of the steels tested.

Linear Elastic Fracture Mechanics

The plane-strain fracture toughness parameter is a material property and as such does not depend on specimen configuration or specimen size. Although this statement is axiomatic it has thus far proved impossible to devise a reasonable experimental set-up such that only plane strain conditions exist ahead of a crack tip. Consequently, and particularly for high toughness steels, a so-called mixed mode of fracture comprising plane strain and plane stress states will be operating. Under these circumstances a material K_{1C} will never be obtained, but in certain circumstances and for certain specimen dimensions, an acceptable K_{1C} value can be determined. Before proceeding to a discussion of these points, with particular relevance to the cast steels examined, it is of value to expand on the influence of 'plane stress' on K_Q .

If, apparent fracture toughness values obtained from experiments, say K_Q 's, are found to vary with specimen dimensions then clearly a mixed mode fracture is taking place and the specimen is undersized. (Usually, increase in specimen dimensions causes a reduction in K_Q , see Figure 3.2). There is therefore a minimum specimen size, below which mixed mode fracture will take place. This size can be shown to depend on the ratio between toughness and yield stress for the material which is also linked to the size of the plastic zone ahead of a crack tip. The limits on specimen dimensions discussed below are based on this ratio which give an indication of whether valid K_{1C} results have been obtained from a given experiment.

The draft British Standard for toughness testing DD3 (102) and ASTM committee (104) have set minimum specimen size limits and recommendations for determining test validity. One recommendation is the linearity condition which states that the deviation of the test record from line OA at a load $0.8 P_Q$ is less than one fourth of the deviation from linearity of the test

record at P_Q as shown in Figure 8.17 For all the cast steels examined, the deviation from linearity on the load/COD curve was negligible at $0.8 P_Q$ as compared with that at P_Q as determined by the secant method. An unusual feature in many of the steels tested, with reference to this linearity condition, is that yield at the crack tip is delayed up to a fairly high load before spreading rapidly ahead of the crack tip. This gives rise to a load/COD curve which appears to be linear elastic, with a deviation arising from a compliance change due to cracking, when in fact no cracking has taken place. In these cases, P_Q does not correspond to crack initiation. Crack initiation actually occurred at a higher load as detected by the electrical potential method. Also, the ratio P_{max}/P_Q was about 1.7 in all cases, showing that the deviation was caused by plastic flow.

More confusing fracture behaviour was observed from the results of experiments on material D, L and A. For these materials sudden yielding did take place giving the appearance of LEFM behaviour. Also, the fracture surfaces showed that fracture had taken place by a predominantly cleavage mechanism as shown in plates 33, 36 & 39 where the lack of shear lips is consistent with plane strain fractures. Such behaviour has been confirmed by other workers on these steels (115) and can only be an artifact in the fracture behaviour of these cast steels. However, the LEFM methods of DD3 (102) should be adequate to exclude this type of behaviour with much larger specimens than those tested here. For the smaller specimens it is necessary to confirm, by direct detection, that cracking has occurred.

The second recommendation for valid K_{1C} results is that no specimen dimension should be less than $2.5 \left(\frac{K_Q}{\sigma_{ys}} \right)^2$. These limits were based on results from tests on what might now be considered materials of medium toughness but are generally accepted to hold for all materials tested using LEFM. In materials M, B and C taken from the centre of the keel block, the basic

specimen size with 25 mm thickness gave valid assessments of the K_{1C} using the above recommendation, however when various thickness specimens were examined it was found that in steels M and B the toughness did not rise above the K_{1C} level down to 10 mm thickness. In steel B, the 5% secant method seemed to be detecting the actual point of initiation down to 10 mm thickness as confirmed by the potential drop method. For steel M however, although the 5% secant method seemed to detect crack initiation down to a specimen thickness of 20 mm, for the 10 mm and 15 mm thick specimens the apparent K_{1C} as shown in Figure 8.1 arose from the sudden onset of plastic behaviour, rather than by crack propagation.

Clearly the factor 2.5 is conservative in these cases giving specimen dimensions well in excess of those necessary to determine valid K_{1C} data, but from overall results obtained for the eight cast steels it is still advisable to use the factor 2.5 for cast steels to cover all materials over a range of toughness, and the final result interpreted in the light of experimental observations on fracture surface appearance, i.e. the mode and mechanisms operating.

The K_{1C} values determined for steels M, B and C can be used with confidence for defect tolerance calculations in actual castings using these steels.

As a result of the many experiments carried out, the general observation can be made that, if the ratio P_{max}/P_Q exceeds 1.10 with a smooth continuous Load-Displacement curve, then the apparent K_Q value will not be a good approximation to the plane strain fracture toughness of the material, K_{1C} . However, as stated above, each test must be considered separately and every variable should be taken into consideration, even the shape of the load/COD curve. For example, in the case of material B, which had a discontinuity in the Load-Displacement record, P_{max}/P_Q did exceed 1.1 but still the

fracture toughness results were valid as can be seen from the shape of the curve, Figure 8.6, which shows a region of increasing displacement with falling applied load followed by a further region of rising applied load prior to the final fracture. For this type of curve, the P_{\max}/P_Q criterion is not an important validity criterion. In other cases, where a smooth load/COD curve is obtained, as for material A, it was found that the linearity condition was satisfied, the dimension criterion was borderline but P_{\max}/P_Q was about 1.7 and the potential drop technique detected crack initiation at a much higher load than P_Q . Clearly the ratio P_{\max}/P_Q is an important parameter in the assessment for valid fracture toughness data.

The linearity condition for cast steels is not a particularly important criterion as sudden yielding took place with most of the steels tested. Larger specimens would not be expected to show this type of behaviour, however, it was inappropriate to fracture large specimens in this work as this would obscure any influence of casting position on toughness values. Also, in cases where casting position had little effect on toughness, the expense of determining plane strain fracture toughness values from exceptionally large specimens is prohibitive.

J-Integral Results

The J-integral method was employed in order to evaluate its usefulness as an alternate method to LEFM and COD for determining fracture toughness properties. At first sight J seems extremely attractive since its derivation was based on elastic-plastic analysis of conditions ahead of a crack tip. Also, the technique has been used successfully by Begley and Landes (51) as an elastic-plastic fracture criterion.

The first experimental measurements of J were obtained from experimental load versus load point displacement curves using a compliance technique where several specimens of varying crack lengths were required (51). In another

method derived by Bucci et al (56), load versus load point displacement curves were analytically derived from test pieces of the geometry of interest in adjacent crack sizes. Both these methods are time consuming and costly. A method by which J can be determined from single specimen is more desirable since the shape, size of keel block casting and the resulting cooling rate may well influence toughness. Also, it is more realistic to compare results obtained from the three methods (J , COD and LEFM) from the results of a single test specimen.

Fortuitously, there is an experimental technique available by which J can be determined from a single test specimen for the particular case of a deep crack in a three point bend specimen. This technique was developed by Rice et al (61) and is described in detail in Section 7.2 of this Thesis. Since the three point bend specimen geometry is used exclusively in this Thesis, J -integral values were determined using the technique referred to above. The method employs a load versus load-point displacement and the most significant feature is being able to locate the point on this curve at which a critical event took place in the fracture process. One possible aid in solving the problem of picking a measurement point may come from presenting the J data in the form of a resistance (R) curve as developed by Landes and Begley (63) which unfortunately also requires a number of test specimens to enable the construction of resistance curve and so for the reasons stated previously this method was not attempted. Although maximum load is sometimes taken as crack initiation this is not generally true and was not considered useful or valid for cast steels. The only real, simple alternative was to use the potential drop technique for locating the point of fracture initiation for measuring a critical J -integral value. This technique is described in detail in Section 7.4. The point of initiation was fixed when material separation had already taken place to some small degree as determined from the potential drop trace. A measurement

point taken earlier in the test would measure J_{1C} for a crack front geometry change only, while a measurement point taken later would introduce specimen size effects artificially. It was felt that a main objection to the use of the potential drop technique, if such be sought, seems to lie in the possible uncertainty concerning the point of failure, since the success of using the potential drop technique to determine J_{1C} could depend on the skill of the investigator in interpreting instrument signals. In fact it was found that by using the procedure outlined in Section 7.4 with a sensitive instrument such as the one used in this work, the point of initiation can be easily obtained with little or no ambiguity.

In those cases where the material behaves in an elastic/brittle manner (e.g. cast steels M, B and C at the centre of the keel block) and valid fracture toughness data is obtained by normal linear elastic method, the J-integral method also gives toughness data which compares well with normal linear elastic results. See for example Tables 8.4, 8.8 and 8.12. Smaller specimens for material M were prepared such that 'invalid' results would be obtained. J-integral values were determined using these small specimens, and the results were converted to K_{1C} values (Table 8.4). These were found to compare well with those previously found using 'valid' LEFM specimens. In terms of figure 8.5, failure was occurring for the small specimens at a moderate amount of plasticity. For cast steel C the results (Table 8.14 and Figure 8.12) offer further support to the concept of using J to determine K_{1C} . These results were for non-valid specimens. Figure 8.12 shows that the ratio of P_{max}/P_Q was about 1.7 indicating that the deviation from linearity was caused by plastic flow in the crack tip region. The mean K_{1C} value obtained from J_{1C} for these bend tests agrees almost exactly with the valid K_{1C} result obtained by the normal linear elastic method (Table 8.12). Note that the results obtained were for J with elastic correction, for an overestimate of toughness arises if the

δ_{total} is used to determine J without subtracting $\delta_{\text{no crack}}$ as shown in Figure 8.11.

These results from materials M and C offers further support that J does provide a one parameter description of the near tip environment, irrespective of the extent of the plastic deformation. This opens up the possibility of scaling the fracture event from a large to a much smaller specimen even though the load deflection behaviour of the two specimens will be very different. Results obtained here appear to indicate that specimen size appears to have little or no effect on J_{1C} values.

A specimen size requirement on the use of J has been recommended as:

$$a, B, b > \alpha \left(\frac{J_{1C}}{\sigma_Y} \right)$$

where a = crack length, B = thickness, b = uncracked ligament
 σ_Y = yield stress and α was assumed to be 25 and 50. Landes and Begley (51) found that from the results obtained that $\alpha = 25$ would give a suitable specimen size requirement for the material. At present this is merely a recommendation and a great many more results are needed to undertake a more thorough evaluation of specimen size effect on J_{1C} . In this Thesis, while all the specimens tested satisfied the above requirement, results seemed to indicate that the factor 25 was rather small. However, until further experimental work is undertaken it is perhaps wise to adhere to this value.

From the above comments it can be concluded that the J-integral technique represents a practical and accurate method of toughness assessment even with specimens as small as 20 mm wide and 10 mm thick as for instance, in the case of steel M. However, experience with K_{1C} testing clearly shows that it is unwise to draw firm conclusions from limited test data, but as

can be seen from the results obtained herein, the K_{1C} values obtained from the J-integral were in excellent agreement with the K_{1C} values obtained using conventional methods. Thus, this agreement between the elastic-plastic and linear elastic critical fracture toughness values indicates that the elastic plastic J_{1C} fracture criterion, based on the path independent J-integral proposed by Rice (49) does extend the concepts of linear elastic fracture mechanics into the elastic-plastic and fully plastic fracture regimes. It should now be possible to obtain critical fracture toughness values with small specimens.

The excellent comparison of results obtained for materials M and C and the ability of J-integral to predict failures in cases of large scale yielding, gave confidence in estimating toughness values for materials L, D, A and F where the material behaved in an elastic/plastic manner. The estimates of K_{1C} for these steels are $86 \text{ MN m}^{-3/2}$ for L, $67 \text{ Mn m}^{-3/2}$ for D, $138 \text{ MN m}^{-3/2}$ for A and $130 \text{ MN m}^{-3/2}$ for F. These are relatively tough materials and critical defect sizes derived from these figures would indicate defect tolerances much greater than appreciated by current codes of practice for pressure containing parts, for instance.

The most important advantage of the development of the critical elastic plastic fracture toughness J_{1C} criterion is its ability to predict failure in cases of large scale yielding, that is, use of small specimens which give tremendous savings in both material and machining costs relative to the specimen sizes required for J_{1C} as opposed to K_{1C} fracture toughness tests. For instance, to obtain a valid fracture toughness value through the LEFM method for material A, a specimen of at least 28 cm thick is required to obtain valid linear elastic K_{1C} fracture toughness test results. Another advantage is that since only small specimens are now required for fracture toughness testing, the effect of cooling rate, casting position or any structural effects can be examined, since ample material is available

to manufacture the necessary fracture toughness test specimens from any position in the casting. For example, in material G where there was segregation of sulphur to the centre of the block it was found that one small specimen had a low toughness in comparison to the others. After further examination it was found that this specimen in particular contained a high percentage of sulphur, so now it is possible to specify minimum fracture toughness standards as an integral part of the material specifications and acceptance standards.

Crack Opening Displacement Results

In order to evaluate the usefulness of COD as a fracture criterion and to present as complete a record of results as possible, COD values were recorded for each specimen tested. The method used for determining COD values is the one described in DD19 (40). At the present time this is the only document which gives details of a recommended procedure for COD testing which is the most widely used method for assessing fracture toughness of elastic/plastic materials. Having decided on a technique of measuring the COD, it was then necessary to make a decision on what point on the load/clip gauge displacement curve was to be taken as representing the critical event in the fracture process. It can be seen from the literature review, Section 4.2 that the established 'material property' appears to be COD at initiation of crack growth. Also, because it is the same point used for measuring critical J-integral values, J_{1C} , this makes it easier to compare results obtained using the two criteria. The potential drop technique described in Section 7.4 was used for locating the point of initiation.

The results will be discussed alongside the two methods proposed in DD19 (40) for the calculation of crack tip COD values from clip gauge displacement V_c :

$$\delta = \frac{V}{\frac{3(a+Z)}{W-a} + 1} \quad (24)$$

This is the simplest relationship (40) and is based on the observed behaviour of COD specimens up to about 50 mm thick. According to the literature in DD19 (40) reasonable approximations to actual behaviour are obtained within the 50 mm thickness range and within the COD range 0.06 to 0.62 mm.

$$\delta = \frac{0.45 (W-a)}{0.45 W + 0.55 a + Z} \quad \left[V < \frac{\gamma \sigma_Y W (1-V^2)}{E} \right]$$

(22, 23)

$$\text{for } V > \frac{2 \gamma \sigma_Y W (1-V^2)}{E}$$

$$\delta = \frac{0.45 (W-a)}{0.45 W + 0.55 a + Z} \quad \left[\frac{V^2 E}{4 \gamma \sigma_Y W (1-V^2)} \right]$$

$$\text{for } V < \frac{2 \gamma \sigma_Y W (1-V^2)}{E}$$

The nomenclature is given in Section 4.2.

This formula (34) predicts a parabolic relationship up to general yield. Based on the formula $G = 2.1 \sigma_Y \delta$ and on boundary collocation estimates of clip gauge displacement, after general yield, the relationship is linear. It can be seen from the results on material G (Table 8.21) that the COD values obtained using the experimental relationship (equation 24) are optimistic at low COD's in comparison to the COD's obtained using the theoretical relationship (equations 22, 23). The difference in COD's values were about 40%. This observation is the same as that made by Veerman and Muller (43) but opposed to that of Archer (110). For higher COD values, for example materials L and A (Tables 8.28, 8.31), the experimental relationship compared well with the theoretical relationship.

The difference in COD values obtained using the two relationships was about 10%. However, since the theoretical relationship derived by Wells (34) is well founded theoretically, it is more advisable to use the theoretical relationship in calculating COD. In addition there was an example when an analysis based on formula 24 was found to give an unsafe answer (111).

The experiment on the effect of reducing specimen thickness varied from one material to another. For example in material D (Table 8.25) results show that there is no significant variation of COD with thickness. This observation is the same as that made by Smith and Knott (46). However the COD values for material L varied with thickness as shown in Table 8.28, COD values for the thinner specimens were higher than those for the thicker specimens. This observation is supported by (112). Using subsized specimens (25, 30, 120) the COD values were lower than that on the standard type specimen (Table 8.28) Material B also showed the same variation of COD with thickness (Table 8.9). This tends to indicate that the sensitivity of COD to thickness is material dependent. It can be seen from the above results that in some cases that COD values are geometry dependent and so it is advisable when determining COD for any one material that a full thickness test be carried out.

Results in Tables 8.28, 8.25 and 8.31, show that the crack opening displacement methods are more accurate with higher toughness materials (L, D and A) than those tested for lower toughness materials (B, M and C). Typically the crack tip displacements at fracture initiation were around 0.02 ± 0.003 mm for the lower toughness materials. This means a maximum error of around 30% in the property measured, arising mostly from the small, absolute size of the displacements.

Finally, the stress intensification factor, that is the degree of elevation of the yield stress, was investigated. This factor also showed

a variation from one material to another. For example in material B it was found that n was between 1 and 2 assuming a $K_{1C} = 44 \text{ MN m}^{-3/2}$ obtained by LEFM. This seems a reasonable experimental confirmation of the estimates by Wells. The n for material L was also between 1 and 2 assuming a $K_{1C} = 86 \text{ MN m}^{-3/2}$ obtained through J , providing further support for the estimates by Wells. However the COD results for material D and material A tend to show stress intensification factors of about 1 assuming a $K_{1C} = 67$ and $138 \text{ MN m}^{-3/2}$ respectively as obtained by the J -integral method. However, there do appear to be other instances of this type. For example work by Robinson & Tetelman (36) gave an experimental value of n equal to 0.93 for cracks propagating with dominantly plane strain plasticity in their plastic zones.

Comparison between J and Crack Opening Displacement

It can be concluded from the above discussion on J and COD, each of which have been proposed for characterising elastic plastic fracture problems, that the fracture toughness values obtained using J were more consistent from elastic behaviour up to elastic/plastic behaviour as compared with COD results. Also the fracture toughness values obtained using J were independent of specimen size for the materials examined in contrast to COD which appeared to be strongly influenced by specimen size. This allows J , at the point of fracture initiation, i.e. J_{1C} , to be considered as a good reflection of the near tip stress-strain environment of cracked elastic-plastic bodies irrespective of overall geometry or state of deformation. In this Thesis only specimen size was investigated but for J to be adopted as a universal fracture criterion, J values must be shown to be geometry, size and state of deformation independent. Work by Begley & Landes (55) proved that J was indeed geometry, size and state of deformation independent. This was an obvious reason for favouring J rather

than COD. Sumpter & Turner (113), as a result of theoretical analysis, found that in most cases it is possible to show that there exists a relationship between J and δ of the form:

$$J = M \sigma_Y \delta$$

For a given definition of δ , M usually shows at least some degree of geometry and load dependence. Sumpter & Turner (113) found, again theoretically, that M varied between 1.15 and 2 over the range of geometries studied. They also found that by considering the experimental method of defining δ in bending, by assuming a plastic hinge a fixed distance $\frac{W-a}{3}$, below the crack, gave a value of M which varies between 0.5, the ASTM limit and approximately 2 which is well after limit load based on data from the 3 point bend, $\frac{a}{W} = 0.5$, finite element analysis. In the results obtained in this Thesis M varied between 0.5 and 1.25, and consequently much more work is needed to relate the two criteria. Also, for COD a particular method of defining δ must be standardised before finding a relation between COD and J-integral.

→ In view of the se comments, the J-integral criterion is preferred to the COD because of its more precise definition, and its ease of calculation. However, most investigators up to the present date still prefer to use the COD method for measuring relative toughness because of the ease of measurement and accumulation of experience. From the work done in this Thesis it can be seen that the method used for estimating J-integral values was successful and the direct measurement of load point displacement makes it as easy as the COD method. Only one condition must be satisfied for measuring J at crack initiation, that is plane strain must be implied for both large and small specimens.

Metallographic and Fractographic Examination

The results presented in Section 8 are only for steels previously shown to be free of defects by radiographic examination. However the results should not be taken as representative of the in-situ properties of similar steels in the form of castings. Variation of casting procedure, shape and size of the casting, the resulting cooling rate and subsequent heat treatment may well influence toughness. These are factors to be examined in a further project. It is worth noting that the heat treatment given to steel B was found, at the end of this testing programme, to be obsolete as far as current industrial practice is concerned. Modified heat treatments have been found to give greater toughness (114). In view of these comments, the micrographs shown in Section 8 can be used simply to relate the various toughness values obtained, with their relevant microstructures. This will assist comparisons in later work. It can be seen from the results of Section 8 that in steels G, C and F the effects of position and the effects of micro and macro segregation need to be carefully assessed. Such a study was beyond the scope of this present work, and all that can be said are general comments concerning the likely variation in fracture properties across a cast section. For these steels, there is a decrease in fracture toughness from the edges to the centre of the block. From the literature review, Section 5, there are a number of compositional and structural factors than can influence the toughness of these materials. For example, material G contained a considerable amount of sulphur which has an effect on toughness but other variables must also be considered before deciding on what factor(s) is affecting the toughness. The presence of upper bainite in tempered martensite and the proportion of bainite in martensite will have an adverse effect on the toughness of the steels. In addition, prior austenite grains will have an effect on toughness, as this influences the distribution and morphology of martensite laths. These factors have been well documented with respect to fracture toughness (76-84). So, in order to determine the

factors affecting the fracture toughness in cast steels F, G and C all these factors must be included in any assessment. Such a study should now be relatively straightforward using the fracture toughness method developed in this Thesis. This method permits the use of small specimens and makes it simpler to measure toughness in the particular region of interest. Generally speaking, this is important since the areas of interest are limited in size necessitating the use of small specimen.

Tables 8.1, 8.22 and 8.26 for materials M, D and L show that casting position had little or no influence on fracture toughness. The fracture toughness values determined for steels L, D and M can be used with confidence for material selection or defect tolerance calculations with the provision that the microstructures in the castings are similar to those shown in Section 8. Also, these toughness values will be independent or at most, vary by a small amount, with the position in the castings.

Details of examination of the fracture surfaces for all the cast steels has been discussed in the results section, Section 8. The appearance of the fracture surfaces, as obtained from the fractographic examination, do in general provide confirmation on the toughness values obtained for the various steels. For example, the fracture surfaces of cast steel G, which gave a fairly low toughness value, showed shallow dimples associated with the large manganese sulphide inclusions and separating small ligaments. This morphology is generally associated with fracture at relatively low loads with the inclusions providing ideal void initiation sites. The results for steel F however, which has a higher toughness is in direct contrast to steel G. In this case the fracture surfaces show fine dimples indicative of fully ductile fracture by the mechanism of void nucleation, growth and eventual coalescence. The fracture surfaces for steels G and F are shown in Plates 27 and 53

respectively. For steels with very low toughness values, in this case steel M and B, fracture occurred by cleavage, as shown in Plates 9 and 13. This type of fracture is typical of a brittle material with a low toughness,

Although the appearance of the fracture surfaces was consistent with the toughness values obtained, there is an important point to note with regard to steel A. In total three keel blocks of steel A were tested, each of which came from different foundaries. Perhaps as a direct consequence of this there is some variability in fracture mechanism for this particular steel. For Al276 for example, the fracture surfaces had a fibrous appearance which indicates that fracture took place by the mechanism of nucleation, growth and coalescence of voids from second phase particles. The fractograph for cast steel Al277 showed that the crack extension process took place by the formation of a large stretch zone at the crack tip as shown in Plate 46. Both these mechanisms are fairly typical of ductile material behaviour which is consistent with the high toughness values obtained for these particular keel blocks. The fracture surfaces of the third keel block of material A however, indicates that fracture took place by cleavage a mechanism associated with low fracture toughness. Unfortunately no valid fracture toughness values were obtained from this block and no definite conclusions can be drawn. It would seem that further work is required here to identify the reasons for the different fracture mode in this keel block. Returning to the previous comments, the change in fracture mode could well have been caused by a different cooling rate for this block but clearly, external variables can have a significant effect on one material's fracture behaviour.

10. CONCLUSIONS

As a consequence of the experience gained during the course of this work and the results obtained from the experiments carried out, the following conclusions have been drawn:-

- 1) The J-Integral provides a practical and accurate method for toughness assessment. It is important however, particularly so for ductile Materials, that the critical J-integral is taken at the onset of crack growth. This value can then be used with confidence as a material constant.
- 2) The Potential Drop Technique as employed in this work, provides an accurate method for determining the onset of crack growth.
- 3) Regarding crack opening displacement results, the theoretical relationship equation 22 gave more consistent results than the experimental relationship, equation 24.
- 4) The fracture toughness results obtained using LEFM techniques for cast steels M, B and C at the centre of the keel block represented valid K_{1C} values, satisfying the criteria of DD3 and ASTM Committee E24.
- 5) With regard to LEFM testing, the single most important criterion for valid test results is that the ratio $P_{max}/P_Q < 1.10$.
- 6) Fracture toughness values for cast steels F, G and C varied through the keel block, minimum values being recorded at the keel block centre. In cast steels B, L, M, D and A toughness was invariant with casting position.

11. ACKNOWLEDGEMENTS

I am pleased to have this opportunity to express my deepest gratitude to my supervisor, Professor J.T. Barnby, for his encouragement and assistance throughout this work.

I am also grateful to the Staff of the Steel Castings Research and Trade Association for the provision and preparation of the Cast Steels used in this work.

The research was carried out in the Department of Metallurgy and Materials at the University of Aston, Birmingham. I am grateful to Professor W.O. Alexander for providing the facilities for this research. In addition I would like to record my appreciation to the College of Engineering Technology, Baghdad, for granting me a Study Leave for the duration of this work.

Finally, I am grateful to Mrs. M. Truman for the typing of this Thesis.

APPENDIX 12.A STATE OF PLANE STRESS AND PLANE STRAINState of Plane Stress

If a thin plate is loaded by forces applied at the boundary parallel to the plane of the plate and distributed uniformly over the thickness, as shown in Figure 12.1, the stress components, σ_z , γ_{xz} , γ_{yz} , are zero on both faces of the plate, and it may be assumed that they are also zero within the plate. The state of stress is then specified by σ_x , σ_y , γ_{xy} only and is called PLANE STRESS. The stresses are functions of x and y only.

In practice a state of plane stress is difficult to achieve. However, if the thickness of the body is very small compared with the other dimensions σ_z , γ_{xz} and γ_{yz} are of negligible magnitude compared with the other stresses so a state of plane stress can be assumed.

State of Plane Strain

If a long cylinder is loaded by forces which are perpendicular to the longitudinal elements and do not vary along the length, it may be assumed that all cross sections are in the same conditions. If also the end sections of the body are confined between fixed smooth rigid planes, so that the displacement in the axial direction is prevented, as shown in Figure 12.2, then ϵ_z , γ_{xz} , γ_{yz} are zero and the body is said to be under a state of PLANE STRAIN.

The plane strain problem like the plane stress problem reduces to the determination of σ_x , σ_y and γ_{xy} as functions of x and y only.

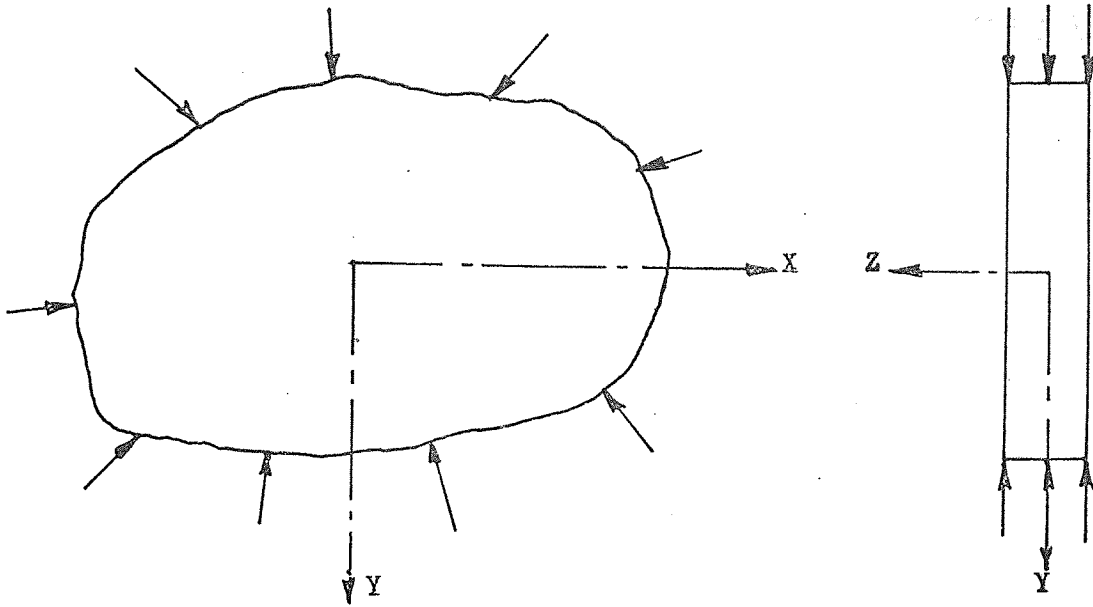


Fig. 12.1 State of Plane Stress.

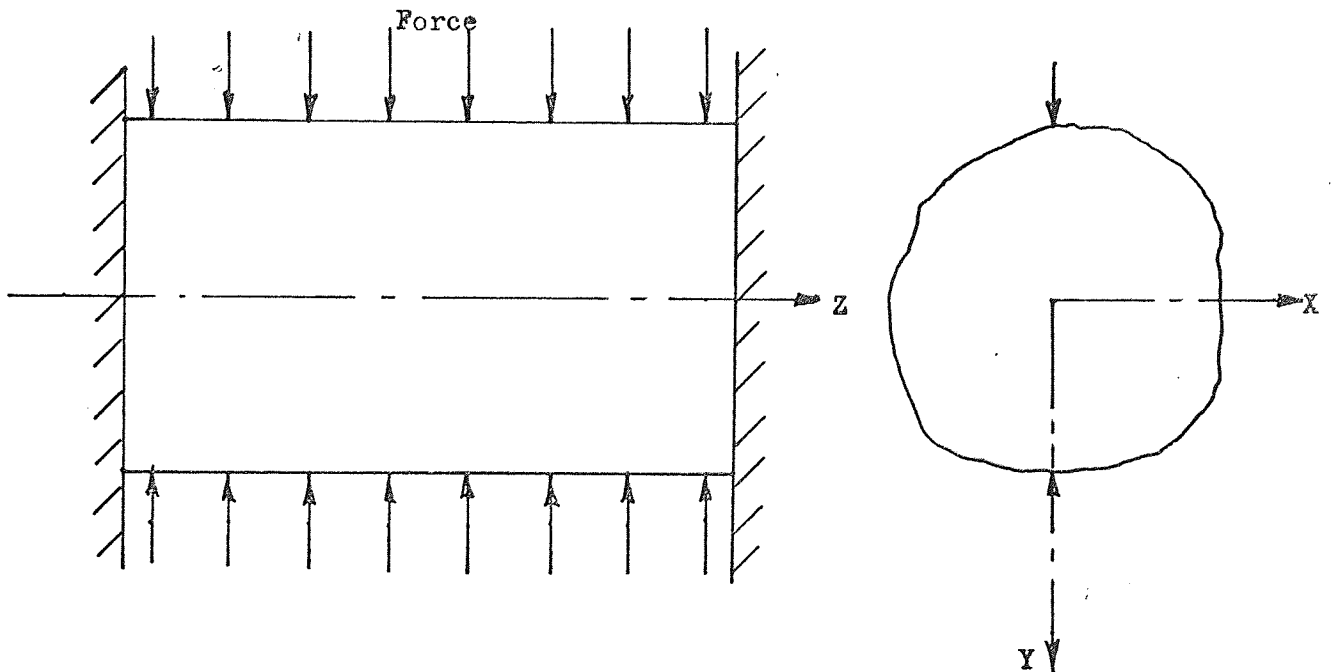


Fig. 12.2 State of Plane Strain.

APPENDIX 12.B DIGITAL COMPUTER PROGRAMME FOR DETERMINING J AND K VALUES FROM LOAD - LOAD POINT DISPLACEMENT CURVES

The following computer program is used to determine the area under experimentally determined Load - Load point displacement (P-LPD) curves. Once calculated, the area under the curve is used to determine values of stress intensity factors, K and J-Integral.

Details of the experimental curves are input to the program as a series of co-ordinates, the value of the co-ordinate points being taken from the experimental record. The area under the curve, to the point of interest, is calculated using two Scientific Sub-routines from the I.C.L. Library. The first of these sub-routines EO2ABA fits a polynomial relating Loads to LPD values, while the second DO1ACA performs the integration necessary to determine the area under the curve. As the area under the curve is required at several different load point displacement values it was considered desirable for program flexibility to fit a polynomial to the P-LPD values rather than integrate numerically using co-ordinates input to the program. A series of numerical trials have been carried out to check the accuracy and stability of the program.

The various program steps are described, with reference to the flow chart as:-

- 1) Number of sets of data are read and loop is constructed for this number.
- 2) For first specimen NPS, B, D, LEN, E and UCW are read.
- 2a) Values input in step 2 are printed to lineprinter.
- 3) Second Moment of Area for the specimen is calculated.
- 4) Number of pairs of points from P-LPD curve are read.
- 5) For the number of points in step 4, values of δ_{LPD} and P are read in order:

$$\delta_1 P_1 \quad \delta_2 P_2 \quad \delta_3 P_3 \quad \dots \quad \dots \quad \dots \quad \dots \quad \delta_m P_m$$

- 6) Procedure EOZABA is called to fit polynomial to points on the P-LPD curve $P = f(\delta_{LPD})$
- 7) Coefficients of best polynomial are printed.
- 8) Loop is constructed round the number of points for which J is to be evaluated (WPS).
- 9) For the first point in step 8 values of UL and P_Q are read, i.e. point on P-LPD curve where K_{1C} and J are to be determined.
- 10) Elastic area under P-LPD curve is calculated for a load P_Q applied to an uncracked specimen ELAR, see Figure 7.1.

$$\left(\frac{1}{2} P_Q \times \delta_{\text{no crack}} \right) \left[\delta_{\text{no crack}} = \frac{P_{QL}^3}{48EI} \right]$$

- 11) Procedure DOLACA called to evaluate area under the actual P-LPD curve up to displacement UL using the polynomial obtained from step 6. (Note. It is possible to integrate the polynomial of degree 4 exactly but the program was originally written for any order of polynomial and can still be used for a higher or lower polynomial by changing the value of DEG. Computational experiments have shown however that a polynomial of degree 4 is satisfactory).
- 12) Total area is printed, ANS.
- 13) Check is performed on procedure DOLACA to ensure that integral reached the required accuracy.
- 14) Plastic area is calculated (ANS-ELAR).
- 15) Values of J and K are calculated for both plane stress and plane strain with and without elastic area correction applied.

16) Values of J and K_I obtained in step 15) are printed ,

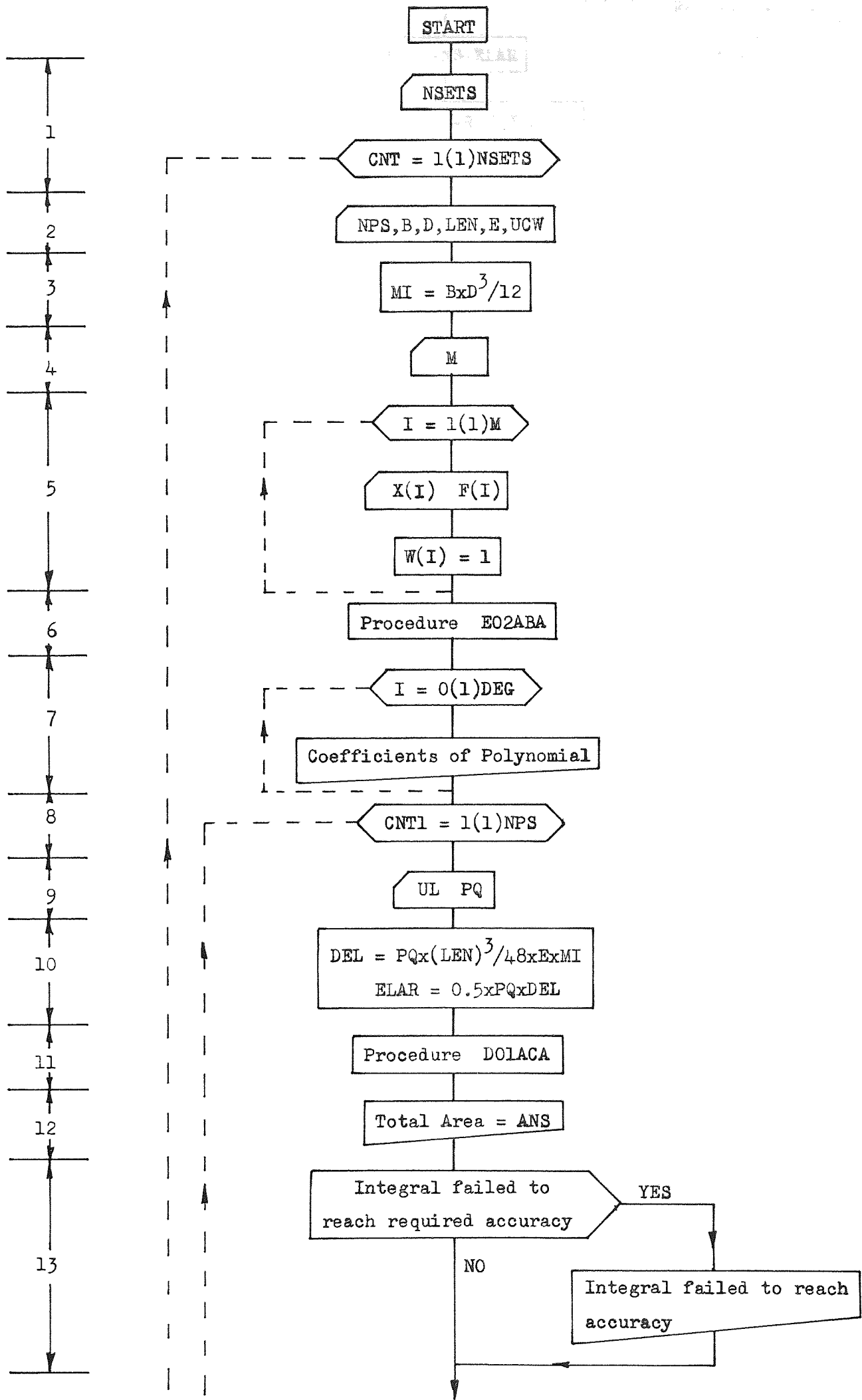
for second and subsequent points at which J and K are to be
evaluated return to step 9)

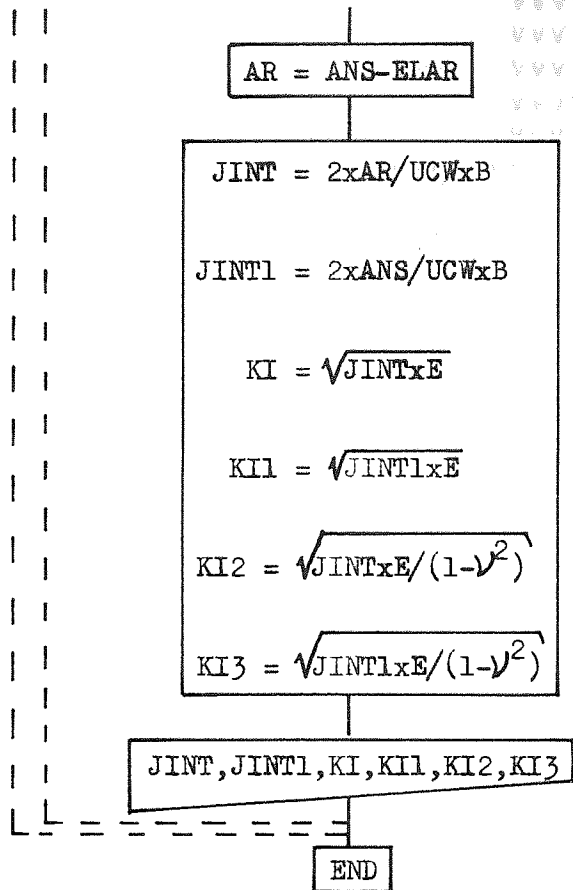
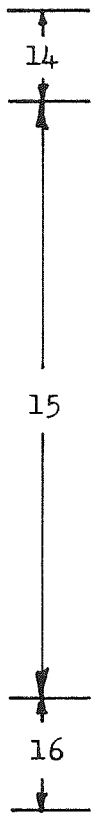
for second and subsequent specimens repeat from step 2).

DESCRIPTION OF PROGRAM VARIABLES

NSETS	Number of sets of data (or specimens)
NPS	Number of points on P-LPD curve at which J is to be evaluated.
B	Specimen Thickness.
D	Specimen Width.
LEN	Specimen Span.
E	Young's Modulus.
UCW	Uncracked Ligament Length.
MI	Moment of Inertia.
M	Number of pairs of points taken from load/Load point deflection curve.
X(I)	Array containing values of LPD, δ_{LPD}
F(I)	Array containing values of Load, P.
W(I)	Weighting values attached to points on P- δ curve, (= 1 in each case).
DEG	Degree of polynomial to be fitted (4 found to be best).
UL	Value of the displacement from P- δ curve at which J is to be found.
P_Q	is the corresponding Load to displacement UL at which J is to be found.
DEL	Elastic displacement of uncracked specimen to load P_Q

ELAR	Elastic area ($\frac{1}{2} P_Q \delta_{\text{no crack}}$)
ANS	Total area
AR	Nett area (ANS-ELAR)
JINT	Value of J with elastic correction applied
JINT1	Value of J without elastic correction
kI	Value of kI for $p\sigma$ with elastic correction
kI2	Value of kI for $p\epsilon$ with elastic correction
kI1	Value of kI for $p\sigma$ without elastic correction
kI3	Value of kI for $p\epsilon$ without elastic correction.






```

'BEGIN' 'REAL' 'ARRAY' X,F,W[1:M],SI,PLU:DEG];
'REAL' 'PROCEDURE' FUN(X);
'VALUE' X; 'REAL' X;
FUN:=P[0]+P[1]*X+P[2]*X*X+P[3]*X*X*X+P[4]*(X↑4);
'FOR' I:=1 'STEP' 1 'UNTIL' M 'DO'
'BEGIN'X[I]:=READ;F[I]:=READ;
W[I]:=1;
NEWLINE(2); SPACE(2); PRINT(X[I],0,6); SPACE(6); PRINT(F[I],0,6);
'END';
EO2ABA(M,X,F,W,DEG,DEF,SI,P,L);
WRITETEXT('('('('205S')'COEFFICIENTS%OF'('10S')'GOODNESS
%OF%FIT'('05S')'BEST%POLYNOMIAL')');
NEWLINE(2);
'FOR' I:=0 'STEP' 1 'UNTIL' DEG 'DO'
'BEGIN'SPACE(6);PRINT(PLI,0,6);
SPACE(11);PRINT(SI[I],0,6);
NEWLINE(1);
'END';
WRITETEXT('('('('0')'DEGREE%OF%BEST%POLYNOMIAL='))');

PRINT(DEF,3,0);
'FOR' CNT1:=1 'STEP' 1 'UNTIL' NPS 'DO'
'BEGIN'UL:=READ;PQ:=READ;
WRITETEXT('('('('80')'J% EVALUATED%FOR:='('22S')'LOAD%=%')');
PRINT(PQ,0,6);
WRITETEXT('('('('031S')'DISPLACEMENT%=%')'); PRINT(UL,0,6);
DEL:=PQ*LEN*LEN+LEN/(48*E*MT);
ELAR:=0.5*PQ*DEL;
DO1ACA(A,UL,FUN,RFLACC,ABSACC,NC,P1,ANS,ACC,SD,IFAIL);
WRITETEXT('('('('20')'TOTAL%AREA,M↑2%=%')'); PRINT(ANS,0,6);
WRITETEXT('('ACC='))'); PRINT(ACC,0,4);
WRITETEXT('('%%NUMBER%OF%POINTS%=%')');
PRINT(SD,2,0);NEWLINE(1);
'IF'IFAIL'LE'0'THEN'GOTO'L1;
WRITETEXT('('INTEGRAL% DID%NOT%REACH%REQUIRED%ACCURACY')');
NEWLINE(1);
L1:AR:=ANS-ELAR;
WRITETEXT('('('('20')'ELASTIC%CORRECTION,M↑2%=%')');
PRINT(ELAR,1,8);
JINT:=2*AR/(UCW*B); JINT1:=2*ANS/(UCW*B);
KI:=(JINT*E)↑0.5; KI1:=(JINT1*E)↑0.5;
KI2:=1.04828*KI; KI3:=KI1*1.04828;
WRITETEXT('('('('3011S')'WITH%ELASTIC%CORRECTION'('33S')'WITHOUT%
ELASTIC%CORRECTION'('202S')'J%INTEGRAL'('9S')'STRESS%INTENSITY
%FACTOR'('16S')'J%INTEGRAL'('9S')'STRESS%INTENSITY%FACTOR'('018S')'
PLANE%STRESS'('5S')'PLANE%STRAIN'('29S')'PLANE%STRESS'('5S')'
PLANE%STRAIN')');
NEWLINE(2); SPACE(1); PRINT(JINT,0,4); SPACE(4);
PRINT(KI,0,4); SPACE(4); PRINT(KI2,0,4); SPACE(11);
PRINT(JINT1,0,4); SPACE(4); PRINT(KI1,0,4); SPACE(4);PRINT(KI3,0,4);
'END'OF CNT1;
'END';
'END'OF CNT;
'END';

```

LENGTH 916

USED 25

xxx EC

(22AM)

AM (DBM)

13. REFERENCES

- 1) Mogford, I.L. The Analysis of Catastrophic Failures,
Central Electricity Research Laboratories,
Leatherhead.
- 2) Holder, R. 'Fatigue Crack Initiation from Stress Concentrations
in Cast Steels', Ph.D. Thesis, University of Aston,
1976.
- 3) Griffith, A.A. The Phenomena of Rupture and Flow in Solids,
Philosophical Transactions, Royal Soc. London,
Series A, Vol. 221, 1920 pp.163-198.
- 4) Knott, J.F. Fundamentals of Fracture Mechanics, Butterwords
1973. pp.98.
- 5) Taylor, G.I. and Proceedings Inst. Mechanical Engineers,
Griffith, A.A. 1917, pp.755-809.
- 6) Inglis, C.E. Stresses in a plate due to the presence of
cracks and sharp corners, Transactions Inst.
Naval Architects, Vol. 60, 1913, p.216.
- 7) Irwin, G.R. 'Fracture Dynamics', in Fracturing of metals
ASM Cleveland, 1948.
- 8) Orowan, E. 'Energy criteria of fracture', Weld J. Res. Suppl.
1955, 20, 157s.
- 9) Orowan, E. 'Fracture' 147-160 1959. New York, Wiley & Sons.
- 10) Irwin, G.R. and Fracturing and fracture dynamics, Weld.
Kies J.A. J. Res. Suppl. 1952, 17, 95s.
- 11) Srawley, J.E. Experimental determination of the dependance of
Jones, M.H. and crack extension force on crack length for a single-
Gross, B. edged notch tension specimen, 1964 NASA TND 2396.
- 12) Irwin G.R. Analysis of stresses and strains near the end of
a crack traversing a plate, J. Applied Mech.
1957, 24, 361.
- 13) Westerguard's, H.M. Bearing pressures and cracks, J. Applied Mech.
1939, 63, A49.
- 14) Paris, P.C. Stress analysis of cracks, ASTM, STP381, 1965.
Sih, G.

- 15) Cartwright, D.J. Evaluation of stress intensity factors,
Rooke, D.P. Journal of strain analysis, Vol. 10, No. 4, 1975.
- 16) A.S.T.M. STP 410, Plane strain crack toughness testing of high
strength metallic materials, 1967.
- 17) Wigglesworth, L.A. Stress distribution in a notched plate,
Mathematika 1957 4, 76.
- 18) Brown, W.F. and Plane strain crack toughness testing 1967
Strawley, J.E. (ASTM STP 410).
- 19) Irwin, G.R. Fracture mode transition for a crack traversing
a plate, Transactions, Am. Soc. Mechanical Engrs.
Vol. 82, Series D, 1960, p.417.
- 20) Barnby, J.T. Welding and Metal Fab. Feb. 1969, p.71.
- 21) A.S.T.M. Standards, 1968, Part 31, pp.1018-1030, Proposed recommended
practice for plane strain fracture toughness testing
of high-strength metallic materials using a fatigue
cracked bend specimen.
- 22) Weiss, V. and ASTM STP 381, 1; 1975 Philadelphia.
Yukawa, S.
- 23) Kies, J.A., Graphical methods for plasticity corrections
Smith, H.L. and in fracture mechanics, NRL Report 6918,
Stonesifer, F.R. September 18, 1969.
- 24) Stonesifer, F.R. Characterization of T16 Welds in 12.5.3 managging
and Smith, H.L. steel plate with application of a new scaling
method for K_{1C} plasticity corrections, NRL
Report 7053 April 16, 1970.
- 25) Witt, F.J. Equivalent energy procedures for predicting gross
plastic fracture, paper presented at Fourth National
Symposium on fracture mechanics, Carnegie Mellon
University, August 1970.
- 26) Chell, G.G., Practical fracture mechanics in the post-yield
Milne, L. regime, Metals Technology Dec. 1975
Kirby, J.H. 549-553.
- 27) Wells, A.A. Unstable crack propagation in metals; cleavage
and fast fracture, crack propagation symposium
College of Aeronautics and the Royal Aeronautical
Society, Cranfield, September 1961.

- 28) Cottrell, A.H. Theoretical aspects of radiation damage and brittle fracture in steel pressure vessels. Steels for reactor pressure circuits, A symposium of the Iron and Steel Inst., November-December 1960, Special Report No. 69.
- 29) Burdekin, F.M. Stone, D.E.W. The crack opening displacement approach to fracture mechanics in yielding materials. Journal of strain analysis, Vol. 1, No. 2, 1966 pp.145-153.
- 30) Dugdale, D.S. Yielding of steel sheets containing slits, J. Mech. Phys. Solids 1960, 8, No. 2, 100.
- 31) Wells, A.A. Application of fracture mechanics at and beyond general yielding, Br. Weld J. 10, 563, 1963.
- 32) Bilby, B.A. Proc. Roy Soc. 1964 A279, 1-9.
Cottrell, A.H.
Smith, E. and
Swindon, K.H.
- 33) Irwin, G.R. Interpretations of the crack opening dislocation concept. Fritz Engineering Lab. Report No. 358.2
Lingarajn, B. and
Tada H. Lehigh University Institute of Research.
- 34) Wells, A.A. The status of COD in fracture mechanics, Eng. Frac. Mech. 1969, 1, 3, 399-410.
- 35) Turner, C.E. A unification of the J contour integral and COD criterion for fracture by use of in-plane constraint factors. Mech. Engineering Dept., Imperial College Report for NDACSS group 'A' CODA Meeting, 6th January 1972.
- 36) Robinson, J.N. and Tetelman A.S. Third International Congress on Fracture, Munich, Vol. 111, paper 9-20 1973.
- 37) Smith, R.F. and Knott, J.F. Crack opening displacement and fibrous fracture in mild steel. Conference on practical application of fracture mechanics to pressure vessel technology London, May 1971, Institution of Mechanical Engineers.
- 38) Wilshaw, T.R. The effect of temp. and strain rate on the deformation and fracture of mild steel charpy specimens, Ph. D. Thesis, 1964, Imperial College, University of London.

- 39) Fearneough, G.D. Int. Journal Fract. Mech., 1968, 4.3,
& Watkins, B. 233-243.
- 40) Methods for Crack Opening Displacement (COD Testing)
Draft British Standard DD19 : 1972.
- 41) Sumpter, J.D.G. Some further Finite Element Results on the
3 point Bend Geometry, Lecture Notes for the
3rd International Post Experience Course on
Fracture Mechanics, Imperial College, July 1974.
- 42) Venzi, S. Determination of a generalised relationship for
COD Calibration Auto Sperimentale Metallurgic
Report, 1973.
- 43) Veerman, C.C. and Eng. Fracture Mech. 1972 4, 25-32.
Muller, T.
- 44) Cowan, A. and Practical fracture mechanics for structural
Kirby, N. steels D1-D27, 1969 London U.K.A.E.A. with
Chapman and Hall.
- 45) Harrison, T.C. and Int. Journal Fracture Mech. 1969, 5, 3, 348-349.
Fearneough, G.D.
- 46) Smith, R.F. and Practical Application of fracture mechanics to
Knott, J.F. pressure vessel technology, Inst. Mech. Eng.
London, 1971.
- 47) Terry, P. and Determining critical crack opening displacement
Barnby, J.T. for the onset of slow tearing in steels.
Metal Construction and British Welding Journal
September 1971, pp. 343-345.
- 48) Gilbey, D.M. and R.A.E. Technical Report 66402, 1966.
Pearson, S.
- 49) Rice, J.R. Journal of Applied Mechanics, Transactions of
the American Society of Mechanical Engineers,
June 1968, pp. 379-386.
- 50) Rice, J.R. Mathematical Analysis in the Mechanics of Fracture,
An Advanced Treatise, Vol. 2 Ed Liebowitz Academic
Press, 1968.
- 51) Begley, J.A. and The J integral as a Fracture Criterion.
Landes J.D. ASTM STP 514 Part II.

- 52) Hutchinson, J.W., Journal of the Mechanics and Physics of Solids, Vol. 16, 1968, pp.13-31.
- 53) Rice, J.R. and Rosengren, G.F. Journal of the Mechanics and Physics of Solids, Vol. 16, 1968, pp.1-12.
- 54) McClintock, F.A. In Fracture, H. Liebowitz, Ed., Vol. 3, Academic Press., New York, 1971, pp.47-225.
- 55) Landes, J.D. and Begley, J.A. "The effect of Specimen Geometry on J_{1C} " Fracture Toughness, Proceedings of the 1971 National Symposium on Fracture Mechanics, Part II, ASTM STP 514 pp.24-39.
- 56) Bucci, R.J., Paris, P.C., Landes, J.D. and Rice, J.R. J. Integral Estimation Procedures, Fracture Toughness Proceedings of the 1971 National Symposium on Fracture Mechanics, Part II, ASTM STP514, pp.40-69.
- 57) Irwin, G.R. and Paris, P.C. In Fracture, Vol. III, Academic Press, New York, 1971.
- 58) Adams, N.J. and Munro H.G. A single test method for evaluation of the J integral as a fracture parameter, Engineering Fracture Mechanics, 1974, Vol. 6, 119-132.
- 59) Hahn, G.T., Sarrate, M. and Rosenfield A.R. Plastic zones in Fe-3 Si steel double-cantilever beam specimens. Int. J. Fracture Mech. 7, 435-446 (1971).
- 60) Munro, H.G. and Adams N.J. Fatigue and Fracture of a 200 k_{si} grade managng steel proposed for use in military bridging Eng. Fracture Mech. 4, 705-715 (1972)
- 61) Rice, J.R. Paris, P.C. and Merkle, J.G. Some further results of J integral analysis and estimates, progress in flow growth and fracture toughness testing, ASTM STP 536, 1973 pp.231-245.
- 62) Paris Discussion in reference 51.
- 63) Landes, J.D. and Begley J.A. Test results from J integral studies. An attempt to establish a J_{1C} testing procedure, Fracture Analysis, ASTM STP 560, 1974, pp.170-186.
- 64) Petch, N.J. J.I.S.I. Vol. 173, 1953, p.25.
- 65) Stroh, A.N. Proc. Roy. Soc. A223, 1954, p.404.

- 66) Smith, E. and Barnby, J.T. Metal Sci. J., V. 1, 1967, 56.
- 67) Cottrell, A.H. I.S.I. Pub. 69, 1960, p.281.
- 68) Hull, D. Acta Met. 8, 11, 1960.
- 69) Knott, J.F. and Cottrell, A.H. J.I.S.I., 201, 249 (1963).
- 70) McMahan, C.J. and Cohen, M. Acta Met., 13, 591 (1965).
- 71) Smith, E. Proc. Conference Physical Basis of Yield and Fracture, 36, Inst. Phys. Soc. Oxford (1966).
- 72) Lindley, T.C. Oates, G and Richards, C.E. Acta Met., 18, 1127 (1970).
- 73) Matas, S.J. Metals Eng. Q., 4 (1964), 48.
- 74) Cottrell, C.L.M. Fracture Toughness of High Strength Materials. Theory and Practice, ISI Publication 120, The Iron and Steel Institute, London, 1970, p.112.
- 75) Sims, C.E. and Dahle, F.B. Effect of Alumina on the Properties of Medium Carbon Cast Steels Trans. AFS 1938, 46, p.65.
- 76) Huang, D. and Thomas, G. Met. Trans. 2 (1971), 1587.
- 77) Huang, D. and Thomas, G. Meta. Trans. 3 (1972), 343.
- 78) Seal, A. and Honeycombe, R.W.K. J. Iron Steel Inst., 188 (1958), 9.
- 79) Webster, D. Met. Trans. 2 (1971), 2097.
- 80) Tanaka, M. and Yamamola, J. Toward Improved Ductility and Toughness, Climex Molybdenum Development CO (Japan) Ltd., 1971, p.195.
- 81) Parker, E.R. and Zackay, V.F. Eng. Fr. Mech. 5 (1973) 147.
- 82) Dolby, R.E. and Knott, J.F. J. Iron and Steel Inst., 210, p.857 (1972).
- 83) Zackay, V.F. Parker, E.R. & Wood, W.F. Microstructure and Design of alloys, Institute of Metals, London, 1973, p.175.

- 84) Zackay, V.F. Nature Physical Science, 236, 108 (1972).
Parker, E.R.,
Goolsby, R.D.
and Wood W.E.
- 85) Spitzig, W.A. ASTM STP 436, Philadelphia 1968 p.17-31.
Pellissier, G.E.
Beachem, C.D.
Brothers, A.J.
Hill, M. and
Warke, W.R.
- 86) Crussard, J.I.S.I. V183, 1956, p.146.
- 87) Beachem C.D. and ASTM STP 436, Philadelphia, 1968, p.59-88.
Meyn, D.A.
- 88) Beachem, C.D. Met. Trans. submitted for publication in 1974.
- 89) Tipper, C.F. Metallurgia 1949, 39, 133.
- 90) Clausing, D.P. Trans. ASM, 1967, Vol. 60, 504.
- 91) Gladman, T. ISI/BISRA Joint Conference, Scarborough,
Holmes, B. and March 1971 or 68, Iron and Steel Institute
McIvor, I.D. London, 1971.
- 92) Joy, G.D. and ibid.
Nutting, J.
- 93) Smith, R.F. and 'Conf. on Practical Applications of Fracture
Knott, J.F. Mechanics to Pressure Vessel Technology'
Inst. Mech. Engrs. 65 (1971).
- 94) McClintock, F.M. Int. Jnl. Fracture Mechanics, 4, 101 (1968).
- 95) Gurland, J. Trans. A.I.M.E. V227, 1963, p.1146.
- 96) Thomason, P.F. Int. J. of Fracture Mech. 7, 409 (1971).
- 97) Edelson, B.I. and Trans. Am. Soc. Met. 55, 230 1962.
Baldwin, W.M.
- 98) Turkalo, A.M. and Trans. Am. Inst. Min. Metall. Petrol Engrs.,
Low, J.R. 212, 750, 1958.
- 99) Rolfe S.T. and ASTM STP 463 American Society for Testing and
Novak, S.R. Materials 1970 124-159.
- 100) Kaufman, J.G., Fracture Toughness of Aluminium Alloy Plate
Nelson, F.G., Jr. determined with Centre-Notched Tension, Single-
and Holt Edged-Notch Tension and Notch Bend Tests.
Presented at the National Symposium on Fracture
Mechanics, Lehigh University, 1967.

- 101) B.I.S.R.A. Proposed Spec. for Fracture Toughness Testing of High Strength Materials. Report MG/EB/312/67.
- 102) Methods for Plane Strain Fracture Toughness (K_{1C}) Testing
Draft British Standard DD3 : 1971.
- 103) Jacquet P.A. Proc. ASTM. 1957 57 1290.
- 104) ASTM E399 - 72 Standard Method of Test for Plane - Strain Fracture Toughness of Metallic Materials.
- 105) Rice, P. Acier-Steel Stahl 40 (1975) 297.
- 106) Lavender, J.D. Proceedings of the Conference on Quality Control and the Significance of Mech. Props., S.C.R.A.T.A. 1975.
- 107) Greenberg, H.D. Mat. Eng. Quart. 9 (1969) 30.
and Clark, D.
- 108) Bradshaw, J. and J. Res. S.C.R.T.A. 8 (1970) 2.
Jackson, W.J.
- 109) Kuzucu, F. Thesis, University of Birmingham 1972.
- 110) Archer, G.L. The Welding Institute Report E/63/75 March 1975.
- 111) Dawes, M.G. The Welding Institute Report E/50/74.
- 112) Burdekin, F.M. J. of Strain Analysis, 1, (2), 145, 1966.
and Stone, D.E.W.
- 113) Sumpter J.D.G. Lecture Notes for the 3rd International Post
and Turner C.E. Experience Course on Fracture Mechanics,
Imperial College, July 1974.
- 114) Kirke, M. Personal Communication.
- 115) Banks, T.M. Personal Communication.